

Review of “Fault-related dolomitization in the Montagna dei Fiori Anticline (Central Apennines, Italy): Record of a dominantly pre-orogenic fluid migration. Se-2018-136

This manuscript presents field, petrographic and geochemical data from non-stratabound dolomites in a complex tectonic setting, and interprets their geofluid origin (parent fluids, timing) in the context of the tectonostratigraphic history.

It is coherent and logically organised. Aspects of the written English need minor improvement (punctuation, plurals, word order, etc); it will benefit from a final revision by a native English speaker.

The data are generally of good quality, and the interpretations are mostly justified from the results presented. In any study such as this, with limitations imposed by the ability to sample all the phases, there is necessarily some latitude or flexibility in the deductions that can be made. However, the authors do a good job of considering alternative possibilities for the fluid sources and timings.

My only issue with the paper is that the authors have not really considered whether there are wider implications or generic advances that can be made from the research. It presents itself as a case study, albeit one with a good integration of structural and diagenetic data. But what is the wider impact that will attract a non-specialist readership? Within the paper the authors all but admit that their findings are only modestly advanced from those of Ronchi and co-workers fifteen years ago (lines 638-642). I had hoped to see more progression in the science, and maybe the authors need to more thoroughly and critically evaluate the Ronchi model in the light of their new data. They could also work the structural data more – rather than just considering fault orientations and timings, what about the character and extent of the damage zones associated with different fault types / generations, and their relationship to the size and shape of dolomite bodies? What determines the lateral extent of dolomites? Is it other faults / fractures, or a gradual reaction front?

One generic aspect that the authors could address is implications for reservoir potential in analogues for this setting. The preponderance of planar dolomite is significant because planar dolomite is usually very beneficial for porperm (unlike many examples of hydrothermal dolomitization that feature tight nonplanar dolomites). Are there dolomitised plays in the Middle East that this study could be compared to (Zagros Mountains for example?), or maybe in Mexico?

Another factor of interest, largely by-passed in the text, is what drove the fluid circulation necessary to cause massive dolomitization when the low temperatures argue against a hydrothermal syn-rift system. Can the authors attempt a mass balance to estimate the order of magnitude fluid volumes needed? Maybe the dolomitization occurred in the down-flowing (cool) limb of a convection cell established on syn-rift faults that breached contemporary sea bed? Or does the dolomite zoning imply a pulsed fluid flow associated with strain cycling or seismic valving? I recommend the recent papers by Hollis and others on the Hammam Faraun fault and related syn-rift dolomitization. Are the D1-2 dolomites formed in a similar manner to this geologically younger example? Likewise, with the later dolomitization, which structures would have been open during compressional tectonics and able to serve as conduits for substantial fluid volumes?

If the authors address these issues their paper, which is already technically good, it will have much greater impact and interest across the sedimentary and structural geoscience community.

I have some more **specific comments** – these are tagged by line number or Figure number:

Line 43: The paper describes the role of evaporite-sourced fluids in the dolomitization process, but I am not sure that it illustrates a controlling role of evaporitic detachments. These may have influenced the tectonic development, but if it is believed that they directly controlled the dolomitization this needs to be specifically discussed later in the paper. **Emphasized more in the text**

Note the abstract is quite long-winded. It would be good to make it more succinct and punchier. **Addressed**

Line 69: The Castel Manfrino Dolostones are not labelled in Fig. 1 or Fig. 2b. **Added in Fig.1**

Line 73, 76: Did Ronchi (2003) base her study on the mapping of Mattei (1987)? Maybe there needs to be a couple of sentences describing Ronchi's findings so that it can be more clearly shown that the understanding has moved on. **Added to text**

Line 79-83: This is very long-winded and vague. It either needs to be shortened or to include specific details. **The sentence is shortened.**

Line 129: Given that the early dolomitization (D1-2) is later ascribed to the syn-rift stage, it would be useful to briefly describe the facies and architectural character of the syn-rift carbonates. For example, were they preferentially developed on footwall highs, in which case there was likely a juxtaposition of permeable high energy facies against faults that later hosted fluid flow? **Addressed**

Line 135-137: It may be a matter of debate, but the authors need to either provide the conflicting evidence or at least express a view and justify it. **The sentence is deleted as further discussion is not the focus of this research**

Line 152: Can the Montagna dei Fiori fault be indicated / labelled on Fig. 1d? **Addressed**

Line 164: Ground truthing implies that the features had previously been mapped out using remote data. If so, this should be included in the methods. **Addressed**

Line 167: So far as I can see, the Sibley and Gregg (1987) terminology (planar-e, planar-s, nonplanar) is <not> used anywhere in the paper, so either it needs to be incorporated or this sentence should be removed. **The sentence and related references are removed**

Line 186: Can the reproducibility ($\pm 0.1\%$) be smaller than the precision ($\pm 0.2\%$)? **The inter-lab reproducibility is $\pm 0.1\%$ means the measurement for the same sample in two different labs has a difference of $\pm 0.1\%$**

Line 224: Bugarone Formation is not shown on Fig. 1 or Fig 2. **Addressed**

Line 231: Is the wider distribution of dolomitized intervals related to the topography of the valley and the exposures? If not, what is the relationship? **Addressed**

Line 238: I suggest not using "overprinted", which implies the original fabric / lithology is lost. Why not just use "cross-cut"? (or even just "cut") **Addressed**

Line 258 and elsewhere: "Dull" is not a colour! **Addressed**

Line 261 onwards: There could be a bit more detail on the dolomite distribution and fabric with respect to host rock facies. Is it all texturally destructive, is there any textural or mineralogical selectivity, were grainy or muddy facies preferentially dolomitized (controls by permeability versus reactive surface area.....?) **Addressed**

Line 272: There is an issue because CV1, CV2 etc. are introduced before they have been defined and described. I suggest starting section 4.2 with a paragenetic summary to alleviate this problem. **Addressed, paragenesis is presented in Fig. 14.**

Line 278: By using “frequently” the text suggests that sometimes (infrequently) D2 post-dates bed-parallel stylolites. Is that the case? **Addressed**

Line 284-285: This sentence needs a figure citation. **Addressed**

Line 297: Repetition of “euhedral to anhedral” (cf. line 295) – note this is not Sibley and Gregg terminology. Nor is “tightly packed texture” in line 279. **Addressed**

Line 305: I do not think one dolomite can “recrystallize” another. Recrystallization is a solid-state process that increased mineral stability. To demonstrate it might need data on the ordering, crystallinity and stoichiometry of D1/2 versus D4 (do the authors have any XRD data?). What is more likely is that D4 has locally replaced D1 and D2 by a dissolution-precipitation mechanism. However, the text lacks a clear description of the evidence for replacement. I recall papers by Mazzullo and by Machel that discuss this – it would be good to list the criteria for this case. **Addressed**

Line 330: In Fig. 11C, D the dolomite does not appear to be yellow-orange, it looks more like orange-brown. **Addressed**

Line 332: How wide was the extensional fault master plane? Please supply the range of widths (and lengths where possible) of the different vein generations. **It is addressed for vein generations.**

Line 335-336: What is meant by “with no evidence of physical disruption”? Does it mean that CV3 always passively overgrows D5 in voids and never cuts it? If so, it is easier to say this. **Addressed**

Line 336: Translucent is not a colour. **Addressed**

Line 334: What colours are the zones? **Addressed**

Line 367-368: Rather than “the presumable Lower Jurassic marine dolomites” – which are hypothetical – it is better to say the values are lower than those expected for Lower Jurassic seawater dolomites. **Addressed**

Line 391: “While.....” indicates there should be a second part to the sentence. **Addressed**

Line 396: What is the lithology of these samples? **Addressed**

Line 401: Please add a sentence or two on the fluid inclusion petrography and distribution – do inclusions follow growth zones or are they randomly distributed? Are they all primary or are some pseudosecondary? What are their shapes and what are the liquid:vapour ratios in the 2-phase examples? Also, in reporting the results for different cements please give the number of inclusions the ranges are based on (n=). **Addressed**

Line 409-410: What is the purpose of nucleating a bubble for measurement of freezing temperatures? **Addressed**

Line 477-478: This sentence appears out of place or at least needs clarification. More than two values are needed to demonstrate a progression. **Addressed**

Line 503-507: Yes, this makes sense if the veins are filling tension gashes associated with stylolites – such as system is likely to be buffered by the dissolving carbonate. Maybe make this point more explicitly, and contrast with vein types that were more extensive and would have allowed allochthonous fluids to pass through with minimal host-rock interaction. **Addressed**

Line 518: Hendry et al. (2015) did not discuss ^{13}C enrichment from CO_2 outgassing due to evaporation. They made the point that negative covariance in C and O isotopes within veins could be due to precipitation during CO_2 outgassing related to pressure changes. **Addressed**

Line 524-551: This is good but is a very long paragraph. Can it be made more succinct? **Addressed**

Line 550-551: The final sentence needs rewriting; what was confined, the thrust wedge or the fluids? **Addressed**

Line 556: In the preceding section there is very little mention of fluid mixing. Could the poorly correlated Th, salinity and stable isotopic data reflect precipitation from allochthonous fluids as they mixed with in situ fluids (and cooled)? Degrees of mixing (and of water-rock interaction) may have different from fault to fault – is it really likely that the hydrogeological systems was as simple as is being presented here? **The obtained data show no systematic variations from fault to fault. Thus, existence of different local hydrological systems cannot be addressed. The sentence is revised ad completed**

Line 575-579: Please rewrite this sentence – it tries to say too many things at the same time. **Addressed**

Line 584: Doesn't the displacement of D1-2 on these faults indicate that the dolomite formed before faulting? What is the critical evidence that it is genuinely syn-rift? **The syn-rift deposits (Corniola Formation) is affected by these dolomites. Addressed more in the text**

Line 590: if D1-2 were related to basement-cutting faults, why are the Sr isotope values much less elevated than for D3 and D4? **There is no other alternative for radiogenic Sr source. This is the case for all of the dolomite types. Maybe less basement derived fluids were involved in D1.**

Line 656-657: Please explain how hydrothermal fluids were able to circulate in the compressional tectonic regime – which structures were able to be in tension and therefore transmissive rather than sealing? **Addressed**

Line 1139: The cross-cutting relationship in Fig. 8a, b is not very evident. **Addressed**

Lines 1142-1148: Should this discussion be in the main text rather than in the caption? **This has been made to avoid a longer discussion.**

Fig. 2b: It would help if the colours and ornaments matched Fig. 8a (e.g. Salinello Fm). The text size needs to be increased for better legibility. **Addressed**

The stereonet data are good, but very little use is made of them in the text of the paper. **Addressed in the figure caption**

Fig. 5: Please increase the text size and make 5c larger – it is too small to see clearly. **Addressed**

Figs 6-9, 11: Some of the CL images could be a bit sharper and maybe with increased contrast to better discriminate the dolomite types. **Addressed**

Fig. 12: The symbols for D3 vs. CV3 and mixed dolomite vs. CV1 are too similar (especially given the small size). I am also not clear how Fig. 12b relates to Fig. 12a; maybe split the legend between the two plots according to what is in them – that might help. **Addressed**

Fig. 14: How were the burial temperatures in the burial history determined? What assumptions are they based on? **Addressed**

Fig. 15: I like this figure but I'm still not sure what the fluid flow pathway is in (b). Maybe a broader tectonic context diagram is needed showing expulsion of fluids from the foreland (if that is where they are coming from?). **The fluids were migrated from hinterland (now indicated on the sketch) rather than forland.**

I hope these comments are helpful, and I look forward to seeing the paper published in revised form.

Jim Hendry

Tullow Oil Ltd, Dublin

Specific comments:

- 1) Abstract: The abstract can be shortened substantially, yet it is missing key information. It provides too much detail of some aspects of this work but lacks equivalent detail in other cases. For example, why are calcite-filled veins not mentioned here? Weren't they a main focus of this study? A more succinct and balanced abstract is required. Also, the abstract would benefit from a "punchline" or statement of the broader implications of this work at the end. What did you learn about the extent of dolomitization near faults? How is this relevant for porosity/permeability evolution and fluid flow in dolomitized, carbonate-hosted hydrocarbon reservoirs and aquifers? **Addressed**
- 2) Introduction: You may want to consider adding a short statement about why some fault-zones become dolomitized but others don't. What are the requirements? What can you learn from outcrops that you cannot from core alone? I would say that the main benefit would be the opportunity to assess the spatial distribution of dolomitized zones, and individual diagenetic events, in 3D. Addition of such a field-relations analysis would greatly improve the impact of this work. **Addressed**
- 3) Geologic setting: This section is a bit long and could be shortened. **Addressed**
- 4) Methodology: A few things are missing:
 - How large of a geographic area did you sample? **Addressed**
 - How did you decide which areas to sample for isotopic analyses? Did you image them first? How? How confident are you that you didn't mix different cements when sampling? **Addressed**
 - How many fluid inclusions in your FIAs? What was your reproducibility and error? How did you make sure you did not measure stretched inclusions? **Addressed**
 - Documentation of where hand samples came from is very poor. This can be improved by showing the location of the thin sections on outcrop photos, and their spatial relationship with faults etc. These might need to be included in an appendix due to space restrictions, but it is important. **Explained in author response**
- 5) Field observations
 - What is the spatial distribution of the dolomitized geobodies? **Addressed**
 - And of the veined sections?
 - 6 outcrop locations are marked on Figure 2 but distributions of the different types of cements are only shown in one image (figure 5b). These are very important relations to assess fluid pathways and the evolution of dolomitization. **Addressed**
 - What are the orientations of CV1–CV4 cement-bearing fractures? **Shown in Storti et al. (2018)**
- 6) Petrography
 - How much calcite cement is there in the breccias? What are the textures? Why are these not included in your diagenetic evolution analysis? How do cements in breccias relate to those in host rocks? Are cements in the host rocks affected by brecciation? Show examples. **Addressed**

- How did dolomitization affect porosity in both host rock and fault rocks? How does porosity compare between limestones and dolostones? **Addressed**
 - Some of the petrographic relationships mentioned need to be backed by images (see my line-specific comments) **Addressed**
 - The order in which dolomite cements and vein-calcite cements are mentioned needs to be improved.
 - What is the relationship between MC and D1/D2? Where is this documented? **Addressed**
 - What is the distribution of CV cements in the host rock (see Laubach, 2003)? This should be properly documented and reported. I don't think vein cement is an appropriate term for these calcite cements. Also, keep in mind that the occlusion of fracture porosity by postkinematic cements can significantly postdate the timing of the opening of the fracture (see Ukar and Laubach, 2016). In other words: the timing of fracturing and cementation are not the same. Keep that in mind in your descriptions. **Addressed**
 - The observation of CV3 in breccias is quite interesting. Document and show images. What other cements are there in breccias? How did you establish the relative timing of these cements and others? Breccia cements should not be referred to as vein cements. **Explained in author response**
 - What are the spatial distributions of the different cement types? **Addressed**
- 7) Geochemistry
- What are the isotopic characteristics of MC and fibrous cements? **Addressed**
 - Interpretations, especially for Sr ratios, should be moved to the discussion.
- 8) Fluid inclusions
- Show images of the different types of fluid inclusions, especially the FIAs.
 - The graphs used to summarize fluid-inclusion thermometric results are not appropriate because key information is lost. Same for salinity. Please replot the data so that the temperature range for each individual FIA is shown. Did you measure an equal amount of FIAs for each type of cement? Otherwise, frequency would not very meaningful in Fig. 13 because it would be sample and cement availability dependent.
 - Why are CV temperatures not shown in these graphs? **For a higher focus on dolomitization case study**
- 9) Discussion
- This section can be significantly shortened by avoiding repetition of results.
 - I think parental fluid calculations should be shown in the results section, not in the discussion. **To emphasize on the nature of parental fluids, we prefer to keep SMOW values in discussion section**
 - Use parallel writing style for stable isotopes and Sr discussion.???
 - D3 shows significantly higher Sr/Sr than D4. How can both be related to the same event and derived from similar fault-related fluids? D1 and D2 are also fault-related. Why the differences in isotopic signatures, especially if all are related to basement-rooted faults???

- The association of D3 and D4 with bed-parallel and shear fractures is mentioned for the first time in the discussion. This needs to be mentioned in the results. Are the cements themselves sheared? Show evidence. **Addressed in petrography**
 - Discuss the spatial distribution of the different cement and vein/breccia types. What do they indicate about fluid-flow patterns? **The breccia types in MDF are not diverse. More details on breccia is out of focus of this study.**
 - The orientation of CV1–CV4-bearing fractures needs to be taken into account in the structural interpretation. **A detailed structural interpretation is discussed in Storti et al. 2018. Its now more emphasized in this manuscript.**
 - Section 5.3: Without a better documentation of the orientations and field relations of the different cements and fracture types it is difficult to assess the validity of the inferred paragenetic sequence and the association of the different cements and structures with tectonic events. Some of the spatial and cross-cutting relationships between different types of cements are first mentioned in this section. Such descriptions should be moved to the results section.
 - What is the driver for fluid circulation? Why are they Mg-rich fluids? What do fluid-inclusion salinities indicate? **Addressed in section 5.2**
 - Why do you go from dolomite replacement and cementation to calcite cementation? **Addressed**
 - How are your findings relevant for porosity/permeability evolution and fluid flow in dolomitized, carbonate-hosted hydrocarbon reservoirs and aquifers associated with similar reservoir-scale structures? **Addressed**
 - How are your conclusions applicable to dolomitization processes associated with faults in general? How far can dolomitizing fluids travel and to what extent do they alter the mechanics and porosity/permeability of the host rock? What are the consequences for fluid-flow in these rocks? **Addressed**
- 10)

Conclusions

- More thought needs to go into the conclusions section.
- I don't think enough data are presented in this study, especially of cross-cutting relationships and orientations of the different “deformation structures” to support the structural interpretation presented in the conclusions. For example, where is the evidence that the opening-mode fractures (no orientations or relationships within the anticline are reported!) and normal faults mentioned in this study are associated with contractional tectonics of the Apenninic orogeny? **All are discussed in details in Storti et al. 2018.**

- 11) Figures and figure captions need work, especially the model shown in Figure 15 (see comments in figure caption).

Lines 29-31: This needs to be re-written. Layer-parallel shortening would not give place to layer-parallel stylolites. Extensional faulting by itself either. Involvement in the Apenninic thrust wedge of what? **Addressed**

Lines 48-54: May I suggest you take a look at the recently published Ferraro et al. (2019) paper for a description of the diagenetic evolution of carbonate fault rocks in the central and southern Apennines? **Addressed**

Lines 54-58: You may want to consider adding a short statement about why some fault zones become dolomitized but others don't. What are the requirements? **Addressed**

Lines 58-61: What can you learn from outcrops that you cannot from core alone? I would say that the main benefit would be the opportunity to assess the spatial distribution of dolomitized zones, and individual diagenetic events, in 3D. Perhaps a missed opportunity in this work?

Line 67: I don't see Bugarone in Figure 1. **Addressed**

Line 69: I don't see catel Manfrino Dolostones in Figures 1 or 2. **All the dolomitized intervals are called Castel Manfrino Dolostones**

Lines 72-73: How is your study better than Ronchi (2003)? **Addressed**

Lines 76-78: In Figure 2 it appears that dolomitized bodies are found quite far away from faults, beyond the typical lateral extent of fault damage zones. What is the explanation? Why are some faults associates with dolomitization while others aren't? Does it have to do with age of faults? Other factors? This would be a good topic for the discussion.

Line: 84: I would have liked to see more "field mapping" of the extent of D1–D5 and CV1–CV4 in this work.

Line 87: This sentence should start with a different word than "therefore". What provides insights? How? **Addressed**

Lines 88-89. Yes. This needs to be discussed in the discussion. **Addressed**

Lines 90-92: Yes. This needs to be discussed in the discussion. **Addressed**

Line 96: evolution of the Apennines has been proposed to be the result of **Addressed**

Line 98: since the Late Cretaceous **Addressed**

Line 103: The Central Apennines involve **OK**

Line 110: lower part of the Burano Formation **Addressed**

Line 115: Deposition of the Hettangian–Sinemurian Calcare Massiccio Formation, with a total thickness ... **Addressed**

Line 117: following facies are present **Addressed**

Line 125: deepening-upward trend **Addressed**

Line 137: olistolith model **This sentence is deleted**

Lines 138-145: So, does this evidence favor the fault-related model or does this evidence provide an alternative model? Why does this sentence start with ‘However’? **This sentence is deleted**

Line 151: at a high angle **Addressed**

Line 162-163: 60 samples distributed across how big of an area? **Addressed**

Line 164: What structures? **Addressed**

Line 187: Vienna Pee Dee Belemnite **Addressed**

Line 215: In order to perform high resolution **Addressed**

Lines 220-221: bed-perpendicular stylolites **Addressed**

Lines 224-230: This belongs in the Geological Setting. **Addressed**

Line 225: There is no evidence of dolomitization **Addressed**

Lines 231-234: Location names need to be included in figure captions. **Addressed**

Lines 235-239: This seems out of place. Start by describing mesoscale relations and distributions of dolomitized geobodies. Then focus on hand-sample and petrographic details. **Addressed**

Line 235: in fault cores are typically **Addressed**

Line 237: is “main slip surface” a better term? **Addressed**

Line 238: cut by rather than overprinted. Are dolomite-filled veins intra- or intergranular?

Line 239: calcite cement **Addressed**

Line 241: cross-cutting bedding surfaces **Addressed**

Line 242: from a few meters to hundreds of meters **Addressed**

Line 243: and the lower part of **Addressed**

Line 246: High amplitude (>1 mm), bed-parallel stylolites **Addressed**

Line 247-248: How does porosity differ between limestones and dolostones?

Line 253: grain-supported intervals **Addressed**

Lines 259-260: Evidence? **Addressed**

Line 265: we can’t see the displacement mentioned in Figure 2A, site 1

Line 267-268: Are they overprinting or overgrowing? Show evidence. We also cannot see the distribution of the different cements at outcrop scale.

271-272: On what basis did you establish that the replacive dolomite within the host rock (D1) and lining fractures is the same?

Lines 275-276: solid inclusions of what? Insert figure call out for concentric zonation. **Addressed**

Line 281: sweeping extinction **Addressed**

Line 282: In some crystals, one... what types of solid and fluid inclusions? **Addressed**

Lines 286-291: Mark locations on map/figure captions and call out the figure. **Addressed**

Line 290-291: Scaglia Formation in the hanging wall. **Addressed**

Lines 293-295: This needs to be moved up **Addressed**

Line 305: bed-parallel shear fractures **Addressed**

Lines 308 on: There is a problem with CV introduction. What does it stand for? Must introduce them in chronological order. If the calcite cement is in veins it is most likely in the host rock as well (see Laubach, 2003). I don't think calling it vein cement is appropriate. **Addressed**

Line 308: What porosity? **Addressed**

Lines 318-320: Show outcrop photo?

Line 319: bed-perpendicular rather than bedding because that's what you use elsewhere. Make sure term usage is consistent throughout. **Addressed**

Line 321: bed-parallel stylolites. CV1 usually shows (often means time. Correct elsewhere in the manuscript). **Addressed**

Lines 324-326: Show image of CV2 in tension gashes **Addressed**

Line 332: extensional fault's master (main?) plane **Addressed**

Line 339-340: More evidence that the use of CV to refer to calcite cements that occur in a variety of textures and petrographic relations is not appropriate.

Lines 361-364: Why is this mentioned here and not with the rest of the calcite cements? **Its ordered based on relative timing**

Line 396: I see 3 values plotted for Scaglia. **Addressed**

Lines 398-399: Interpretation. Move to discussion. Same comment for previous paragraphs. **Addressed**

Lines 401-411: This belongs in the Methods section. **Addressed**

Lines 409 and 439: all-liquid inclusions **Addressed**

Lines 439-445: This belongs in the Methods section. **Addressed**

Lines 469-470: This belongs in the methods/results. Why did you avoid them? Could mottled D be a different type than those reported? **Addressed**

Lines 471-474: Move to methods. Report parental fluid calculations in the results section.

Line 478: Progressively higher than what? **Fixed**

Line 481: siliciclastic rocks,... Correct here and elsewhere. **Addressed**

Line 493: , or values recorded... Add references. **Addressed**

Lines 499 and 505: Replace comparable with similar. Here and elsewhere. **Addressed**

Line 507: stylolitization of the host rock (otherwise we do not know what dissolution etc. you are referring to). **Addressed**

Lines 527-528: fluids related to Late Messinian... overlying Upper Miocene Laga Formation and their possible... **Addressed**

Line 543: burial-related temperature **Addressed**

Line 544: it is unlikely that the.. **Addressed**

Line 546: located at higher stratigraphic levels **Addressed**

Line 564: calcite cements (FC) in grain-supported stratigraphic levels of the CMF is interpreted to be... **Addressed**

Line 570: bed-parallel stylolites **Addressed**

Line 574 and 575: are cut by **Addressed**

Line 579: Figure 15A call out. **Addressed**

Line 585: We cannot see the distribution described in Figure 2A.

Line 587: attributed to post-rift **Addressed**

Line 588: Although an absolute age cannot be provided, **Addressed**

Line 603: bed-parallel fractures. This is the first mention of shear veins for D4. Are the cements sheared? Show evidence. **Cements are not sheared. Addressed**

Line 604: Contractional deformations? How? Describe relationships better. Bed-perpendicular dilation alone would not cause shear.

Lines 608-610: First mention of this. Move to results.

Lines 618-619: bed-parallel veins **Addressed**

Line 622: fragments suggests that... late-stage evolution **Addressed**

Line 624: bed-perpendicular stylolites **Addressed**

Line 624-629. This is way too long. In any case, there is new information here that needs to be moved to the results section. **Addressed**

Line 629: low homogenization temperatures of fluid inclusions trapped within these cements **Addressed**

Lines 638-642: So, how is your study better? How are your conclusions applicable to dolomitization processes associated with faults in general?

Figures: Documentation of where samples came from is poor. Locations of samples need to be shown on outcrop photos and/or detailed maps. Add in appendix if space is limited.

Figure 1: Tiny name in a) is unreadable. Mark location of cross-section (A-A') shown in d).

Figure 2: Add names of each field site to the figure caption. **Addressed**

Figure 3: The picture in a) is too close up to see the context. Mark distribution of D1 etc. as in Fig 5d. Why isn't there more on these breccias (c) in the manuscript? Explain what arrows point to. Pressure solution seams. You are not showing intensity (it would be a number). Perhaps say showing abundant pressure solution seams. What are the abutting relationships? Which abuts which? Move arrow in b) so that the vein is actually visible. Are the other white pods also considered "veins"?

Figure 4: Show spatial distribution of D1, D3, CV1... etc. at the outcrop scale. The sentence seems to say that CV1 veins are dolomitized. Is that what you really mean? What is the dolomite type in b) and c)? Good opportunity to show cross-cutting relationships summarized in Figure 14.

Figure 5: What field site(s) and formation(s) are these from? In b) the zone shown in c) is marked as only having D1 but as D1 + D2 in c). Which one is correct? Any CV2-CV4 here? **Addressed**

Figure 6: What field site is this? rimmed by fibrous cements (FC), which are overgrown by mosaic cements (MC). overprinted. bed-parallel stylolites. D1 cements lining a fracture. What do

arrows point to in f) If it is D1, then what is to the right of it? Line 1123: which is cemented by CV1 in the center. **Addressed**

Figure 7: What field site(s) and formation(s) are these from? What is beyond D3 in e) and f)? Is D3 only present in breccias in this site? What is the CL signal of D3 in breccias and how did you establish correspondence with D3 in host rocks? What is the context of the sample? in e) and f) **Addressed**

Figure 8: What field site(s) and formation(s)? D3 and D4 are not cross-cutting but it appears that D4 overgrows D3. What is the D4 arrow in b) exactly pointing to? What cement is in the rhomb on the upper right corner? d) I am having a hard time seeing the microfracture. What CV is this? Or do you have dolomite-filled veins as well? Where are these described? What other cements are in e) and f) and what do arrows point to? Lines 1141-1150 belongs in the discussion. **Addressed**

Figure 9: What field site(s) and formation(s)? If D4 also occurs in fractures why is it not called vein cement as in your CV scheme? What other cements and/or host rock are in these photographs? Add labels. **Addressed**

Figure 10: These photographs are too close up to see the context. Outlining obscures fractures in a). c-d) These do not look like tension gashes to me (as mentioned in text?). Misabeled as CV2 on the picture (?) but CV3 in the figure caption. **Addressed**

Figure 11: What field site(s) and formation(s)? What is a) a sample of? And the rest? Show field context. **Addressed**

Figure 12: Why aren't these figures in color? The symbols are too similar and they are hard to distinguish from one another. I would assign a color to each formation and a symbol to each diagenetic feature. **Addressed**

Figure 13: These plots are not very useful because key information is lost. Plot homogenization and ice melting T ranges so that variability within individual FIAs is captured. Color would help, Also, where are the data for CV cements?

Figure 15: The fracture in a) would not have that orientation if σ_1 were vertical. Indicate which fault you are referring to in b). The vein in b) would not develop in that orientation if σ_1 were horizontal. Also, keep in mind that the timing of cementation of the veins by postkinematic cements (see Ukar and Laubach, 2016) postdates timing of opening of the fracture. Don't mix the two! I had no idea that CV4 is restricted to the MdFF until now, because it is not mentioned anywhere in the text. How do you reconcile D3 to be surrounding breccia clasts within the MdFF in this model and sequence? **Addressed**

Estibalitz Ukar
Research Associate
Jackson School of Geosciences
The University of Texas at Austin

Dear Dr. Hendry and Dr. Ukar,

Thank you for the very constructive comments. They not only helped us to improve the quality of the manuscript but also our knowledge of dolomitization process. We have tried our best to address your suggestions in this new version of the manuscript.

Regarding the advancement of our research in comparison with the work previously presented by Ronchi et al. (2003), the current study gives much more details about the dolomite characterization and their relation to the structural evolution of the anticline on the regional and local scale. Furthermore, the obtained geochemical and microthermometry analyses do not confirm the role of marly or shaly basinal successions in providing the Mg-rich fluids during the first event of dolomitization (i.e. syn-rift), as proposed by Ronchi et al. (2003). We have tried to be modest in criticizing the latter authors limited research since the current research was build up on their findings. Another important question about the studied dolomites was the role of Scaglia Formation in providing the Mg-rich fluids during compression, because this formation is juxtaposed with the dolostones by the Montagna dei Fiori Fault. Our results do not support this hypothesis.

During our research, we also performed some other advance analyses such as clumped isotopes and U/Pb dating. However, the consecutive overgrowth pattern of dolomites and difficulties in isolating them to get enough and good quality samples increased the uncertainty in the results. Therefore, we decided not to include those data in the manuscript.

In the Montagna dei Fiori Anticline, the structures and their relative chronology are very complicated. A comprehensive structural study on the evolution of the Montagna dei Fiori Anticline was performed parallel with the current study, and published by Storti et al. (2018) in *Tectonics*. The target of the current study was to focus on dolomitization, and to use the structural model proposed by Storti et al. (2018) to deduce the most likely timing for dolomitization.

The distribution of dolomitization and sampled locations are way larger than the out crop photo scale. The dolomitized intervals are tens of meters mostly exposed in vertical to subvertical outcrops. To be able to show their 3D distribution properly a photogrammetry or LiDAR imaging is required.

The brecciated zones are mostly clast-support with minor calcite and negligible dolomite cement. Moreover, a detailed classification of breccia is not the focus of this research and does not give relevant information regarding this dolomitization case study.

This new version of the manuscript has been reviewed by a native English speaker.

Best regards,

Mozafari et al.

1 **Fault-controlled dolomitization in the Montagna dei Fiori Anticline (Central Apennines,**
2 **Italy): Record of a dominantly pre-orogenic fluid migration**

3 Mahtab Mozafari¹, Rudy Swennen², Fabrizio Balsamo¹, Hamdy El Desouky^{2,3}, Fabrizio Storti¹
4 and Conxita Taberner⁴

5

6 *1- NEXT - Natural and Experimental Tectonics Research Group - Department of Chemistry,*
7 *Life Sciences and Environmental Sustainability, University of Parma, Italy.*

8 *2- Department of Earth and Environmental Sciences, KU Leuven, Belgium.*

9 *3- Geology Department, Faculty of Science, Menoufia University, Menoufia, Egypt*

10 *4- Shell Global Solutions International B.V., Amsterdam, The Netherlands*

11 Correspondence: Mahtab Mozafari (mahtab_mozafari@yahoo.com) and Fabrizio Storti
12 (Fabrizio.Storti@unipr.it)

13

14 **Abstract**

15 The Lower Jurassic platform and basinal deposits exposed in the Montagna dei Fiori
16 Anticline (Central Apennines, Italy) are pervasively affected by dolomitization. Based on the
17 integration of field work, petrography, and geochemistry, two fault-related dolomitization events
18 were recognized and interpreted as having occurred before and during the Apenninic orogeny,
19 respectively. Fluid inclusion analysis indicates moderate to elevated salinity values of 3.5 to 20.5
20 and 12.8 to 18.6 eq. wt. % NaCl, in the first and the second event, respectively. The estimated
21 salinities, in combination with $\delta^{18}\text{O}$ values and $^{87}\text{Sr}/^{86}\text{Sr}$ ratios, suggest significant involvement
22 of evaporitic fluids in both events, most likely derived from the underlying Upper Triassic
23 Burano Formation. In addition, the $^{87}\text{Sr}/^{86}\text{Sr}$ ratios up to 0.70963 suggest the circulation of deep-
24 sourced fluids that interacted with siliciclastic rocks and/or the crystalline basement
25 during the dolomitization events. ~~The first dolomitization event which is also considered as the~~
26 ~~most pervasive one started prior to the significant burial conditions, as reflected in~~
27 ~~homogenization temperatures of their fluid inclusions being mostly below about 40–50°C.~~

28 Two major dolomite types (D1 and D2) were recognized as pertaining to this the first
29 event, both postdated by high amplitude bed-parallel stylolites. ~~, supporting This relationship~~
30 ~~supports~~ a syn-burial, pre layer-parallel shortening dolomitization, ~~interpreted as controlled by~~
31 ~~the extensional fault pattern affecting the carbonate succession before its involvement in the~~

32 ~~Apenninic thrust wedge~~. A possible geodynamic framework for this dolomitization event is
33 Early to Late Jurassic rift-related extensional tectonism. ~~The second dolomitization event (D3,~~
34 ~~D4 and D5) initiated with a dolomite type (D3) is~~ characterized by a ~~slight~~ temperature upturn
35 ~~(up to 73°C), followed by a second type (D4) with markedly higher homogenization~~
36 ~~temperatures~~ (up to 105°C), ~~and~~ interpreted as associated with the inflow of hydrothermal fluids,
37 possibly related to major changes in the permeability architecture of faults during early- to syn-
38 thrusting and folding activity. ~~Eventually, D4 was overprinted by a late generation of dolomite~~
39 ~~veins (D5) interpreted as associated with late orogenic extensional faulting in the backlimb of the~~
40 ~~Montagna dei Fiori Anticline~~. Based on the timing of deformation in the Montagna dei Fiori
41 Anticline, ~~D3 to D5~~ the second dolomitization event likely occurred in Late Miocene to Pliocene
42 times. The findings regarding characteristics and timing of dolomitization here illustrates the
43 long-term controlling role of the ~~evaporitic~~ evaporitic detachments in dolomitization process.
44 ~~Our data~~ This study shows that the Mg-rich fluids that were most likely derived from ~~these~~
45 evaporites may prime the tectonically involved successions for repeated dolomitization, and
46 hence formation of potential reservoirs ~~in~~ during sequential tectonic modifications (extensional
47 vs. compressional).

48 **1 Introduction**

49 Fault-controlled dolomitization has been the focus of attention in many studies during the last
50 decades due to its influential role in modifying the petrophysical properties of rocks and, hence,
51 anisotropy in fluid migration pathways, and, ultimately on reservoir quality (e.g. Purser et al.,
52 1994; Montanez, 1994; Zempolich and Hardie, 1997; Vandeginste et al., 2005; Davies and
53 Smith, 2006; Sharp et al. 2010). The mechanical and hydrological behaviour of fault zones are in
54 turn influenced by fluid-rock interactions and diagenetic modifications (e.g. Gale et al., 2004;
55 Laubach et al., 2010; Clemenzi et al., 2015; Ferraro et al., 2019). It follows that the mutual
56 interplay between fault activity and ~~fluid-driven~~ rock-fluid interaction can trigger dolomitization
57 of carbonates when exposing to Mg saturated or oversaturated fluids and, consequently,
58 variations in physico-chemical properties of fluids through time and space.

59 -Leaking or sealing behaviours of fault zones during deformation are key controls for fault-
60 related fluid circulation. A detailed understanding of such an interplay is thus necessary to
61 improve our capability of making reliable predictions of fault-related dolomitization in carbonate
62 reservoirs. Studying outcrop analogues provides fundamental support to meet this requirement

63 ~~(e.g. Swennen et al., 2012; Dewit et al., 2014; Bistacchi et al., 2015).~~ and the opportunity to
64 assess the spatial distribution of dolomitized zones, and individual diagenetic events, in 3D (e.g.
65 Swennen et al., 2012; Dewit et al., 2014; Bistacchi et al., 2015).

66 The Lower Jurassic to Lower Cretaceous Umbria-Marche passive margin carbonate
67 succession, in the Central Apennines (Italy), is intensely affected by localized dolomitization
68 both in the onshore fold-and-thrust belt and in offshore foredeep and foreland areas (e.g. Murgia
69 et al., 2004; Pierantoni et al., 2013). The dolomitized intervals which are the focus of this study
70 are well-exposed in the core of the Montagna dei Fiori Anticline ~~(e.g. Ronchi et al., 2003)~~, where
71 the dolomitized Lower Jurassic intervals (Calcare Massiccio, Bugarone and Corniola
72 Formations) and their relationships with fault zones allow to study the mutual influence between
73 deformation structures and dolomitized intervals (Fig. 1). These intervals, known as the Castel
74 Manfrino Dolostones (Crescenti, 1969; Mattei, 1987; Koopman, 1983), have been previously
75 studied by Ronchi et al. (2003) only at its reference section, exposed at the Castel Manfrino
76 location (Fig. 1b), in the central sector of the Montagna dei Fiori Anticline (Fig. 2). A
77 fault-controlled dolomitization model and the relative timing of dolomitization were proposed by
78 ~~Ronchi (2003)~~ the latter authors— based on the homogenization temperatures obtained from
79 microthermometry of the fluid inclusions, and their relation with the thermal history of the area
80 studied. However, no clear relation between dolomitization and structural evolution of the
81 Montagna dei Fiori Anticline on a local scale was provided to confidently link the occurrence of
82 dolomitization to a particular tectonic event. Moreover, the nature and origin of the dolomitizing
83 fluids were not well constrained. Recent re-evaluation of dolostone distribution in the Montagna
84 dei Fiori Anticline (Storti et al., 2017a), showed that the dimension of the dolomitized geobodies
85 (Fig. 2) is much more significant than what was previously mapped by Mattei (1987).
86 Dolostones are distributed within fault damage zones and in the laterally adjacent carbonate
87 rocks, and in intersection areas between fault sets, for a total area in map view of more than 1.5
88 km² (Storti et al., 2017a).

89 The structural pattern of the Montagna dei Fiori Anticline documents the overprinting of
90 extensional and contractional deformation along major fault zones. ~~Although challenging, the~~ The
91 preserved structural framework in this anticline provides an opportunity to study the direct but
92 complex regional tectonic controls on dolomitization in carbonate successions undergoing
93 multiple deformation events, from rifting to folding and thrusting. This contribution integrates

94 ~~field mapping~~, new petrographic, geochemical, and microthermometric analyses, with structural
95 studies ([Storti et al., 2018](#)) to characterize the temporal record of fault-controlled diagenetic
96 phases and, more specifically, dolomitization in the carbonatic succession outcropping in the
97 Montagna dei Fiori Anticline. ~~Therefore provides insights into the structural controls on regional~~
98 ~~fluid flow and their chemical evolution through time.~~ These findings might be of relevance for
99 exploration and reservoir quality prediction ~~in the region of onshore and offshore~~ the Apennines
100 and Southern Alps, ~~both onshore and offshore~~. Moreover, this work provides additional evidence
101 of the potential influence of fluids derived from evaporitic detachment levels in modifications of
102 geochemical trends and petrophysical properties of the overlying carbonate rocks.

103 2 Geological setting

104 The Montagna dei Fiori Anticline is a NNW-SSE striking, thrust-related fold located at
105 the mountain front of the Central Apennines (Fig. 1). The geodynamic evolution of the
106 Apennines ~~is generally known~~ [has been proposed](#) to be the result of the superposition of NE-SW
107 compression (in present-day geographic coordinates), related to the convergence between
108 Eurasia and Africa plates since ~~the~~ Late Cretaceous times (Elter et al., 1975; Dewey et al., 1989;
109 Patacca et al., 1992), on a rifting-related tectono-sedimentary architecture produced by Early
110 Jurassic extension (e.g., Centamore et al., 1971). In such a framework, the Central Apennines
111 developed during Miocene to Plio-Pleistocene times (e.g. Parotto and Praturlon, 1975; Barchi et
112 al., 1998; Mazzoli et al., 2002; Bollati et al., 2012).

113 The Central Apennines involves the Umbria-Marche succession, which essentially
114 includes Triassic to Miocene carbonates and marls, covered by Miocene to Pliocene syn-
115 orogenic clastic sediments (Fig. 1). The pre-orogenic succession, from bottom to top, includes
116 Late Triassic evaporites, dolomites and limestones ~~(of the Burano Formation)~~, ~~which the basal~~
117 ~~detachment runs within its evaporitic interval (Ghissetti and Vezzani, 2000).~~ Early to Late
118 Jurassic platform and basinal limestones and dolostones (Calcare Massiccio, Corniola, Rosso
119 Ammonitico, Calcari a Posidonia and Calcari ad Aptici Formations), and Cretaceous to Early
120 Miocene basinal carbonates (Maiolica, Marne a Fucoidi, Scaglia and Biscaro Formations). In
121 general, the lower part of ~~the~~ Burano Formation is overlaid by the fluvio-deltaic ~~siliciclastics~~
122 ~~siliciclastic rocks~~ of the Verrucano Formation (Middle-Late Triassic) (Tongiorgi et al., 1977;
123 Ghissetti and Vezzani, 2000; Tavani et al., 2008). Nevertheless, the existence of these
124 ~~siliciclastics~~ ~~siliciclastic rocks~~ in the Montagna dei Fiori area is not yet ~~proved~~ [proven](#). Syn-

125 orogenic deposits include Miocene marls and turbiditic sandstones (Marne con Cerroigna and
126 Laga Formations) (Artoni, 2013 and references therein).

127 The deposition of the Calcare Massiccio Formation, ~~(dated as Hettangian-Sinemurian) and~~ with
128 a total thickness varying between 300 to 700 m (Pialli, 1971), records an important extension
129 pulse in the evolution of Tethyan rifting. The ~~following facies are observed in the~~ lower part of
130 ~~the Calcare Massiccio Formation~~ this formation which has been interpreted as having been
131 deposited in a peritidal environment:- consists of oenoid-rich peloidal pack- to grainstones in
132 alternation with peloidal wacke- to packstones including horizons of algal bindstones (Calcare
133 Massiccio A; Brandano et al., 2016). The upper part is made up of beds of skeletal and coated
134 grain wacke- to grainstones ~~including microoncooids, echinoderms, calcareous and siliceous~~
135 ~~sponges, bivalves, gastropods and ammonites~~ (Calcare Massiccio B; Brandano et al., 2016). It
136 The lower part has been interpreted as having been deposited in a peritidal environment, while
137 the upper part corresponds to lower to middle shelf depositional environments, characterized by
138 a general ~~deepening-deepening~~ upward trend ~~associated with extensional faulting and drowning~~
139 ~~of the platform, coupled with subsidence and deposition of the overlying Corniola Formation in~~
140 ~~the pelagic areas~~. Overall, the Early Jurassic rifting led to the growth of the Calcare Massiccio
141 Formation in a carbonate platform setting, followed by faulting and drowning, and development
142 of pelagic intrabasins filled by syn-rift sediments (Fig. 1c; Bernoulli et al. 1979; Santantonio and
143 Carminati, 2011). The syn-rift sediments include pelagic limestones of the Bugarone and
144 Corniola Formations. Condensed pelagic limestones of the Bugarone Formation (Lower
145 Pliensbachian-Lower Tithonian; Bugarone Group in Pierantoni et al., 2013) occur at the top of
146 the Calcare Massiccio Formation where it formed fault-controlled highs marking the regional
147 drowning of the carbonate platform (Santantonio and Carminati, 2011). The pelagic limestones
148 of the Corniola Formation (Sinemurian-Toarcian; Colacicchi et al., 1975; Morettini et al., 2002;
149 Bosence et al., 2009; Marino and Santantonio, 2010; Brandano et al., 2016) occur within the
150 fault-controlled (half)grabens in lateral continuation with the Calcare Massiccio Formation. The
151 Corniola Formation in the lower part consists of turbiditic lobes which originated from tectonic
152 brecciation of the Calcare Massiccio Formation. The upper part consists of a well-bedded pelagic
153 mudstone with chert nodules (Di Francesco et al., 2010). In the Montagna dei Fiori, the geologic
154 framework of the outcropping Calcare Massiccio Formation is still a matter of debate between a

155 ~~fault-related tectonosedimentary pattern (Mattei, 1987; Storti et al., 2017b), and a gravity-driven,~~
156 ~~olistolith hypothesis (Di Francesco et al., 2010; Santantonio et al., 2017). However, recent~~

157 2.1 Structural Framework

158 The Montagna dei Fiori Anticline is intersected by two major fault categories (Storti et al.,
159 2018), which based on the chronological order include: detailed work in the Salinello valley
160 (Storti et al., 2017a; 2018) Firstly, ~ E-W and ~ N-S striking fault zones showing extensional
161 kinematics bounding the documented that major outcrops of Calcare Massiccio are bounded by
162 mostly ~ E-W and ~ N-S striking fault zones showing extensional kinematics and dominantly
163 affecting the Jurassic rocks older than the Maiolica Formation (Fig. 2A2a, e.g. sites 1 to 4).
164 Overprinting relations indicate that ~ E-W deformation structures are systematically younger
165 than the ~ N-S ones. Similar trends were observed in syn-rift fault zones in other anticlines of the
166 Central Apennines (e.g. Cooper and Burbi, 1986; Alvarez, 1989; Chilovi et al., 2002). Such a
167 tectonosedimentary inheritance was involved in the growth of the Montagna dei Fiori Anticline,
168 which initiated during the Late Miocene (Mazzoli et al., 2002; Artoni, 2003) and progressively
169 evolved into the upper thrust sheet of a well-developed antiformal stack until Plio-Pleistocene
170 times (e.g. Ghisetti et al., 1993; Calamita et al., 1994; Artoni, 2013). The second set of faults is A
171 a major structural feature trending parallel to the Montagna dei Fiori Anticline and dissecting it
172 is the Montagna dei Fiori Fault, a NNW-SSE striking extensional fault system cutting at a high
173 angle through the folded footwall rocks, typically at the forelimb-crest transition (Figs. 1, 2).
174 This fault consists of two partially overlapping main fault zones with an extensional stratigraphic
175 separation exceeding 900 m, and ~~This fault system~~ juxtaposes intensely deformed Late Miocene
176 sediments in the hanging wall, against dolomitized and undolomitized Lower Jurassic and
177 Cretaceous limestones in the footwall (Figs. 1 and 2). The development of the Montagna dei
178 Fiori Fault has been alternatively interpreted as either a pre- (e.g. Calamita et al., 1994, Mazzoli,
179 2002; Scisciani et al., 2002) or late-folding (Ghisetti and Vezzani, 2000) feature. More recently,
180 the origin of the Montagna dei Fiori Fault has been ascribed to the mutual interaction between
181 horizontal shortening and uplift, and episodic gravitational re-equilibration during antiformal
182 stacking underneath the anticline during Plio-Pleistocene times (Storti et al., 2018). The
183 dolomitized intervals are exposed in the damage zones of the both aforementioned fault
184 categories.

185 **3 Methodology**

186 | The fieldwork covered an area of over 4 km² to delineate the distribution of dolostones.

187 | The stratigraphic and deformational features of dolostones were analyzed in more than 60
188 | outcrops. The distribution of dolomitized intervals as well as their cross-cutting relationships
189 | with bedding planes, stylolites, veins and ~~structures-faults~~ were ~~ground-truthed~~documented and
190 | sampled. For petrographic analyses, 130 polished thin sections were studied with standard
191 | petrographic methods (transmitted and UV-fluorescent light microscopy). Dolomite crystal
192 | morphology and texture is based on the classification proposed by Sibley and Gregg (1987).

193 | The rock slabs and thin sections were stained using Alizarine Red S and potassium
194 | ferricyanide (Dickson, 1966) to discriminate dolomite from calcite and evaluate their iron
195 | content. Cold cathodoluminescence microscopy (CL) was carried out on representative thin
196 | sections (n = 80) at KU Leuven University (Belgium) using a Technosyn cathodoluminescence
197 | device (8-15 kV, 200-400 μ A gun current, 0.05 Torr vacuum and 5 mm beam width).

198 | $\delta^{13}\text{C}$ and $\delta^{18}\text{O}$ analysis were carried out on 117 samples. To ensure the sampling quality
199 | and avoid physical mixing of different diagenetic phases, the thin section images were mapped
200 | and the sampling targets were determined. Nevertheless, some diagenetic phases could not be
201 | isolated due to their sequential overgrowth and small size. Powder samples (150 - 200 μ g) were
202 | obtained by applying a New Wave Research micromilling device and a dental drill at KU
203 | Leuven University (Belgium). The analysis was conducted at Parma University (Italy) and the
204 | Friedrich-Alexander-Universität (Erlangen-Nürnberg, Germany) laboratories using Finnigan
205 | DeltaPlus V and ThermoFinnigan 252 mass spectrometers, respectively. The carbonate powders
206 | were reacted with 100% phosphoric acid at constant temperature of 75°C. Several additional CO₂
207 | reference gases (NBS18, NBS19, MAB99, and a pure Carrara marble) with known isotopic ratio
208 | were analyzed during the measurements to determine the $\delta^{13}\text{C}$ and $\delta^{18}\text{O}$ values of the sample.
209 | Reproducibility was checked by replicate analysis of laboratory standards and was better than
210 | $\pm 0.1\text{‰}$ for $\delta^{13}\text{C}$ and $\pm 0.2\text{‰}$ for $\delta^{18}\text{O}$ at Parma University and ± 0.04 for $\delta^{13}\text{C}$ and $\pm 0.05\text{‰}$ for
211 | $\delta^{18}\text{O}$ at Friedrich-Alexander-Universität. Oxygen isotope composition of dolomites was
212 | corrected using the acid fractionation factors given by Rosenbaum and Sheppard (1986).
213 | Duplicate homogeneous samples measured in both labs for inter-laboratory reproducibility ~~show~~
214 | ~~$\delta^{13}\text{C}$ and $\delta^{18}\text{O}$ values within the acceptable range of error deviation ($\pm 0.1\text{‰}$) both for $\delta^{13}\text{C}$ and~~
215 | ~~$\delta^{18}\text{O}$.~~ All carbon and oxygen values are reported in per mil, relative to the “Vienna Pee Dee
216 | Belemnite Vienna-PDB scale” (V-PDB).

217 A total number of 21 samples were analyzed for their $^{87}\text{Sr}/^{86}\text{Sr}$ ratios. The analyses were
218 conducted at the Department of Analytical Chemistry, Ghent University (Belgium) and at the
219 Vrije Universiteit Amsterdam (the Netherlands). NIST SRM 987 was used as the international Sr
220 standard in both labs. At Ghent University, 15 sample powders (20 mg) were collected using a
221 dental drill device. The $^{87}\text{Sr}/^{86}\text{Sr}$ ratio measurements were performed using a Thermo Scientific
222 Neptune Multi-collector Inductively Coupled Plasma Mass Spectrometer (MC-ICP-MS)
223 instrument. Within the external precision, repeated analyses of the international Sr standard
224 yielded an average $^{87}\text{Sr}/^{86}\text{Sr}$ ratio of 0.710271 ± 0.000023 (2SD, $n = 43$), in agreement with the
225 accepted $^{87}\text{Sr}/^{86}\text{Sr}$ ratio of 0.710248 for this reference sample (Thirlwall, 1991). At Vrije
226 Universiteit Amsterdam, 6 sample powders (2 - 3 mg) were collected using a New Wave
227 Research micromilling device. Analyses were performed using a ThermoElectron Triton plus
228 TIMS instrument. In order to monitor and document the system's performance, repeated analyses
229 of the international Sr standard ($n = 58$) were carried out on load sizes of 10 ng and 100 ng which
230 yielded average $^{87}\text{Sr}/^{86}\text{Sr}$ ratios of 0.710245 ± 0.000022 (2SD) and 0.710242 ± 0.000008 (2SD),
231 respectively. In both labs mass discrimination correction was performed via internal
232 normalization using Russell's exponential law and the accepted value (0.1194; Steiger and Jager,
233 1977) of the invariant $^{86}\text{Sr}/^{88}\text{Sr}$ ratio.

234 Fluid inclusion microthermometry analysis was performed on 11 doubly polished wafers
235 (80-130 μm in thickness). Measurements were carried out at Parma University (Italy) using
236 Linkam THMSG-600 and Linkam MDS-600 heating-cooling stages coupled with a Leica DM
237 2500 microscope. The final melt ($T_{m_{ice}}$) and homogenization temperatures (T_h) were
238 reproducible within 0.5°C and 5°C, respectively. The stages were calibrated by synthetic Syn
239 FliTM fluid inclusion standards. A 100x objective was used during the microthermometry runs
240 of the small inclusions. The microthermometry data were collected following the Fluid Inclusion
241 Assemblage (FIA) approach described in Goldstein and Reynolds (1994) for carbonate minerals.
242 The inconsistent homogenization temperatures and salinities obtained for these fluid inclusions,
243 within the framework of an individual fluid inclusion assemblage (FIA) described by Goldstein
244 and Reynolds (1994), indicate possible re-equilibration (stretched) of these inclusions and thus
245 are not used in the interpretations. It is common for small inclusions ($< 3 \mu\text{m}$) to remain mono-
246 phase all-liquid at room temperature due to their metastability (Goldstein and Reynolds, 1994).
247 Thus, to eliminate the possible role of metastability, the samples were placed in a freezer for

248 several days following the procedures described in detail by Goldstein and Reynolds (1994). All-
249 liquid inclusions remained unchanged and no vapor bubble was developed within them, which
250 discards the metastability effect. In order to properly observe the phase transitions and determine
251 the final melting temperature of ice in the all-liquid inclusions, they were rapidly heated up to
252 ~200°C to stretch and nucleate a bubble at room temperature (Goldstein, 1990). The salinities
253 are reported in equivalent weight percent NaCl (eq. wt. % NaCl) and were calculated based on
254 the equation of Bodnar (1993). The homogenization temperatures obtained in all fluid inclusion
255 assemblages indicate the minimum temperatures at which the fluids could have been trapped
256 (Goldstein and Reynolds, 1994). No correction was made for pressure effects on entrapment
257 temperatures since no data regarding the exact depth and pressure of entrapment are available. In
258 absence of independent thermal indicators such as Conodont Alteration Index (CIA) and
259 Vitrinite Reflectance (VR), the accuracy of pressure correction cannot be well constrained
260 (Slobodník et al, 2006), and thus no correction was made for pressure effects on homogenization
261 temperatures.

262 In order to perform a high resolution petrography, Scanning Electron Microscope (SEM)
263 and Back-scattered Scanning Electron Microscope (BSEM) analyses were conducted using a
264 Jeol 6400 Scanning Electron Microscope (SEM) equipped with an Oxford EDS (Energy
265 Dispersive System). Operating conditions were 15 kV and 1.2 nA, electron beam about 1 µm in
266 diameter and 100 s counting time; errors are ±2-5% for major elements and ±5-10% for minor
267 components. The analysis focused mainly on detecting possible dolomite crystals inside the bed-
268 perpendicular stylolites affecting the Cretaceous Scaglia Formation.

269 **4 Results**

270 **4.1 Field observation and distribution of the dolomitized bodies**

271 ~~Dolomitization affected the Calcare Massiccio, Bugarone and Corniola Formations.~~

272 There is no evidences of dolomitization in the overlying and immediate surrounding successions
273 of the Calcare Massiccio, Bugarone and Corniola Formations (e.g. Maiolica and Scaglia
274 Formations), though the base of Maiolica Formation is reported as dolomitized in the Central
275 Apennines onshore (e.g. Pierantoni et al., 2013) and offshore areas (Murgia et al., 2004).

276 Dolomitized intervals are folded in the forelimb of the Montagna dei Fiori Anticline and
277 are abruptly truncated by the Montagna dei Fiori Fault, which juxtaposes them against intensely
278 foliated Scaglia, Bisciaro and Marne con Cerrognia Formations (Figs. 2 and 3). The distribution

279 of dolomitized intervals is wider in the Salinello ~~valley creek~~ (Figs. ~~4B1b, 2A2a~~) perhaps due to
280 a better exposure. In the Corano Quarry location, dolomitization occur in the Calcare Massiccio
281 and Bugarone Formations only as meter-sized dolostone geobodies in the footwall of the
282 Montagna dei Fiori Fault (Fig. 4). The map pattern (Fig. 2) of dolostones indicates that their
283 distribution is maximized in the Castel Manfrino-Osso Caprino hill area and fades out both
284 southward and eastward.

285 ~~Dolostone breccias in fault cores is typically clast supported, with angular and~~
286 ~~millimeter to centimeter sized fragments (Fig. 3C), changing to crackle breccia (Woodcock and~~
287 ~~Mort, 2008) away from the master slip surface. In the proximity of the master slip surface,~~
288 ~~dolostone fragments are sporadically overprinted by millimeter-sized dolomite veins. The~~
289 ~~breccia fragments, where cemented, are commonly surrounded by calcite.~~

290 ~~Dolomitization does not follow a systematic pattern. The lateral extent of dolomitization~~
291 is gradual. In some outcrops, dolomitization fronts show irregular outlines following, but also
292 cross-cutting, ~~the~~ bedding surfaces (Fig. 5). ~~–~~ Dolomitized intervals vary in thickness from a few
293 meters to hundred meters affecting the totality of the exposed Calcare Massiccio and ~~only~~ the
294 lower part of Corniola Formation, where no clay interlayers are present. In the Calcare Massiccio
295 Formation, dolomitization does not follow a systematic pattern. In the northern side of the Osso
296 Caprino hill (Fig. 2), the top of formation is dolomitized but moving toward the Salinello creek,
297 a thick non dolomitized limestone is exposed. The same situation occurs on the opposite side of
298 the creek and to the east of Castel Manfrino.

299 Dolomitized intervals in the Corniola Formation have a darker color relative to the host
300 rock and are systematically more fractured than the hosting limestone. High amplitude (> 1 mm),
301 bed-parallel stylolites are clearly visible in both limestones and dolostones (Fig. 5). However, in
302 some dolostones only ghosts of stylolite traces can be seen. No apparent porosity could be
303 observed in host rock limestones but ~~The~~ dolostones locally contain porosity, appearing as
304 millimetre- to centimetre-sized pores. Dolostone breccias in fault cores are typically clast-
305 supported, with angular and millimeter- to centimeter-sized fragments (Fig. 3C), changing to
306 crackle breccia (Woodcock and Mort, 2008) away from the main slip surface. In the proximity of
307 the main slip surface, dolostone fragments are sporadically cross-cut by millimeter-sized
308 dolomite veins. The breccia fragments, where cemented, are commonly surrounded by calcite
309 cement.

310 4.2 Petrography

311 4.2.1 Early calcite cementation

312 The early diagenetic products in the studied intervals are generally non-ferroan calcite
313 cements. The first calcite cements precipitated following a phase of bioclast micritization (*sensu*
314 Bathurst, 1975) in grain-grain-supported intervals. In chronological order, they include: 1)
315 fibrous cements (FC) riming the bioclasts, mostly in the peloidal facies of the Calcare Massiccio
316 Formation (Fig. 6A6a). These cements are dull-dark brown to non-luminescent under
317 cathodoluminescence; 2) mosaic cements (MC), commonly fill the intergranular pore spaces
318 (Fig. 6B6b), and also occur as syntaxial overgrowths on echinoderm fragments. ~~These~~
319 ~~cements~~They exhibit deformation twinning and show a well-developed dull-brown and orange
320 concentrically-zoned cathodoluminescence pattern (Figs. 6C-6c and Dd). They contain only
321 mono-phase all-liquid inclusions. All of these cements are postdated by dolomites and high
322 amplitude bed-parallel stylolites (Fig. 6b).

323 4.2.2 Dolomitization

324 All the dolomite types are non-ferroan and dominantly fabric destructive. Dolomitization
325 developed in all the facies types of the Calcare Massiccio and the overlying Bugarone
326 Formations, but only at the lower part of the Corniola Formation which consists of reseedimented
327 Calcare Massiccio breccias (turbiditic lobes).

328 The two first dolomite types (D1 and D2) are the dominant dolomite types in the studied
329 outcrops. These dolomites are distributed within the damage zones of the ~ N-S and E-W
330 Jurassic rift-related extensional faults and, in places, displaced by them (Fig. 2A2a, site 1). The
331 third and fourth dolomite types (D3 and D4) are mainly observed within the damage zone of the
332 Montagna dei Fiori Fault (NNW-SSE), and appear only as dolomitic pockets locally replacing
333 the host rock and overprinting-overgrowing D1 and D2 at the proximity of the ~ N-S and E-W
334 extensional faults. The fifth dolomite type (D5) is found only within the brecciated zones
335 associated with the Montagna dei Fiori Fault damage zone. The distinctive petrographic features
336 of the recognized dolomite types are summarized below:

337 **Dolomite 1 (D1)** is a replacive dolomite which commonly appears as dispersed rhombs and
338 aggregates, and locally rims fracture walls cemented by calcite (CV1) (Figs. 6E-6e and Ff). D1
339 postdates the micritic envelopes and early calcite cements, and predates high amplitude bed-
340 parallel stylolites (Figs. 6G-6g and Hh). The crystals are fine to medium sized (< 350 μm) ~~and~~

341 ~~with planar-e and planar-s textures, consists~~ consisting of relatively turbid, rich in host rock
342 solid-inclusions ~~rich~~, well-developed ~~eu~~hedral to subhedral crystals, ~~-. They show with~~ red
343 luminescence when viewed under cathodoluminescence, ~~occasionally developing a concentric~~
344 zonation.

345 **Dolomite 2 (D2)** is a replacive dolomite (Figs. ~~7A-7a~~ and ~~Bb~~), infrequently occluding existing
346 pore spaces. Like D1, it also ~~frequently~~ predates high amplitude bed-parallel stylolites (Figs. ~~6G~~
347 ~~6g~~ and ~~Hh~~). D2 generally exhibits a tightly-closely packed texture with no or little
348 intercrystalline porosity. The crystals are medium to coarse sized ($\leq 500 \mu\text{m}$) with planar-s to
349 non-planar textures. ~~They include~~ing a turbid core followed by a transparent ~~subhedral to~~
350 ~~anhedral~~ rim and trace quantities of saddle dolomite developing swiping-sweeping extinction. In
351 some crystals, one additional turbid zone rich in host rock solid inclusions and fluid inclusions of
352 mostly mono-phase is present. Cathodoluminescence observations enabled to recognize the
353 presence of D1 in their turbid cores. D2 crystals are characterized by zones of bright red-pink
354 luminescence separated by purple luminescence zones (Fig. 7b).

355 **Dolomite 3 (D3)** is present as small localized bodies in the Calcare Massiccio (at the Castel
356 Manfrino reference section), in the Corniola Formation (at the Osso Caprino Road), and in the
357 Calcare Massiccio and Bugarone Formations (at the Corano Quarry) (Figs. 1b and 2a). In the
358 Corano Quarry the dolomitized Bugarone and Calcare Massiccio Formations are in the footwall
359 of the Montagna dei Fiori Fault; and juxtaposed to the ~~undolomitezed~~undolomitized, intensely
360 foliated Scaglia Formation in (the hanging wall). The SEM and BSEM analysis performed on the
361 samples from the immediate adjacent Scaglia Formation within the aforementioned fault damage
362 zone did not indicate the presence of any dolomite in this formation. Within the Bugarone
363 Formation in this fault damage zone, D3 locally cements the millimeter-sized angular breccias
364 that are in turn affected by ~~fault-fault~~-parallel stylolites (Figs. ~~7C-7c~~ and ~~Dd~~). ~~The SEM and~~
365 ~~BSEM analysis performed on the samples from the immediate adjacent Scaglia Formation within~~
366 ~~the aforementioned fault damage zone did not indicate the presence of any dolomite in this~~
367 ~~formation.~~ D3 crystals are fine to medium sized ($< 300 \mu\text{m}$) mostly transparent ~~eu~~hedral to
368 ~~anhedral~~exhibiting planar-e to non-planar textures ($< 300 \mu\text{m}$), with minor development of
369 saddle morphologies ~~in~~of larger crystals ($> 500 \mu\text{m}$) with planar-c texture (Figs. ~~7E-7e~~ to ~~Hh~~).
370 The ~~eu~~hedral to anhedral replacive crystals ~~are generally replacive~~, displaying a faint core, which
371 compared to previous dolomite types has fewer solid inclusions. The saddle crystals are

372 | occasionally replacive ~~but majorly appear as cement in fractures~~. They display typical curved
373 | and slightly serrated crystal terminations with ~~swiping~~sweeping extinction. These saddle
374 | dolomites were only observed in the Castel Manfrino reference section. D3 generally exhibit a
375 | ~~dull-dark~~ purple color with bright orange zones and subzones in core and/or rims when viewed
376 | under cathodoluminescence (Figs. ~~7E-7e~~ to ~~Hh~~).

377 | **Dolomite 4 (D4)** appears as a matrix replacive and dolomite cement surrounding porosity, and
378 | locally ~~recrystallizing-replacing~~ D1 and D2 (Figs. ~~8A-8a~~ to ~~Ff~~). D4 also occludes ~~bed-bed-~~
379 | parallel shear fractures and appears along the ~~bed-bed-~~parallel stylolites (Figs. ~~9A-9a~~ to ~~Dd~~). In
380 | the Castel Manfrino reference section, some intercrystalline vuggy porosity is filled with fine
381 | dolomite rhombs including D4 with relics of D2 within their core (Figs. ~~8E-8e~~ and ~~Ff~~). ~~The-This~~
382 | porosity may be preserved or partially to completely filled by calcite (CV4C4). D4 crystals have
383 | a turbid, solid-inclusion rich core and transparent rim. They are fine to medium sized (< 200-350
384 | μm), presenting ~~subhedral-planar-s to-and~~ infrequent ~~euhedral-crystals~~non-planar textures. D4
385 | exhibits a distinct luminescence pattern including a purple zone and an irregular green subzone.

386 | **Dolomite 5 (D5)** occurs as crystals cementing micro-veins that cross-cut precursor dolomite
387 | types including dolomitic breccia fragments. In cemented breccias, D5 is postdated by ~~CV3C3~~.
388 | D5 presents a planar-c texture is transparent, anhedral and is characterized by a bright red
389 | luminescence (Figs. ~~9E-9e~~ and ~~Ff~~).

390 | 4.2.3 Late calcite cementation

391 | Four generations of calcite ~~veins~~ postdating dolomitization and distributed only within
392 | the fault damage zones have been identified (Figs. 10 and 11):

393 | 1) ~~Calcite-vein~~ 1 (CV1) occurs only in Calcare Massiccio limestones and dolostones and is
394 | represented as centimeter-sized veins with thickness that does not exceed 1.5 cm. It is not clear
395 | whether the fracture opening and calcite precipitation was simultaneous (as shown in Ukar and
396 | Laubach, 2016). These veins are strata-bound, ~~bedding~~-perpendicular ~~veins~~ with irregular
397 | fracture walls, exhibiting white color in the outcrops. They are present within the syn-rift related
398 | extensional fault damage zones, postdate postdating the first dolomite type (D1) and abutted
399 | riming the same fractures that abut the highly high amplitude ~~bed-bed-~~parallel stylolites. CV1
400 | ~~often-usually~~ shows blocky to elongated crystal morphologies and displays well-developed
401 | deformation twinning planes (Type II of Burkhard, 1993). This calcite exhibits concentric ~~al~~

402 zonation and ~~dull-brown~~ zones alternate with orange luminescence zones (Figs. ~~11A-11a~~ and
403 ~~Bb~~).

404 ~~2)~~ Calcite vein 2 (CV2) exclusively occurs in the intensely deformed Scaglia Formation
405 within the fault damage zones (Figs. 11b, c and d) and correspond to tension gashes associated
406 with stylolites (*sensu* Nelson, 1981). The thickness of these veins does exceed 1 cm. They are
407 usually discontinuous and branch to several microveins (thickness < 1mm) when their tips are
408 not intersected by stylolites. CV2C2 veins are mostly recorded in foliated shear deformation
409 zones with well-defined S-C fabrics, exhibiting blocky, elongated to fibrous shapes with strongly
410 developed tightly spaced deformation twinning planes (Type II of Burkhard, 1993). CV2C2
411 displays ~~yellow-brown~~ to orange luminescence with locally darker sector zones. The ~~yellow~~
412 ~~brown~~ to orange luminescence characteristic of CV2C2 is ~~comparable with~~ similar to those of
413 encasing Scaglia host rocks (Figs. ~~11C-11c~~ and ~~Dd~~).

414 ~~3)~~ Calcite vein 3 (CV3) occurs as cement, filling the ~~extensional faults~~ Montagna dei
415 Fiori master-main fault plane and isolated veins within ~~the extensional faults~~ damage zones.
416 These veins are centimeter-sized with thicknesses of less than 2 cm. The breccias are generally
417 clast-supported, but locally CV3C3 cements the brecciated fault-infillings containing angular
418 fragments of host rock limestones, dolostones and earlier calcites. In the brecciated zones ~~at the~~
419 ~~backlimb of the anticline (Montagna dei Fiori Fault), CV3C3 always passively overgrows D5 in~~
420 ~~fractures and never cuts it. postdates the last dolomitization phase (D5) with no evidence of~~
421 ~~physical disruption.~~ CV3C3 exhibits a translucent white ~~to translucent~~ color in hand specimen.
422 The crystals are blocky with no or weakly developed deformation twinning planes, and are
423 characterized by a dark orange to brown luminescence with distinct darker sector zones (Figs.
424 ~~11E-11e~~ and ~~Ff~~).

425 ~~4)~~ Calcite vein 4 (CV4) exists as centimeter-sized isolated veins, pore-filling as well as
426 breccia cements postdating all the preceding dolomites and calcites in the Montagna dei Fiori
427 main fault plane. The breccia fragments are ~~more often~~ usually dolostones. CV4C4 has a
428 translucent white ~~to translucent white~~ color in hand specimen with blocky crystal morphology
429 and no evidence of subsequent deformation (e.g. deformation twinning planes), and is
430 characterized by distinct concentric ~~al~~ zonation (Figs. ~~11G-11g~~ and ~~Hh~~).

431 4.3 Geochemistry

432 4.3.1 Carbon and oxygen stable isotopes

433 The carbon and oxygen stable isotopic data ($\delta^{13}\text{C}$ and $\delta^{18}\text{O}$) of host rocks, dolomites and
434 calcites are given in Table 1 and shown in Figures [12A-12a](#) and [Bb](#). The marine stable isotopic
435 compositions reported by Veizer et al. (1999) were used as marine reference values.
436 Accordingly, Lower Jurassic marine limestones are characterized by $\delta^{13}\text{C}$ values of -0.5 to
437 +4.5‰ and $\delta^{18}\text{O}$ values of -2.5 to +1.0‰ V-PDB. The $\delta^{18}\text{O}$ values of the marine dolomites are
438 known to be 3-4‰ V-PDB more enriched than those of co-genetic marine limestones (Land,
439 1980; Major et al., 1992; Horita, 2014). In order to avoid data ambiguity due to physical mixing,
440 this analysis was not separately performed on early calcite cements (FC and MC). The $\delta^{13}\text{C}$ and
441 $\delta^{18}\text{O}$ values measured on bulk samples of host rock limestones. Both $\delta^{13}\text{C}$ and $\delta^{18}\text{O}$ values of the
442 host rocks are within the expected range of the Lower Jurassic marine limestones but the
443 Corniola host rocks show slightly lower values comparing to those of Calcare Massiccio. In the
444 Calcare Massiccio host rocks, the $\delta^{13}\text{C}$ values plot between +2.4 and +3.1‰ and $\delta^{18}\text{O}$ values are
445 within the range of -1.6 and 0.0‰ V-PDB. The $\delta^{13}\text{C}$ values in the Corniola host rocks are +2.0
446 and +2.5‰ while the $\delta^{18}\text{O}$ values are -3.1 to -1.4‰ V-PDB. The $\delta^{13}\text{C}$ and $\delta^{18}\text{O}$ values of the
447 Scaglia host rocks range between +1.0 to +3.3‰ for $\delta^{13}\text{C}$ and -2.2 to -1.0‰ V-PDB for $\delta^{18}\text{O}$.
448 The ~~obtained~~-values obtained are characterized in the mean range of Upper Cretaceous to
449 Paleogene marine limestones (Veizer et al., 1999; +1.0 to +4.5‰ for $\delta^{13}\text{C}$ and -4.0 to +2.0‰
450 V-PDB for $\delta^{18}\text{O}$).

451 The $\delta^{13}\text{C}$ values of [CV1C1](#) are between +1.6 and +2.1‰ which plot within the range of
452 reference values (Jurassic) but are slightly lower than the surrounding host rock values. The $\delta^{18}\text{O}$
453 values are between -4.7 and -2.7‰ V-PDB which are lower than those of reference and host rock
454 values.

455 The $\delta^{13}\text{C}$ values of all dolomite types (+0.6 to +3.4‰) fall within the range of host rocks
456 and Jurassic marine limestones (Veizer et al., 1999). The $\delta^{18}\text{O}$ shows a wider range of values,
457 ~~somehow~~ overlapping but also lower than ~~those of~~ host rocks (-4.5 to -0.9‰ V-PDB) and those
458 expected for the ~~presumable~~-Lower Jurassic marine dolomites. The majority of values plot
459 between -3.5 and -1.5‰ V-PDB. The small size and overgrowth nature of certain dolomite types
460 (e.g. D2 and D5) limits their proper isolation for geochemical analyses. Only one sample from
461 D1 dolomite could be measured for $\delta^{13}\text{C}$ and $\delta^{18}\text{O}$ values, showing +2.5 and -1.9‰ V-PDB,
462 respectively. The $\delta^{13}\text{C}$ and $\delta^{18}\text{O}$ values of D3 dolomite range from +2.0 to +2.6‰ and -2.8
463 to -1.9‰ V-PDB, respectively, with values lower than those of the host rock.

464 D4 dolomite has $\delta^{13}\text{C}$ values between +2.4 and +2.5‰, and $\delta^{18}\text{O}$ values of -3.0 to -2.5‰
465 V-PDB. The $\delta^{13}\text{C}$ and $\delta^{18}\text{O}$ values of ~~CV2C2~~ are +1.2 to +3.1‰ and -1.7 to -1.7‰ V-PDB,
466 respectively. The $\delta^{13}\text{C}$ values of ~~CV3C3~~ are between +0.5 and +2.4‰, and the $\delta^{18}\text{O}$ values cover
467 a range of -2.2 to 0.0‰ V-PDB. The $\delta^{13}\text{C}$ and $\delta^{18}\text{O}$ values of ~~CV4C4~~ are +3.8 to +4.9‰ and -9.4
468 to -9.1‰ V-PDB, respectively. The $\delta^{13}\text{C}$ values are slightly higher but the $\delta^{18}\text{O}$ values are
469 considerably lower compared to preceding calcite generations and the measured values from host
470 rocks.

471 4.3.2 $^{87}\text{Sr}/^{86}\text{Sr}$ ratios

472 Samples from host rocks (i.e. Calcare Massiccio and Corniola Formations), dolomites
473 (D1, D3 and D4) and the Scaglia Formation in juxtaposition with the dolostones were analyzed
474 for their $^{87}\text{Sr}/^{86}\text{Sr}$ isotopic ratios. The obtained ratios versus $\delta^{18}\text{O}$ values of the analyzed samples
475 are shown in Fig. 12C. The $^{87}\text{Sr}/^{86}\text{Sr}$ ratios obtained from the Calcare Massiccio and Corniola
476 limestones are 0.70766 and 0.70725 ($n = 2$), respectively, which is in agreement with the values
477 of the Lower Jurassic marine carbonates (0.70704-0.70768) reported by McArthur et al. (2012).
478 CV1 show a value equal to 0.70773.

479 All the dolomite types display higher $^{87}\text{Sr}/^{86}\text{Sr}$ ratios when compared to the host rocks
480 and reference values of the Lower Jurassic marine carbonates. D1 (replacive) and D4 cements
481 show a ~~comparable-similar~~ narrow range with values between 0.70784 and 0.70790, respectively.
482 ~~While, the The~~ two D3 samples (replacive and cement) display higher $^{87}\text{Sr}/^{86}\text{Sr}$ ratios (0.70858
483 and 0.70963, respectively). The $^{87}\text{Sr}/^{86}\text{Sr}$ ratios obtained for dolomites do not show co-variation
484 with corresponding $\delta^{18}\text{O}$ values. The radiogenic Sr analysis was not performed on D2 and D5
485 since the physical mixing with other dolomite types could not be avoided.

486 The $^{87}\text{Sr}/^{86}\text{Sr}$ ratios of the ~~two-three marly limestone~~ samples of Scaglia Formation are
487 0.70784 to 0.70790. The ~~CV2C2~~ veins in Scaglia Formation show ~~comparable-similar~~ ratios of
488 0.70779 and 0.70787. These values fit within the limits of values assigned by McArthur et al.
489 (2012) for the Cenomanian-Bartonian (Scaglia age) marine carbonates (0.70730-0.70790).

490 4.4 Fluid inclusion microthermometry

491 The overview of microthermometry measurements is given in Table 1 and Figs. 13A to
492 C. All the measured fluid inclusions are primary and occur in growth zones. Based on optical and
493 fluorescence microscopy analysis of wafers all the inclusions are aqueous mono-phase (liquid)

494 and two-phase (liquid and vapor) with relatively consistent L:V ratio of 10-15% within a single
495 FIA (fluid inclusion assemblage). Special care was taken to avoid the samples that occasionally
496 displayed scattered mottled luminescence that may indicate recrystallization.

497 ~~On the basis of optical microscopy analysis of wafers,~~ D1 contain dominantly mono-
498 phase aqueous inclusions with sizes greater than 5 μm . ~~It is common for small inclusions~~
499 ~~(<3 μm) to remain mono-phase all liquid at room temperature due to their metastability~~
500 ~~(Goldstein and Reynolds, 1994). Thus, to eliminate the possible role of metastability, the~~
501 ~~samples were placed in a freezer for several days following the procedures described in detail by~~
502 ~~Goldstein and Reynolds (1994). All liquid inclusions remained unchanged and no vapor bubble~~
503 ~~was developed within them, which discards the metastability effect. In order to properly observe~~
504 ~~the phase transitions in the all liquid inclusions, they were rapidly heated up to -200°C to stretch~~
505 ~~and nucleate a bubble at room temperature (Goldstein, 1990).~~ All the inclusions froze at -65
506 to -49°C . The first melting (T_e) was detected between -22 to -19.3°C . The final ice melting (T_m)
507 appeared at temperatures between -7.7 and -2°C . Applying Bodnar's (1993) equation, the
508 obtained final melting temperatures correspond to salinity ranges of 3.5 to 11.3 eq. wt. % NaCl.

509 D2 is characterized by the presence of mono-phase and infrequent two-phase inclusions
510 generally within their growth zones. The homogenization temperature of two-phase inclusions
511 varies between 58 and 71°C . Upon cooling, a complete freezing of the fluid phase is reached
512 at -56 to -40°C . The first ice melting temperature was distinguished at -22°C . The final ice
513 melting temperatures fall within -17.5 and -5°C , corresponding to salinities between 7.9 and
514 20.5 eq. wt. % NaCl.

515 D3 is commonly inclusion poor. The measurable inclusions were detected and examined
516 only in saddle dolomite crystals. These crystals contain only two-phase aqueous inclusions. Their
517 homogenization temperatures are within the narrow range of 70 to 73°C . The complete freezing
518 and first ice melting temperatures could not be distinguished but the final ice melting
519 temperature occurred at temperatures between -13 and -6°C equal to salinity ranges of 9.2 to
520 16.9 eq. wt.% NaCl. The first melting temperatures of fluid inclusions in D1, D2 and D3 were
521 about -21°C , suggesting a H_2O -NaCl fluid system.

522 D4 contains only two-phase aqueous inclusions. The homogenization temperatures in D4
523 vary between 79 and 105°C . Complete freezing of inclusions occurred at temperatures
524 between -86 and -54°C . The first ice melting was detected at -35 to -40°C indicating the

525 possible presence of divalent cations such as Ca^{2+} and/or Mg^{2+} in the fluids (Shepherd et al.,
526 1985; Goldstein and Reynolds, 1994). The final ice melting temperatures fall within a range
527 of -15 and -9°C corresponding to salinities of 12.8 to 18.6 eq. wt. % NaCl. A couple of
528 inclusions show homogenization temperatures exceeding 120°C with salinities higher than
529 20 eq. wt. % NaCl. ~~The inconsistent homogenization temperatures and salinities obtained for
530 these fluid inclusions, within the framework of an individual fluid inclusion assemblage (FIA)
531 described by Goldstein and Reynolds (1994), indicate possible re-equilibration of these
532 inclusions and thus are not used in the interpretations.~~

533 ~~The obtained homogenization temperatures in all fluid inclusion assemblages indicate the
534 minimum temperatures at which the fluids could have been trapped (Goldstein and Reynolds,
535 1994). No correction was made for pressure effects on entrapment temperatures since no data
536 regarding the exact depth and pressure of entrapment are available. In absence of independent
537 thermal indicators such as Conodont Alteration Index (CIA) and Vitrinite Reflectance (VR), the
538 accuracy of pressure correction cannot be well constrained (Slobodník et al, 2006), and thus no
539 correction was made for pressure effects on homogenization temperatures.~~

540 No measurable fluid inclusion could be identified in EV1C1 and EV2C2 due to intense
541 deformation twinning. EV3C3 and EV4C4 contain only primary mono-phase aqueous
542 inclusions, indicating an entrapment temperature of below about 40-50°C (Goldstein and
543 Reynolds, 1994). A complete freezing of the inclusions in EV3C3 occurred at temperatures
544 between -40 and -52.5°C. The first melting temperature was detected at about -21 to -22°C,
545 suggesting a H_2O -NaCl composition. The final melting temperatures range between -6.4
546 and -2.7°C, corresponding to salinities between 9.7 and 4.5 eq. wt. % NaCl. The majority of the
547 values cluster between 7.8 and 5 eq. wt. % NaCl.

548 The complete freezing temperatures of the inclusions in EV4C4 fall within -46
549 and -35.5°C. The first melting temperature could not be determined with confidence but the final
550 melting temperatures were reached at about -0.1 to -1.8°C, corresponding to salinities of 0.17 to
551 3.0 eq. wt. % NaCl.

552 **5 Discussion**

553 **5.1 Stable and radiogenic isotopic composition of the parental fluids**

554 The $\delta^{13}\text{C}$ values of all dolomite types mimic the range of host rock and Jurassic marine
555 limestones and, consequently, they can be interpreted as largely rock-buffered. Their $\delta^{18}\text{O}$ values

556 | are partly ~~comparable-similar~~ to those of their respective host rocks as well as Jurassic marine
557 | reference values but more depleted when compared to the presumable Jurassic marine dolomites.
558 | The relatively depleted $\delta^{18}\text{O}_{\text{dolomite}}$ values could indicate the contribution of heated fluids in
559 | dolomitization process, although it could also relate to recrystallization of a precursor dolomite
560 | by fluids at higher temperature or ^{18}O -depleted (Land, 1980; 1985). The absence of distinctive
561 | textural evidence in the analyzed samples such as enlarged crystal size and/or systematic mottled
562 | cathodoluminescence pattern, and their co-variation with $\delta^{18}\text{O}$ values do not confirm
563 | recrystallization (Mazzullo, 1992 and ref. therein). ~~Nevertheless, special care was taken to avoid~~
564 | ~~the samples that occasionally displayed scattered mottled luminescence.~~

565 | The oxygen isotope fractionation relation between water and dolomite (Land, 1983) was
566 | used to determine the most plausible parental fluids. In order to avoid erroneous results due to
567 | rock-buffered $\delta^{18}\text{O}$ values, only the $\delta^{18}\text{O}$ values of dolomite cements, especially from the ~~bed~~
568 | ~~bed~~-parallel veins containing D4 were used. These values may provide the closest approximation
569 | to the $\delta^{18}\text{O}$ signature of the parental fluids (Barker and Cox, 2011). Accordingly, a $\delta^{18}\text{O}$ value of
570 | $\approx +2.5$ to $+4\%$ V-SMOW was calculated for D3, while this values increase to $\approx +5$ to $+7.5\%$
571 | V-SMOW for D4 (Fig. ~~13D13d~~). ~~The calculated compositions of the potential parental fluids are~~
572 | ~~progressively higher~~—The higher $\delta^{18}\text{O}$ composition of the dolomitizing fluids relative to the
573 | Mesozoic seawater, which is estimated at -1.2 to -1% V-SMOW (Shackleton and Kennett, 1975;
574 | Marshall, 1992; Saelen et al., 1996), is compatible with fluids derived from or that had interacted
575 | with ~~siliciclastic rocks~~, crystalline basement (Taylor, 1997) and/or evaporite-derived
576 | brines.

577 | The $^{87}\text{Sr}/^{86}\text{Sr}$ ratios obtained for all dolomite types are higher than the Lower Jurassic
578 | marine carbonate values (0.70704-0.70768; McArthur et al., 2012). Since marine carbonates
579 | have very low rubidium (Rb) concentrations they produce negligible *in situ* radiogenic ^{87}Sr after
580 | their deposition (Stueber et al. 1972; Burke et al. 1982). Therefore, the higher $^{87}\text{Sr}/^{86}\text{Sr}$ ratios can
581 | be explained by the contribution of fluids originated or interacted with potassium rich
582 | ~~siliciclastic rocks~~ (K-feldspars), crystalline basement and/or stratigraphic levels with
583 | higher $^{87}\text{Sr}/^{86}\text{Sr}$ ratios (Emery and Robinson 1993; Banner, 2004). Taking into account that the
584 | Upper Triassic Burano Formation underlying the studied intervals ~~as the basal detachment~~ has
585 | $^{87}\text{Sr}/^{86}\text{Sr}$ ratios between 0.70774 and 0.70794 (Boschetti et al., 2005), the $^{87}\text{Sr}/^{86}\text{Sr}$ ratios (D1 and
586 | D4) can partially be explained by their contribution. However, this contribution cannot justify

587 much higher $^{87}\text{Sr}/^{86}\text{Sr}$ ratios recorded in D3, being higher than values reported for Phanerozoic
588 seawater (McArthur et al., 2012), and the values ~~recorded~~inobtained for the adjacent basinal
589 deposits (i.e. Corniola and Scaglia Formations). Therefore, parental fluids most likely originated
590 from or had interacted with the ~~siliciclastic~~siliciclastic rocks underlying the Burano Formation
591 (Verrucano Formation), if present, and/or with the crystalline basement with common elevated
592 $^{87}\text{Sr}/^{86}\text{Sr}$ ratios (0.71500-0.72650; Del Moro et al., 1982). The significantly higher $^{87}\text{Sr}/^{86}\text{Sr}$ ratios
593 in D3 in comparison with other studied dolomites indicates a higher influence of $^{87}\text{Sr}/^{86}\text{Sr}$ -rich
594 fluids either due to major changes in the permeability architecture of faults or availability of such
595 fluids. The lack of any ferroan diagenetic phase minimizes the interaction of fluids produced by
596 clay transformation/dewatering (i.e. smectite to illite transformation; Boles and Franks, 1979).

597 CV1C1 is characterized by $\delta^{13}\text{C}$ and $\delta^{18}\text{O}$ values lower than the host limestones (i.e.
598 Calcare Massiccio), while its $^{87}\text{Sr}/^{86}\text{Sr}$ ratio is ~~comparable~~similar to them. The salinity and
599 composition of the parental fluids cannot be inferred here since no measurable fluid inclusions
600 were found within this cement. The $^{87}\text{Sr}/^{86}\text{Sr}$ ratio being within the range of the corresponding
601 host rocks and the reference values, points to a rock-buffered system for $^{87}\text{Sr}/^{86}\text{Sr}$.

602 The $\delta^{13}\text{C}$ and $\delta^{18}\text{O}$ values obtained for CV2C2, as well as $^{87}\text{Sr}/^{86}\text{Sr}$ ratios, fall within the
603 range of the Scaglia host rocks, thus reflecting their rock-buffered nature. This interpretation is
604 further supported by the ~~comparable~~similar luminescence characteristics of CV2C2 with that of
605 encasing Scaglia host rocks. The fluids from which CV2C2 calcite precipitated, as expected for
606 tension gashes, were most likely derived from carbonate dissolution during pressure-solution and
607 stylolitization of host rock-, pointing to a closed fluid system in contrast with the subsequent vein
608 generations.

609 CV3C3 is characterized by $\delta^{13}\text{C}$ values within the Jurassic marine values but are
610 generally lower than the host rocks, while their $\delta^{18}\text{O}$ values partially overlap both the hosting
611 limestones and dolostones. Microthermometry of fluid inclusions revealed only mono-phase
612 aqueous inclusions and thus precipitation at relatively low temperature ($\leq 40\text{-}50^\circ\text{C}$) with
613 moderate salinity (4.5-9.7 eq. wt. % NaCl). Such levels of salinity can be assigned to evaporated
614 seawater, residual brines or fluids derived from evaporite dissolution, and thus makes it difficult
615 here to interpret their exact origin with the available data.

616 CV4C4 is the latest calcite phase, and records the $\delta^{13}\text{C}$ and $\delta^{18}\text{O}$ values, respectively
617 enriched and significantly depleted when compared to their hosting rocks and preceding

618 diagenetic products. Generally, the enrichment of ^{13}C could suggest CO_2 outgassing due to
619 | evaporation or pressure changes (Friedman, 1970; Hendry et al., 2015) or bacterial fermentation
620 | (methanogenesis) of organic matter (Hudson, 1977) in low temperature diagenetic environments.
621 | The homogenization temperature of CV4C4, being below about 40-50°C, could support any of
622 | these processes. Their low $\delta^{18}\text{O}$ values and fluid inclusions with salinities comparable-similar to,
623 | but also significantly lower than, seawater reflect the contribution of meteoric fluids during
624 | precipitation of this calcite.

625 **5.2 Origin of the dolomitizing fluids**

626 | The contribution of brines that derived from highly evaporated seawater or evaporites is
627 | suggested by the elevated salinity values obtained from microthermometry of the fluid inclusions
628 | (3.5 to 20.5 eq. wt. % NaCl). Accordingly, two sources that could potentially provide such fluids
629 | can be proposed: 1) fluids related to the Late Messinian evaporites, associated with the overlying
630 | Upper Miocene Laga Formation, ~~deposited during the Upper Miocene time,~~ and their possible
631 | downward percolation through fault zones by density driven flow and/or seismic pumping
632 | mechanisms (Sibson, 1981; McCaig, 1988, 1990); or their tectonic involvement into the
633 | Apenninic thrust wedge during its propagation (underthrusting; Lobato et al., 1983); and 2)
634 | fluids related to the underlying décollement-detachment horizon of the Burano evaporites (Upper
635 | Triassic) and their upward flow through fault zones during development of the Montagna dei
636 | Fiori Anticline. The first scenario is valid if the dolomitization would have occurred only from
637 | the Upper Miocene time onwards. Moreover, Several-several researchers (e.g. Vai and Ricci
638 | Lucchi, 1977; Bassetti et al., 1998; Roveri et al. 2001) have shown that the occurrence of
639 | primary shallow-water evaporites, which were dominantly gypsum, was limited only to the
640 | western and central parts of the northern Apennines consisting of thrust-top marginal basins. ~~In~~
641 | ~~contrast, evaporites never precipitated in parts of the central Apennines including the Montagna~~
642 | ~~dei Fiori region (Marche area)~~ (Roveri et al. 2001). Hence, the evaporitic horizons existing
643 | within the Laga Formation corresponds to re-sedimentation (gypsum debris) of those previously
644 | precipitated in the marginal basins. This interpretation makes the Messinian evaporites an
645 | unlikely source of Mg-rich brines. ~~Moreover, taking~~ Taking into account that the maximum
646 | burial-burial-related temperature of the Calcare Massiccio Formation did not exceed 80°C in the
647 | Montagna dei Fiori region (Ronchi et al., 2003), ~~it's-it is not-unlikely~~ that the downward
648 | percolation of relatively low-temperature brines derived from the Messinian evaporites, located

649 | at ~~the~~ higher stratigraphic levels, could reach or exceed the high temperatures recorded in fluid
650 | inclusions of the studied dolomites ~~in the Calcare Massiccio Formation~~ (D4; up to 105°C), given
651 | that the homogenization temperatures reflect the minimum entrapment temperatures (Goldstein
652 | and Reynolds, 1994). Deep circulation of these brines, if they existed, can also be excluded by
653 | the fact that their limited ~~tectonic~~ involvement ~~with~~in the thrust wedge ~~being~~ was confined
654 | merely to the off shore wards of the Montagna dei Fiori region (Artoni, 2013).

655 | Accordingly, the Upper Triassic Burano Formation, the basal detachment, appears as the
656 | most plausible source for the high salinity brines recorded in fluid inclusions, and likewise, the
657 | Mg-rich fluids could have been originated from post-evaporite brines associated with them
658 | (Carpenter, 1978; McCaffrey et al., 1987). The fluctuations in salinity may argue for ~~different~~
659 | degrees of diverse range of fault connectivity, different degrees of rock-water interaction and
660 | contribution of pore waters of lower salinity (e.g. marine or meteoric).

661 | **5.3 Timing and structural controls on the evolution of parental fluids**

662 | A generalized paragenesis and the relative chronology of dolomitization in relation to the
663 | structural evolution of the Montagna dei Fiori Anticline are illustrated in Figs. 14 and 15. The
664 | structural episodes are based on the evolutionary stages of the Montagna dei Fiori Anticline
665 | suggested by Storti et al. (2018). The paragenesis is constructed on the basis of direct evidences
666 | recorded during observations at outcrop scale and microscopic observations (e.g. cross-cutting
667 | relationships between diagenetic phases, stylolites, fractures and other structural kinematics), and
668 | indirect evidences (e.g. regional geodynamics and burial history).

669 | The occurrence of micritic envelopes and fibrous calcite cements (FC), in ~~grain-grain-~~
670 | supported stratigraphic levels of the Calcare Massiccio Formation, is interpreted to be of
671 | eogenetic origin (i.e. marine phreatic diagenesis; Moore, 1989), reflecting an early diagenesis
672 | shortly after deposition. The well-developed ~~dull~~ brown and orange concentric
673 | cathodoluminescence pattern of the succeeding mosaic calcite cement (MC) suggests a
674 | progressive shift to more reducing conditions during precipitation in a phreatic diagenetic
675 | environment (as shown in Li et al., 2017). High amplitude ~~bed-bed-~~parallel stylolites postdate
676 | both cements, which confirm their precipitation before significant burial. The observations made
677 | here are in agreement with earlier work by Giacometti and Ronchi (2000), interpreting that the
678 | Calcare Massiccio Formation was cemented during the early diagenetic stages.

679 D1, ~~CV1C1~~ and D2 are ~~postdated-cut~~ by well-developed, high amplitude bed-parallel
680 stylolites. Presence of D1 and ~~CV1C1~~ in bed-perpendicular veins typically ~~abutted-cut~~ by these
681 stylolites (see Figs. ~~6E-6e~~ to ~~Hh~~) support the interpretation that the first dolomitization event (D1
682 and D2) took place before significant burial and stylolite development, ~~being-t~~The latter and
683 bed-perpendicular veins are dynamically compatible within the same stress field which is
684 characterized by a vertical, load-related maximum principal axis of the stress ellipsoid (Fig. 15a).
685 The dominantly mono-phase fluid inclusions within D1 and D2 are in agreement with
686 precipitation temperatures below about 40-50°C, suggesting a relatively shallow to intermediate
687 burial environment and hence supporting a pre-Apenninic orogeny age of precipitation from a
688 mix of formational and extra-formational fluids with elevated $^{87}\text{Sr}/^{86}\text{Sr}$ ratios. The distribution of
689 D1 and D2 localized nearby the rifting-related ~ N-S and E-W striking extensional faults and
690 even their displacement along them (Fig. 2A2a, e.g. site 1), point to the possible contribution of
691 these faults in occurrence of D1 and D2. These faults dominantly affect the Jurassic rocks older
692 than the Maiolica Formation which is attributed to ~~the~~ post-rift deposits, therefore suggesting a
693 pre-Maiolica age for these dolomite types. Although, an absolute age cannot be provided, based
694 on the evidence discussed above, the circulation of Mg-rich fluids during this dolomitization
695 event was most likely controlled by rifting-related Jurassic extensional fault zones cutting
696 through the crystalline basement. Precipitation of D1 and D2 at the lower part of Corniola
697 Formation which is known as the syn-rift deposit discards a pre-rift origin for these dolomites.
698 The displacement of dolomites along the aforementioned faults is possibly related to their
699 prolonged activation during Early to Late Jurassic. In addition to the role of these faults in
700 channelizing the fluids, their mobilization must have been intensified by some deriving
701 mechanisms. A thermal convection system derived from high hit flux during rifting was
702 interpreted by Hollis et al. (2017) to be responsible for circulation of seawater in a syn-rift
703 dolomitization case in the Hammam Faraun fault block (Suez Rift, Egypt). In such scenario, the
704 salinity of the fluids and their $^{87}\text{Sr}/^{86}\text{Sr}$ ratios are expected to be more or less within the range of
705 seawater. Furthermore, this scenario seems unlikely in the studied area given the lack of a deep
706 aquifer to accommodate the fault tips and promotes the lateral fluid flux from basin to the rift
707 shoulders and vice versa. Taking into account that D1 and D2 are the volumetrically more
708 relevant dolomites within the studied intervals, and assuming the likely role of syn-rift
709 extensional faults (Early to Late Jurassic) in their precipitation, a dominantly syn-rift

710 dolomitization process is proposed for the dolostones in the Montagna dei Fiori Anticline.
711 Although the CL zonation pattern observed in D2 may indicate changes in flow condition or
712 fluid composition, the lack of physical disruptions such as multiple fracturing suggests external
713 regional controls rather than slip along the same faults (Eichhubl and Boles, 2000). The absence
714 of pervasive syn-dolomitization fracturing and brecciation as well as zebra fabrics in these
715 dolomites, perhaps indicate a relatively calm tectonic period during dolomite development (e.g.
716 Hollis et al., 2017).

717 D3 and D4 both record elevated $^{87}\text{Sr}/^{86}\text{Sr}$ ratios which accounts for their fault-controlled
718 origin. However, their occurrence at the top of the Calcare Massiccio and overlaying Bugarone
719 Formation (Corano Quarry site) which is < 1 m thick in Montagna dei Fiori region, and is
720 marked as the final rift deposit (Cardello and Doglioni, 2015) discards a syn-rift origin for these
721 dolomites. Moreover, D3 and D4 postdate the development of high amplitude ~~bed-bed~~-parallel
722 stylolites. The formation of stylolites requires an approximate overburden of 600 to 1500 m
723 (Lind, 1993; Machel, 1999; Mountjoy et al., 1999; Schulz et al., 2016), corresponding to a late to
724 post-Maiolica deposition time (Early Cretaceous time onwards). The presence of D3 and D4
725 dolomites in ~~bed-bed~~-parallel fractures and as shear veins (D4) (Figs. 9a and b) suggests their
726 association with contractional deformations, i.e. the most likely tectonic regime for explaining
727 bed-perpendicular dilation. Therefore, the volumetrically minor second stage of dolomite
728 precipitation may possibly be related to the Late- to post-Miocene compressional tectonics
729 recorded in this region (e.g. Mazzoli et al., 2002; Artoni, 2013; Storti et al., 2018).

730 Dolostones containing D3 and D4 appear commonly as clast-supported breccias along
731 fault zones pertaining to the Montagna dei Fiori Fault, then overprinted by fault-parallel
732 stylolites (Figs. 3 and 7). Accordingly, the occurrence of these dolomites was probably
733 synchronous with the incipient stages of fault development, predating fault buttressing (Storti et
734 al., 2018). Homogenization temperatures recorded in D4 (up to 105°C), much higher than the
735 maximum temperatures recorded in the host rocks (below about 80°C; Ronchi et al., 2003),
736 suggest hydrothermal fluid circulation. The development of the Montagna dei Fiori Anticline at
737 the toe of the Late Miocene Central Apennines thrust wedge could have favored the
738 forelandward migration of hydrothermal fluids expelled from the more internal regions of the
739 belt, similarly to what has been proposed for the Rocky Mountains foreland (i.e. squeegee flow
740 model; Machel and Cavell, (1999). Such a migration may have possibly favored the precipitation

741 of D4 in ~~bed-bed~~-parallel veins, generally considered as evidence for syn-compressional fluid
742 overpressure (Sibson, 2001; Hiemstra and Goldstein, 2015). At this stage, in addition to dilation
743 of the pre-existing ~ N-S and E-W striking rift-related extensional faults and their possible role
744 in fluid migration, the excess of pore pressure at the base of the thrust ramp, in the fold hinge and
745 during fold tightening could promote the localization of the fractures (Smith and Wiltschko,
746 1996; Ghisetti and Vezzani, 2000), with fluid migration within this zone and eventually
747 dolomitization. These fractures could have been corridors that later on formed the insipient NW-
748 SE Montagna dei Fiori Fault. Their localization at the back-limb cross-cutting the core,
749 explaining best the distribution of D3 and D4 at this locality. The presence of only D5 ~~only~~
750 within the damage zone of the Montagna dei Fiori Fault, postdating dolostone brecciation and, in
751 places, cementing breccia fragments, ~~may~~ suggest that D5 dolomite precipitation was associated
752 with the late stage evolution of the Montagna dei Fiori Fault, predating late stage calcite
753 precipitation. The shift from dolomite to calcite precipitation can be ascribed to attenuation of
754 Mg-rich fluids and/or calcite saturation. This condition was perhaps initiated during the late
755 stages of anticline evolution due to changes in fault conductivity sealing the upward migration of
756 Mg-rich fluids.

757 The presence of several generations of ~~bed-bed~~-perpendicular stylolites bounding and
758 intersecting EV2C2 veins (Fig. 10), supports the postulation that late stage calcite cements
759 precipitated in close ~~elosely associated~~-association with the deformation history of the Scaglia
760 Formation in the hanging wall of the Montagna dei Fiori Fault (Fig. 3). This deformation
761 occurred; during buttressing against Calcare Massiccio and Corniola Formations in the footwall,
762 and related with the positive inversion event induced by thrust-sheet stacking at depth (Storti et
763 al., 2018). Precipitation of EV3C3 and EV4C4 ~~in-is~~ interpreted to have occurred during uplift
764 and cooling as revealed by their relatively low homogenization temperatures ($\leq 40-50^{\circ}\text{C}$). of fluid
765 inclusions trapped within these cements. Deformation twining is either absent or weakly
766 developed, reflecting the lack of significant tectonic deformation after calcite precipitation.
767 These cements postdate the dolomitization events, high amplitude ~~bed-bed~~-perpendicular and
768 parallel stylolites, and are precipitated as cements bounding the breccia fragments within the
769 damage zone of the Montagna dei Fiori Fault. Salinities calculated from their fluid inclusions,
770 particularly in EV4C4, suggests precipitation from meteoric waters, which should have been
771 favored during the late evolutionary stages of antiformal stacking beneath the Montagna dei Fiori

772 Anticline, and eventual late extensional slip along the Montagna dei Fiori Fault (Storti et al.,
773 2018). The results obtained in this study are in relative agreement with the earlier work by
774 Ronchi et al. (2003) and Murgia et al. (2004) in the Central Apennines, assigning dolomitization
775 phases to the pre- and syn-orogenic deformations, although they did not specify the direct
776 relation between the local structures and the different types of dolomite.

777 The textures of the studied dolomites vary from planar-e to non-planar, the preponderance of
778 planar dolomite, as in D4, creates a rock with interesting poroperm characteristics (e.g. Woody et
779 al., 1996; Wilson et al., 2007; Wenzhi et al., 2012). This case-study is certainly relevant for
780 many potential reservoirs elsewhere in the world. Similar multistage burial dolomitization events
781 enhancing the reservoir quality have been reported from the carbonate successions of the Jurassic
782 in the Kopet-Dagh Basin, north eastern Iran (Adabi, 2009) and Devonian of the Rainbow sub-
783 Basin, western Canada (Qing and Mountjoy, 1989; Lonnee, 1999).

784 **6 Conclusions**

785 The Lower Jurassic limestones outcropping at the core of the Montagna dei Fiori
786 Anticline (Central Apennines, Italy) are massively affected by dolomitization, in damage zones
787 of the pre-orogenic faults inherited from the Tethyan rifting and the ones formed during the
788 Apenninic orogeny. Cross-cutting relationships between deformation structures, and results from
789 optical and cold cathodoluminescence petrography, fluid inclusion microthermometry, and
790 isotope geochemistry, support the occurrence of two major dolomitization events. The first event
791 is interpreted as having developed during the late stages of Tethyan rifting in Jurassic and
792 resulted in volumetrically significant dolostone geobodies. These dolostones are majorly-largely
793 matrix replacive, and their precipitation initiated prior to the significant burial as reflected in
794 their cross-cutting relationship with bed-bed-parallel stylolites, and by homogenization
795 temperatures in fluid inclusions that are dominantly below about 40-50°C. The second
796 dolomitization event corresponds to volumetrically less relevant replacive dolomite and dolomite
797 cements occluding fractures. These dolomites precipitated during hydrothermal fluid circulation
798 associated with contractional tectonics during the Apenninic orogeny, possibly at the onset of the
799 growth of the Montagna dei Fiori Anticline (Late Miocene).

800 Dolomitizing fluids in both events were most likely sourced from evaporitic brines
801 associated to the underlying Burano evaporites and their interaction with silicelasties-siliciclastic
802 rocks and/or the crystalline basement.

803

804 *Author contributions.* M. Mozafari participated in fieldwork, performed petrographic and
805 microthermometric analyses, provided their interpretation, and wrote the manuscript; R.
806 Swennen participated in fieldwork, discussed the results of the diagenetic study, and critically
807 reviewed the manuscript; F. Balsamo contributed to collect and interpret structural data,
808 discussed structural diagenesis data interpretation, and critically reviewed the manuscript; H. El
809 Desouky collected $^{87}\text{Sr}/^{86}\text{Sr}$ data; F. Storti conceived the research, contributed to collect and
810 interpret structural data, discussed structural diagenesis data interpretation, and critically
811 reviewed the manuscript; C. Taberner participated in fieldwork, discussed the results of the
812 diagenetic study and their framing into the proposed structural evolution, and critically reviewed
813 the manuscript.

814

815 *Acknowledgments.* This research was performed by collaboration between Parma and KU
816 Leuven universities in the framework of a research project (PT12432 and GFSTE 1100942)
817 funded by Shell Global Solutions International (Carbonate Research Team, now Geology and
818 New Reservoir Types Team). We thank E.M. Selmo (Parma University) and M. Joachimski
819 (University of Erlangen, Germany) for the stable carbon and oxygen analysis. G. Davis (VU
820 Amsterdam, the Netherlands) is thanked for the strontium isotope analysis. A. Comelli and H.
821 Nijs are kindly thanked for the careful preparation of the wafers and thin sections. L. Barchi is
822 gratefully appreciated for his help in SEM analysis. We ~~gratefully~~ acknowledge A. Koopman for
823 the constructive discussions during field work. We appreciate D. Smith (Energie Beheer
824 Nederland, the Netherlands) for the careful reviewing of the manuscript. We are very grateful to
825 reviewers J. Hendry and E. Ukar for their suggestions that allowed us to significantly improve
826 the manuscript.

827

828 **References**

- 829 Adabi, M. H.: Multistage dolomitization of upper jurassic mozduran formation, Kopet-Dagh
830 Basin, NE Iran. Carbonates and Evaporites, 24, 16-32,
831 <https://doi.org/10.1007/BF03228054>, 2009.
- 832 Alvarez, W.: Evolution of the Monte Nerone Seamount in the Umbria-Marches Apennines; I,
833 Jurassic-Tertiary stratigraphy, B. Soc. Geol. Ital., 108, 3-21, 1989.
- 834 Amieux, P.: La cathodoluminescence: méthode d'étude sédimentologique des carbonates, B.
835 Cent. Rech. Explor.-Prod. Elf-Aquitaine, 6, 437-483, 1982.
- 836 Artoni, A.: Messinian events within the tectono-stratigraphic evolution of the Southern Laga
837 Basin (Central Apennines, Italy), B. Soc Geol. Ital., 122, 447-466, 2003.
- 838 Artoni, A.: The Pliocene-Pleistocene stratigraphic and tectonic evolution of the central sector of
839 the Western Periadriatic Basin of Italy, Mar. Pet. Geol., 42, 82-106,
840 <https://doi.org/10.1016/j.marpetgeo.2012.10.005>, 2013.
- 841 Banner, J. L.: Radiogenic isotopes: systematics and applications to earth surface processes and
842 chemical stratigraphy, Earth. Sci. Rev., 65, 141-194, [https://doi.org/10.1016/S0012-](https://doi.org/10.1016/S0012-8252(03)00086-2)
843 [8252\(03\)00086-2](https://doi.org/10.1016/S0012-8252(03)00086-2), 2004.
- 844 Barchi, M., Minelli, G., and Pialli G.: The CROP 03 profile: a synthesis of results of deep
845 structures of the Northern Apennines, Mem. Soc. Geol. It., 52, 383-400, 1998.
- 846 Barker, S. L., and Cox, S. F.: Evolution of fluid chemistry and fluid-flow pathways during
847 folding and faulting: an example from Taemas, NSW, Australia, Geol. Soc. London
848 Spec. Publ., 359, 203-227, <https://doi.org/10.1144/SP359.12>, 2011.
- 849 Bassetti, M. A., Ricci Lucchi, F., Roveri, M., Taviani, M.: Messinian facies in a critical section
850 of northern Apennines (Montepetra-Perticara, Pesaro), Giorn. Geol., 60, 261-263,
851 1998.
- 852 Bathurst, R. G. C. (Eds.): Carbonate sediments and their diagenesis, Dev. Sedimentol., Ser.,
853 Elsevier, 12, 658 pp., 1975.
- 854 Bathurst, R. G. C.: Deep crustal diagenesis in limestones: Revista del Instituto de Investigaciones
855 Geológicas, Deputacion Provincial, Universidad Barcelona, 34, 89-100, 1980.
- 856 Bernoulli, D., Kälin, O., and Patacca, E.: A sunken continental margin of the Mesozoic Tethys:
857 The Northern and Central Apennines, Symposium" Sédimentation jurassique W
858 Européen", Spec. Publ. Ass. Sedim. Francis, 1, 179-210, 1979.

- 859 Bodnar, R. J.: Revised equation and table for determining the freezing point depression of H₂O-
860 NaCl solutions, *Geochim. Cosmochim. Acta*, 57, 683-684, 10.1016/0016-
861 7037(93)90378-A, 1993.
- 862 Boles, J. R. and Franks, S. G.: Clay diagenesis in Wilcox Sandstone of southwest Texas:
863 Implications of smectite diagenesis and sandstone cementation, *J. Sediment. Petrol.*,
864 49, 55-70, <https://doi.org/10.1306/212F76BC-2B24-11D7-8648000102C1865D>,
865 1979.
- 866 Bollati, A., Corrado, S., and Marino, M.: Inheritance of Jurassic rifted margin architecture into
867 the Apennines Neogene mountain building: a case history from the Lucretili Mts.
868 (Latium, Central Italy), *Int. J. Earth Sci.*, 101, 1011-1031,
869 <https://doi.org/10.1007/s00531-011-0694-7>, 2012.
- 870 Bosence, D., Procter, E., Aurell, M., Kahla, A. B., Boudagher-Fadel, M., Casaglia, F., Cirilli, S.,
871 Mehdie, M., Nieto, L., Rey, J., Scherreiks, R., Soussi, M., and Waltham, D.: A
872 dominant tectonic signal in high-frequency, peritidal carbonate cycles? A regional
873 analysis of Liassic platforms from western Tethys, *J. Sediment. Res.*, 79, 389-415,
874 <https://doi.org/10.2110/jsr.2009.038>, 2009.
- 875 Boschetti, T., Venturelli, G., Toscani, L., Barbieri, M., and Mucchino, C.: The Bagni di Lucca
876 thermal waters (Tuscany, Italy): an example of CaSO₄ waters with high Na/Cl and
877 low Ca/SO₄ ratios, *J. Hydrol.*, 307, 270-293,
878 <https://doi.org/10.1016/j.jhydrol.2004.10.015>, 2005.
- 879 Brandano, M., Cornacchia, I., Raffi, I., and Tomassetti, L.: The Oligocene-Miocene stratigraphic
880 evolution of the Majella carbonate platform (Central Apennines, Italy), *Sediment.*
881 *Geol.*, 333, 1-14, <https://doi.org/10.1016/j.sedgeo.2015.12.002>, 2016.
- 882 Burke, W. H., Denison, R. E., Hetherington, E. A., Koepnick, R. B., Nelson, H. F., and Otto, J.
883 B.: Variation of seawater ⁸⁷Sr/⁸⁶Sr throughout Phanerozoic time, *Geology*, 10, 516-
884 519, [https://doi.org/10.1130/0091-7613\(1982\)10<516:VOSSTP>2.0.CO;2](https://doi.org/10.1130/0091-7613(1982)10<516:VOSSTP>2.0.CO;2), 1982.
- 885 Burkhard, M.: Calcite twins, their geometry, appearance and significance as stress-strain markers
886 and indicators of tectonic regime: a review, *J. Struct. Geol.*, 15, 351-368,
887 [https://doi.org/10.1016/0191-8141\(93\)90132-T](https://doi.org/10.1016/0191-8141(93)90132-T), 1993.
- 888 Calamita, F., Cello, G., Deiana, G., and Paltrinieri, W.: Structural styles, chronology rates of
889 deformation, and time-space relationships in the Umbria-Marche thrust system

890 (central Apennines, Italy), *Tectonics*, 13, 873-881,
891 <https://doi.org/10.1029/94TC00276>, 1994.

892 Cardello, G. L., and Doglioni, C.: From mesozoic rifting to Apennine orogeny: the gran Sasso
893 range (Italy), *Gondwana Res.*, 27, 1307-1334,
894 <https://doi.org/10.1016/j.gr.2014.09.009>, 2015.

895 Carpenter, B.: Origin and chemical evolution of brines in sedimentary basins, *Oklahoma Geol.*
896 *Surv.*, 79, 60-77, <https://doi.org/10.2118/7504-MS>, 1978.

897 Centamore, E., Chiocchini, U., and Moretti, A.. *Geologia della zona tra Acerenza e Avigliano*
898 (Prov. di Potenza), *Studi Geol. Camerti*, 1, 97-122,
899 <http://dx.doi.org/10.15165/studgeocam-1462>, 1971.

900 Chilovi, C., De Feyter, A. J., Minelli, G., and Barchi, M. R.. Neogene strike-slip reactivation of
901 Jurassic normal faults in the M. Nerone-M. Catria Anticline (Umbro-Marchean Apennines,
902 Italy), *Boll. Soc. Geol. It.*, 121, 199-207, 2002.

903 Choukroune, P., Gapais, D., and Merle, O.: Shear criteria and structural symmetry, *J. Struct.*
904 *Geol.*, 9, 525-530, [https://doi.org/10.1016/0191-8141\(87\)90137-4](https://doi.org/10.1016/0191-8141(87)90137-4), 1987.

905 Clemenzi, L., Storti, F., Balsamo, F., Molli, G., Ellam, R., Mucchez, P., and Swennen, R.: Fluid
906 pressure cycles, variations in permeability, and weakening mechanisms along low-
907 angle normal faults: The Tellaro detachment, Italy, *Am. Assoc. Pet. Geol. Bull.*, 127,
908 1689-1710, <https://doi.org/10.1130/B31203.1>, 2015.

909 Colacicchi, R., Passeri, L., and Piali, G.: Evidences of tidal environment deposition in the
910 Calcare Massiccio formation (Central Apennines-Lower Lias), in: *Tidal Deposits*,
911 edited by: Ginsburg, R. N., Springer, Berlin, Heidelberg, Germany, 345-353,
912 <https://doi.org/10.1007/978-3-642-88494-8>, 1975.

913 Cooper, J. C., and Burbi, L.: The geology of the central Sibillini Mountains, *Mem. Soc. Geol. It.*,
914 35, 323-347, 1986.

915 Crescenti, U.: Serie stratigrafiche della serie calcarea dal Lias al Miocene nella regione
916 Marchigiano Abruzzese: parte I and II, *Mem. Soc. Geol. It.*, 8, 155-420, 1969.

917 Davies, G. R., and Smith, L. B. J.: Structurally controlled hydrothermal dolomite reservoir
918 facies: an overview, *Am. Assoc. Pet. Geol. Bull.*, 90, 1641-1690, 2006.

919 Del Moro, A., Puxeddu, M., Radicati di Brozolo, F., and Villa, I. M.: Rb-Sr and K-Ar ages of
920 minerals at temperatures of 300-400°C from deep wells in the Larderello geothermal

- 921 field (Italy), *Contrib. Mineral. Petr.*, 81, 349-349,
922 <https://doi.org/10.1007/BF00371688>, 1982.
- 923 Dewever, B., Swennen, R., and Breesch, L.: Fluid flow compartmentalization in the Sicilian fold
924 and thrust belt: implications for the regional aqueous fluid flow and oil migration
925 history, *Tectonophysics*, 591, 194-209, <https://doi.org/10.1016/j.tecto.2011.08.009>,
926 2013.
- 927 Dewey, J. F., Helman, M. L., Turco, E., Hutton, D. H. W., and Knott, S. D.: Kinematics of the
928 western Mediterranean, in: *Alpine Tectonics*, edited by: Coward, M. P., Dietrich, D.,
929 Park, R. G., *Geol. Soc. London Spec. Publ.*, 45, 265-283,
930 <https://doi.org/10.1144/GSL.SP.1989.045.01.15>, 1989.
- 931 Dewit, J., Foubert, A., El Desouky, H. A., Muchez, P., Hunt, D., Vanhaecke, F., and Swennen,
932 R.: Characteristics, genesis and parameters controlling the development of a large
933 stratabound HTD body at Matienzo (Ramales Platform, Basque-Cantabrian Basin,
934 northern Spain), *Mar. Pet. Geol.*, 55, 6-25, [10.1016/j.marpetgeo.2013.12.021](https://doi.org/10.1016/j.marpetgeo.2013.12.021), 2014.
- 935 Dickson, J. A. D.: Carbonate identification and genesis as revealed by staining, *J. Sediment.*
936 *Petrol.*, 36, 491-505, [https://doi.org/10.1306/74D714F6-2B21-11D7-](https://doi.org/10.1306/74D714F6-2B21-11D7-8648000102C1865D)
937 [8648000102C1865D](https://doi.org/10.1306/74D714F6-2B21-11D7-8648000102C1865D), 1966.
- 938 Di Francesco, L., Fabbi, S., Santantonio, M., Bigi, S., and Poblet, J.: Contribution of different
939 kinematic models and a complex Jurassic stratigraphy in the construction of a
940 forward model for the Montagna dei Fiori fault-related fold (Central Apennines,
941 Italy), *Geol. J.*, 45, 489-505, <https://doi.org/10.1002/gj.1191>, 2010.
- 942 [Eichhubl, P., and Boles, J. R.: Rates of fluid flow in fault systems: evidence for episodic rapid](#)
943 [fluid flow in the Miocene Monterey Formation, coastal California, *Am. J. Sci.*, 300,](#)
944 [571-600, doi: 10.2475/ajs.300.7.571, 2000.](#)
- 945 Elter, P., Giglia, G., Tongiorgi, M., and Trevisan, L.: Tensional and contractional areas in the
946 recent (Tortonian to Present) evolution of the Northern Apennines, *B. Geofis. Teor.*
947 *Appl.*, 17, 3-18, 1975.
- 948 Emery, D., and Robinson, A. (Eds.): *Inorganic Geochemistry: Applications to Petroleum*
949 *Geology*, Blackwell Science, Oxford, United Kingdom, 101-128, 1993.
- 950 Fantoni, R., and Franciosi, R.: Tectono-sedimentary setting of the Po Plain and Adriatic foreland,
951 *Rend. Lincei*, 21, 197-209, <https://doi.org/10.1007/s12210-010-0102-4>, 2010.

- 952 [Ferraro, F., Agosta, F., Ukar, E., Grieco, D. S., Cavalcante, F., Belviso, C., and Prosser, G.:](#)
953 [Structural diagenesis of carbonate fault rocks exhumed from shallow crustal depths:](#)
954 [An example from the central-southern Apennines, Italy, *J. Struct. Geol.*, 122, 58-80,](#)
955 <https://doi.org/10.1016/j.jsg.2019.02.008>, 2019.
- 956 Flecker, R., De Villiers, S., and Ellam, R. M.: Modelling the effect of evaporation on the
957 salinity-⁸⁷Sr/⁸⁶Sr relationship in modern and ancient marginal-marine systems: the
958 Mediterranean Messinian Salinity Crisis, *Earth Planet. Sci. Lett.*, 203, 221-233,
959 10.1016/S0012-821X(02)00848-8, 2002.
- 960 Friedman, I.: Some investigations of the deposition of travertine from Hot Springs-I. The
961 isotopic chemistry of a travertine-depositing spring, *Geochim. Cosmochim. Acta*, 34,
962 1303-1315, [https://doi.org/10.1016/0016-7037\(70\)90043-8](https://doi.org/10.1016/0016-7037(70)90043-8), 1970.
- 963 Gale, J. F., Laubach, S. E., Marrett, R. A., Olson, J. E., Holder, J., and Reed, R. M.: Predicting
964 and characterizing fractures in dolostone reservoirs: Using the link between
965 diagenesis and fracturing, *Geol. Soc. London Spec. Publ.*, 235, 177-192,
966 <https://doi.org/10.1144/GSL.SP.2004.235.01.08>, 2004.
- 967 Giacometti, A., and Ronchi, P.: Early Lias Carbonate Platform: Facies and Diagenesis Analogies
968 between the Calcare Massiccio (Umbro-Marchean Apennines) and the Inici Fm.
969 (Sicily Channel), *Mem. Soc. Geol. It.*, 55, 271-278, 2000.
- 970 Ghisetti, F., and Vezzani, L.: Detachments and normal faulting in the Marche fold-and-thrust belt
971 (Central Apennines, Italy): inferences on fluid migration paths, *J. Geodyn.*, 29, 345-
972 369, [https://doi.org/10.1016/S0264-3707\(99\)00057-5](https://doi.org/10.1016/S0264-3707(99)00057-5), 2000.
- 973 Ghisetti, F., and Vezzani, L.: Interfering paths of deformation and development of arcs in the
974 fold-and-thrust belt of the central Apennines (Italy), *Tectonics*, 16, 523-536,
975 <https://doi.org/10.1029/97TC00117>, 1997.
- 976 Goldstein, R. H., and Reynolds, T. J.: Systematics of Fluid Inclusions in Diagenetic Minerals,
977 *Soc. Sediment. Geol., Short Course*, 31, 199 pp., 1994.
- 978 Gregg, J. M.: On the formation and occurrence of saddle dolomite-discussion, *J. Sediment.*
979 *Petrol.*, 53, 1025-1033, 1983.
- 980 Gregg, J. M., Shelton, K. L., Johnson, A. W., Somerville, I. D., and Wright, W. R.:
981 Dolomitization of the Waulsortian limestone (lower Carboniferous) in the Irish

982 Midlands, *Sedimentology*, 48, 745-766, <https://doi.org/10.1046/j.1365->
983 3091.2001.00397.x, 2001.

984 Habermann, D., Neuser, R. D., and Richter, D. K.: REE-activated cathodoluminescence of
985 calcite and dolomite: high-resolution spectrometric analysis of CL emission (HRS-
986 CL), *Sediment. Geol.*, 101, 1-7, [https://doi.org/10.1016/0037-0738\(95\)00086-0](https://doi.org/10.1016/0037-0738(95)00086-0),
987 1996.

988 Hendry, J. P., Gregg, J. M., Shelton, K. L., Somerville, I. D., and Crowley, S. F.: Origin,
989 characteristics and distribution of fault-related and fracture-related dolomitization:
990 Insights from Mississippian carbonates, Isle of Man, *Sedimentology*, 62, 717-752,
991 <https://doi.org/10.1111/sed.12160>, 2015.

992 Hiemstra, E. J., and Goldstein, R. H.: Repeated injection of hydrothermal fluids into downdip
993 carbonates: a diagenetic and stratigraphic mechanism for localization of reservoir
994 porosity, Indian Basin Field, New Mexico, USA, *Geol. Soc. London Spec. Publ.*,
995 406, 141-177, <https://doi.org/10.1144/SP406.1>, 2015.

996 [Hollis, C., Bastesen, E., Boyce, A., Corlett, H., Gawthorpe, R., Hirani, J. Rotevatn, A., and](#)
997 [Whitaker, F.: Fault-controlled dolomitization in a rift basin. *Geology*, 45, 219-222.](#)
998 <https://doi.org/10.1130/G38s394.1>, 2017.

999 Horita, J.: Oxygen and carbon isotope fractionation in the system dolomite-water-CO₂ to
1000 elevated temperatures, *Geochim. Cosmochim. Acta*, 129, 111-124,
1001 <https://doi.org/10.1016/j.gca.2013.12.027>, 2014.

1002 Horvath, F.: Towards a mechanical model for the formation of the Pannonian basin,
1003 *Tectonophysics*, 226, 333-357, [https://doi.org/10.1016/0040-1951\(93\)90126-5](https://doi.org/10.1016/0040-1951(93)90126-5), 1993.

1004 Hudson, J. D.: Stable isotopes and limestone lithification, *Geol. Soc. London*, 133, 637-660,
1005 <https://doi.org/10.1144/gsjgs.133.6.0637>, 1977.

1006 Koopman, A.: Detachment tectonics in the central Apennines, Italy, Ph.D. thesis, Utrecht
1007 University, The Netherlands, 155 pp., 1983.

1008 Land L. S.: The isotopic and trace element geochemistry of dolomite: the state of the art, in:
1009 Concepts and Models of dolomitization, edited by: Zenger D. H., Dunham J. B. and
1010 Ethington R. L., *Soc. Econ. Paleontol. and Mineral., Spec. Pub.*, 28, 87-110, 1980.

1011 Land L. S.: The application of stable isotopes to studies of the origin of dolomite and to
1012 problems of diagenesis of clastic sediments, in: *Stable Isotopes in Sedimentary*

- 1013 Geology, edited by: Arthur M. A., Soc. Econ. Paleontol. and Mineral, Short Course,
1014 10, 4-1 , 1983.
- 1015 Land L. S.: The origin of massive dolomite. Jour. Geol. Educ., 33, 112-125, 1985.
- 1016 Laubach, S. E., Eichhubl, P., Hilgers, C., and Lander, R. H.: Structural diagenesis, J. Struct.
1017 Geol., 32, 1866-1872, <https://doi.org/10.1016/j.jsg.2010.10.001>, 2010.
- 1018 Li, Z., Goldstein, R. H. and Franseen, E. K.: Meteoric calcite cementation: diagenetic response to
1019 relative fall in sea-level and effect on porosity and permeability, Las Negras area,
1020 southeastern Spain, Sediment. Geol., 348, 1-18,
1021 <https://doi.org/10.1016/j.sedgeo.2016.12.002>, 2017.
- 1022 Lind, I. L., Berger, W. H., and Kroenke, L. W.: Stylolites in chalk from leg 130, Ontong Java
1023 Plateau, in: Proceedings of the Ocean Drilling Program, scientific results, 445-451,
1024 1993.
- 1025 Lobato, L. M., Forman, J. M. A., Fazikawa, K., Fyfe, W. S., and Kerrich, R.: Uranium in
1026 overthrust Archean basement, Bahia, Brazil. Canadian Mineral., 21, 647-654, 1983.
- 1027 [Lonnee, J. S.: Sedimentology, dolomitization and diagenetic fluid evolution of the Middle](#)
1028 [Devonian Sulphur Point Formation, northwestern Alberta, Ph.D. thesis, University of](#)
1029 [Windsor, Canada, 133 pp., 1999.](#)
- 1030 Luczaj, J. A., and Goldstein, R. H.: Diagenesis of the Lower Permian Krider Member, southwest
1031 Kansas, USA: fluid-inclusion, U-Pb, and fission-track evidence for reflux
1032 dolomitization during latest Permian time, J. Sediment. Res., 70, 762-773,
1033 <https://doi.org/10.1306/2DC40936-0E47-11D7-8643000102C1865D>, 2000.
- 1034 Machel, H. G.: Effects of groundwater flow on mineral diagenesis, with emphasis on carbonate
1035 aquifers, Hydrol. J., 7, 94-107, <https://doi.org/10.1007/s100400050>, 1999.
- 1036 Machel, H. G., Mason, R. A., Mariano, A. N., and Mucci, A.: Causes and emission of
1037 luminescence in calcite and dolomite, in: Luminescence microscopy and
1038 spectroscopy : Qualitative and quantitative applications, edited by: Barker, C. E., and
1039 Kopp, O. C, Soc. Sediment. Geol., Short Course, 9-25, 1991.
- 1040 Machel, H. G., and Cavell, P. A.: Low-flux, tectonically-induced squeegee fluid flow, Bull. Can.
1041 Petrol. Geol., 47, 510-533, 1999.

- 1042 Major, R. P., Lloyd, R. M. and Lucia, F. J.: Oxygen isotope composition of Holocene dolomite
1043 formed in a humid hypersaline setting, *Geology*, 20, 586-588,
1044 [https://doi.org/10.1130/0091-7613\(1992\)020<0586:OICOHD>2.3.CO;2](https://doi.org/10.1130/0091-7613(1992)020<0586:OICOHD>2.3.CO;2), 1992.
- 1045 Marchegiani, L., Deiana, G., and Tondi, E.: Tettonica pre-orogenica in Appennino centrale, *Stud.*
1046 *Geol. Camerti*, 14, 211-228, <http://dx.doi.org/10.15165/studgeocam-807>, 1999.
- 1047 Marino, M., and Santantonio, M.: Understanding the geological record of carbonate platform
1048 drowning across rifted Tethyan margins: Examples from the Lower Jurassic of the
1049 Apennines and Sicily (Italy), *Sediment. Geol.*, 225, 116-137,
1050 <https://doi.org/10.1016/j.sedgeo.2010.02.002>, 2010.
- 1051 Marshall, J. D.: Climatic and oceanographic isotopic signals from the carbonate rock record and
1052 their preservation, *Geol. Mag.*, 129, 143-160,
1053 <https://doi.org/10.1017/S0016756800008244>, 1992.
- 1054 Mattei, M.: Analisi geologico-strutturale della Montagna dei Fiori (Ascoli Piceno, Italia
1055 Centrale), *Geol. Romana*, 26, 327-347, 1987.
- 1056 Mazzoli, S., Deiana, G., Galdenzi, S., and Cello, G.: Miocene fault-controlled sedimentation and
1057 thrust propagation in the previously faulted external zones of the Umbria-Marche
1058 Apennines, Italy, *EGU Stephan Mueller Spec. Publ. Ser.*, 1, 195-209, 2002.
- 1059 Mazzullo, S. J.: Geochemical and neomorphic alteration of dolomite: a review, *Carbonates*
1060 *Evaporites*, 7, 21-37, <https://doi.org/10.1007/BF03175390>, 1992.
- 1061 McArthur, J. M., Howarth, R. J., and Shields, G. A.: Strontium isotope stratigraphy, in: *The*
1062 *Geologic Time Scale 2012*, edited by: Gradstein, F. M., Ogg, J. G., Schmitz, M., and
1063 Ogg, G., Elsevier, 127-144, <https://doi.org/10.1016/C2011-1-08249-8>, 2012.
- 1064 McCaffrey, M. A., Lazar, B., Holland, H. D.: The evaporation path of seawater and the
1065 coprecipitation of Br- and K⁺ with halite, *J. Sediment. Res.*, 57, 928-937,
1066 <https://doi.org/10.1306/212F8CAB-2B24-11D7-8648000102C1865D>, 1987.
- 1067 McCaig, A. M.: Deep fluid circulation in fault zones, *Geology*, 16, 867-870,
1068 [https://doi.org/10.1130/0091-7613\(1988\)016<0867:DFCIFZ>2.3.CO;2](https://doi.org/10.1130/0091-7613(1988)016<0867:DFCIFZ>2.3.CO;2), 1988.
- 1069 McCaig, A. M., Wickham, S. M., and Taylor, H. P.: Deep fluid circulation in alpine shear zones,
1070 Pyrenees, France: field and oxygen isotope studies, *Contrib. Mineral. Petr.*, 106, 41-
1071 60, <https://doi.org/10.1007/BF00306407>, 1990.

- 1072 Montanez, I. P.: Late diagenetic dolomitization of Lower Ordovician, upper Knox carbonates: A
1073 record of the hydrodynamic evolution of the southern Appalachian Basin, *Am.*
1074 *Assoc. Pet. Geol. Bull.*, 78, 1210-1239, 1994.
- 1075 Moore, C. H. (Eds.): Carbonate diagenesis and porosity, *Dev. Sedimentol.*, 46, Elsevier Sci.
1076 Publ., Amsterdam, The Netherlands, 338 pp., 1989.
- 1077 Morettini, E., Santantonio, M., Bartolini, A., Cecca, F., Baumgartner, P. O., and Hunziker, J. C.:
1078 Carbon isotope stratigraphy and carbonate production during the Early-Middle
1079 Jurassic: examples from the Umbria-Marche-Sabina Apennines (central Italy),
1080 *Paleog., Paleocl., Paleoec.*, 184, 251-273, [https://doi.org/10.1016/S0031-](https://doi.org/10.1016/S0031-0182(02)00258-4)
1081 [0182\(02\)00258-4](https://doi.org/10.1016/S0031-0182(02)00258-4), 2002.
- 1082 Mountjoy, E. W., Machel, H. G., Green, D., Duggan, J., and Williams-Jones, A. E.: Devonian
1083 matrix dolomites and deep burial carbonate cements: a comparison between the
1084 Rimbe-Meadowbrook reef trend and the deep basin of west-central Alberta, *B. Can.*
1085 *Petrol. Geol.*, 47, 487-509, 1999.
- 1086 Murgia, M. V., Ronchi, P., and Ceriani, A.: Dolomitization processes and their relationships with
1087 the evolution of an orogenic belt (Central Apennines and peri-adriatic foreland,
1088 Italy), *AAPG Hedberg series*, 1, 277-294, <https://doi.org/10.1306/1025695H13121>,
1089 2004.
- 1090 Nelson, R. A: Significance of fracture sets associated with stylolite zones, *Am. Assoc. Pet. Geol.*
1091 *Bull.*, 65, 2417-2425, 1981.
- 1092 Parotto, M., and Praturlon, A.: Geological summary of the Central Apennines, *Quad. Ric. Sci.*,
1093 90, 257-311, 1975.
- 1094 Patacca, E., Sartori, R., and Scandone, P.: Tyrrhenian basin and Apenninic arcs: Kinematic
1095 relations since late Tortonian times, *Mem. Soc. Geol. It.*, 45, 425-451,
1096 <http://hdl.handle.net/11568/11610>, 1992.
- 1097 Piali, G.: Facies di piana cotidale nel Calcarea Massiccio dell'Appennino umbro marchigiano,
1098 *Boll. Soc. Geol. It.*, 90, 481-507, 1971.
- 1099 Pierantoni, P., Deiana, G., and Galdenzi, S.: Stratigraphic and structural features of the Sibillini
1100 Mountains (Umbria-Marche Apennines, Italy), *Ital. J. Geosci.*, 132, 497-520,
1101 <https://doi.org/10.3301/IJG.2013.08>, 2013.

- 1102 Purser, B., Tucker, M. and Zenger, D.: Problems, progress and future research concerning
1103 dolomites and dolomitization, in: Dolomites: a Volume in Honour of Dolomieu,
1104 edited by: Purser, B., Tucker, M. and Zenger, D., IAS Spec. Publ., 21, 3-20, 1994.
- 1105 [Qing, H., and Mountjoy, E. W.: Multistage dolomitization in Rainbow buildups, Middle](#)
1106 [Devonian Keg River Formation, Alberta, Canada. J. of Sediment. Res., 59, 114-126,](#)
1107 <https://doi.org/10.1306/212F8F30-2B24-11D7-8648000102C1865D>, 1989.
- 1108 Radke, B. M., and Mathis, R. L.: On the formation and occurrence of saddle dolomite, J.
1109 Sediment. Res., 50, 1149-1168, [https://doi.org/10.1306/212F7B9E-2B24-11D7-](https://doi.org/10.1306/212F7B9E-2B24-11D7-8648000102C1865D)
1110 [8648000102C1865D](https://doi.org/10.1306/212F7B9E-2B24-11D7-8648000102C1865D), 1980.
- 1111 Ronchi, P., Casaglia, F., and Ceriani, A.: The multiphase dolomitization of the Liassic Calcare
1112 Massiccio and Corniola successions (Montagna dei Fiori, Northern Apennines, Italy),
1113 Boll. Soc. Geol. It., 122, 157-172, 2003.
- 1114 Rosenbaum, J., and Sheppard, S. M.: An isotopic study of siderites, dolomites, and ankerites at
1115 high temperatures, Geochim. Cosmochim. Acta, 50, 1147-1150,
1116 [https://doi.org/10.1016/0016-7037\(86\)90396-0](https://doi.org/10.1016/0016-7037(86)90396-0), 1986.
- 1117 Roveri, M., Bassetti, M. A., and Lucchi, F. R.: The Mediterranean Messinian salinity crisis: an
1118 Apennine foredeep perspective, Sediment. Geol., 140, 201-214,
1119 [https://doi.org/10.1016/S0037-0738\(00\)00183-4](https://doi.org/10.1016/S0037-0738(00)00183-4), 2001.
- 1120 Saelen, G., Doyle, P., and Talbot, M. R.: Stable-isotope analyses of belemnite rostra from the
1121 Whitby Mudstone Fm., England: Surface water conditions during deposition of a
1122 marine black shale, Palaios, 11, 97-117, <https://doi.org/10.2307/3515065>, 1996.
- 1123 Santantonio, M, and Carminati, E.: Jurassic rifting evolution of the Apennines and Southern Alps
1124 (Italy): Parallels and differences, Geol. Soc. Am. B., 123, 464-484,
1125 <https://doi.org/10.1130/B30104.1>, 2011.
- 1126 Santantonio, M. and Muraro, C.: The Sabina Plateau, Palaeoescrapment, and Basin-Central
1127 Apennines, 6th international symposium on the Jurassic system, General Field Trip
1128 Guidebook, Palermo, Italy, 271-315, 2002.
- 1129 Santantonio, M., Fabbi, S., and Bigi, S.: Discussion on «Geological map of the partially
1130 dolomitized Jurassic succession exposed in the central sector of the Montagna dei
1131 Fiori Anticline, Central Apennines, Italy», Ital. J. Geosci., 136, 312-316,
1132 <https://doi.org/10.3301/IJG.2017.04>, 2017.

- 1133 Schulz, H. M., Wirth, R., and Schreiber, A.: Organic-inorganic rock-fluid interactions in
1134 stylolitic micro-environments of carbonate rocks: a FIB-TEM study combined with a
1135 hydrogeochemical modelling approach, *Geofluids*, 16, 909-924,
1136 <https://doi.org/10.1111/gfl.12195>, 2016.
- 1137 Scisciani V., Tavarnelli, E., and Calamita, F.: The interaction of extensional and contractional
1138 deformations in the outer zones of the Central Apennines, Italy, *J. Struct. Geol.*, 24,
1139 1647-1658, [https://doi.org/10.1016/S0191-8141\(01\)00164-X](https://doi.org/10.1016/S0191-8141(01)00164-X), 2002.
- 1140 Shackleton, N. J., and Kennett, J. P.: Paleotemperature History of the Cenozoic and the Initiation
1141 of Antarctic Glaciation Oxygen and Carbon Isotope Analyses in DSDP Sites 277, 279,
1142 and 281, Initial reports of Deep Sea Drilling Project, 29, 743-755, 1975.
- 1143 Sharp, I., Gillespie, P., Morsalnezhad, D., Taberner, C., Karpuz, R., Vergés, J., Horbury, A.,
1144 Pickard, N., J. Garland, J., and Hunt, D.: Stratigraphic architecture and fracture-
1145 controlled dolomitization of the Cretaceous Khami and Bangestan groups: an outcrop
1146 case study, Zagros Mountains, Iran, *Geol. Soc. London Spec. Publ.*, 329, 343-396,
1147 <https://doi.org/10.1144/SP329.14>, 2010.
- 1148 Shepherd, T., Rankin, A. H., and Alderton, D. H. M. (Eds.): *A Practical Guide to Fluid Inclusion*
1149 *Studies*, Glasgow: Blackie, 239 pp., 1985.
- 1150 Sibley, D. F., and Gregg, J. M.: Classification of dolomite rock textures, *J. Sediment. Petrol.*, 57,
1151 967-975, <https://doi.org/10.1306/212F8CBA-2B24-11D7-8648000102C1865D>,
1152 1987.
- 1153 Sibson, R. H.: Fluid flow accompanying faulting: field evidence and models, *Earthquake*
1154 *prediction: an international review*, AGU, 4, 593-603,
1155 <https://doi.org/10.1029/ME004p0593>, 1981.
- 1156 Slobodník, M., Mucchez, P., Kral, J., and Keppens, E.: Variscan veins: record of fluid circulation
1157 and Variscan tectonothermal events in Upper Palaeozoic limestones of the Moravian
1158 Karst, Czech Republic, *Geol. Mag.*, 143, 491-508,
1159 <https://doi.org/10.1017/S0016756806001981>, 2006.
- 1160 Smith, R. E., Wiltschko, D. V.: Generation and maintenance of abnormal fluid pressures beneath
1161 a ramping thrust sheet: isotropic permeability experiments, *J. Struct. Geol.*, 18, 951-
1162 970, [https://doi.org/10.1016/0191-8141\(96\)00023-5](https://doi.org/10.1016/0191-8141(96)00023-5), 1996.

- 1163 Steiger, R., and Jäger, E.: Subcommittee on geochronology: convention on the use of decay
1164 constants in geo and cosmochemistry, *Earth Planet. Sci. Lett.*, 36, 359-362,
1165 [https://doi.org/10.1016/0012-821X\(77\)90060-7](https://doi.org/10.1016/0012-821X(77)90060-7), 1977.
- 1166 Storti, F., Balsamo, F., and Koopman, A.: Geological map of the partially dolomitized Jurassic
1167 succession exposed in the core of the Montagna dei Fiori Anticline, Central
1168 Apennines, Italy, *Ital. J. Geosci.*, 136, 125-135, <https://doi.org/10.3301/IJG.2016.05>,
1169 2017a.
- 1170 Storti F., Balsamo, F., and Koopman, A.: Reply to: discussion on «Geological map of the
1171 partially dolomitized Jurassic succession exposed in the central sector of the
1172 Montagna dei Fiori Anticline, Central Apennines, Italy» by Santantonio, M., Fabbì,
1173 S. and Bigi, S., *Ital. J. Geosci.*, 136, 317-319, <https://doi.org/10.3301/IJG.2017.04>,
1174 2017b.
- 1175 Storti, F., Balsamo F., Mozafari M., Koopman A., Swennen R. and Taberner C.: Syn-
1176 contractional overprinting between extension and shortening along the Montagna dei
1177 Fiori Fault during Plio-Pleistocene antiformal stacking at the Central Apennines
1178 thrust wedge toe, *Tectonics*, <https://doi.org/10.1029/2018TC005072>, 2018.
- 1179 Stueber, A. M., Pushkar, P., and Baldwin, A. D., JR.: Survey of $^{87}\text{Sr}/^{86}\text{Sr}$ ratios and total
1180 strontium concentrations in Ohio stream and ground waters, *Ohio J. Sci.*, 72, 98-104,
1181 1972.
- 1182 Sommer, S. E.: Cathodoluminescence of carbonates, 1. Characterization of cathodoluminescence
1183 from carbonate solid solutions, *Chemical Geology*, 9, 257-273,
1184 [https://doi.org/10.1016/0009-2541\(72\)90064-2](https://doi.org/10.1016/0009-2541(72)90064-2), 1972.
- 1185 Swennen, R., Dewit, J., Fierens, E., Muchez, Ph., Shah, M., Nader, F. H., Hunt, D.: Multiple
1186 dolomitisation events along the Ranero fault (Pozalagua Quarry, Basque-Cantabrian
1187 Basin): episodic earthquake activity, *Sedimentology*, 59, 1345-1374,
1188 <https://doi.org/10.1111/j.1365-3091.2011.01309.x>, 2012.
- 1189 Tavani, S., Storti, F., Salvini, F., and Toscano, C.: Stratigraphic versus structural control on the
1190 deformation pattern associated with the evolution of the Mt. Catria anticline, Italy, *J.*
1191 *Struct. Geol.*, 30, 664-681, <https://doi.org/10.1016/j.jsg.2008.01.011>, 2008.

- 1192 Taylor, H. P.: Oxygen and hydrogen isotope relationships in hydrothermal mineral deposits, In:
1193 Geochemistry of hydrothermal ore deposits, edited by: Barnes, H. L., Wiley and
1194 Sons, New York, 229-302, 1997.
- 1195 Thirlwall, M. F.: Long-term reproducibility of multicollector Sr and Nd isotope ratio analysis,
1196 Chemical Geology, 94, 85-104, [https://doi.org/10.1016/S0009-2541\(10\)80021-X](https://doi.org/10.1016/S0009-2541(10)80021-X),
1197 1991.
- 1198 Tongiorgi, M., Rau, A., and Martini, I. P.: Sedimentology of early-alpine, fluvio-marine, clastic
1199 deposits (Verrucano, Triassic) in the Monti Pisani (Italy), Sediment. Geol., 17, 311-
1200 332, [https://doi.org/10.1016/0037-0738\(77\)90051-3](https://doi.org/10.1016/0037-0738(77)90051-3), 1977.
- 1201 [Ukar, E., and Laubach, S. E.: Syn-and postkinematic cement textures in fractured carbonate](#)
1202 [rocks: Insights from advanced cathodoluminescence imaging, Tectonophysics, 690,](#)
1203 [190-205, https://doi.org/10.1016/j.tecto.2016.05.001, 2016.](#)
- 1204 Vai, G. B., and Ricci Lucchi, F.: Algal crusts, autochthonous and clastic gypsum in a
1205 cannibalistic evaporite basin: a case history from the Messinian of northern
1206 Apennines. Sedimentology, 24, 221-244, <https://doi.org/10.1111/j.1365-3091.1977.tb00255.x>, 1977.
- 1208 Vandeginste, V., Swennen, R., Gleeson, S. A., Ellam, R. M., Osadetz, K., and Roure, F.: Zebra
1209 dolomitization as a result of focused fluid flow in the Rocky Mountains Fold and
1210 Thrust Belt, Canada. Sedimentology, 52, 1067-1095, <https://doi.org/10.1111/j.1365-3091.2005.00724.x>, 2005.
- 1212 Vandeginste, V., Swennen, R., Gleeson, S. A., Ellam, R. M., Osadetz, K., and Roure, F.:
1213 Geochemical constraints on the origin of the Kicking Horse and Monarch Mississippi
1214 Valley-type lead-zinc ore deposits, southeast British Columbia, Canada, Mineralium
1215 Deposita, 42, 913-935, <https://doi.org/10.1007/s00126-007-0142-6>, 2007.
- 1216 Veizer, J., Ala, D., Azmy, K., Bruckshen, P., Buhl, D., Bruhn, F., Carden, G. A. F., Diener, A.,
1217 Ebner, S., Godderis, Y., Jasper, T., Korte, C., Pawellek, F., Podlaha, O. G., and
1218 Strauss, H.: $^{87}\text{Sr}/^{86}\text{Sr}$, $\delta^{13}\text{C}$ and evolution of Phanerozoic seawater, Chemical
1219 Geology, 161, 59-88, [https://doi.org/10.1016/S0009-2541\(99\)00081-9](https://doi.org/10.1016/S0009-2541(99)00081-9), 1999.
- 1220 Walker, G., Abumere, O. E., and Kamaluddin, B.: Luminescence spectroscopy of Mn²⁺ rock-
1221 forming carbonates, Mineral. Mag., 53, 201-11, 10.1180/minmag.1989.053.370.07,
1222 1989.

1223 Wenzhi, Z., Anjiang, S., Suyun, H., Baomin, Z., Wenqing, P., Jingao, Z. and Zecheng, W.:
1224 Geological conditions and distributional features of large-scale carbonate reservoirs
1225 onshore China. *Petrol. Explor. Develop.*, 39, 1-14, [https://doi.org/10.1016/S1876-](https://doi.org/10.1016/S1876-3804(12)60010-X)
1226 [3804\(12\)60010-X](https://doi.org/10.1016/S1876-3804(12)60010-X), 2012.

1227 Wilson, A., and Ruppel, C.: Salt tectonics and shallow subsea floor fluid convection: models of
1228 coupled fluid-heat-salt transport, *Geofluids*, 7, 377-386,
1229 <https://doi.org/10.1111/j.1468-8123.2007.00191.x>, 2007.

1230 Wilson, M. E. J., Evans, M. J., Oxtoby, N. H., Nas, D. S., Donnelly, T. and Thirlwall, M.:
1231 Reservoir quality, textural evolution, and origin of fault-associated
1232 dolomites. *AAPB Bull.*, 91, 1247-1272, 2007.

1233 Woodcock, N. H., and Mort, K.: Classification of fault breccias and related fault rocks, *Geol.*
1234 *Mag.*, 145, 435-440, <https://doi.org/10.1017/S0016756808004883>, 2008.

1235 Woody, R. E., Gregg, J. M. and Koederitz, L. F.: Effect of texture on petrophysical properties of
1236 dolomite: Evidence from the Cambrian-Ordovician of Southeastern Missouri. *AAPG*
1237 *Bull.*, 80, 119-131, 1996.

1238 Zempolich, W. G., and Hardie, L. A.: Geometry of dolomite bodies within deep-water
1239 resedimented oolite of the Middle Jurassic Vajont Limestone, Venetian Alps, Italy:
1240 Analogs for hydrocarbon reservoirs created through fault-related burial
1241 dolomitization, in: *Reservoir quality prediction in sandstones and carbonates*, edited
1242 by: Kupecz, A., Gluyas, J., and Bloch, S., *AAPG Mem.*, 69, 127-162, 1997.

1243

1244

1245

1246

1247

1248

1249

1250

1251 **Table captions**

1252 **Table. 1.** Stable carbon and oxygen isotopes, $^{87}\text{Sr}/^{86}\text{Sr}$ ratios, and fluid inclusion
1253 microthermometry data (not pressure corrected) of host rocks and diagenetic phases in the
1254 Montagna dei Fiori Anticline. Stable carbon and oxygen isotopes values are expressed in
1255 ‰ V-PDB and salinity values in eq. wt. % NaCl.

1256 **Figure captions**

1257 Fig. 1. **Aa)** Simplified regional map (modified after Ghisetti and Vezzani, 1997) showing the
1258 tectonic outlines of the Central Apennines and the study area (rectangle). **Bb)** Schematic
1259 geological map of the Montagna dei Fiori Anticline showing the distribution of dolostones
1260 (modified after Storti et al., 2017a). **Cc)** Lithostratigraphical column of the successions exposed
1261 in Montagna dei Fiori (modified after Mattei, 1987; Di Francesco et al, 2010; Storti et al., 2018).
1262 Letter B stands for the Bugarone Formation. Lithologies are mentioned in the text. Note that the
1263 thickness of the not-outcropping formations (Triassic evaporites and the crystalline basement) is
1264 not to scale. **Dd)** Regional Geological-geological transect across present day Central Apennines
1265 and the Adriatic Sea (modified after Fantoni and Franciosi, 2010) with vertical exaggeration of
1266 2:1. The dashed rectangle indicates the Montagna dei Fiori Anticline region.

1267

1268 Fig. 2. **Aa, Bb)** Geological map of the central sector of the Montagna dei Fiori Anticline, and
1269 cross-section oriented parallel (a-b) to the hinge line representing the tectono-stratigraphic
1270 architecture of the faulted anticline (modified after Storti et al., 2017a). The stereonets (Schmidt
1271 equal area projection lower hemisphere) provide the attitude of the extensional faults. The
1272 locations of the corresponding field sites are indicated by ~~numbers~~letters. **c)** At this location, well
1273 exposed N-S striking extensional fault zones offset the dolomitized Corniola Formation. The
1274 fault zone is characterized by near-horizontal stylolites localized in the footwall damage zone (4
1275 fault data). **d, e and f)** These locations consist of mostly ~ E-W striking extensional fault zones.
1276 Particularly the boundary fault zones delimiting Calcare Massiccio Formation in the main horst
1277 block is evident (site d: 20 fault data; site e: 24 fault data; site f: 9 fault data). **g and h)** At these
1278 locations, dip-slip slickenlines support major extensional movements related to the Montagna dei
1279 Fiori Fault. Contractional deformation structures are preserved in the bed-perpendicular

1280 | stylolites, shear surfaces and tension gashes arranged as S-C arrays (site g: 21 fault data; site h:
1281 | 14 fault data). Equal area projection, lower hemisphere.

1282 |
1283 | Fig. 3. Aa) Field photograph showing the deformed Scaglia Formation in the hanging wall (HW)
1284 | and brecciated, dolomitized Calcare Massiccio Formation in the footwall (FW) of the Montagna
1285 | dei Fiori Fault. The red arrow indicates the sense of fault movement. Bb) A hand specimen from
1286 | the deformed Scaglia formation showing ~~the intensity of the abundant~~ pressure ~~solutions-solution~~
1287 | ~~seems~~ (TS), indicated by arrows, and their abutting relationship with cross-cutting calcite veins
1288 | (CV2C2). Cc) A transmitted light photomicrograph of the dolomitized, brecciated Calcare
1289 | Massiccio Formation. Note all the breccia fragments are composed of dolomite (D4 here).

1290 |
1291 | Fig. 4. Field photographs (Corano Quarry) showing the field relations between dolostones (only
1292 | D3 here), host limestones and the Montagna dei Fiori Fault: Aa) Panoramic view showing the
1293 | spatial relationship between limestones and dolostones (orange) in the damage zone of the
1294 | Montagna dei Fiori Fault (F). Note that the limestones and including dolostones of the Calcare
1295 | Massiccio and Bugarone Formations on the footwall (FW) and marly limestones of the Scaglia
1296 | Formation on the hangingwall (HW) are intensely deformed. Bb) Plan view of the dolomitized
1297 | Calcare Massiccio limestone in the footwall damage zone: intersected by calcite veins (CV4C1),
1298 | which are partially dolomitized, and affected by ~~bed-bed~~-perpendicular stylolites (arrows). Cc)
1299 | Distinct transition (dashed line) between dolomitized and undolomitized Calcare Massiccio
1300 | limestone in the footwall damage zone.

1301 |
1302 | Fig. 5. Field photograph (Aa) and a simplified sketch (Bb) in field site d showing of a dolomitic
1303 | pocket (grey color) ~~within the folded Calcare Massiccio (grey color)~~ and ~~their-its~~ relation with
1304 | ~~bed-bed~~-parallel stylolites within the Calcare Massiccio Formation (hammer is 40 cm long). Note
1305 | C1 is the only calcite cement here.

1306 |
1307 | Fig. 6. Undolomitized and dolomitized Calcare Massiccio Formation in field site d: Aa)
1308 | Transmitted light image showing a micritic peloid rimmed by ~~the~~-fibrous cements (FC) which
1309 | are ~~followed-overgrown~~ by ~~the~~-mosaic cements (MC). Bb) Transmitted light image showing
1310 | mosaic cements (MC) in a peloidal limestone over-printed by high amplitude ~~bed-bed~~-parallel

1311 stylolites (dotted white line). Note the core of some of the peloids is partially cemented as well.
1312 **Cc, Dd**) Respectively, transmitted light and corresponding cathodoluminescence image of FC
1313 and MC cements. **Ee**) Transmitted light photomicrograph showing D1 crystals (arrows) rimming
1314 lining a fracture which is cemented by EV1C1. The fracture is in turn affected by a bed-bed-
1315 parallel stylolite. **Ff**) Cathodoluminescence image showing D1 scattered in the host rock and
1316 riming the fracture. **Gg, Hh**) Respectively, transmitted light and corresponding
1317 cathodoluminescence image showing part of a bed-bed-parallel stylolite (dotted white line)
1318 overprinting D1 and D2 crystals.

1319

1320 Fig. 7. **Aa, Bb**) Photomicrographs of respectively, transmitted light and corresponding
1321 cathodoluminescence image showing the zoned rhombs of D2 with the remnants of D1 preserved
1322 in their cloudy core sampled from dolomitized Calcare Massiccio Formation in field site d. The
1323 pore space is occluded by D4. **Cc, Dd**) D3 cementing angular breccia fragments of the Bugarone
1324 Formation in the damage zone of the Montagna dei Fiori Fault in the Corano Quarry site. Note
1325 the breccia is overprinted by a fault-fault-parallel bed-bed-perpendicular stylolite. **Ee, Ff**)
1326 Photomicrographs of respectively, transmitted light and corresponding cathodoluminescence
1327 image showing the euhedral to subhedral crystals of D3 entirely replacing the matrix and also
1328 present as cement developing a bright subzone and rim sampled from dolomitized Corniola
1329 Formation in Osso-caprino road. **Gg, Hh**) D3 with a saddle crystal outline (SD) postdating calcite
1330 cements (MC) and a zoned D2 crystal. The saddle morphology is outlined by a dotted white line.

1331

1332 Fig. 8. Photomicrographs of respectively, transmitted light and corresponding
1333 cathodoluminescence image of dolomite types: **Aa, Bb**) The cross-cutting relationship between
1334 D3 and D4 sampled from dolomitized Corniola Formation in Osso-caprino road. Note the
1335 presence of D3 within the core of dolomite crystals overgrown by D4. **Cc, Dd**) Successions of
1336 dolomite types sampled from dolomitized Calcare Massiccio Formation in field site f. Note the
1337 green CL color of D4 crystals. Typically, luminescent dolomites are known to show yellow,
1338 orange to red colors (Machel et al., 1991). Green luminescence in carbonates including dolomite
1339 have been attributed by a number of researchers to the incorporation of three valent rare earth
1340 elements (REE) such as Dy^{3+} and U^{3+} as luminescence activators within their crystal lattice
1341 (Luczaj and Goldstein, 2000). Another possibility is the emplacement of Mn^{2+} , with yellow

1342 luminescence, in Ca²⁺ sites with blue luminescence in the dolomite crystal lattice instead of
1343 preferential incorporation in the Mg²⁺ site (Sommer, 1972b; Amieux, 1982; Walker et al., 1989;
1344 Habermann et al., 1999). Accordingly, non-stoichiometric, Ca-rich and poorly ordered dolomites
1345 may favor Mn²⁺ incorporation into their Ca²⁺ site. ~~Ee, Ff~~) Vuggy porosity rimmed by D4 (green
1346 CL). Note the porosity is filled with fine dolomite rhombs including traces of D2 in their core
1347 and D4 overgrowths.

1348

1349 Fig. 9. Photomicrographs showing respectively, transmitted light and corresponding
1350 cathodoluminescence image of D4 and D5 in relation to stylolites and fracturing: ~~Aa, Bb~~) D4,
1351 exploiting a ~~bed-bed~~-parallel stylolite that crossed-cuts D1 and D2 sampled from dolomitized
1352 Calcare Massiccio Formation in field site d. ~~Ec, Dd~~) A sub-horizontal fracture cemented by D4
1353 sampled from dolomitized Corniola Formation in field site f. ~~Ee, Ff~~) D5 microveins (arrows)
1354 intersecting all the predating dolomite types in the footwall brecciated zone of the Montagna dei
1355 Fiori Fault-, sampled from dolomitized Calcare Massiccio Formation in Castel Manfrino site.

1356

1357 Fig. 10. Field photographs showing the major calcite vein settings observed in Montagna dei
1358 Fiori: ~~Aa~~) Cross-sectional view of bed normal Calcite vein 1 (~~CV1C1~~) abutting ~~bed-bed~~-parallel
1359 stylolites in folded beds of the Calcare Massiccio Formation. ~~Bb~~) Plan view of the Calcite vein 2
1360 (~~CV2C2~~) intensely affecting the deformed Scaglia (Rossa) Formation. ~~Ec, Dd~~) Cross-sectional
1361 view of the Scaglia Formation, intensely affected by pressure solution seams of tectonic origin
1362 crossed-over by populations of bed-perpendicular Calcite veins (~~CV3C3~~) in en echelon
1363 extensional arrays.

1364

1365 Fig. 11. ~~Aa~~) Cathodoluminescence and transmitted light (in set) image showing blocky to
1366 elongated crystals of ~~CV1C1~~ with zoned CL pattern in the Corano Quarry site. ~~Bb~~) Transmitted
1367 light image showing intensely twinned ~~CV1C1~~ crystals overprinted by euhedral to subhedral
1368 crystals of D3 in the Corano Quarry site. Photomicrographs of respectively, transmitted light and
1369 corresponding cathodoluminescence image: ~~Ec, Dd~~) ~~CV2C2~~ in the Scaglia Formation abutted by
1370 a ~~bed-bed~~-perpendicular stylolite (indicated by white arrows and dashed line) in the Corano
1371 Quarry site. The crystals display blocky to fibrous morphologies, deformation twinning, and a
1372 similar orange luminescence pattern ~~comparable with~~ similar to the adjacent host rock. ~~Ee, Ff~~)

1373 | [EV3C3](#) cementing the breccia fragments in the damage zone of the Montagna dei Fiori Fault.
1374 | The crystals are blocky and show faint deformation twinning. They are brown-orange with
1375 | distinct darker luminescence sector zones. [Gg](#), [Hh](#)) [EV4C4](#) present as a cement within a
1376 | polygonal pore space rimmed by dolomite-, [sampled from dolomitized Calcare Massiccio](#)
1377 | [Formation in field site f](#). Note the blocky crystals, absence of deformation twinning and distinct
1378 | concentric luminescence zonation pattern. [EV4C4](#) is corroded and followed by a late telogenetic
1379 | calcite.

1380

1381 | Fig. 12. ~~A, B~~ Overview of the $\delta^{13}\text{C}$ and $\delta^{18}\text{O}$ values of dolomites ([Aa](#)) host rocks from
1382 | Montagna dei Fiori as well as calcite veins ([Bb](#)). The stable isotope value of Lower Jurassic
1383 | marine limestones based on Veizer et al. (1999) is indicated by a dashed rectangle in subset B.
1384 | The $\delta^{18}\text{O}$ values of the marine dolomites are considered to be 3-4‰ V-PDB higher than those of
1385 | marine limestones (Land, 1980; Major et al., 1992; Horita, 2014). [Cc](#)) Cross-plot of $^{87}\text{Sr}/^{86}\text{Sr}$
1386 | ratios and corresponding $\delta^{18}\text{O}$ values of host rocks, dolomites and calcite veins compared with
1387 | Lower Jurassic marine carbonates $^{87}\text{Sr}/^{86}\text{Sr}$ (dashed rectangle) framework reported by McArthur
1388 | et al. (2012).

1389

1390 | Fig. 13. Overview of microthermometry analysis of primary inclusions in Montagna dei Fiori:
1391 | [Aa](#)) Frequency distribution of the $T_{m_{ice}}$ (°C) in dolomite [phases types](#). [Bb](#)) Frequency distribution
1392 | of the T_h (°C) in dolomite [phases types](#). [Cc](#)) Salinity (eq. wt. % NaCl) versus T_h (°C) of dolomite
1393 | and calcite phases. [Dd](#)) Isotopic fractionation diagram from Land (1983) used to determine the
1394 | isotopic composition (‰ V-SMOW) of parental fluids in equilibrium with dolomites in
1395 | Montagna dei Fiori.

1396

1397 | Fig. 14. ~~A~~) Generalized paragenesis of diagenetic phases in relation to deformational stages and
1398 | burial history of the Calcare Massiccio Formation in the Montagna dei Fiori Anticline. The
1399 | deformational stages are from Storti et al. (2018), and the burial curve is based on Ronchi et al.
1400 | (2003). [The burial curve was made based on paleo-depth, paleo-temperatures, sedimentation rate](#)
1401 | [and paleo-heat flow.](#)

1402

1403 Fig. 15. Sketch showing the successive fault-related diagenetic phases, of most importantly
1404 dolomitization, recorded in the carbonate succession exposed at the core of the Montagna dei
1405 Fiori Anticline (not scaled). Different diagenetic phases are indicated with different colors. **Aa)**
1406 The first dolomitization event is pre-orogenic (syn-rift), triggered from the fluids channelized
1407 along Jurassic ~ E-W and ~ N-S striking extensional faults. This event occurred during burial
1408 compaction and development of bed-bed-parallel stylolites (BS). It is represented by scattered
1409 dolomite rhombs (D1) followed by calcite cementation (**CV1C1**). The dolomitization continued
1410 with precipitation of larger crystals of D2. **Bb)** Second dolomitization event: syn-orogenic (early
1411 folding/ faulting) dolomitization from fluids that migrated from more internal regions of the
1412 thrust belt and were channelized along the basal detachment level into the fold core. This
1413 dolomitization event presents matrix replacive and cements displaying infrequent saddle outlines
1414 (SD) in pore spaces, within bed-bed-parallel veins and shear fractures. These dolostones postdate
1415 compaction but are affected by bed-bed-perpendicular stylolites (TS) generated by horizontal to
1416 sub-horizontal layer-layer-parallel shortening related to the growth of the Montagna dei Fiori
1417 Anticline. **Cc)** Extensional collapse of the anticline and development of the Montagna dei Fiori
1418 Fault, followed by buttressing of the Scaglia against Calcare Massiccio and Corniola Formations
1419 during positive inversion induced by continuing underthrusting at depth. Precipitation of D5 in
1420 micro-veins and cements in breccia zones, followed by late stage calcite cementation in the
1421 Montagna dei Fiori Fault damage zone (**CV2C2**, **CV3C3** and **CV4C4**).

	Stable isotopes		Sr isotopes	Fluid inclusion microthermometry		
	$\delta^{13}\text{C}$	$\delta^{18}\text{O}$	$^{87}\text{Sr}/^{86}\text{Sr}$	Th (°C)	Salinity	n
Calcare Massiccio Fm.	+2.4 to +3.1	-1.6 to 0.0	0.70766	-	-	
Corniola Fm.	+2.0 to +2.5	-3.1 to -1.4	0.70725	-	-	
Scaglia Fm.	+1.0 to +3.1	-2.2 to -1.0	0.70784-0.70791	-	-	
D1	+2.5	-1.9	0.70789	≤ 40-50	3.5 to 11.3	<u>27</u>
CV1	+1.6 to +2.1	-4.7 to -2.7	0.70773	-	-	=
D2	-	-	-	≤ 40-50 to 71	7.9 to 20.5	<u>37</u>
D3	+2.0 to +2.6	-2.8 to -1.9	0.70859-0.70964	70 to 73	9.2 to 16.9	<u>9</u>
D4	+2.4 to +2.5	-3.0 to -2.5	0.70790	79 to 105	12.8 to 18.6	<u>7</u>
CV2	+1.2 to +3.1	-1.7 to -1.6	0.70779 - 0.70787	-	-	
CV3	+0.5 to +2.4	-2.2 to 0.0	-	≤ 40-50	4.5 to 9.7	<u>9</u>
CV4	+3.8 to +4.9	-9.4 to -9.1	-	≤ 40-50	0.17 to 3.0	<u>19</u>

Table. 1

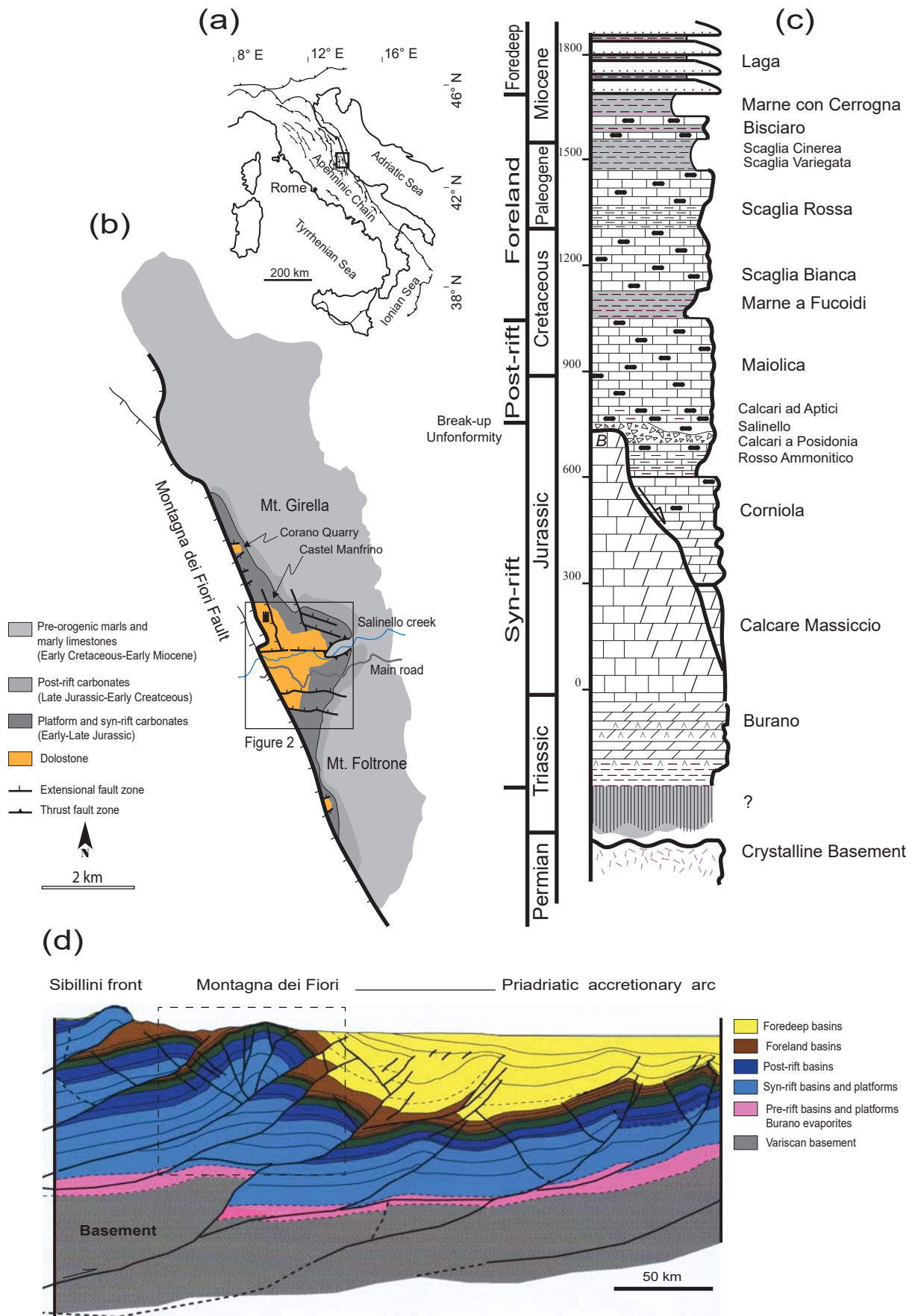


Fig. 1

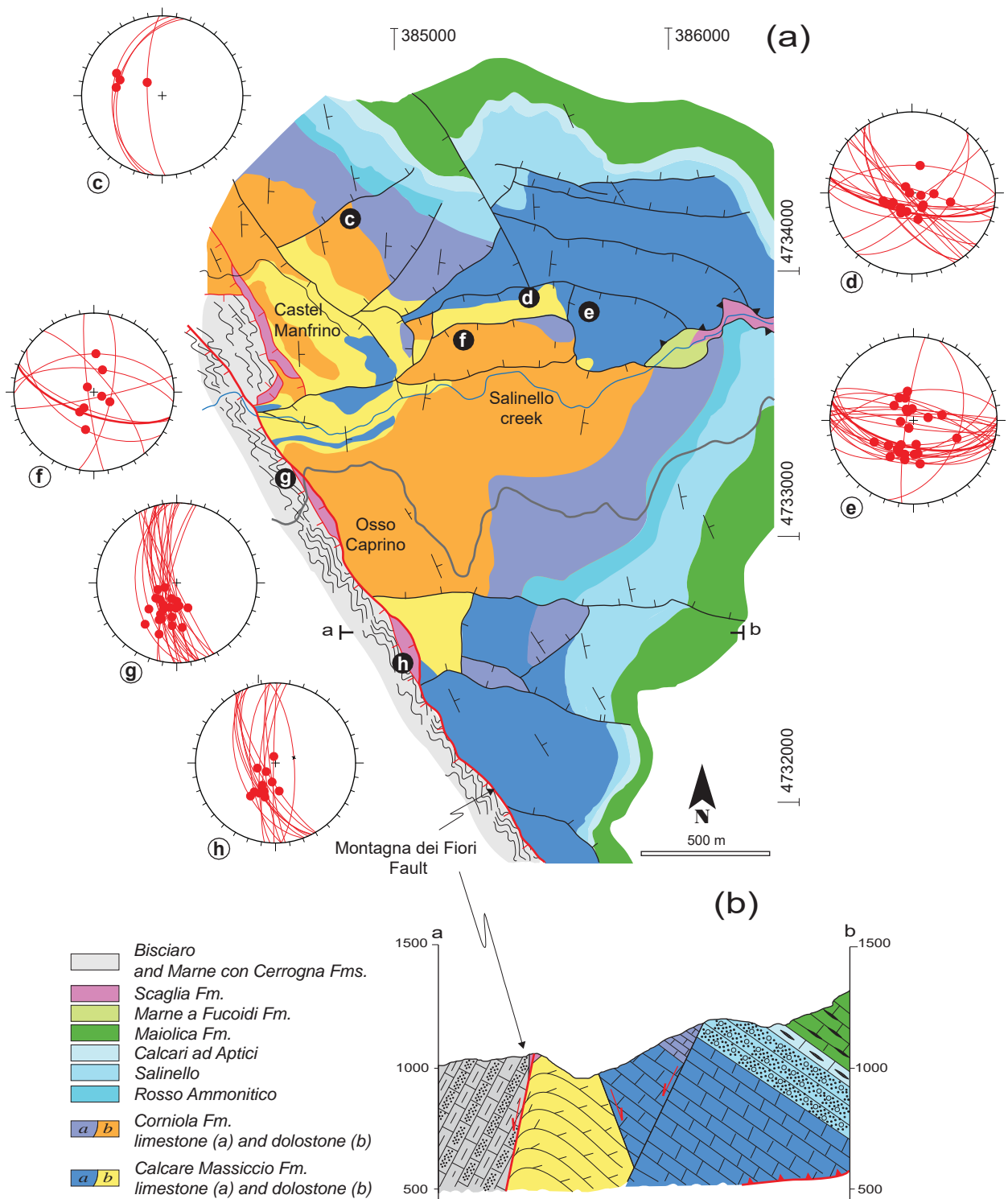


Fig. 2

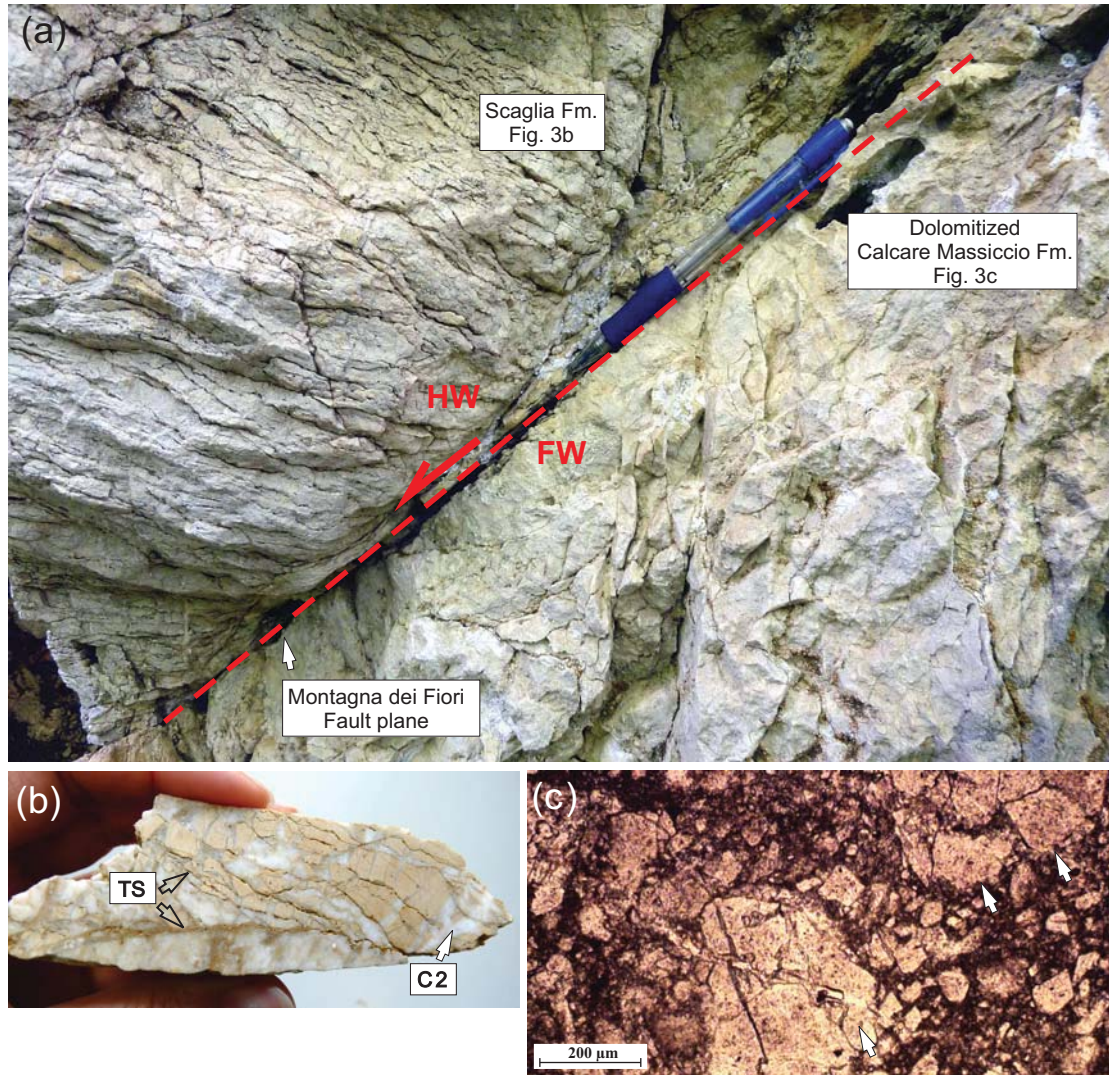


Fig. 3

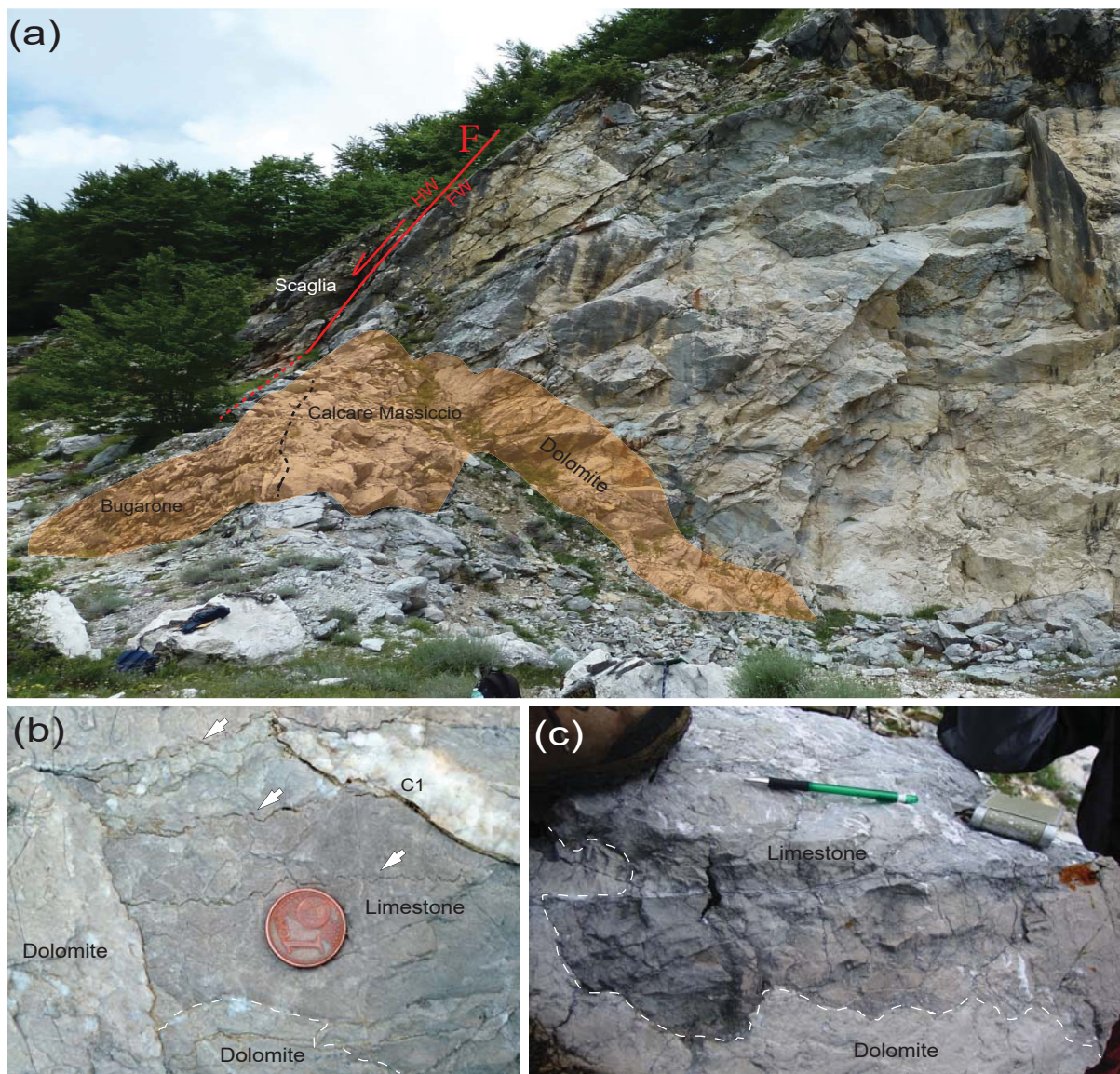


Fig. 4

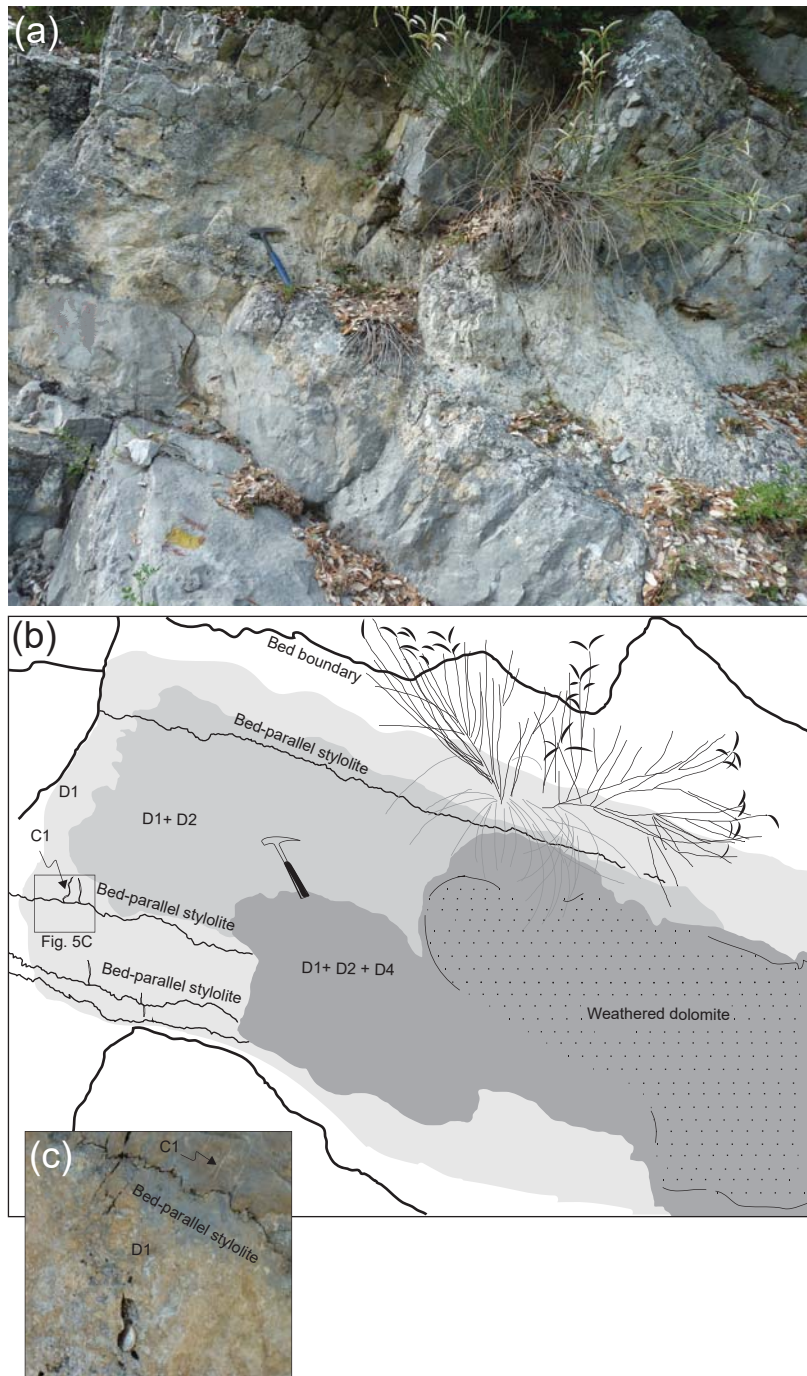


Fig. 5

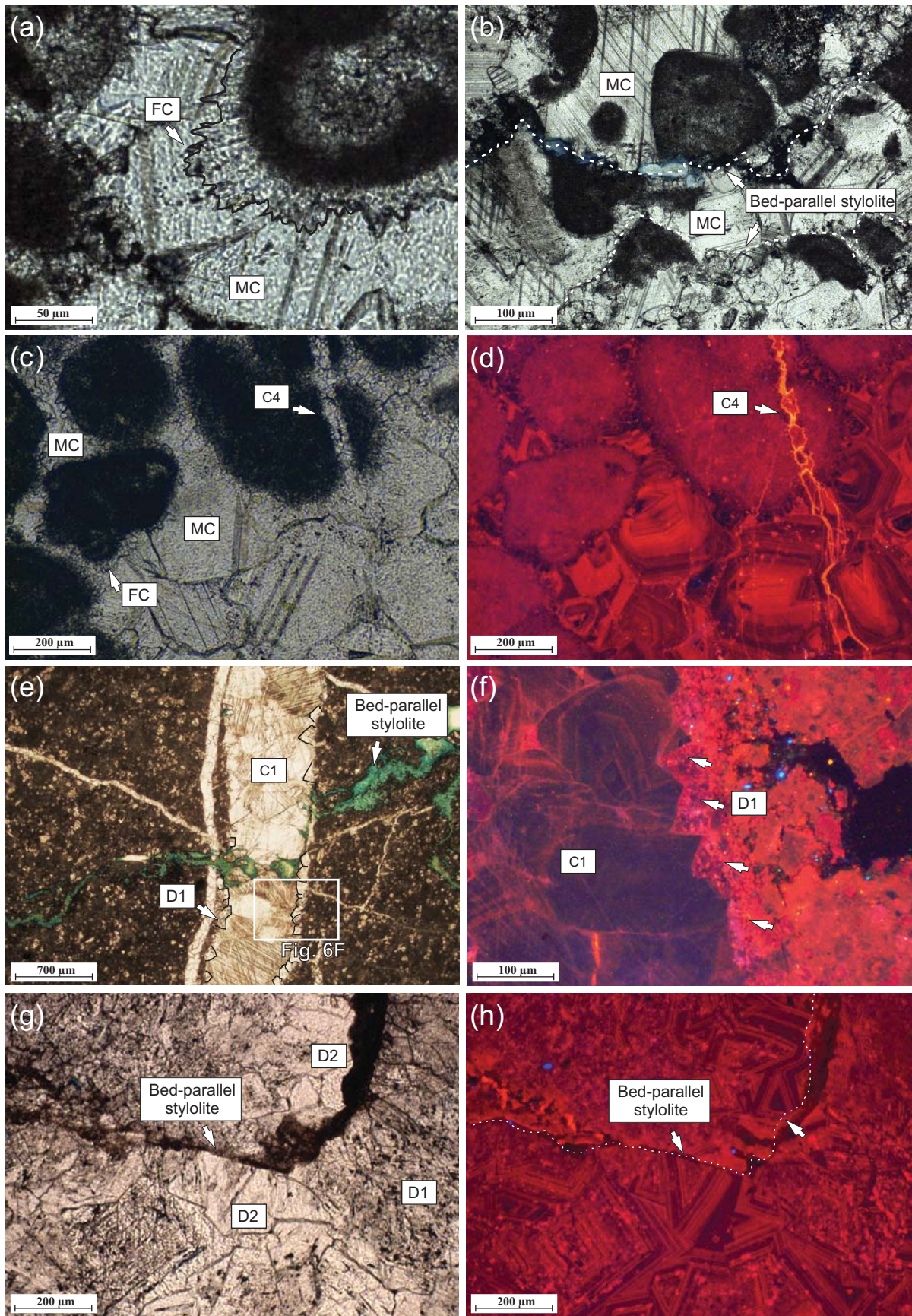


Fig. 6

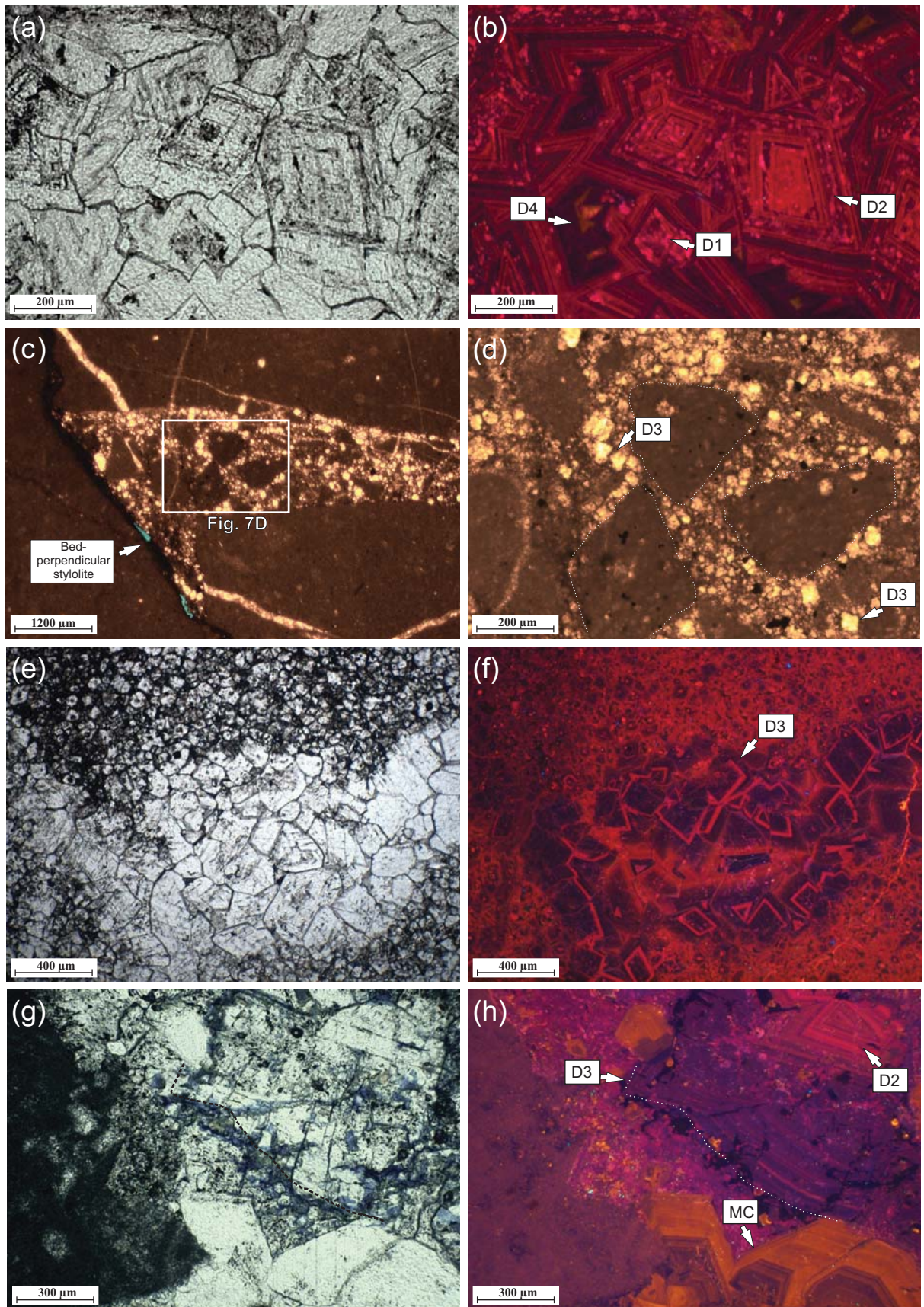


Fig. 7

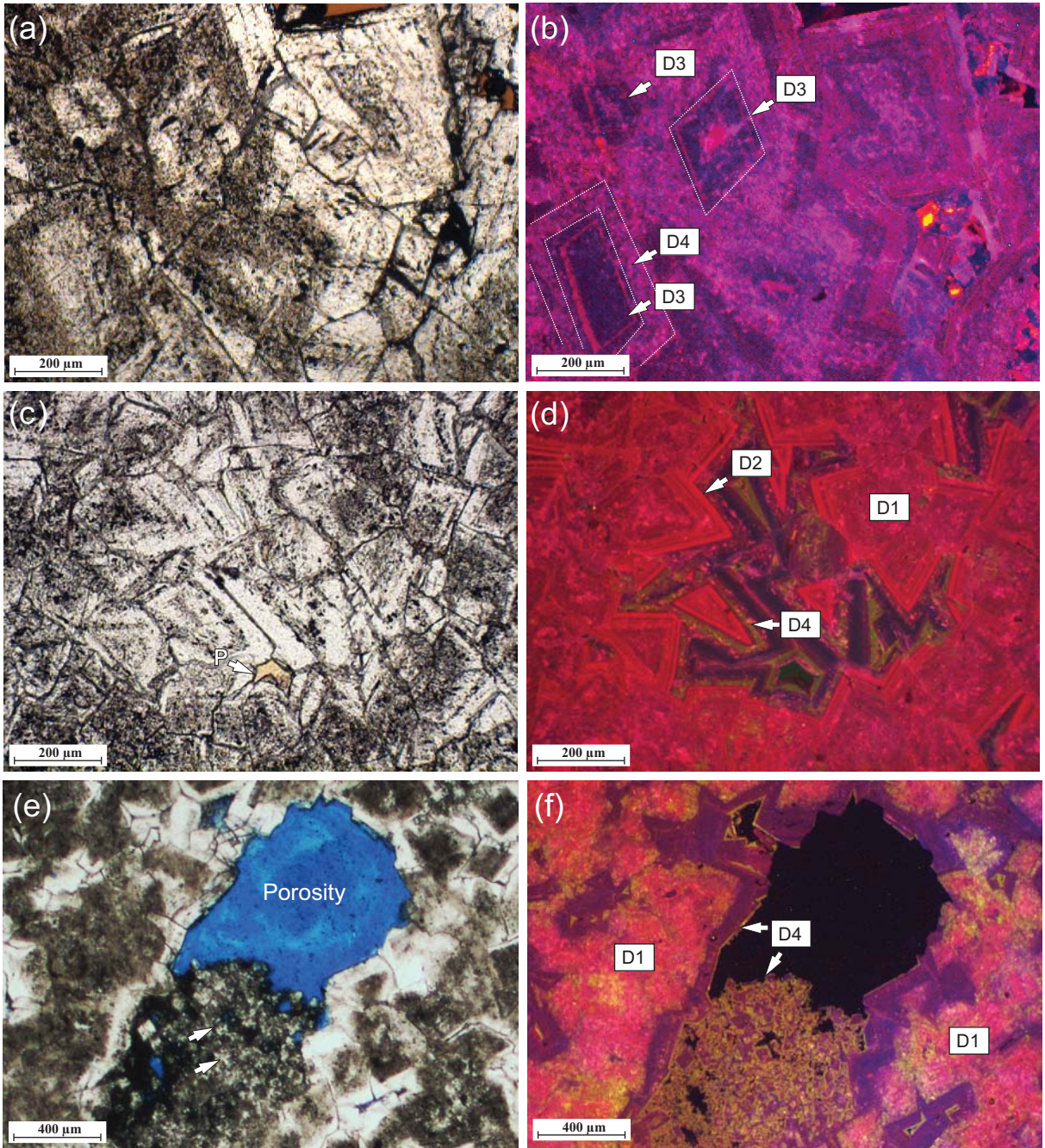


Fig. 8

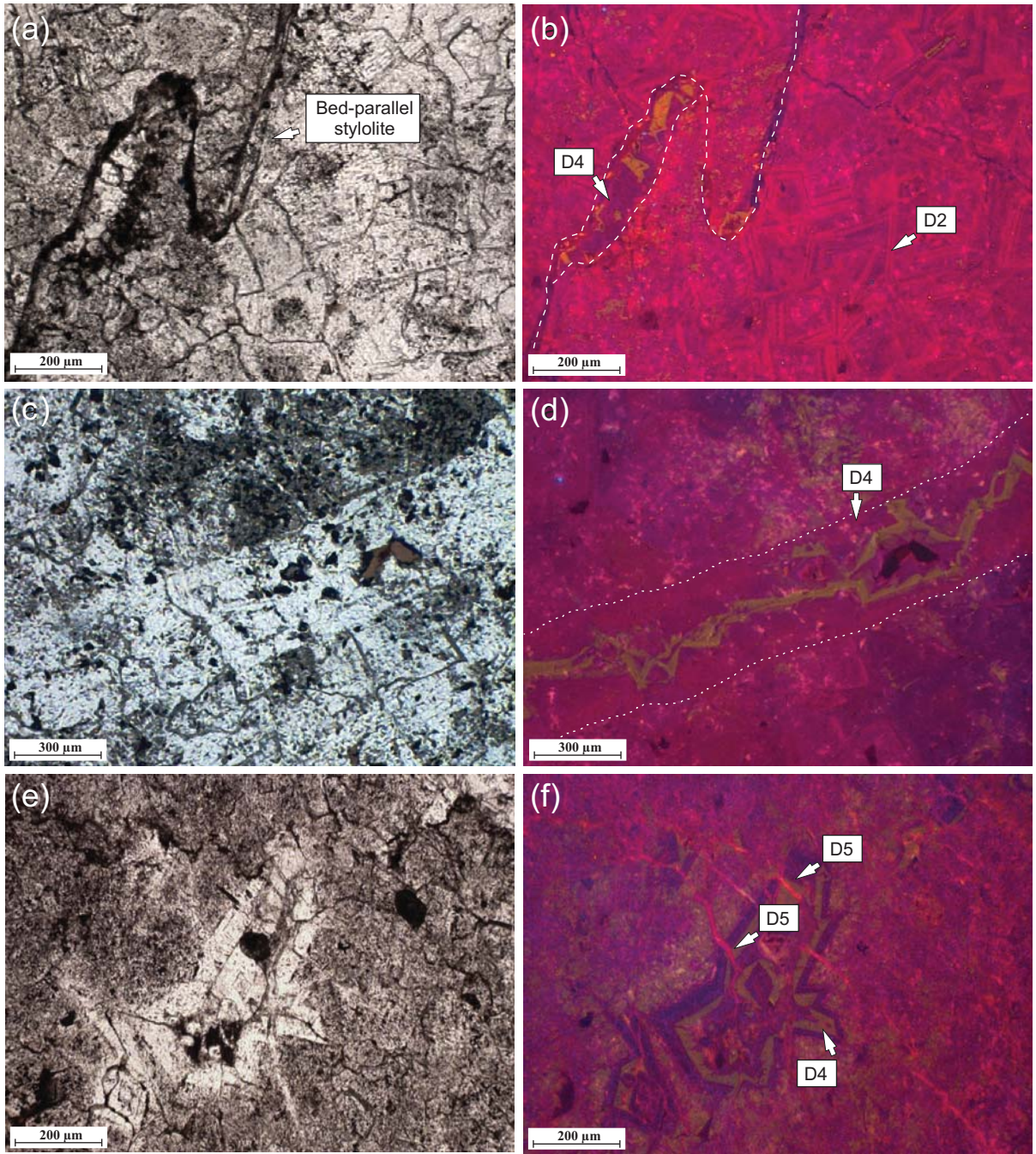


Fig. 9

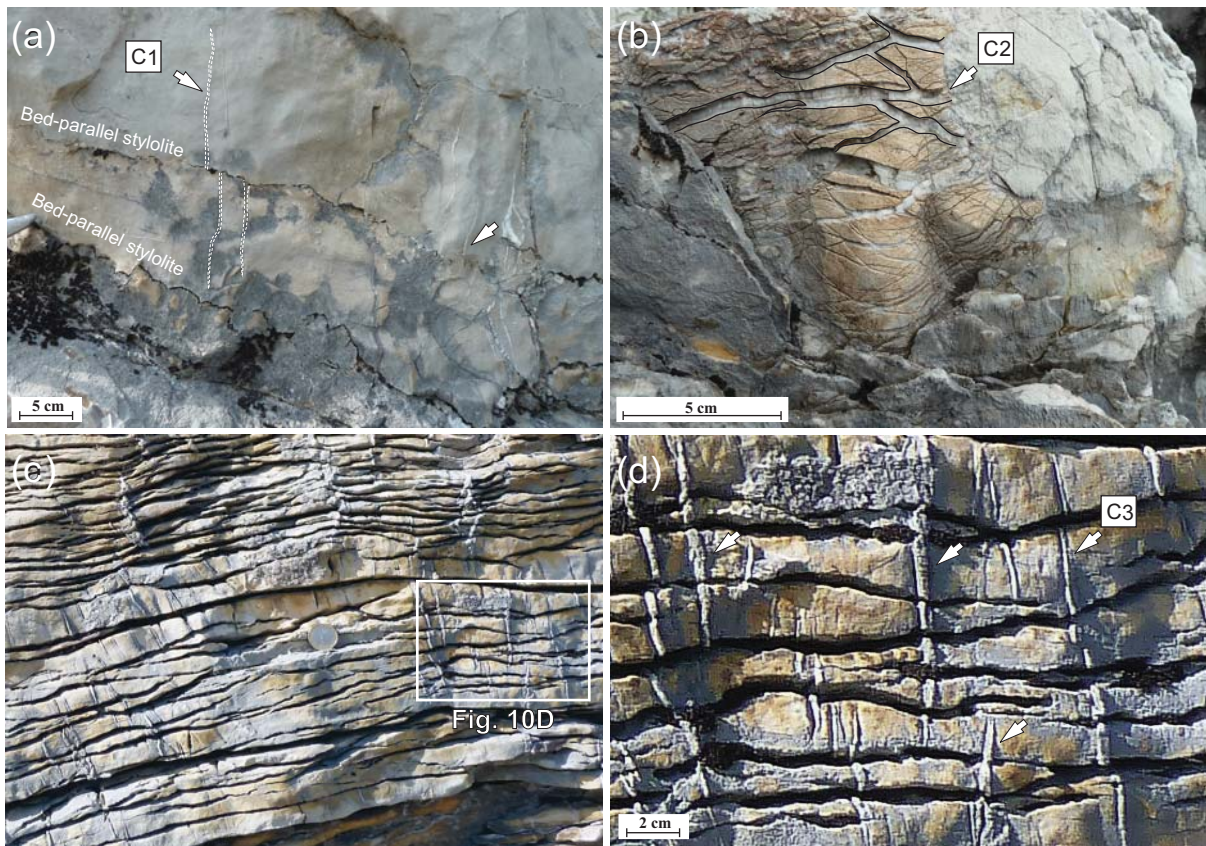


Fig. 10

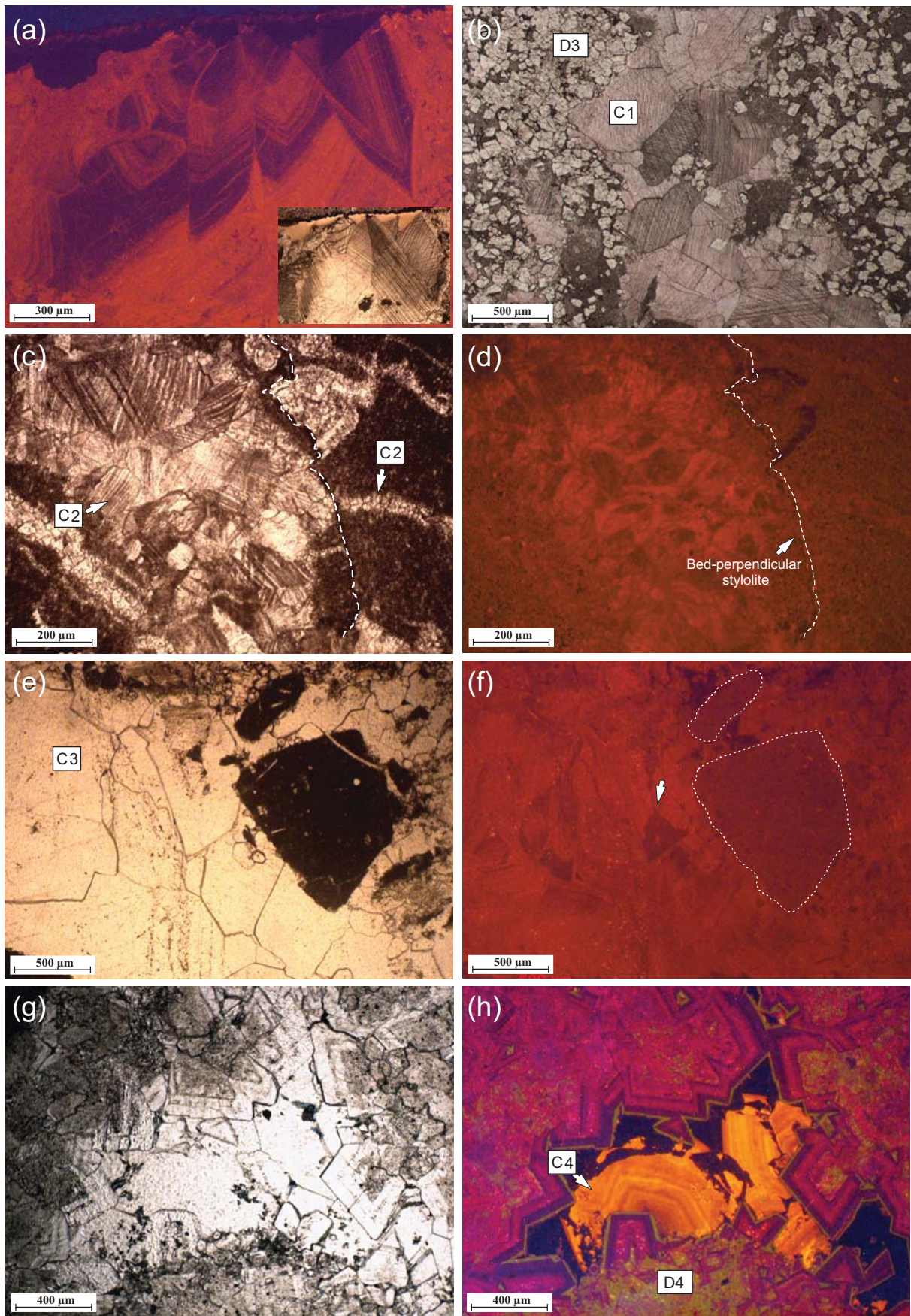


Fig. 11

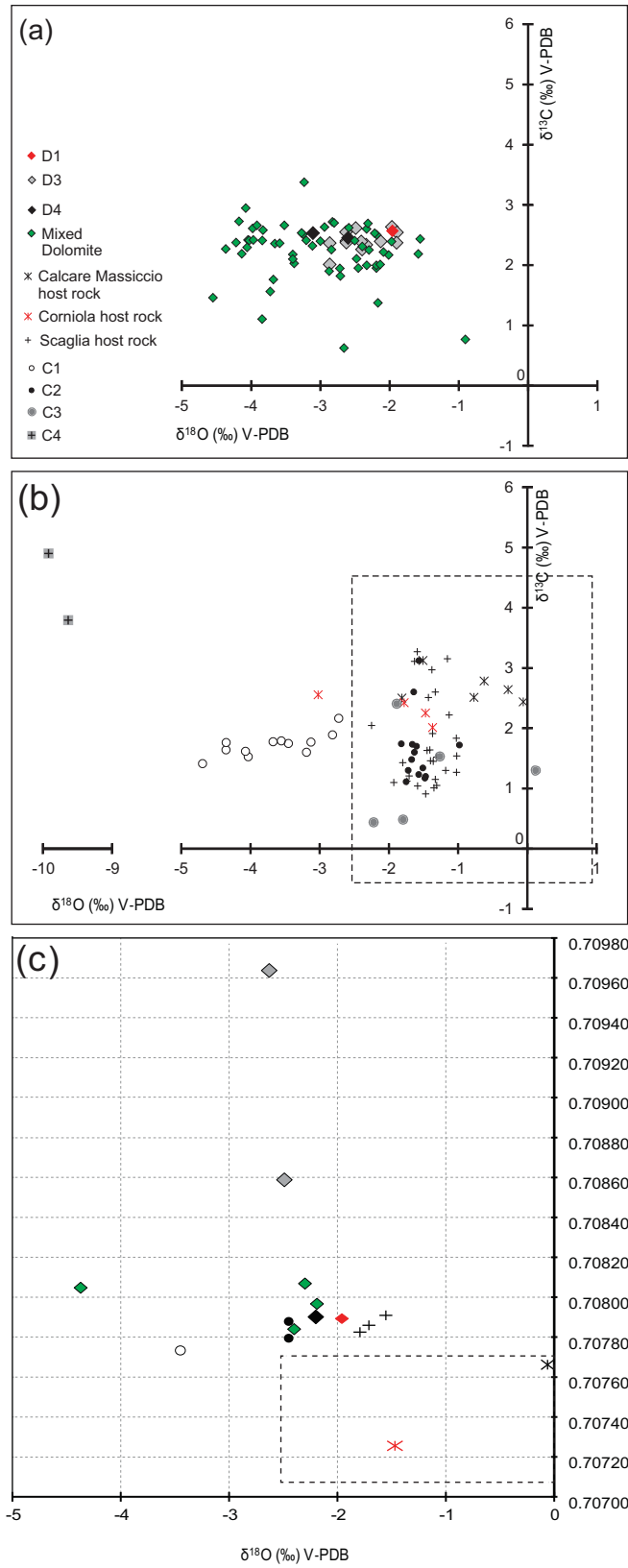


Fig. 12

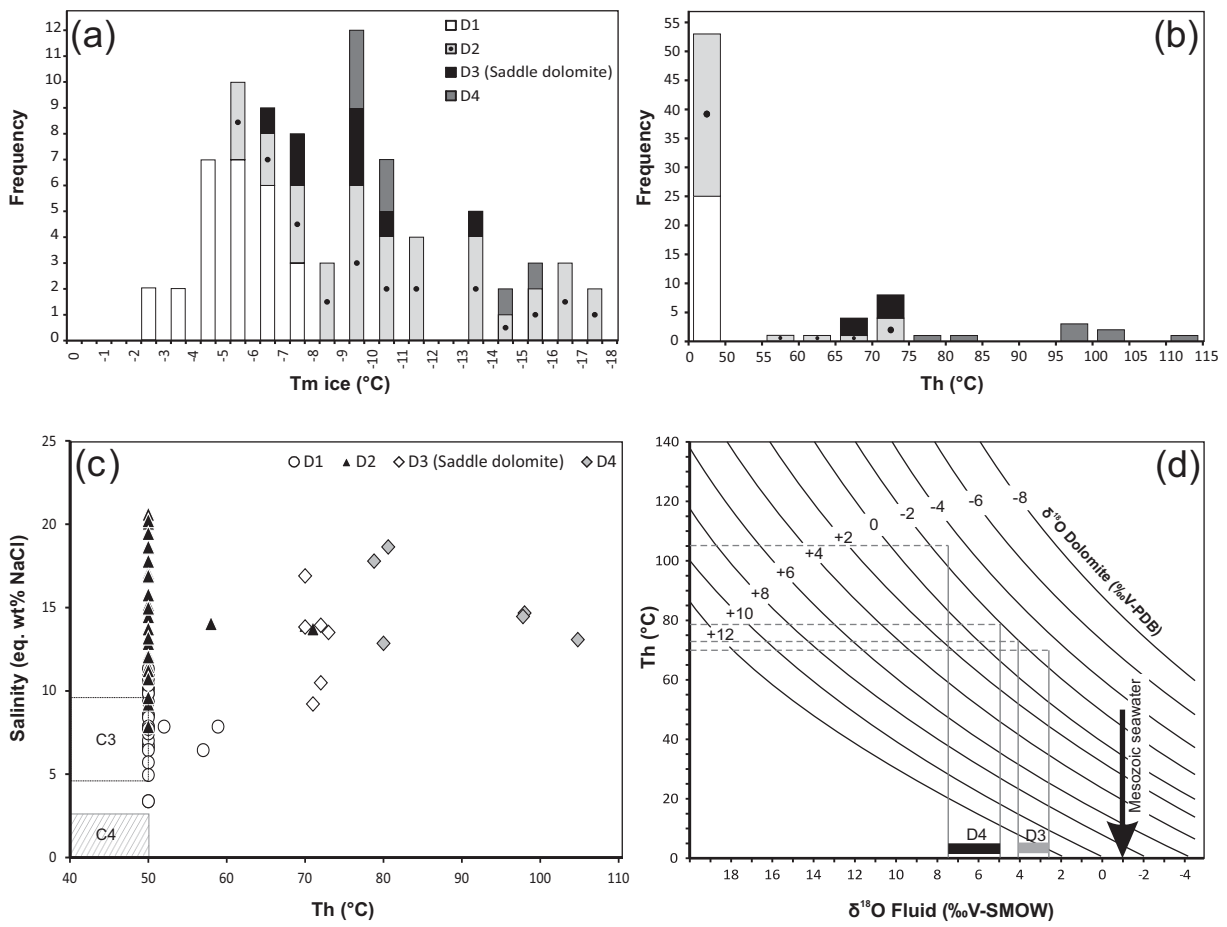


Fig. 13

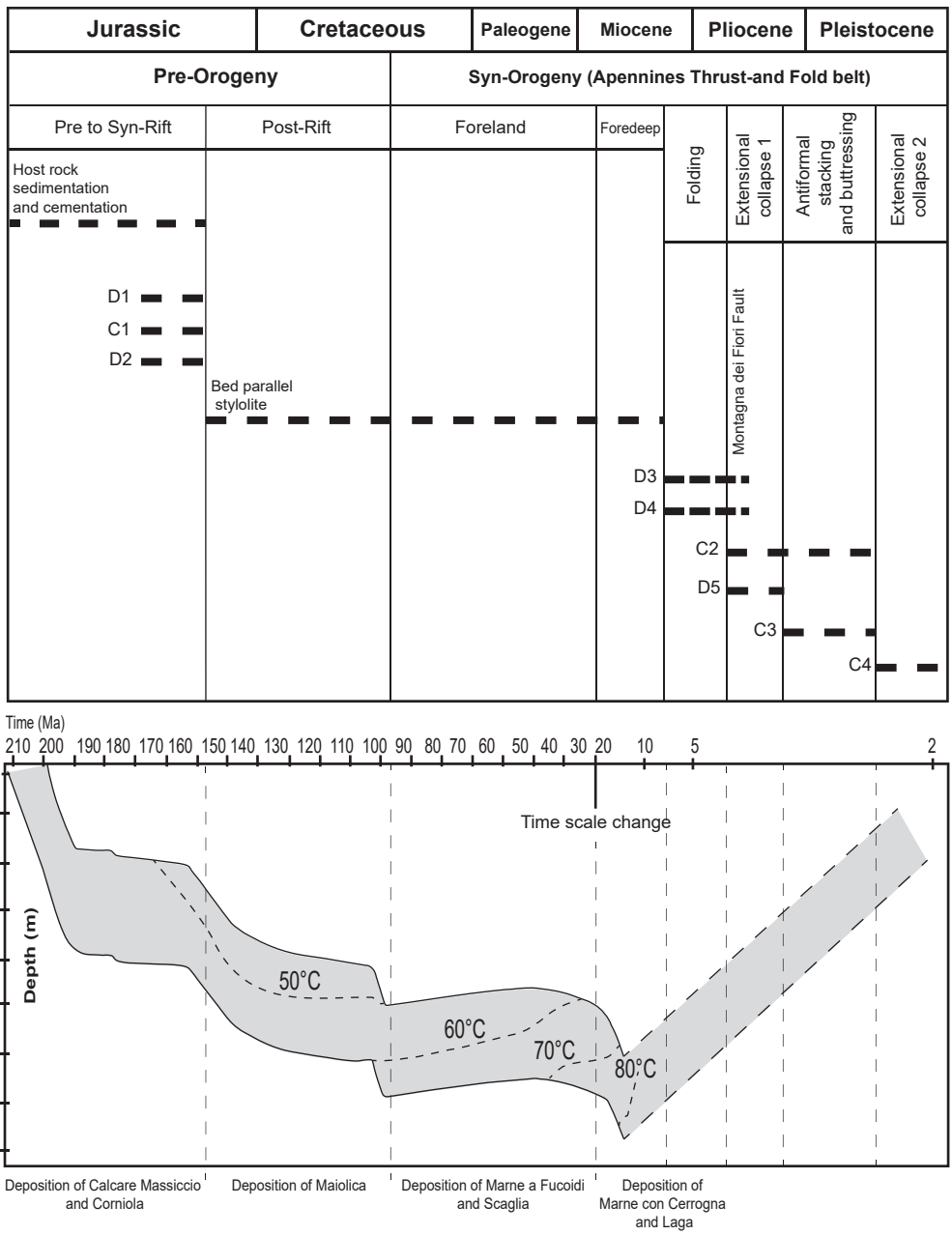


Fig. 14

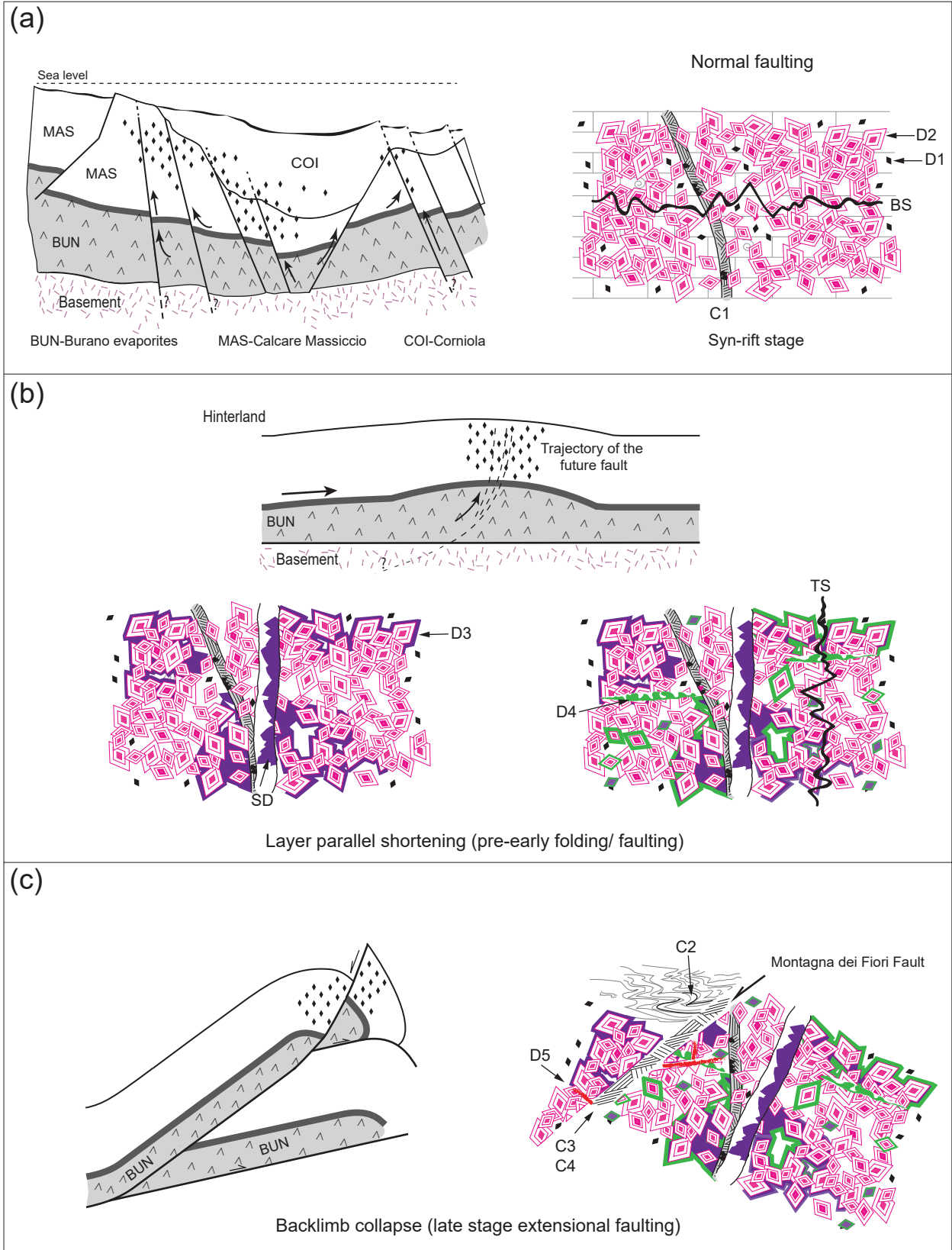


Fig. 15

Review of “Fault-related dolomitization in the Montagna dei Fiori Anticline (Central Apennines, Italy): Record of a dominantly pre-orogenic fluid migration. Se-2018-136

This manuscript presents field, petrographic and geochemical data from non-stratabound dolomites in a complex tectonic setting, and interprets their geofluid origin (parent fluids, timing) in the context of the tectonostratigraphic history.

It is coherent and logically organised. Aspects of the written English need minor improvement (punctuation, plurals, word order, etc); it will benefit from a final revision by a native English speaker.

The data are generally of good quality, and the interpretations are mostly justified from the results presented. In any study such as this, with limitations imposed by the ability to sample all the phases, there is necessarily some latitude or flexibility in the deductions that can be made. However, the authors do a good job of considering alternative possibilities for the fluid sources and timings.

My only issue with the paper is that the authors have not really considered whether there are wider implications or generic advances that can be made from the research. It presents itself as a case study, albeit one with a good integration of structural and diagenetic data. But what is the wider impact that will attract a non-specialist readership? Within the paper the authors all but admit that their findings are only modestly advanced from those of Ronchi and co-workers fifteen years ago (lines 638-642). I had hoped to see more progression in the science, and maybe the authors need to more thoroughly and critically evaluate the Ronchi model in the light of their new data. They could also work the structural data more – rather than just considering fault orientations and timings, what about the character and extent of the damage zones associated with different fault types / generations, and their relationship to the size and shape of dolomite bodies? What determines the lateral extent of dolomites? Is it other faults / fractures, or a gradual reaction front?

One generic aspect that the authors could address is implications for reservoir potential in analogues for this setting. The preponderance of planar dolomite is significant because planar dolomite is usually very beneficial for porperm (unlike many examples of hydrothermal dolomitization that feature tight nonplanar dolomites). Are there dolomitised plays in the Middle East that this study could be compared to (Zagros Mountains for example?), or maybe in Mexico?

Another factor of interest, largely by-passed in the text, is what drove the fluid circulation necessary to cause massive dolomitization when the low temperatures argue against a hydrothermal syn-rift system. Can the authors attempt a mass balance to estimate the order of magnitude fluid volumes needed? Maybe the dolomitization occurred in the down-flowing (cool) limb of a convection cell established on syn-rift faults that breached contemporary sea bed? Or does the dolomite zoning imply a pulsed fluid flow associated with strain cycling or seismic valving? I recommend the recent papers by Hollis and others on the Hammam Faraun fault and related syn-rift dolomitization. Are the D1-2 dolomites formed in a similar manner to this geologically younger example? Likewise, with the later dolomitization, which structures would have been open during compressional tectonics and able to serve as conduits for substantial fluid volumes?

If the authors address these issues their paper, which is already technically good, it will have much greater impact and interest across the sedimentary and structural geoscience community.

I have some more **specific comments** – these are tagged by line number or Figure number:

Line 43: The paper describes the role of evaporite-sourced fluids in the dolomitization process, but I am not sure that it illustrates a controlling role of evaporitic detachments. These may have influenced the tectonic development, but if it is believed that they directly controlled the dolomitization this needs to be specifically discussed later in the paper. **Emphasized more in the text**

Note the abstract is quite long-winded. It would be good to make it more succinct and punchier. **Addressed**

Line 69: The Castel Manfrino Dolostones are not labelled in Fig. 1 or Fig. 2b. **Added in Fig.1**

Line 73, 76: Did Ronchi (2003) base her study on the mapping of Mattei (1987)? Maybe there needs to be a couple of sentences describing Ronchi's findings so that it can be more clearly shown that the understanding has moved on. **Added to text**

Line 79-83: This is very long-winded and vague. It either needs to be shortened or to include specific details. **The sentence is shortened.**

Line 129: Given that the early dolomitization (D1-2) is later ascribed to the syn-rift stage, it would be useful to briefly describe the facies and architectural character of the syn-rift carbonates. For example, were they preferentially developed on footwall highs, in which case there was likely a juxtaposition of permeable high energy facies against faults that later hosted fluid flow? **Addressed**

Line 135-137: It may be a matter of debate, but the authors need to either provide the conflicting evidence or at least express a view and justify it. **The sentence is deleted as further discussion is not the focus of this research**

Line 152: Can the Montagna dei Fiori fault be indicated / labelled on Fig. 1d? **Addressed**

Line 164: Ground truthing implies that the features had previously been mapped out using remote data. If so, this should be included in the methods. **Addressed**

Line 167: So far as I can see, the Sibley and Gregg (1987) terminology (planar-e, planar-s, nonplanar) is <not> used anywhere in the paper, so either it needs to be incorporated or this sentence should be removed. **The sentence and related references are removed**

Line 186: Can the reproducibility ($\pm 0.1\%$) be smaller than the precision ($\pm 0.2\%$)? **The inter-lab reproducibility is $\pm 0.1\%$ means the measurement for the same sample in two different labs has a difference of $\pm 0.1\%$**

Line 224: Bugarone Formation is not shown on Fig. 1 or Fig 2. **Addressed**

Line 231: Is the wider distribution of dolomitized intervals related to the topography of the valley and the exposures? If not, what is the relationship? **Addressed**

Line 238: I suggest not using "overprinted", which implies the original fabric / lithology is lost. Why not just use "cross-cut"? (or even just "cut") **Addressed**

Line 258 and elsewhere: "Dull" is not a colour! **Addressed**

Line 261 onwards: There could be a bit more detail on the dolomite distribution and fabric with respect to host rock facies. Is it all texturally destructive, is there any textural or mineralogical selectivity, were grainy or muddy facies preferentially dolomitized (controls by permeability versus reactive surface area.....?) **Addressed**

Line 272: There is an issue because CV1, CV2 etc. are introduced before they have been defined and described. I suggest starting section 4.2 with a paragenetic summary to alleviate this problem. **Addressed, paragenesis is presented in Fig. 14.**

Line 278: By using “frequently” the text suggests that sometimes (infrequently) D2 post-dates bed-parallel stylolites. Is that the case? **Addressed**

Line 284-285: This sentence needs a figure citation. **Addressed**

Line 297: Repetition of “euhedral to anhedral” (cf. line 295) – note this is not Sibley and Gregg terminology. Nor is “tightly packed texture” in line 279. **Addressed**

Line 305: I do not think one dolomite can “recrystallize” another. Recrystallization is a solid-state process that increased mineral stability. To demonstrate it might need data on the ordering, crystallinity and stoichiometry of D1/2 versus D4 (do the authors have any XRD data?). What is more likely is that D4 has locally replaced D1 and D2 by a dissolution-precipitation mechanism. However, the text lacks a clear description of the evidence for replacement. I recall papers by Mazzullo and by Machel that discuss this – it would be good to list the criteria for this case. **Addressed**

Line 330: In Fig. 11C, D the dolomite does not appear to be yellow-orange, it looks more like orange-brown. **Addressed**

Line 332: How wide was the extensional fault master plane? Please supply the range of widths (and lengths where possible) of the different vein generations. **It is addressed for vein generations.**

Line 335-336: What is meant by “with no evidence of physical disruption”? Does it mean that CV3 always passively overgrows D5 in voids and never cuts it? If so, it is easier to say this. **Addressed**

Line 336: Translucent is not a colour. **Addressed**

Line 334: What colours are the zones? **Addressed**

Line 367-368: Rather than “the presumable Lower Jurassic marine dolomites” – which are hypothetical – it is better to say the values are lower than those expected for Lower Jurassic seawater dolomites. **Addressed**

Line 391: “While.....” indicates there should be a second part to the sentence. **Addressed**

Line 396: What is the lithology of these samples? **Addressed**

Line 401: Please add a sentence or two on the fluid inclusion petrography and distribution – do inclusions follow growth zones or are they randomly distributed? Are they all primary or are some pseudosecondary? What are their shapes and what are the liquid:vapour ratios in the 2-phase examples? Also, in reporting the results for different cements please give the number of inclusions the ranges are based on (n=). **Addressed**

Line 409-410: What is the purpose of nucleating a bubble for measurement of freezing temperatures? **Addressed**

Line 477-478: This sentence appears out of place or at least needs clarification. More than two values are needed to demonstrate a progression. **Addressed**

Line 503-507: Yes, this makes sense if the veins are filling tension gashes associated with stylolites – such as system is likely to be buffered by the dissolving carbonate. Maybe make this point more explicitly, and contrast with vein types that were more extensive and would have allowed allochthonous fluids to pass through with minimal host-rock interaction. **Addressed**

Line 518: Hendry et al. (2015) did not discuss ^{13}C enrichment from CO_2 outgassing due to evaporation. They made the point that negative covariance in C and O isotopes within veins could be due to precipitation during CO_2 outgassing related to pressure changes. **Addressed**

Line 524-551: This is good but is a very long paragraph. Can it be made more succinct? **Addressed**

Line 550-551: The final sentence needs rewriting; what was confined, the thrust wedge or the fluids? **Addressed**

Line 556: In the preceding section there is very little mention of fluid mixing. Could the poorly correlated Th, salinity and stable isotopic data reflect precipitation from allochthonous fluids as they mixed with in situ fluids (and cooled)? Degrees of mixing (and of water-rock interaction) may have different from fault to fault – is it really likely that the hydrogeological systems was as simple as is being presented here? **The obtained data show no systematic variations from fault to fault. Thus, existence of different local hydrological systems cannot be addressed. The sentence is revised ad completed**

Line 575-579: Please rewrite this sentence – it tries to say too many things at the same time. **Addressed**

Line 584: Doesn't the displacement of D1-2 on these faults indicate that the dolomite formed before faulting? What is the critical evidence that it is genuinely syn-rift? **The syn-rift deposits (Corniola Formation) is affected by these dolomites. Addressed more in the text**

Line 590: if D1-2 were related to basement-cutting faults, why are the Sr isotope values much less elevated than for D3 and D4? **There is no other alternative for radiogenic Sr source. This is the case for all of the dolomite types. Maybe less basement derived fluids were involved in D1.**

Line 656-657: Please explain how hydrothermal fluids were able to circulate in the compressional tectonic regime – which structures were able to be in tension and therefore transmissive rather than sealing? **Addressed**

Line 1139: The cross-cutting relationship in Fig. 8a, b is not very evident. **Addressed**

Lines 1142-1148: Should this discussion be in the main text rather than in the caption? **This has been made to avoid a longer discussion.**

Fig. 2b: It would help if the colours and ornaments matched Fig. 8a (e.g. Salinello Fm). The text size needs to be increased for better legibility. **Addressed**

The stereonet data are good, but very little use is made of them in the text of the paper. **Addressed in the figure caption**

Fig. 5: Please increase the text size and make 5c larger – it is too small to see clearly. **Addressed**

Figs 6-9, 11: Some of the CL images could be a bit sharper and maybe with increased contrast to better discriminate the dolomite types. **Addressed**

Fig. 12: The symbols for D3 vs. CV3 and mixed dolomite vs. CV1 are too similar (especially given the small size). I am also not clear how Fig. 12b relates to Fig. 12a; maybe split the legend between the two plots according to what is in them – that might help. **Addressed**

Fig. 14: How were the burial temperatures in the burial history determined? What assumptions are they based on? **Addressed**

Fig. 15: I like this figure but I'm still not sure what the fluid flow pathway is in (b). Maybe a broader tectonic context diagram is needed showing expulsion of fluids from the foreland (if that is where they are coming from?). **The fluids were migrated from hinterland (now indicated on the sketch) rather than forland.**

I hope these comments are helpful, and I look forward to seeing the paper published in revised form.

Jim Hendry

Tullow Oil Ltd, Dublin

Specific comments:

- 1) Abstract: The abstract can be shortened substantially, yet it is missing key information. It provides too much detail of some aspects of this work but lacks equivalent detail in other cases. For example, why are calcite-filled veins not mentioned here? Weren't they a main focus of this study? A more succinct and balanced abstract is required. Also, the abstract would benefit from a "punchline" or statement of the broader implications of this work at the end. What did you learn about the extent of dolomitization near faults? How is this relevant for porosity/permeability evolution and fluid flow in dolomitized, carbonate-hosted hydrocarbon reservoirs and aquifers? **Addressed**
- 2) Introduction: You may want to consider adding a short statement about why some fault-zones become dolomitized but others don't. What are the requirements? What can you learn from outcrops that you cannot from core alone? I would say that the main benefit would be the opportunity to assess the spatial distribution of dolomitized zones, and individual diagenetic events, in 3D. Addition of such a field-relations analysis would greatly improve the impact of this work. **Addressed**
- 3) Geologic setting: This section is a bit long and could be shortened. **Addressed**
- 4) Methodology: A few things are missing:
 - How large of a geographic area did you sample? **Addressed**
 - How did you decide which areas to sample for isotopic analyses? Did you image them first? How? How confident are you that you didn't mix different cements when sampling? **Addressed**
 - How many fluid inclusions in your FIAs? What was your reproducibility and error? How did you make sure you did not measure stretched inclusions? **Addressed**
 - Documentation of where hand samples came from is very poor. This can be improved by showing the location of the thin sections on outcrop photos, and their spatial relationship with faults etc. These might need to be included in an appendix due to space restrictions, but it is important. **Explained in author response**
- 5) Field observations
 - What is the spatial distribution of the dolomitized geobodies? **Addressed**
 - And of the veined sections?
 - 6 outcrop locations are marked on Figure 2 but distributions of the different types of cements are only shown in one image (figure 5b). These are very important relations to assess fluid pathways and the evolution of dolomitization. **Addressed**
 - What are the orientations of CV1–CV4 cement-bearing fractures? **Shown in Storti et al. (2018)**
- 6) Petrography
 - How much calcite cement is there in the breccias? What are the textures? Why are these not included in your diagenetic evolution analysis? How do cements in breccias relate to those in host rocks? Are cements in the host rocks affected by brecciation? Show examples. **Addressed**

- How did dolomitization affect porosity in both host rock and fault rocks? How does porosity compare between limestones and dolostones? **Addressed**
 - Some of the petrographic relationships mentioned need to be backed by images (see my line-specific comments) **Addressed**
 - The order in which dolomite cements and vein-calcite cements are mentioned needs to be improved.
 - What is the relationship between MC and D1/D2? Where is this documented? **Addressed**
 - What is the distribution of CV cements in the host rock (see Laubach, 2003)? This should be properly documented and reported. I don't think vein cement is an appropriate term for these calcite cements. Also, keep in mind that the occlusion of fracture porosity by postkinematic cements can significantly postdate the timing of the opening of the fracture (see Ukar and Laubach, 2016). In other words: the timing of fracturing and cementation are not the same. Keep that in mind in your descriptions. **Addressed**
 - The observation of CV3 in breccias is quite interesting. Document and show images. What other cements are there in breccias? How did you establish the relative timing of these cements and others? Breccia cements should not be referred to as vein cements. **Explained in author response**
 - What are the spatial distributions of the different cement types? **Addressed**
- 7) Geochemistry
- What are the isotopic characteristics of MC and fibrous cements? **Addressed**
 - Interpretations, especially for Sr ratios, should be moved to the discussion.
- 8) Fluid inclusions
- Show images of the different types of fluid inclusions, especially the FIAs.
 - The graphs used to summarize fluid-inclusion thermometric results are not appropriate because key information is lost. Same for salinity. Please replot the data so that the temperature range for each individual FIA is shown. Did you measure an equal amount of FIAs for each type of cement? Otherwise, frequency would not very meaningful in Fig. 13 because it would be sample and cement availability dependent.
 - Why are CV temperatures not shown in these graphs? **For a higher focus on dolomitization case study**
- 9) Discussion
- This section can be significantly shortened by avoiding repetition of results.
 - I think parental fluid calculations should be shown in the results section, not in the discussion. **To emphasize on the nature of parental fluids, we prefer to keep SMOW values in discussion section**
 - Use parallel writing style for stable isotopes and Sr discussion.???
 - D3 shows significantly higher Sr/Sr than D4. How can both be related to the same event and derived from similar fault-related fluids? D1 and D2 are also fault-related. Why the differences in isotopic signatures, especially if all are related to basement-rooted faults???

- The association of D3 and D4 with bed-parallel and shear fractures is mentioned for the first time in the discussion. This needs to be mentioned in the results. Are the cements themselves sheared? Show evidence. **Addressed in petrography**
 - Discuss the spatial distribution of the different cement and vein/breccia types. What do they indicate about fluid-flow patterns? **The breccia types in MDF are not diverse. More details on breccia is out of focus of this study.**
 - The orientation of CV1–CV4-bearing fractures needs to be taken into account in the structural interpretation. **A detailed structural interpretation is discussed in Storti et al. 2018. Its now more emphasized in this manuscript.**
 - Section 5.3: Without a better documentation of the orientations and field relations of the different cements and fracture types it is difficult to assess the validity of the inferred paragenetic sequence and the association of the different cements and structures with tectonic events. Some of the spatial and cross-cutting relationships between different types of cements are first mentioned in this section. Such descriptions should be moved to the results section.
 - What is the driver for fluid circulation? Why are they Mg-rich fluids? What do fluid-inclusion salinities indicate? **Addressed in section 5.2**
 - Why do you go from dolomite replacement and cementation to calcite cementation? **Addressed**
 - How are your findings relevant for porosity/permeability evolution and fluid flow in dolomitized, carbonate-hosted hydrocarbon reservoirs and aquifers associated with similar reservoir-scale structures? **Addressed**
 - How are your conclusions applicable to dolomitization processes associated with faults in general? How far can dolomitizing fluids travel and to what extent do they alter the mechanics and porosity/permeability of the host rock? What are the consequences for fluid-flow in these rocks? **Addressed**
- 10)

Conclusions

- More thought needs to go into the conclusions section.
- I don't think enough data are presented in this study, especially of cross-cutting relationships and orientations of the different "deformation structures" to support the structural interpretation presented in the conclusions. For example, where is the evidence that the opening-mode fractures (no orientations or relationships within the anticline are reported!) and normal faults mentioned in this study are associated with contractional tectonics of the Apenninic orogeny? **All are discussed in details in Storti et al. 2018.**

- 11) Figures and figure captions need work, especially the model shown in Figure 15 (see comments in figure caption).

Lines 29-31: This needs to be re-written. Layer-parallel shortening would not give place to layer-parallel stylolites. Extensional faulting by itself either. Involvement in the Apenninic thrust wedge of what? **Addressed**

Lines 48-54: May I suggest you take a look at the recently published Ferraro et al. (2019) paper for a description of the diagenetic evolution of carbonate fault rocks in the central and southern Apennines? **Addressed**

Lines 54-58: You may want to consider adding a short statement about why some fault zones become dolomitized but others don't. What are the requirements? **Addressed**

Lines 58-61: What can you learn from outcrops that you cannot from core alone? I would say that the main benefit would be the opportunity to assess the spatial distribution of dolomitized zones, and individual diagenetic events, in 3D. Perhaps a missed opportunity in this work?

Line 67: I don't see Bugarone in Figure 1. **Addressed**

Line 69: I don't see catel Manfrino Dolostones in Figures 1 or 2. **All the dolomitized intervals are called Castel Manfrino Dolostones**

Lines 72-73: How is your study better than Ronchi (2003)? **Addressed**

Lines 76-78: In Figure 2 it appears that dolomitized bodies are found quite far away from faults, beyond the typical lateral extent of fault damage zones. What is the explanation? Why are some faults associates with dolomitization while others aren't? Does it have to do with age of faults? Other factors? This would be a good topic for the discussion.

Line: 84: I would have liked to see more "field mapping" of the extent of D1–D5 and CV1–CV4 in this work.

Line 87: This sentence should start with a different word than "therefore". What provides insights? How? **Addressed**

Lines 88-89. Yes. This needs to be discussed in the discussion. **Addressed**

Lines 90-92: Yes. This needs to be discussed in the discussion. **Addressed**

Line 96: evolution of the Apennines has been proposed to be the result of **Addressed**

Line 98: since the Late Cretaceous **Addressed**

Line 103: The Central Apennines involve **OK**

Line 110: lower part of the Burano Formation **Addressed**

Line 115: Deposition of the Hettangian–Sinemurian Calcare Massiccio Formation, with a total thickness ... **Addressed**

Line 117: following facies are present **Addressed**

Line 125: deepening-upward trend **Addressed**

Line 137: olistolith model **This sentence is deleted**

Lines 138-145: So, does this evidence favor the fault-related model or does this evidence provide an alternative model? Why does this sentence start with ‘However’? **This sentence is deleted**

Line 151: at a high angle **Addressed**

Line 162-163: 60 samples distributed across how big of an area? **Addressed**

Line 164: What structures? **Addressed**

Line 187: Vienna Pee Dee Belemnite **Addressed**

Line 215: In order to perform high resolution **Addressed**

Lines 220-221: bed-perpendicular stylolites **Addressed**

Lines 224-230: This belongs in the Geological Setting. **Addressed**

Line 225: There is no evidence of dolomitization **Addressed**

Lines 231-234: Location names need to be included in figure captions. **Addressed**

Lines 235-239: This seems out of place. Start by describing mesoscale relations and distributions of dolomitized geobodies. Then focus on hand-sample and petrographic details. **Addressed**

Line 235: in fault cores are typically **Addressed**

Line 237: is “main slip surface” a better term? **Addressed**

Line 238: cut by rather than overprinted. Are dolomite-filled veins intra- or intergranular?

Line 239: calcite cement **Addressed**

Line 241: cross-cutting bedding surfaces **Addressed**

Line 242: from a few meters to hundreds of meters **Addressed**

Line 243: and the lower part of **Addressed**

Line 246: High amplitude (>1 mm), bed-parallel stylolites **Addressed**

Line 247-248: How does porosity differ between limestones and dolostones?

Line 253: grain-supported intervals **Addressed**

Lines 259-260: Evidence? **Addressed**

Line 265: we can’t see the displacement mentioned in Figure 2A, site 1

Line 267-268: Are they overprinting or overgrowing? Show evidence. We also cannot see the distribution of the different cements at outcrop scale.

271-272: On what basis did you establish that the replacive dolomite within the host rock (D1) and lining fractures is the same?

Lines 275-276: solid inclusions of what? Insert figure call out for concentric zonation. **Addressed**

Line 281: sweeping extinction **Addressed**

Line 282: In some crystals, one... what types of solid and fluid inclusions? **Addressed**

Lines 286-291: Mark locations on map/figure captions and call out the figure. **Addressed**

Line 290-291: Scaglia Formation in the hanging wall. **Addressed**

Lines 293-295: This needs to be moved up **Addressed**

Line 305: bed-parallel shear fractures **Addressed**

Lines 308 on: There is a problem with CV introduction. What does it stand for? Must introduce them in chronological order. If the calcite cement is in veins it is most likely in the host rock as well (see Laubach, 2003). I don't think calling it vein cement is appropriate. **Addressed**

Line 308: What porosity? **Addressed**

Lines 318-320: Show outcrop photo?

Line 319: bed-perpendicular rather than bedding because that's what you use elsewhere. Make sure term usage is consistent throughout. **Addressed**

Line 321: bed-parallel stylolites. CV1 usually shows (often means time. Correct elsewhere in the manuscript). **Addressed**

Lines 324-326: Show image of CV2 in tension gashes **Addressed**

Line 332: extensional fault's master (main?) plane **Addressed**

Line 339-340: More evidence that the use of CV to refer to calcite cements that occur in a variety of textures and petrographic relations is not appropriate.

Lines 361-364: Why is this mentioned here and not with the rest of the calcite cements? **Its ordered based on relative timing**

Line 396: I see 3 values plotted for Scaglia. **Addressed**

Lines 398-399: Interpretation. Move to discussion. Same comment for previous paragraphs. **Addressed**

Lines 401-411: This belongs in the Methods section. **Addressed**

Lines 409 and 439: all-liquid inclusions **Addressed**

Lines 439-445: This belongs in the Methods section. **Addressed**

Lines 469-470: This belongs in the methods/results. Why did you avoid them? Could mottled D be a different type than those reported? **Addressed**

Lines 471-474: Move to methods. Report parental fluid calculations in the results section.

Line 478: Progressively higher than what? **Fixed**

Line 481: siliciclastic rocks,... Correct here and elsewhere. **Addressed**

Line 493: , or values recorded... Add references. **Addressed**

Lines 499 and 505: Replace comparable with similar. Here and elsewhere. **Addressed**

Line 507: stylolitization of the host rock (otherwise we do not know what dissolution etc. you are referring to). **Addressed**

Lines 527-528: fluids related to Late Messinian... overlying Upper Miocene Laga Formation and their possible... **Addressed**

Line 543: burial-related temperature **Addressed**

Line 544: it is unlikely that the.. **Addressed**

Line 546: located at higher stratigraphic levels **Addressed**

Line 564: calcite cements (FC) in grain-supported stratigraphic levels of the CMF is interpreted to be... **Addressed**

Line 570: bed-parallel stylolites **Addressed**

Line 574 and 575: are cut by **Addressed**

Line 579: Figure 15A call out. **Addressed**

Line 585: We cannot see the distribution described in Figure 2A.

Line 587: attributed to post-rift **Addressed**

Line 588: Although an absolute age cannot be provided, **Addressed**

Line 603: bed-parallel fractures. This is the first mention of shear veins for D4. Are the cements sheared? Show evidence. **Cements are not sheared. Addressed**

Line 604: Contractional deformations? How? Describe relationships better. Bed-perpendicular dilation alone would not cause shear.

Lines 608-610: First mention of this. Move to results.

Lines 618-619: bed-parallel veins **Addressed**

Line 622: fragments suggests that... late-stage evolution **Addressed**

Line 624: bed-perpendicular stylolites **Addressed**

Line 624-629. This is way too long. In any case, there is new information here that needs to be moved to the results section. **Addressed**

Line 629: low homogenization temperatures of fluid inclusions trapped within these cements **Addressed**

Lines 638-642: So, how is your study better? How are your conclusions applicable to dolomitization processes associated with faults in general?

Figures: Documentation of where samples came from is poor. Locations of samples need to be shown on outcrop photos and/or detailed maps. Add in appendix if space is limited.

Figure 1: Tiny name in a) is unreadable. Mark location of cross-section (A-A') shown in d).

Figure 2: Add names of each field site to the figure caption. **Addressed**

Figure 3: The picture in a) is too close up to see the context. Mark distribution of D1 etc. as in Fig 5d. Why isn't there more on these breccias (c) in the manuscript? Explain what arrows point to. Pressure solution seams. You are not showing intensity (it would be a number). Perhaps say showing abundant pressure solution seams. What are the abutting relationships? Which abuts which? Move arrow in b) so that the vein is actually visible. Are the other white pods also considered "veins"?

Figure 4: Show spatial distribution of D1, D3, CV1... etc. at the outcrop scale. The sentence seems to say that CV1 veins are dolomitized. Is that what you really mean? What is the dolomite type in b) and c)? Good opportunity to show cross-cutting relationships summarized in Figure 14.

Figure 5: What field site(s) and formation(s) are these from? In b) the zone shown in c) is marked as only having D1 but as D1 + D2 in c). Which one is correct? Any CV2-CV4 here? **Addressed**

Figure 6: What field site is this? rimmed by fibrous cements (FC), which are overgrown by mosaic cements (MC). overprinted. bed-parallel stylolites. D1 cements lining a fracture. What do

arrows point to in f) If it is D1, then what is to the right of it? Line 1123: which is cemented by CV1 in the center. **Addressed**

Figure 7: What field site(s) and formation(s) are these from? What is beyond D3 in e) and f)? Is D3 only present in breccias in this site? What is the CL signal of D3 in breccias and how did you establish correspondence with D3 in host rocks? What is the context of the sample? in e) and f) **Addressed**

Figure 8: What field site(s) and formation(s)? D3 and D4 are not cross-cutting but it appears that D4 overgrows D3. What is the D4 arrow in b) exactly pointing to? What cement is in the rhomb on the upper right corner? d) I am having a hard time seeing the microfracture. What CV is this? Or do you have dolomite-filled veins as well? Where are these described? What other cements are in e) and f) and what do arrows point to? Lines 1141-1150 belongs in the discussion. **Addressed**

Figure 9: What field site(s) and formation(s)? If D4 also occurs in fractures why is it not called vein cement as in your CV scheme? What other cements and/or host rock are in these photographs? Add labels. **Addressed**

Figure 10: These photographs are too close up to see the context. Outlining obscures fractures in a). c-d) These do not look like tension gashes to me (as mentioned in text?). Misabeled as CV2 on the picture (?) but CV3 in the figure caption. **Addressed**

Figure 11: What field site(s) and formation(s)? What is a) a sample of? And the rest? Show field context. **Addressed**

Figure 12: Why aren't these figures in color? The symbols are too similar and they are hard to distinguish from one another. I would assign a color to each formation and a symbol to each diagenetic feature. **Addressed**

Figure 13: These plots are not very useful because key information is lost. Plot homogenization and ice melting T ranges so that variability within individual FIAs is captured. Color would help, Also, where are the data for CV cements?

Figure 15: The fracture in a) would not have that orientation if σ_1 were vertical. Indicate which fault you are referring to in b). The vein in b) would not develop in that orientation if σ_1 were horizontal. Also, keep in mind that the timing of cementation of the veins by postkinematic cements (see Ukar and Laubach, 2016) postdates timing of opening of the fracture. Don't mix the two! I had no idea that CV4 is restricted to the MdFF until now, because it is not mentioned anywhere in the text. How do you reconcile D3 to be surrounding breccia clasts within the MdFF in this model and sequence? **Addressed**

Estibalitz Ukar
Research Associate
Jackson School of Geosciences
The University of Texas at Austin

Dear Dr. Hendry and Dr. Ukar,

Thank you for the very constructive comments. They not only helped us to improve the quality of the manuscript but also our knowledge of dolomitization process. We have tried our best to address your suggestions in this new version of the manuscript.

Regarding the advancement of our research in comparison with the work previously presented by Ronchi et al. (2003), the current study gives much more details about the dolomite characterization and their relation to the structural evolution of the anticline on the regional and local scale. Furthermore, the obtained geochemical and microthermometry analyses do not confirm the role of marly or shaly basal successions in providing the Mg-rich fluids during the first event of dolomitization (i.e. syn-rift), as proposed by Ronchi et al. (2003). We have tried to be modest in criticizing the latter authors limited research since the current research was build up on their findings. Another important question about the studied dolomites was the role of Scaglia Formation in providing the Mg-rich fluids during compression, because this formation is juxtaposed with the dolostones by the Montagna dei Fiori Fault. Our results do not support this hypothesis.

During our research, we also performed some other advance analyses such as clumped isotopes and U/Pb dating. However, the consecutive overgrowth pattern of dolomites and difficulties in isolating them to get enough and good quality samples increased the uncertainty in the results. Therefore, we decided not to include those data in the manuscript.

In the Montagna dei Fiori Anticline, the structures and their relative chronology are very complicated. A comprehensive structural study on the evolution of the Montagna dei Fiori Anticline was performed parallel with the current study, and published by Storti et al. (2018) in *Tectonics*. The target of the current study was to focus on dolomitization, and to use the structural model proposed by Storti et al. (2018) to deduce the most likely timing for dolomitization.

The distribution of dolomitization and sampled locations are way larger than the out crop photo scale. The dolomitized intervals are tens of meters mostly exposed in vertical to subvertical outcrops. To be able to show their 3D distribution properly a photogrammetry or LiDAR imaging is required.

The brecciated zones are mostly clast-support with minor calcite and negligible dolomite cement. Moreover, a detailed classification of breccia is not the focus of this research and does not give relevant information regarding this dolomitization case study.

This new version of the manuscript has been reviewed by a native English speaker.

Best regards,

Mozafari et al.

1 **Fault-controlled dolomitization in the Montagna dei Fiori Anticline (Central Apennines,**
2 **Italy): Record of a dominantly pre-orogenic fluid migration**

3 Mahtab Mozafari¹, Rudy Swennen², Fabrizio Balsamo¹, Hamdy El Desouky^{2,3}, Fabrizio Storti¹
4 and Conxita Taberner⁴

5

6 *1- NEXT - Natural and Experimental Tectonics Research Group - Department of Chemistry,*
7 *Life Sciences and Environmental Sustainability, University of Parma, Italy.*

8 *2- Department of Earth and Environmental Sciences, KU Leuven, Belgium.*

9 *3- Geology Department, Faculty of Science, Menoufia University, Menoufia, Egypt*

10 *4- Shell Global Solutions International B.V., Amsterdam, The Netherlands*

11 Correspondence: Mahtab Mozafari (mahtab_mozafari@yahoo.com) and Fabrizio Storti
12 (Fabrizio.Storti@unipr.it)

13

14 **Abstract**

15 The Lower Jurassic platform and basinal deposits exposed in the Montagna dei Fiori
16 Anticline (Central Apennines, Italy) are pervasively affected by dolomitization. Based on the
17 integration of field work, petrography, and geochemistry, two fault-related dolomitization events
18 were recognized and interpreted as having occurred before and during the Apenninic orogeny,
19 respectively. Fluid inclusion analysis indicates moderate to elevated salinity values of 3.5 to 20.5
20 and 12.8 to 18.6 eq. wt. % NaCl, in the first and the second event, respectively. The estimated
21 salinities, in combination with $\delta^{18}\text{O}$ values and $^{87}\text{Sr}/^{86}\text{Sr}$ ratios, suggest significant involvement
22 of evaporitic fluids in both events, most likely derived from the underlying Upper Triassic
23 Burano Formation. In addition, the $^{87}\text{Sr}/^{86}\text{Sr}$ ratios up to 0.70963 suggest the circulation of deep-
24 sourced fluids that interacted with siliciclastic rocks and/or the crystalline basement
25 during the dolomitization events. ~~The first dolomitization event which is also considered as the~~
26 ~~most pervasive one started prior to the significant burial conditions, as reflected in~~
27 ~~homogenization temperatures of their fluid inclusions being mostly below about 40–50°C.~~

28 Two major dolomite types (D1 and D2) were recognized as pertaining to this the first
29 event, both postdated by high amplitude bed-parallel stylolites. ~~, supporting This relationship~~
30 ~~supports~~ a syn-burial, pre layer-parallel shortening dolomitization, ~~interpreted as controlled by~~
31 ~~the extensional fault pattern affecting the carbonate succession before its involvement in the~~

32 ~~Apenninic thrust wedge~~. A possible geodynamic framework for this dolomitization event is
33 Early to Late Jurassic rift-related extensional tectonism. ~~The second dolomitization event (D3,~~
34 ~~D4 and D5) initiated with a dolomite type (D3) is~~ characterized by a ~~slight~~ temperature upturn
35 ~~(up to 73°C), followed by a second type (D4) with markedly higher homogenization~~
36 ~~temperatures~~ (up to 105°C), ~~and~~ interpreted as associated with the inflow of hydrothermal fluids,
37 possibly related to major changes in the permeability architecture of faults during early- to syn-
38 thrusting and folding activity. ~~Eventually, D4 was overprinted by a late generation of dolomite~~
39 ~~veins (D5) interpreted as associated with late orogenic extensional faulting in the backlimb of the~~
40 ~~Montagna dei Fiori Anticline~~. Based on the timing of deformation in the Montagna dei Fiori
41 Anticline, ~~D3 to D5~~ the second dolomitization event likely occurred in Late Miocene to Pliocene
42 times. The findings regarding characteristics and timing of dolomitization here illustrates the
43 long-term controlling role of the ~~evaporitic~~ evaporitic detachments in dolomitization process.
44 ~~Our data~~ This study shows that the Mg-rich fluids that were most likely derived from ~~these~~
45 evaporites may prime the tectonically involved successions for repeated dolomitization, and
46 hence formation of potential reservoirs ~~in~~ during sequential tectonic modifications (extensional
47 vs. compressional).

48 **1 Introduction**

49 Fault-controlled dolomitization has been the focus of attention in many studies during the last
50 decades due to its influential role in modifying the petrophysical properties of rocks and, hence,
51 anisotropy in fluid migration pathways, and, ultimately on reservoir quality (e.g. Purser et al.,
52 1994; Montanez, 1994; Zempolich and Hardie, 1997; Vandeginste et al., 2005; Davies and
53 Smith, 2006; Sharp et al. 2010). The mechanical and hydrological behaviour of fault zones are in
54 turn influenced by fluid-rock interactions and diagenetic modifications (e.g. Gale et al., 2004;
55 Laubach et al., 2010; Clemenzi et al., 2015; Ferraro et al., 2019). It follows that the mutual
56 interplay between fault activity and ~~fluid-driven~~ rock-fluid interaction can trigger dolomitization
57 of carbonates when exposing to Mg saturated or oversaturated fluids and, consequently,
58 variations in physico-chemical properties of fluids through time and space.

59 -Leaking or sealing behaviours of fault zones during deformation are key controls for fault-
60 related fluid circulation. A detailed understanding of such an interplay is thus necessary to
61 improve our capability of making reliable predictions of fault-related dolomitization in carbonate
62 reservoirs. Studying outcrop analogues provides fundamental support to meet this requirement

63 ~~(e.g. Swennen et al., 2012; Dewit et al., 2014; Bistacchi et al., 2015).~~ and the opportunity to
64 assess the spatial distribution of dolomitized zones, and individual diagenetic events, in 3D (e.g.
65 Swennen et al., 2012; Dewit et al., 2014; Bistacchi et al., 2015).

66 The Lower Jurassic to Lower Cretaceous Umbria-Marche passive margin carbonate
67 succession, in the Central Apennines (Italy), is intensely affected by localized dolomitization
68 both in the onshore fold-and-thrust belt and in offshore foredeep and foreland areas (e.g. Murgia
69 et al., 2004; Pierantoni et al., 2013). The dolomitized intervals which are the focus of this study
70 are well-exposed in the core of the Montagna dei Fiori Anticline ~~(e.g. Ronchi et al., 2003)~~, where
71 the dolomitized Lower Jurassic intervals (Calcere Massiccio, Bugarone and Corniola
72 Formations) and their relationships with fault zones allow to study the mutual influence between
73 deformation structures and dolomitized intervals (Fig. 1). These intervals, known as the Castel
74 Manfrino Dolostones (Crescenti, 1969; Mattei, 1987; Koopman, 1983), have been previously
75 studied by Ronchi et al. (2003) only at its reference section, exposed at the Castel Manfrino
76 location (Fig. 1b), in the central sector of the Montagna dei Fiori Anticline (Fig. 2). A
77 fault-controlled dolomitization model and the relative timing of dolomitization were proposed by
78 ~~Ronchi (2003)~~ the latter authors— based on the homogenization temperatures obtained from
79 microthermometry of the fluid inclusions, and their relation with the thermal history of the area
80 studied. However, no clear relation between dolomitization and structural evolution of the
81 Montagna dei Fiori Anticline on a local scale was provided to confidently link the occurrence of
82 dolomitization to a particular tectonic event. Moreover, the nature and origin of the dolomitizing
83 fluids were not well constrained. Recent re-evaluation of dolostone distribution in the Montagna
84 dei Fiori Anticline (Storti et al., 2017a), showed that the dimension of the dolomitized geobodies
85 (Fig. 2) is much more significant than what was previously mapped by Mattei (1987).
86 Dolostones are distributed within fault damage zones and in the laterally adjacent carbonate
87 rocks, and in intersection areas between fault sets, for a total area in map view of more than 1.5
88 km² (Storti et al., 2017a).

89 The structural pattern of the Montagna dei Fiori Anticline documents the overprinting of
90 extensional and contractional deformation along major fault zones. ~~Although challenging, the~~ The
91 preserved structural framework in this anticline provides an opportunity to study the direct but
92 complex regional tectonic controls on dolomitization in carbonate successions undergoing
93 multiple deformation events, from rifting to folding and thrusting. This contribution integrates

94 ~~field mapping~~, new petrographic, geochemical, and microthermometric analyses, with structural
95 studies ([Storti et al., 2018](#)) to characterize the temporal record of fault-controlled diagenetic
96 phases and, more specifically, dolomitization in the carbonatic succession outcropping in the
97 Montagna dei Fiori Anticline. ~~Therefore provides insights into the structural controls on regional~~
98 ~~fluid flow and their chemical evolution through time.~~ These findings might be of relevance for
99 exploration and reservoir quality prediction ~~in the region of onshore and offshore~~ the Apennines
100 and Southern Alps, ~~both onshore and offshore~~. Moreover, this work provides additional evidence
101 of the potential influence of fluids derived from evaporitic detachment levels in modifications of
102 geochemical trends and petrophysical properties of the overlying carbonate rocks.

103 2 Geological setting

104 The Montagna dei Fiori Anticline is a NNW-SSE striking, thrust-related fold located at
105 the mountain front of the Central Apennines (Fig. 1). The geodynamic evolution of the
106 Apennines ~~is generally known~~ [has been proposed](#) to be the result of the superposition of NE-SW
107 compression (in present-day geographic coordinates), related to the convergence between
108 Eurasia and Africa plates since ~~the~~ Late Cretaceous times (Elter et al., 1975; Dewey et al., 1989;
109 Patacca et al., 1992), on a rifting-related tectono-sedimentary architecture produced by Early
110 Jurassic extension (e.g., Centamore et al., 1971). In such a framework, the Central Apennines
111 developed during Miocene to Plio-Pleistocene times (e.g. Parotto and Praturlon, 1975; Barchi et
112 al., 1998; Mazzoli et al., 2002; Bollati et al., 2012).

113 The Central Apennines involves the Umbria-Marche succession, which essentially
114 includes Triassic to Miocene carbonates and marls, covered by Miocene to Pliocene syn-
115 orogenic clastic sediments (Fig. 1). The pre-orogenic succession, from bottom to top, includes
116 Late Triassic evaporites, dolomites and limestones ~~(of the Burano Formation)~~, ~~which the basal~~
117 ~~detachment runs within its evaporitic interval (Ghissetti and Vezzani, 2000).~~ Early to Late
118 Jurassic platform and basinal limestones and dolostones (Calcare Massiccio, Corniola, Rosso
119 Ammonitico, Calcari a Posidonia and Calcari ad Aptici Formations), and Cretaceous to Early
120 Miocene basinal carbonates (Maiolica, Marne a Fucoidi, Scaglia and Biscaro Formations). In
121 general, the lower part of ~~the~~ Burano Formation is overlaid by the fluvio-deltaic ~~siliciclastics~~
122 ~~siliciclastic rocks~~ of the Verrucano Formation (Middle-Late Triassic) (Tongiorgi et al., 1977;
123 Ghissetti and Vezzani, 2000; Tavani et al., 2008). Nevertheless, the existence of these
124 ~~siliciclastics~~ ~~siliciclastic rocks~~ in the Montagna dei Fiori area is not yet ~~proved~~ [proven](#). Syn-

125 orogenic deposits include Miocene marls and turbiditic sandstones (Marne con Cerroigna and
126 Laga Formations) (Artoni, 2013 and references therein).

127 The deposition of the Calcare Massiccio Formation, ~~(dated as Hettangian-Sinemurian) and~~ with
128 a total thickness varying between 300 to 700 m (Pialli, 1971), records an important extension
129 pulse in the evolution of Tethyan rifting. The ~~following facies are observed in the~~ lower part of
130 ~~the Calcare Massiccio Formation~~ this formation which has been interpreted as having been
131 deposited in a peritidal environment:- consists of oolite-rich peloidal pack- to grainstones in
132 alternation with peloidal wacke- to packstones including horizons of algal bindstones (Calcare
133 Massiccio A; Brandano et al., 2016). The upper part is made up of beds of skeletal and coated
134 grain wacke- to grainstones ~~including microoncolites, echinoderms, calcareous and siliceous~~
135 ~~sponges, bivalves, gastropods and ammonites~~ (Calcare Massiccio B; Brandano et al., 2016). It
136 The lower part has been interpreted as having been deposited in a peritidal environment, while
137 the upper part corresponds to lower to middle shelf depositional environments, characterized by
138 a general ~~deepening-deepening~~ upward trend ~~associated with extensional faulting and drowning~~
139 ~~of the platform, coupled with subsidence and deposition of the overlying Corniola Formation in~~
140 ~~the pelagic areas~~. Overall, the Early Jurassic rifting led to the growth of the Calcare Massiccio
141 Formation in a carbonate platform setting, followed by faulting and drowning, and development
142 of pelagic intrabasins filled by syn-rift sediments (Fig. 1c; Bernoulli et al. 1979; Santantonio and
143 Carminati, 2011). The syn-rift sediments include pelagic limestones of the Bugarone and
144 Corniola Formations. Condensed pelagic limestones of the Bugarone Formation (Lower
145 Pliensbachian-Lower Tithonian; Bugarone Group in Pierantoni et al., 2013) occur at the top of
146 the Calcare Massiccio Formation where it formed fault-controlled highs marking the regional
147 drowning of the carbonate platform (Santantonio and Carminati, 2011). The pelagic limestones
148 of the Corniola Formation (Sinemurian-Toarcian; Colacicchi et al., 1975; Morettini et al., 2002;
149 Bosence et al., 2009; Marino and Santantonio, 2010; Brandano et al., 2016) occur within the
150 fault-controlled (half)grabens in lateral continuation with the Calcare Massiccio Formation. The
151 Corniola Formation in the lower part consists of turbiditic lobes which originated from tectonic
152 brecciation of the Calcare Massiccio Formation. The upper part consists of a well-bedded pelagic
153 mudstone with chert nodules (Di Francesco et al., 2010). In the Montagna dei Fiori, the geologic
154 framework of the outcropping Calcare Massiccio Formation is still a matter of debate between a

155 ~~fault-related tectonosedimentary pattern (Mattei, 1987; Storti et al., 2017b), and a gravity-driven,~~
156 ~~olistolith hypothesis (Di Francesco et al., 2010; Santantonio et al., 2017). However, recent~~

157 2.1 Structural Framework

158 The Montagna dei Fiori Anticline is intersected by two major fault categories (Storti et al.,
159 2018), which based on the chronological order include: detailed work in the Salinello valley
160 (Storti et al., 2017a; 2018) Firstly, ~ E-W and ~ N-S striking fault zones showing extensional
161 kinematics bounding the documented that major outcrops of Calcare Massiccio are bounded by
162 mostly ~ E-W and ~ N-S striking fault zones showing extensional kinematics and dominantly
163 affecting the Jurassic rocks older than the Maiolica Formation (Fig. 2A2a, e.g. sites 1 to 4).
164 Overprinting relations indicate that ~ E-W deformation structures are systematically younger
165 than the ~ N-S ones. Similar trends were observed in syn-rift fault zones in other anticlines of the
166 Central Apennines (e.g. Cooper and Burbi, 1986; Alvarez, 1989; Chilovi et al., 2002). Such a
167 tectonosedimentary inheritance was involved in the growth of the Montagna dei Fiori Anticline,
168 which initiated during the Late Miocene (Mazzoli et al., 2002; Artoni, 2003) and progressively
169 evolved into the upper thrust sheet of a well-developed antiformal stack until Plio-Pleistocene
170 times (e.g. Ghisetti et al., 1993; Calamita et al., 1994; Artoni, 2013). The second set of faults is A
171 a major structural feature trending parallel to the Montagna dei Fiori Anticline and dissecting it
172 is the Montagna dei Fiori Fault, a NNW-SSE striking extensional fault system cutting at a high
173 angle through the folded footwall rocks, typically at the forelimb-crest transition (Figs. 1, 2).
174 This fault consists of two partially overlapping main fault zones with an extensional stratigraphic
175 separation exceeding 900 m, and ~~This fault system~~ juxtaposes intensely deformed Late Miocene
176 sediments in the hanging wall, against dolomitized and undolomitized Lower Jurassic and
177 Cretaceous limestones in the footwall (Figs. 1 and 2). The development of the Montagna dei
178 Fiori Fault has been alternatively interpreted as either a pre- (e.g. Calamita et al., 1994, Mazzoli,
179 2002; Scisciani et al., 2002) or late-folding (Ghisetti and Vezzani, 2000) feature. More recently,
180 the origin of the Montagna dei Fiori Fault has been ascribed to the mutual interaction between
181 horizontal shortening and uplift, and episodic gravitational re-equilibration during antiformal
182 stacking underneath the anticline during Plio-Pleistocene times (Storti et al., 2018). The
183 dolomitized intervals are exposed in the damage zones of the both aforementioned fault
184 categories.

185 **3 Methodology**

186 | The fieldwork covered an area of over 4 km² to delineate the distribution of dolostones.

187 | The stratigraphic and deformational features of dolostones were analyzed in more than 60
188 | outcrops. The distribution of dolomitized intervals as well as their cross-cutting relationships
189 | with bedding planes, stylolites, veins and ~~structures-faults~~ were ~~ground-truthed~~documented and
190 | sampled. For petrographic analyses, 130 polished thin sections were studied with standard
191 | petrographic methods (transmitted and UV-fluorescent light microscopy). Dolomite crystal
192 | morphology and texture is based on the classification proposed by Sibley and Gregg (1987).

193 | The rock slabs and thin sections were stained using Alizarine Red S and potassium
194 | ferricyanide (Dickson, 1966) to discriminate dolomite from calcite and evaluate their iron
195 | content. Cold cathodoluminescence microscopy (CL) was carried out on representative thin
196 | sections (n = 80) at KU Leuven University (Belgium) using a Technosyn cathodoluminescence
197 | device (8-15 kV, 200-400 μ A gun current, 0.05 Torr vacuum and 5 mm beam width).

198 | $\delta^{13}\text{C}$ and $\delta^{18}\text{O}$ analysis were carried out on 117 samples. To ensure the sampling quality
199 | and avoid physical mixing of different diagenetic phases, the thin section images were mapped
200 | and the sampling targets were determined. Nevertheless, some diagenetic phases could not be
201 | isolated due to their sequential overgrowth and small size. Powder samples (150 - 200 μ g) were
202 | obtained by applying a New Wave Research micromilling device and a dental drill at KU
203 | Leuven University (Belgium). The analysis was conducted at Parma University (Italy) and the
204 | Friedrich-Alexander-Universität (Erlangen-Nürnberg, Germany) laboratories using Finnigan
205 | DeltaPlus V and ThermoFinnigan 252 mass spectrometers, respectively. The carbonate powders
206 | were reacted with 100% phosphoric acid at constant temperature of 75°C. Several additional CO₂
207 | reference gases (NBS18, NBS19, MAB99, and a pure Carrara marble) with known isotopic ratio
208 | were analyzed during the measurements to determine the $\delta^{13}\text{C}$ and $\delta^{18}\text{O}$ values of the sample.
209 | Reproducibility was checked by replicate analysis of laboratory standards and was better than
210 | $\pm 0.1\text{‰}$ for $\delta^{13}\text{C}$ and $\pm 0.2\text{‰}$ for $\delta^{18}\text{O}$ at Parma University and ± 0.04 for $\delta^{13}\text{C}$ and $\pm 0.05\text{‰}$ for
211 | $\delta^{18}\text{O}$ at Friedrich-Alexander-Universität. Oxygen isotope composition of dolomites was
212 | corrected using the acid fractionation factors given by Rosenbaum and Sheppard (1986).
213 | Duplicate homogeneous samples measured in both labs for inter-laboratory reproducibility ~~show~~
214 | ~~$\delta^{13}\text{C}$ and $\delta^{18}\text{O}$ values within the acceptable range of error deviation ($\pm 0.1\text{‰}$) both for $\delta^{13}\text{C}$ and~~
215 | ~~$\delta^{18}\text{O}$.~~ All carbon and oxygen values are reported in per mil, relative to the “Vienna Pee Dee
216 | Belemnite Vienna-PDB scale” (V-PDB).

217 A total number of 21 samples were analyzed for their $^{87}\text{Sr}/^{86}\text{Sr}$ ratios. The analyses were
218 conducted at the Department of Analytical Chemistry, Ghent University (Belgium) and at the
219 Vrije Universiteit Amsterdam (the Netherlands). NIST SRM 987 was used as the international Sr
220 standard in both labs. At Ghent University, 15 sample powders (20 mg) were collected using a
221 dental drill device. The $^{87}\text{Sr}/^{86}\text{Sr}$ ratio measurements were performed using a Thermo Scientific
222 Neptune Multi-collector Inductively Coupled Plasma Mass Spectrometer (MC-ICP-MS)
223 instrument. Within the external precision, repeated analyses of the international Sr standard
224 yielded an average $^{87}\text{Sr}/^{86}\text{Sr}$ ratio of 0.710271 ± 0.000023 (2SD, $n = 43$), in agreement with the
225 accepted $^{87}\text{Sr}/^{86}\text{Sr}$ ratio of 0.710248 for this reference sample (Thirlwall, 1991). At Vrije
226 Universiteit Amsterdam, 6 sample powders (2 - 3 mg) were collected using a New Wave
227 Research micromilling device. Analyses were performed using a ThermoElectron Triton plus
228 TIMS instrument. In order to monitor and document the system's performance, repeated analyses
229 of the international Sr standard ($n = 58$) were carried out on load sizes of 10 ng and 100 ng which
230 yielded average $^{87}\text{Sr}/^{86}\text{Sr}$ ratios of 0.710245 ± 0.000022 (2SD) and 0.710242 ± 0.000008 (2SD),
231 respectively. In both labs mass discrimination correction was performed via internal
232 normalization using Russell's exponential law and the accepted value (0.1194; Steiger and Jager,
233 1977) of the invariant $^{86}\text{Sr}/^{88}\text{Sr}$ ratio.

234 Fluid inclusion microthermometry analysis was performed on 11 doubly polished wafers
235 (80-130 μm in thickness). Measurements were carried out at Parma University (Italy) using
236 Linkam THMSG-600 and Linkam MDS-600 heating-cooling stages coupled with a Leica DM
237 2500 microscope. The final melt ($T_{m_{ice}}$) and homogenization temperatures (T_h) were
238 reproducible within 0.5°C and 5°C, respectively. The stages were calibrated by synthetic Syn
239 FliTM fluid inclusion standards. A 100x objective was used during the microthermometry runs
240 of the small inclusions. The microthermometry data were collected following the Fluid Inclusion
241 Assemblage (FIA) approach described in Goldstein and Reynolds (1994) for carbonate minerals.
242 The inconsistent homogenization temperatures and salinities obtained for these fluid inclusions,
243 within the framework of an individual fluid inclusion assemblage (FIA) described by Goldstein
244 and Reynolds (1994), indicate possible re-equilibration (stretched) of these inclusions and thus
245 are not used in the interpretations. It is common for small inclusions (< 3 μm) to remain mono-
246 phase all-liquid at room temperature due to their metastability (Goldstein and Reynolds, 1994).
247 Thus, to eliminate the possible role of metastability, the samples were placed in a freezer for

248 several days following the procedures described in detail by Goldstein and Reynolds (1994). All-
249 liquid inclusions remained unchanged and no vapor bubble was developed within them, which
250 discards the metastability effect. In order to properly observe the phase transitions and determine
251 the final melting temperature of ice in the all-liquid inclusions, they were rapidly heated up to
252 ~200°C to stretch and nucleate a bubble at room temperature (Goldstein, 1990). The salinities
253 are reported in equivalent weight percent NaCl (eq. wt. % NaCl) and were calculated based on
254 the equation of Bodnar (1993). The homogenization temperatures obtained in all fluid inclusion
255 assemblages indicate the minimum temperatures at which the fluids could have been trapped
256 (Goldstein and Reynolds, 1994). No correction was made for pressure effects on entrapment
257 temperatures since no data regarding the exact depth and pressure of entrapment are available. In
258 absence of independent thermal indicators such as Conodont Alteration Index (CIA) and
259 Vitrinite Reflectance (VR), the accuracy of pressure correction cannot be well constrained
260 (Slobodník et al, 2006), and thus no correction was made for pressure effects on homogenization
261 temperatures.

262 In order to perform a high resolution petrography, Scanning Electron Microscope (SEM)
263 and Back-scattered Scanning Electron Microscope (BSEM) analyses were conducted using a
264 Jeol 6400 Scanning Electron Microscope (SEM) equipped with an Oxford EDS (Energy
265 Dispersive System). Operating conditions were 15 kV and 1.2 nA, electron beam about 1 µm in
266 diameter and 100 s counting time; errors are ±2-5% for major elements and ±5-10% for minor
267 components. The analysis focused mainly on detecting possible dolomite crystals inside the bed-
268 perpendicular stylolites affecting the Cretaceous Scaglia Formation.

269 **4 Results**

270 **4.1 Field observation and distribution of the dolomitized bodies**

271 ~~Dolomitization affected the Calcare Massiccio, Bugarone and Corniola Formations.~~

272 There is no evidences of dolomitization in the overlying and immediate surrounding successions
273 of the Calcare Massiccio, Bugarone and Corniola Formations (e.g. Maiolica and Scaglia
274 Formations), though the base of Maiolica Formation is reported as dolomitized in the Central
275 Apennines onshore (e.g. Pierantoni et al., 2013) and offshore areas (Murgia et al., 2004).

276 Dolomitized intervals are folded in the forelimb of the Montagna dei Fiori Anticline and
277 are abruptly truncated by the Montagna dei Fiori Fault, which juxtaposes them against intensely
278 foliated Scaglia, Bisciaro and Marne con Cerrognia Formations (Figs. 2 and 3). The distribution

279 of dolomitized intervals is wider in the Salinello ~~valley creek~~ (Figs. ~~4B1b, 2A2a~~) perhaps due to
280 a better exposure. In the Corano Quarry location, dolomitization occur in the Calcare Massiccio
281 and Bugarone Formations only as meter-sized dolostone geobodies in the footwall of the
282 Montagna dei Fiori Fault (Fig. 4). The map pattern (Fig. 2) of dolostones indicates that their
283 distribution is maximized in the Castel Manfrino-Osso Caprino hill area and fades out both
284 southward and eastward.

285 ~~Dolostone breccias in fault cores is typically clast supported, with angular and~~
286 ~~millimeter to centimeter sized fragments (Fig. 3C), changing to crackle breccia (Woodcock and~~
287 ~~Mort, 2008) away from the master slip surface. In the proximity of the master slip surface,~~
288 ~~dolostone fragments are sporadically overprinted by millimeter-sized dolomite veins. The~~
289 ~~breccia fragments, where cemented, are commonly surrounded by calcite.~~

290 ~~Dolomitization does not follow a systematic pattern. The lateral extent of dolomitization~~
291 is gradual. In some outcrops, dolomitization fronts show irregular outlines following, but also
292 cross-cutting, ~~the~~ bedding surfaces (Fig. 5). ~~–~~ Dolomitized intervals vary in thickness from a few
293 meters to hundred meters affecting the totality of the exposed Calcare Massiccio and ~~only~~ the
294 lower part of Corniola Formation, where no clay interlayers are present. In the Calcare Massiccio
295 Formation, dolomitization does not follow a systematic pattern. In the northern side of the Osso
296 Caprino hill (Fig. 2), the top of formation is dolomitized but moving toward the Salinello creek,
297 a thick non dolomitized limestone is exposed. The same situation occurs on the opposite side of
298 the creek and to the east of Castel Manfrino.

299 Dolomitized intervals in the Corniola Formation have a darker color relative to the host
300 rock and are systematically more fractured than the hosting limestone. High amplitude (> 1 mm),
301 bed-parallel stylolites are clearly visible in both limestones and dolostones (Fig. 5). However, in
302 some dolostones only ghosts of stylolite traces can be seen. No apparent porosity could be
303 observed in host rock limestones but ~~The~~ dolostones locally contain porosity, appearing as
304 millimetre- to centimetre-sized pores. Dolostone breccias in fault cores are typically clast-
305 supported, with angular and millimeter- to centimeter-sized fragments (Fig. 3C), changing to
306 crackle breccia (Woodcock and Mort, 2008) away from the main slip surface. In the proximity of
307 the main slip surface, dolostone fragments are sporadically cross-cut by millimeter-sized
308 dolomite veins. The breccia fragments, where cemented, are commonly surrounded by calcite
309 cement.

310 4.2 Petrography

311 4.2.1 Early calcite cementation

312 The early diagenetic products in the studied intervals are generally non-ferroan calcite
313 cements. The first calcite cements precipitated following a phase of bioclast micritization (*sensu*
314 Bathurst, 1975) in ~~grain-grain~~-supported intervals. In chronological order, they include: 1)
315 fibrous cements (FC) riming the bioclasts, mostly in the peloidal facies of the Calcare Massiccio
316 Formation (Fig. ~~6A6a~~). These cements are ~~dull-dark brown~~ to non-luminescent under
317 cathodoluminescence; 2) mosaic cements (MC), commonly fill the intergranular pore spaces
318 (Fig. ~~6B6b~~), and also occur as syntaxial overgrowths on echinoderm fragments. ~~These~~
319 ~~cements~~~~They~~ exhibit deformation twinning and show ~~a~~ well-developed ~~dull-brown~~ and orange
320 concentrically-zoned cathodoluminescence pattern (Figs. ~~6C-6c~~ and ~~Dd~~). They contain only
321 mono-phase all-liquid inclusions. All of these cements are postdated by ~~dolomites and~~ high
322 amplitude bed-parallel stylolites (Fig. ~~6b~~).

323 4.2.2 Dolomitization

324 All the dolomite types are non-ferroan and dominantly fabric destructive. ~~Dolomitization~~
325 ~~developed in all the facies types of the Calcare Massiccio and the overlying Bugarone~~
326 ~~Formations, but only at the lower part of the Corniola Formation which consists of reseedimented~~
327 ~~Calcare Massiccio breccias (turbiditic lobes).~~

328 The two first dolomite types (D1 and D2) are the dominant dolomite types in the studied
329 outcrops. These dolomites are distributed within the damage zones of the ~ N-S and E-W
330 Jurassic rift-related extensional faults and, in places, displaced by them (Fig. ~~2A2a~~, site 1). The
331 third and fourth dolomite types (D3 and D4) are mainly observed within the damage zone of the
332 Montagna dei Fiori Fault (NNW-SSE), and appear only as dolomitic pockets ~~locally replacing~~
333 ~~the host rock and overprinting-overgrowing~~ D1 and D2 at the proximity of the ~ N-S and E-W
334 extensional faults. The fifth dolomite type (D5) is found only within the brecciated zones
335 associated with the Montagna dei Fiori Fault damage zone. The distinctive petrographic features
336 of the recognized dolomite types are summarized below:

337 **Dolomite 1 (D1)** is a replacive dolomite which commonly appears as dispersed rhombs and
338 aggregates, and locally rims fracture walls cemented by calcite (~~CV1~~) (Figs. ~~6E-6e~~ and ~~Ff~~). D1
339 postdates the micritic envelopes and early calcite cements, and predates high amplitude bed-
340 parallel stylolites (Figs. ~~6G-6g~~ and ~~Hh~~). The crystals are fine to medium sized (< 350 μm) ~~and~~

341 ~~with planar-e and planar-s textures, consists-consisting~~ of relatively turbid, rich in host rock
342 solid-inclusions-rich, well-developed ~~eu~~hedral to subhedral crystals, ~~-. They show with~~ red
343 luminescence when viewed under cathodoluminescence, occasionally developing a concentric
344 zonation.

345 **Dolomite 2 (D2)** is a replacive dolomite (Figs. ~~7A-7a~~ and ~~Bb~~), infrequently occluding existing
346 pore spaces. Like D1, it also ~~frequently~~ predates high amplitude bed-parallel stylolites (Figs. ~~6G~~
347 ~~6g~~ and ~~Hh~~). D2 generally exhibits a tightly-closely packed texture with no or little
348 intercrystalline porosity. The crystals are medium to coarse sized ($\leq 500 \mu\text{m}$) with planar-s to
349 non-planar textures. They includeing a turbid core followed by a transparent ~~subhedral to~~
350 ~~anhedral~~ rim and trace quantities of saddle dolomite developing swiping-sweeping extinction. In
351 some crystals, one additional turbid zone rich in host rock solid inclusions and fluid inclusions of
352 mostly mono-phase is present. Cathodoluminescence observations enabled to recognize the
353 presence of D1 in their turbid cores. D2 crystals are characterized by zones of bright red-pink
354 luminescence separated by purple luminescence zones (Fig. 7b).

355 **Dolomite 3 (D3)** is present as small localized bodies in the Calcare Massiccio (at the Castel
356 Manfrino reference section), in the Corniola Formation (at the Osso Caprino Road), and in the
357 Calcare Massiccio and Bugarone Formations (at the Corano Quarry) (Figs. 1b and 2a). In the
358 Corano Quarry the dolomitized Bugarone and Calcare Massiccio Formations are in the footwall
359 of the Montagna dei Fiori Fault; and juxtaposed to the ~~undolomitezedundolomitized~~, intensely
360 foliated Scaglia Formation in (the hanging wall). The SEM and BSEM analysis performed on the
361 samples from the immediate adjacent Scaglia Formation within the aforementioned fault damage
362 zone did not indicate the presence of any dolomite in this formation. Within the Bugarone
363 Formation in this fault damage zone, D3 locally cements the millimeter-sized angular breccias
364 that are in turn affected by ~~fault-fault~~-parallel stylolites (Figs. ~~7C-7c~~ and ~~Dd~~). ~~The SEM and~~
365 ~~BSEM analysis performed on the samples from the immediate adjacent Scaglia Formation within~~
366 ~~the aforementioned fault damage zone did not indicate the presence of any dolomite in this~~
367 ~~formation.~~ D3 crystals are fine to medium sized ($< 300 \mu\text{m}$) mostly transparent eu
368 hedral exhibiting planar-e to non-planar textures ($< 300 \mu\text{m}$), with minor development of
369 saddle morphologies in-of larger crystals ($> 500 \mu\text{m}$) with planar-c texture (Figs. ~~7E-7e~~ to ~~Hh~~).
370 The ~~eu~~hedral to anhedral replacive crystals ~~are generally replacive,~~ displaying a faint core, which
371 compared to previous dolomite types has fewer solid inclusions. The saddle crystals are

372 | occasionally replacive ~~but majorly appear as cement in fractures~~. They display typical curved
373 | and slightly serrated crystal terminations with ~~swiping~~sweeping extinction. These saddle
374 | dolomites were only observed in the Castel Manfrino reference section. D3 generally exhibit a
375 | ~~dull-dark~~ purple color with bright orange zones and subzones in core and/or rims when viewed
376 | under cathodoluminescence (Figs. ~~7E-7e~~ to Hh).

377 | **Dolomite 4 (D4)** appears as a matrix replacive and dolomite cement surrounding porosity, and
378 | locally ~~recrystallizing-replacing~~ D1 and D2 (Figs. ~~8A-8a~~ to Ff). D4 also occludes ~~bed-bed-~~
379 | parallel shear fractures and appears along the ~~bed-bed-~~parallel stylolites (Figs. ~~9A-9a~~ to Dd). In
380 | the Castel Manfrino reference section, some intercrystalline vuggy porosity is filled with fine
381 | dolomite rhombs including D4 with relics of D2 within their core (Figs. ~~8E-8e~~ and Ff). ~~The-This~~
382 | porosity may be preserved or partially to completely filled by calcite (CV4C4). D4 crystals have
383 | a turbid, solid-inclusion rich core and transparent rim. They are fine to medium sized (< 200-350
384 | μm), presenting ~~subhedral-planar-s to-and~~ infrequent ~~euhedral-crystals~~non-planar textures. D4
385 | exhibits a distinct luminescence pattern including a purple zone and an irregular green subzone.

386 | **Dolomite 5 (D5)** occurs as crystals cementing micro-veins that cross-cut precursor dolomite
387 | types including dolomitic breccia fragments. In cemented breccias, D5 is postdated by CV3C3.
388 | D5 presents a planar-c texture is transparent, anhedral and is characterized by a bright red
389 | luminescence (Figs. ~~9E-9e~~ and Ff).

390 | 4.2.3 Late calcite cementation

391 | Four generations of calcite ~~veins~~ postdating dolomitization and distributed only within
392 | the fault damage zones have been identified (Figs. 10 and 11):

393 | 1) ~~Calcite-vein~~ 1 (CV1) occurs only in Calcare Massiccio limestones and dolostones and is
394 | represented as centimeter-sized veins with thickness that does not exceed 1.5 cm. It is not clear
395 | whether the fracture opening and calcite precipitation was simultaneous (as shown in Ukar and
396 | Laubach, 2016). These veins are strata-bound, ~~bedding~~-perpendicular ~~veins~~ with irregular
397 | fracture walls, exhibiting white color in the outcrops. They are present within the syn-rift related
398 | extensional fault damage zones, postdate postdating the first dolomite type (D1) and abutted
399 | riming the same fractures that abut the highly high amplitude ~~bed-bed-~~parallel stylolites. CV1
400 | ~~often-usually~~ shows blocky to elongated crystal morphologies and displays well-developed
401 | deformation twinning planes (Type II of Burkhard, 1993). This calcite exhibits concentric ~~al~~

402 zonation and ~~dull-brown~~ zones alternate with orange luminescence zones (Figs. ~~H1A-11a~~ and
403 ~~Bb~~).

404 ~~2)~~ Calcite vein 2 (CV2) exclusively occurs in the intensely deformed Scaglia Formation
405 within the fault damage zones (Figs. 11b, c and d) and correspond to tension gashes associated
406 with stylolites (*sensu* Nelson, 1981). The thickness of these veins does exceed 1 cm. They are
407 usually discontinuous and branch to several microveins (thickness < 1mm) when their tips are
408 not intersected by stylolites. CV2C2 veins are mostly recorded in foliated shear deformation
409 zones with well-defined S-C fabrics, exhibiting blocky, elongated to fibrous shapes with strongly
410 developed tightly spaced deformation twinning planes (Type II of Burkhard, 1993). CV2C2
411 displays ~~yellow-brown~~ to orange luminescence with locally darker sector zones. The ~~yellow~~
412 ~~brown~~ to orange luminescence characteristic of CV2C2 is ~~comparable with~~ similar to those of
413 encasing Scaglia host rocks (Figs. ~~H1C-11c~~ and ~~Dd~~).

414 ~~3)~~ Calcite vein 3 (CV3) occurs as cement, filling the ~~extensional faults~~ Montagna dei
415 Fiori master-main fault plane and isolated veins within ~~the extensional faults~~ damage zones.
416 These veins are centimeter-sized with thicknesses of less than 2 cm. The breccias are generally
417 clast-supported, but locally CV3C3 cements the brecciated fault-infillings containing angular
418 fragments of host rock limestones, dolostones and earlier calcites. In the brecciated zones ~~at the~~
419 ~~backlimb of the anticline (Montagna dei Fiori Fault), CV3C3 always passively overgrows D5 in~~
420 ~~fractures and never cuts it. postdates the last dolomitization phase (D5) with no evidence of~~
421 ~~physical disruption.~~ CV3C3 exhibits a translucent white ~~to translucent~~ color in hand specimen.
422 The crystals are blocky with no or weakly developed deformation twinning planes, and are
423 characterized by a dark orange to brown luminescence with distinct darker sector zones (Figs.
424 ~~H1E-11e~~ and ~~Ff~~).

425 ~~4)~~ Calcite vein 4 (CV4) exists as centimeter-sized isolated veins, pore-filling as well as
426 breccia cements postdating all the preceding dolomites and calcites in the Montagna dei Fiori
427 main fault plane. The breccia fragments are ~~more often~~ usually dolostones. CV4C4 has a
428 translucent white ~~to translucent white~~ color in hand specimen with blocky crystal morphology
429 and no evidence of subsequent deformation (e.g. deformation twinning planes), and is
430 characterized by distinct concentric ~~al~~ zonation (Figs. ~~H1G-11g~~ and ~~Hh~~).

431 4.3 Geochemistry

432 4.3.1 Carbon and oxygen stable isotopes

433 The carbon and oxygen stable isotopic data ($\delta^{13}\text{C}$ and $\delta^{18}\text{O}$) of host rocks, dolomites and
434 calcites are given in Table 1 and shown in Figures [12A-12a](#) and [Bb](#). The marine stable isotopic
435 compositions reported by Veizer et al. (1999) were used as marine reference values.
436 Accordingly, Lower Jurassic marine limestones are characterized by $\delta^{13}\text{C}$ values of -0.5 to
437 +4.5‰ and $\delta^{18}\text{O}$ values of -2.5 to +1.0‰ V-PDB. The $\delta^{18}\text{O}$ values of the marine dolomites are
438 known to be 3-4‰ V-PDB more enriched than those of co-genetic marine limestones (Land,
439 1980; Major et al., 1992; Horita, 2014). In order to avoid data ambiguity due to physical mixing,
440 this analysis was not separately performed on early calcite cements (FC and MC). The $\delta^{13}\text{C}$ and
441 $\delta^{18}\text{O}$ values measured on bulk samples of host rock limestones. Both $\delta^{13}\text{C}$ and $\delta^{18}\text{O}$ values of the
442 host rocks are within the expected range of the Lower Jurassic marine limestones but the
443 Corniola host rocks show slightly lower values comparing to those of Calcare Massiccio. In the
444 Calcare Massiccio host rocks, the $\delta^{13}\text{C}$ values plot between +2.4 and +3.1‰ and $\delta^{18}\text{O}$ values are
445 within the range of -1.6 and 0.0‰ V-PDB. The $\delta^{13}\text{C}$ values in the Corniola host rocks are +2.0
446 and +2.5‰ while the $\delta^{18}\text{O}$ values are -3.1 to -1.4‰ V-PDB. The $\delta^{13}\text{C}$ and $\delta^{18}\text{O}$ values of the
447 Scaglia host rocks range between +1.0 to +3.3‰ for $\delta^{13}\text{C}$ and -2.2 to -1.0‰ V-PDB for $\delta^{18}\text{O}$.
448 The ~~obtained~~-values obtained are characterized in the mean range of Upper Cretaceous to
449 Paleogene marine limestones (Veizer et al., 1999; +1.0 to +4.5‰ for $\delta^{13}\text{C}$ and -4.0 to +2.0‰
450 V-PDB for $\delta^{18}\text{O}$).

451 The $\delta^{13}\text{C}$ values of [CV1C1](#) are between +1.6 and +2.1‰ which plot within the range of
452 reference values (Jurassic) but are slightly lower than the surrounding host rock values. The $\delta^{18}\text{O}$
453 values are between -4.7 and -2.7‰ V-PDB which are lower than those of reference and host rock
454 values.

455 The $\delta^{13}\text{C}$ values of all dolomite types (+0.6 to +3.4‰) fall within the range of host rocks
456 and Jurassic marine limestones (Veizer et al., 1999). The $\delta^{18}\text{O}$ shows a wider range of values,
457 ~~somehow~~ overlapping but also lower than ~~those of~~ host rocks (-4.5 to -0.9‰ V-PDB) and those
458 expected for the ~~presumable~~-Lower Jurassic marine dolomites. The majority of values plot
459 between -3.5 and -1.5‰ V-PDB. The small size and overgrowth nature of certain dolomite types
460 (e.g. D2 and D5) limits their proper isolation for geochemical analyses. Only one sample from
461 D1 dolomite could be measured for $\delta^{13}\text{C}$ and $\delta^{18}\text{O}$ values, showing +2.5 and -1.9‰ V-PDB,
462 respectively. The $\delta^{13}\text{C}$ and $\delta^{18}\text{O}$ values of D3 dolomite range from +2.0 to +2.6‰ and -2.8
463 to -1.9‰ V-PDB, respectively, with values lower than those of the host rock.

464 D4 dolomite has $\delta^{13}\text{C}$ values between +2.4 and +2.5‰, and $\delta^{18}\text{O}$ values of -3.0 to -2.5‰
465 V-PDB. The $\delta^{13}\text{C}$ and $\delta^{18}\text{O}$ values of ~~CV2C2~~ are +1.2 to +3.1‰ and -1.7 to -1.7‰ V-PDB,
466 respectively. The $\delta^{13}\text{C}$ values of ~~CV3C3~~ are between +0.5 and +2.4‰, and the $\delta^{18}\text{O}$ values cover
467 a range of -2.2 to 0.0‰ V-PDB. The $\delta^{13}\text{C}$ and $\delta^{18}\text{O}$ values of ~~CV4C4~~ are +3.8 to +4.9‰ and -9.4
468 to -9.1‰ V-PDB, respectively. The $\delta^{13}\text{C}$ values are slightly higher but the $\delta^{18}\text{O}$ values are
469 considerably lower compared to preceding calcite generations and the measured values from host
470 rocks.

471 4.3.2 $^{87}\text{Sr}/^{86}\text{Sr}$ ratios

472 Samples from host rocks (i.e. Calcare Massiccio and Corniola Formations), dolomites
473 (D1, D3 and D4) and the Scaglia Formation in juxtaposition with the dolostones were analyzed
474 for their $^{87}\text{Sr}/^{86}\text{Sr}$ isotopic ratios. The obtained ratios versus $\delta^{18}\text{O}$ values of the analyzed samples
475 are shown in Fig. 12C. The $^{87}\text{Sr}/^{86}\text{Sr}$ ratios obtained from the Calcare Massiccio and Corniola
476 limestones are 0.70766 and 0.70725 ($n = 2$), respectively, which is in agreement with the values
477 of the Lower Jurassic marine carbonates (0.70704-0.70768) reported by McArthur et al. (2012).
478 CV1 show a value equal to 0.70773.

479 All the dolomite types display higher $^{87}\text{Sr}/^{86}\text{Sr}$ ratios when compared to the host rocks
480 and reference values of the Lower Jurassic marine carbonates. D1 (replacive) and D4 cements
481 show a ~~comparable-similar~~ narrow range with values between 0.70784 and 0.70790, respectively.
482 ~~While, the The~~ two D3 samples (replacive and cement) display higher $^{87}\text{Sr}/^{86}\text{Sr}$ ratios (0.70858
483 and 0.70963, respectively). The $^{87}\text{Sr}/^{86}\text{Sr}$ ratios obtained for dolomites do not show co-variation
484 with corresponding $\delta^{18}\text{O}$ values. The radiogenic Sr analysis was not performed on D2 and D5
485 since the physical mixing with other dolomite types could not be avoided.

486 The $^{87}\text{Sr}/^{86}\text{Sr}$ ratios of the ~~two-three marly limestone~~ samples of Scaglia Formation are
487 0.70784 to 0.70790. The ~~CV2C2~~ veins in Scaglia Formation show ~~comparable-similar~~ ratios of
488 0.70779 and 0.70787. These values fit within the limits of values assigned by McArthur et al.
489 (2012) for the Cenomanian-Bartonian (Scaglia age) marine carbonates (0.70730-0.70790).

490 4.4 Fluid inclusion microthermometry

491 The overview of microthermometry measurements is given in Table 1 and Figs. 13A to
492 C. All the measured fluid inclusions are primary and occur in growth zones. Based on optical and
493 fluorescence microscopy analysis of wafers all the inclusions are aqueous mono-phase (liquid)

494 and two-phase (liquid and vapor) with relatively consistent L:V ratio of 10-15% within a single
495 FIA (fluid inclusion assemblage). Special care was taken to avoid the samples that occasionally
496 displayed scattered mottled luminescence that may indicate recrystallization.

497 ~~On the basis of optical microscopy analysis of wafers,~~ D1 contain dominantly mono-
498 phase aqueous inclusions with sizes greater than 5 μm . ~~It is common for small inclusions~~
499 ~~(<3 μm) to remain mono-phase all liquid at room temperature due to their metastability~~
500 ~~(Goldstein and Reynolds, 1994). Thus, to eliminate the possible role of metastability, the~~
501 ~~samples were placed in a freezer for several days following the procedures described in detail by~~
502 ~~Goldstein and Reynolds (1994). All liquid inclusions remained unchanged and no vapor bubble~~
503 ~~was developed within them, which discards the metastability effect. In order to properly observe~~
504 ~~the phase transitions in the all liquid inclusions, they were rapidly heated up to -200°C to stretch~~
505 ~~and nucleate a bubble at room temperature (Goldstein, 1990).~~ All the inclusions froze at -65
506 to -49°C . The first melting (T_e) was detected between -22 to -19.3°C . The final ice melting (T_m)
507 appeared at temperatures between -7.7 and -2°C . Applying Bodnar's (1993) equation, the
508 obtained final melting temperatures correspond to salinity ranges of 3.5 to 11.3 eq. wt. % NaCl.

509 D2 is characterized by the presence of mono-phase and infrequent two-phase inclusions
510 generally within their growth zones. The homogenization temperature of two-phase inclusions
511 varies between 58 and 71°C . Upon cooling, a complete freezing of the fluid phase is reached
512 at -56 to -40°C . The first ice melting temperature was distinguished at -22°C . The final ice
513 melting temperatures fall within -17.5 and -5°C , corresponding to salinities between 7.9 and
514 20.5 eq. wt. % NaCl.

515 D3 is commonly inclusion poor. The measurable inclusions were detected and examined
516 only in saddle dolomite crystals. These crystals contain only two-phase aqueous inclusions. Their
517 homogenization temperatures are within the narrow range of 70 to 73°C . The complete freezing
518 and first ice melting temperatures could not be distinguished but the final ice melting
519 temperature occurred at temperatures between -13 and -6°C equal to salinity ranges of 9.2 to
520 16.9 eq. wt.% NaCl. The first melting temperatures of fluid inclusions in D1, D2 and D3 were
521 about -21°C , suggesting a H_2O -NaCl fluid system.

522 D4 contains only two-phase aqueous inclusions. The homogenization temperatures in D4
523 vary between 79 and 105°C . Complete freezing of inclusions occurred at temperatures
524 between -86 and -54°C . The first ice melting was detected at -35 to -40°C indicating the

525 possible presence of divalent cations such as Ca^{2+} and/or Mg^{2+} in the fluids (Shepherd et al.,
526 1985; Goldstein and Reynolds, 1994). The final ice melting temperatures fall within a range
527 of -15 and -9°C corresponding to salinities of 12.8 to 18.6 eq. wt. % NaCl. A couple of
528 inclusions show homogenization temperatures exceeding 120°C with salinities higher than
529 20 eq. wt. % NaCl. ~~The inconsistent homogenization temperatures and salinities obtained for
530 these fluid inclusions, within the framework of an individual fluid inclusion assemblage (FIA)
531 described by Goldstein and Reynolds (1994), indicate possible re-equilibration of these
532 inclusions and thus are not used in the interpretations.~~

533 ~~The obtained homogenization temperatures in all fluid inclusion assemblages indicate the
534 minimum temperatures at which the fluids could have been trapped (Goldstein and Reynolds,
535 1994). No correction was made for pressure effects on entrapment temperatures since no data
536 regarding the exact depth and pressure of entrapment are available. In absence of independent
537 thermal indicators such as Conodont Alteration Index (CIA) and Vitrinite Reflectance (VR), the
538 accuracy of pressure correction cannot be well constrained (Slobodník et al, 2006), and thus no
539 correction was made for pressure effects on homogenization temperatures.~~

540 No measurable fluid inclusion could be identified in EV1C1 and EV2C2 due to intense
541 deformation twinning. EV3C3 and EV4C4 contain only primary mono-phase aqueous
542 inclusions, indicating an entrapment temperature of below about 40-50°C (Goldstein and
543 Reynolds, 1994). A complete freezing of the inclusions in EV3C3 occurred at temperatures
544 between -40 and -52.5°C. The first melting temperature was detected at about -21 to -22°C,
545 suggesting a H_2O -NaCl composition. The final melting temperatures range between -6.4
546 and -2.7°C, corresponding to salinities between 9.7 and 4.5 eq. wt. % NaCl. The majority of the
547 values cluster between 7.8 and 5 eq. wt. % NaCl.

548 The complete freezing temperatures of the inclusions in EV4C4 fall within -46
549 and -35.5°C. The first melting temperature could not be determined with confidence but the final
550 melting temperatures were reached at about -0.1 to -1.8°C, corresponding to salinities of 0.17 to
551 3.0 eq. wt. % NaCl.

552 **5 Discussion**

553 **5.1 Stable and radiogenic isotopic composition of the parental fluids**

554 The $\delta^{13}\text{C}$ values of all dolomite types mimic the range of host rock and Jurassic marine
555 limestones and, consequently, they can be interpreted as largely rock-buffered. Their $\delta^{18}\text{O}$ values

556 | are partly ~~comparable-similar~~ to those of their respective host rocks as well as Jurassic marine
557 | reference values but more depleted when compared to the presumable Jurassic marine dolomites.
558 | The relatively depleted $\delta^{18}\text{O}_{\text{dolomite}}$ values could indicate the contribution of heated fluids in
559 | dolomitization process, although it could also relate to recrystallization of a precursor dolomite
560 | by fluids at higher temperature or ^{18}O -depleted (Land, 1980; 1985). The absence of distinctive
561 | textural evidence in the analyzed samples such as enlarged crystal size and/or systematic mottled
562 | cathodoluminescence pattern, and their co-variation with $\delta^{18}\text{O}$ values do not confirm
563 | recrystallization (Mazzullo, 1992 and ref. therein). ~~Nevertheless, special care was taken to avoid~~
564 | ~~the samples that occasionally displayed scattered mottled luminescence.~~

565 | The oxygen isotope fractionation relation between water and dolomite (Land, 1983) was
566 | used to determine the most plausible parental fluids. In order to avoid erroneous results due to
567 | rock-buffered $\delta^{18}\text{O}$ values, only the $\delta^{18}\text{O}$ values of dolomite cements, especially from the ~~bed~~
568 | ~~bed~~-parallel veins containing D4 were used. These values may provide the closest approximation
569 | to the $\delta^{18}\text{O}$ signature of the parental fluids (Barker and Cox, 2011). Accordingly, a $\delta^{18}\text{O}$ value of
570 | $\approx +2.5$ to $+4\%$ V-SMOW was calculated for D3, while this values increase to $\approx +5$ to $+7.5\%$
571 | V-SMOW for D4 (Fig. ~~13D13d~~). ~~The calculated compositions of the potential parental fluids are~~
572 | ~~progressively higher~~—The higher $\delta^{18}\text{O}$ composition of the dolomitizing fluids relative to the
573 | Mesozoic seawater, which is estimated at -1.2 to -1% V-SMOW (Shackleton and Kennett, 1975;
574 | Marshall, 1992; Saelen et al., 1996), is compatible with fluids derived from or that had interacted
575 | with ~~siliciclastic rocks~~, crystalline basement (Taylor, 1997) and/or evaporite-derived
576 | brines.

577 | The $^{87}\text{Sr}/^{86}\text{Sr}$ ratios obtained for all dolomite types are higher than the Lower Jurassic
578 | marine carbonate values (0.70704-0.70768; McArthur et al., 2012). Since marine carbonates
579 | have very low rubidium (Rb) concentrations they produce negligible *in situ* radiogenic ^{87}Sr after
580 | their deposition (Stueber et al. 1972; Burke et al. 1982). Therefore, the higher $^{87}\text{Sr}/^{86}\text{Sr}$ ratios can
581 | be explained by the contribution of fluids originated or interacted with potassium rich
582 | ~~siliciclastic rocks~~ (K-feldspars), crystalline basement and/or stratigraphic levels with
583 | higher $^{87}\text{Sr}/^{86}\text{Sr}$ ratios (Emery and Robinson 1993; Banner, 2004). Taking into account that the
584 | Upper Triassic Burano Formation underlying the studied intervals ~~as the basal detachment~~ has
585 | $^{87}\text{Sr}/^{86}\text{Sr}$ ratios between 0.70774 and 0.70794 (Boschetti et al., 2005), the $^{87}\text{Sr}/^{86}\text{Sr}$ ratios (D1 and
586 | D4) can partially be explained by their contribution. However, this contribution cannot justify

587 much higher $^{87}\text{Sr}/^{86}\text{Sr}$ ratios recorded in D3, being higher than values reported for Phanerozoic
588 seawater (McArthur et al., 2012), and the values ~~recorded in~~obtained for the adjacent basinal
589 deposits (i.e. Corniola and Scaglia Formations). Therefore, parental fluids most likely originated
590 from or had interacted with the ~~siliciclastic~~siliciclastic rocks underlying the Burano Formation
591 (Verrucano Formation), if present, and/or with the crystalline basement with common elevated
592 $^{87}\text{Sr}/^{86}\text{Sr}$ ratios (0.71500-0.72650; Del Moro et al., 1982). The significantly higher $^{87}\text{Sr}/^{86}\text{Sr}$ ratios
593 in D3 in comparison with other studied dolomites indicates a higher influence of $^{87}\text{Sr}/^{86}\text{Sr}$ -rich
594 fluids either due to major changes in the permeability architecture of faults or availability of such
595 fluids. The lack of any ferroan diagenetic phase minimizes the interaction of fluids produced by
596 clay transformation/dewatering (i.e. smectite to illite transformation; Boles and Franks, 1979).

597 CV1C1 is characterized by $\delta^{13}\text{C}$ and $\delta^{18}\text{O}$ values lower than the host limestones (i.e.
598 Calcare Massiccio), while its $^{87}\text{Sr}/^{86}\text{Sr}$ ratio is ~~comparable to~~similar to them. The salinity and
599 composition of the parental fluids cannot be inferred here since no measurable fluid inclusions
600 were found within this cement. The $^{87}\text{Sr}/^{86}\text{Sr}$ ratio being within the range of the corresponding
601 host rocks and the reference values, points to a rock-buffered system for $^{87}\text{Sr}/^{86}\text{Sr}$.

602 The $\delta^{13}\text{C}$ and $\delta^{18}\text{O}$ values obtained for CV2C2, as well as $^{87}\text{Sr}/^{86}\text{Sr}$ ratios, fall within the
603 range of the Scaglia host rocks, thus reflecting their rock-buffered nature. This interpretation is
604 further supported by the ~~comparable to~~similar luminescence characteristics of CV2C2 with that of
605 encasing Scaglia host rocks. The fluids from which CV2C2 calcite precipitated, as expected for
606 tension gashes, were most likely derived from carbonate dissolution during pressure-solution and
607 stylolitization of host rock-, pointing to a closed fluid system in contrast with the subsequent vein
608 generations.

609 CV3C3 is characterized by $\delta^{13}\text{C}$ values within the Jurassic marine values but are
610 generally lower than the host rocks, while their $\delta^{18}\text{O}$ values partially overlap both the hosting
611 limestones and dolostones. Microthermometry of fluid inclusions revealed only mono-phase
612 aqueous inclusions and thus precipitation at relatively low temperature ($\leq 40\text{-}50^\circ\text{C}$) with
613 moderate salinity (4.5-9.7 eq. wt. % NaCl). Such levels of salinity can be assigned to evaporated
614 seawater, residual brines or fluids derived from evaporite dissolution, and thus makes it difficult
615 here to interpret their exact origin with the available data.

616 CV4C4 is the latest calcite phase, and records the $\delta^{13}\text{C}$ and $\delta^{18}\text{O}$ values, respectively
617 enriched and significantly depleted when compared to their hosting rocks and preceding

618 diagenetic products. Generally, the enrichment of ^{13}C could suggest CO_2 outgassing due to
619 | evaporation or pressure changes (Friedman, 1970; Hendry et al., 2015) or bacterial fermentation
620 | (methanogenesis) of organic matter (Hudson, 1977) in low temperature diagenetic environments.
621 | The homogenization temperature of CV4C4, being below about 40-50°C, could support any of
622 | these processes. Their low $\delta^{18}\text{O}$ values and fluid inclusions with salinities comparable-similar to,
623 | but also significantly lower than, seawater reflect the contribution of meteoric fluids during
624 | precipitation of this calcite.

625 **5.2 Origin of the dolomitizing fluids**

626 | The contribution of brines that derived from highly evaporated seawater or evaporites is
627 | suggested by the elevated salinity values obtained from microthermometry of the fluid inclusions
628 | (3.5 to 20.5 eq. wt. % NaCl). Accordingly, two sources that could potentially provide such fluids
629 | can be proposed: 1) fluids related to the Late Messinian evaporites, associated with the overlying
630 | Upper Miocene Laga Formation, ~~deposited during the Upper Miocene time,~~ and their possible
631 | downward percolation through fault zones by density driven flow and/or seismic pumping
632 | mechanisms (Sibson, 1981; McCaig, 1988, 1990); or their tectonic involvement into the
633 | Apenninic thrust wedge during its propagation (underthrusting; Lobato et al., 1983); and 2)
634 | fluids related to the underlying décollement-detachment horizon of the Burano evaporites (Upper
635 | Triassic) and their upward flow through fault zones during development of the Montagna dei
636 | Fiori Anticline. The first scenario is valid if the dolomitization would have occurred only from
637 | the Upper Miocene time onwards. Moreover, Several-several researchers (e.g. Vai and Ricci
638 | Lucchi, 1977; Bassetti et al., 1998; Roveri et al. 2001) have shown that the occurrence of
639 | primary shallow-water evaporites, which were dominantly gypsum, was limited only to the
640 | western and central parts of the northern Apennines consisting of thrust-top marginal basins. ~~In~~
641 | ~~contrast, evaporites never precipitated in parts of the central Apennines including the Montagna~~
642 | ~~dei Fiori region (Marche area)~~ (Roveri et al. 2001). Hence, the evaporitic horizons existing
643 | within the Laga Formation corresponds to re-sedimentation (gypsum debris) of those previously
644 | precipitated in the marginal basins. This interpretation makes the Messinian evaporites an
645 | unlikely source of Mg-rich brines. ~~Moreover, taking~~ Taking into account that the maximum
646 | burial-burial-related temperature of the Calcare Massiccio Formation did not exceed 80°C in the
647 | Montagna dei Fiori region (Ronchi et al., 2003), ~~it's-it is not-unlikely~~ that the downward
648 | percolation of relatively low-temperature brines derived from the Messinian evaporites, located

649 | at ~~the~~ higher stratigraphic levels, could reach or exceed the high temperatures recorded in fluid
650 | inclusions of the studied dolomites ~~in the Calcare Massiccio Formation~~ (D4; up to 105°C), given
651 | that the homogenization temperatures reflect the minimum entrapment temperatures (Goldstein
652 | and Reynolds, 1994). Deep circulation of these brines, if they existed, can also be excluded by
653 | the fact that their limited ~~tectonic~~ involvement ~~with~~in the thrust wedge ~~being~~ was confined
654 | merely to the off shore wards of the Montagna dei Fiori region (Artoni, 2013).

655 | Accordingly, the Upper Triassic Burano Formation, the basal detachment, appears as the
656 | most plausible source for the high salinity brines recorded in fluid inclusions, and likewise, the
657 | Mg-rich fluids could have been originated from post-evaporite brines associated with them
658 | (Carpenter, 1978; McCaffrey et al., 1987). The fluctuations in salinity may argue for ~~different~~
659 | degrees of diverse range of fault connectivity, different degrees of rock-water interaction and
660 | contribution of pore waters of lower salinity (e.g. marine or meteoric).

661 | **5.3 Timing and structural controls on the evolution of parental fluids**

662 | A generalized paragenesis and the relative chronology of dolomitization in relation to the
663 | structural evolution of the Montagna dei Fiori Anticline are illustrated in Figs. 14 and 15. The
664 | structural episodes are based on the evolutionary stages of the Montagna dei Fiori Anticline
665 | suggested by Storti et al. (2018). The paragenesis is constructed on the basis of direct evidences
666 | recorded during observations at outcrop scale and microscopic observations (e.g. cross-cutting
667 | relationships between diagenetic phases, stylolites, fractures and other structural kinematics), and
668 | indirect evidences (e.g. regional geodynamics and burial history).

669 | The occurrence of micritic envelopes and fibrous calcite cements (FC), in ~~grain-grain-~~
670 | supported stratigraphic levels of the Calcare Massiccio Formation, is interpreted to be of
671 | eogenetic origin (i.e. marine phreatic diagenesis; Moore, 1989), reflecting an early diagenesis
672 | shortly after deposition. The well-developed ~~dull~~ brown and orange concentric
673 | cathodoluminescence pattern of the succeeding mosaic calcite cement (MC) suggests a
674 | progressive shift to more reducing conditions during precipitation in a phreatic diagenetic
675 | environment (as shown in Li et al., 2017). High amplitude ~~bed-bed-~~parallel stylolites postdate
676 | both cements, which confirm their precipitation before significant burial. The observations made
677 | here are in agreement with earlier work by Giacometti and Ronchi (2000), interpreting that the
678 | Calcare Massiccio Formation was cemented during the early diagenetic stages.

679 D1, ~~CV1C1~~ and D2 are ~~postdated-cut~~ by well-developed, high amplitude bed-parallel
680 stylolites. Presence of D1 and ~~CV1C1~~ in bed-perpendicular veins typically ~~abutted-cut~~ by these
681 stylolites (see Figs. ~~6E-6e~~ to ~~Hh~~) support the interpretation that the first dolomitization event (D1
682 and D2) took place before significant burial and stylolite development, ~~being-t~~The latter and
683 bed-perpendicular veins are dynamically compatible within the same stress field which is
684 characterized by a vertical, load-related maximum principal axis of the stress ellipsoid (Fig. 15a).
685 The dominantly mono-phase fluid inclusions within D1 and D2 are in agreement with
686 precipitation temperatures below about 40-50°C, suggesting a relatively shallow to intermediate
687 burial environment and hence supporting a pre-Apenninic orogeny age of precipitation from a
688 mix of formational and extra-formational fluids with elevated $^{87}\text{Sr}/^{86}\text{Sr}$ ratios. The distribution of
689 D1 and D2 localized nearby the rifting-related ~ N-S and E-W striking extensional faults and
690 even their displacement along them (Fig. 2A2a, e.g. site 1), point to the possible contribution of
691 these faults in occurrence of D1 and D2. These faults dominantly affect the Jurassic rocks older
692 than the Maiolica Formation which is attributed to ~~the~~ post-rift deposits, therefore suggesting a
693 pre-Maiolica age for these dolomite types. Although, an absolute age cannot be provided, based
694 on the evidence discussed above, the circulation of Mg-rich fluids during this dolomitization
695 event was most likely controlled by rifting-related Jurassic extensional fault zones cutting
696 through the crystalline basement. Precipitation of D1 and D2 at the lower part of Corniola
697 Formation which is known as the syn-rift deposit discards a pre-rift origin for these dolomites.
698 The displacement of dolomites along the aforementioned faults is possibly related to their
699 prolonged activation during Early to Late Jurassic. In addition to the role of these faults in
700 channelizing the fluids, their mobilization must have been intensified by some deriving
701 mechanisms. A thermal convection system derived from high heat flux during rifting was
702 interpreted by Hollis et al. (2017) to be responsible for circulation of seawater in a syn-rift
703 dolomitization case in the Hammam Faraun fault block (Suez Rift, Egypt). In such scenario, the
704 salinity of the fluids and their $^{87}\text{Sr}/^{86}\text{Sr}$ ratios are expected to be more or less within the range of
705 seawater. Furthermore, this scenario seems unlikely in the studied area given the lack of a deep
706 aquifer to accommodate the fault tips and promotes the lateral fluid flux from basin to the rift
707 shoulders and vice versa. Taking into account that D1 and D2 are the volumetrically more
708 relevant dolomites within the studied intervals, and assuming the likely role of syn-rift
709 extensional faults (Early to Late Jurassic) in their precipitation, a dominantly syn-rift

710 dolomitization process is proposed for the dolostones in the Montagna dei Fiori Anticline.
711 Although the CL zonation pattern observed in D2 may indicate changes in flow condition or
712 fluid composition, the lack of physical disruptions such as multiple fracturing suggests external
713 regional controls rather than slip along the same faults (Eichhubl and Boles, 2000). The absence
714 of pervasive syn-dolomitization fracturing and brecciation as well as zebra fabrics in these
715 dolomites, perhaps indicate a relatively calm tectonic period during dolomite development (e.g.
716 Hollis et al., 2017).

717 D3 and D4 both record elevated $^{87}\text{Sr}/^{86}\text{Sr}$ ratios which accounts for their fault-controlled
718 origin. However, their occurrence at the top of the Calcare Massiccio and overlaying Bugarone
719 Formation (Corano Quarry site) which is < 1 m thick in Montagna dei Fiori region, and is
720 marked as the final rift deposit (Cardello and Doglioni, 2015) discards a syn-rift origin for these
721 dolomites. Moreover, D3 and D4 postdate the development of high amplitude ~~bed-bed~~-parallel
722 stylolites. The formation of stylolites requires an approximate overburden of 600 to 1500 m
723 (Lind, 1993; Machel, 1999; Mountjoy et al., 1999; Schulz et al., 2016), corresponding to a late to
724 post-Maiolica deposition time (Early Cretaceous time onwards). The presence of D3 and D4
725 dolomites in ~~bed-bed~~-parallel fractures and as shear veins (D4) (Figs. 9a and b) suggests their
726 association with contractional deformations, i.e. the most likely tectonic regime for explaining
727 bed-perpendicular dilation. Therefore, the volumetrically minor second stage of dolomite
728 precipitation may possibly be related to the Late- to post-Miocene compressional tectonics
729 recorded in this region (e.g. Mazzoli et al., 2002; Artoni, 2013; Storti et al., 2018).

730 Dolostones containing D3 and D4 appear commonly as clast-supported breccias along
731 fault zones pertaining to the Montagna dei Fiori Fault, then overprinted by fault-parallel
732 stylolites (Figs. 3 and 7). Accordingly, the occurrence of these dolomites was probably
733 synchronous with the incipient stages of fault development, predating fault buttressing (Storti et
734 al., 2018). Homogenization temperatures recorded in D4 (up to 105°C), much higher than the
735 maximum temperatures recorded in the host rocks (below about 80°C; Ronchi et al., 2003),
736 suggest hydrothermal fluid circulation. The development of the Montagna dei Fiori Anticline at
737 the toe of the Late Miocene Central Apennines thrust wedge could have favored the
738 forelandward migration of hydrothermal fluids expelled from the more internal regions of the
739 belt, similarly to what has been proposed for the Rocky Mountains foreland (i.e. squeegee flow
740 model; Machel and Cavell, (1999). Such a migration may have possibly favored the precipitation

741 of D4 in ~~bed-bed~~-parallel veins, generally considered as evidence for syn-compressional fluid
742 overpressure (Sibson, 2001; Hiemstra and Goldstein, 2015). At this stage, in addition to dilation
743 of the pre-existing ~ N-S and E-W striking rift-related extensional faults and their possible role
744 in fluid migration, the excess of pore pressure at the base of the thrust ramp, in the fold hinge and
745 during fold tightening could promote the localization of the fractures (Smith and Wiltschko,
746 1996; Ghisetti and Vezzani, 2000), with fluid migration within this zone and eventually
747 dolomitization. These fractures could have been corridors that later on formed the insipient NW-
748 SE Montagna dei Fiori Fault. Their localization at the back-limb cross-cutting the core,
749 explaining best the distribution of D3 and D4 at this locality. The presence of only D5 ~~only~~
750 within the damage zone of the Montagna dei Fiori Fault, postdating dolostone brecciation and, in
751 places, cementing breccia fragments, ~~may~~ suggest that D5 dolomite precipitation was associated
752 with the late stage evolution of the Montagna dei Fiori Fault, predating late stage calcite
753 precipitation. The shift from dolomite to calcite precipitation can be ascribed to attenuation of
754 Mg-rich fluids and/or calcite saturation. This condition was perhaps initiated during the late
755 stages of anticline evolution due to changes in fault conductivity sealing the upward migration of
756 Mg-rich fluids.

757 The presence of several generations of ~~bed-bed~~-perpendicular stylolites bounding and
758 intersecting EV2C2 veins (Fig. 10), supports the postulation that late stage calcite cements
759 precipitated in close ~~elosely associated~~-association with the deformation history of the Scaglia
760 Formation in the hanging wall of the Montagna dei Fiori Fault (Fig. 3). This deformation
761 occurred; during buttressing against Calcare Massiccio and Corniola Formations in the footwall,
762 and related with the positive inversion event induced by thrust-sheet stacking at depth (Storti et
763 al., 2018). Precipitation of EV3C3 and EV4C4 ~~in-is~~ interpreted to have occurred during uplift
764 and cooling as revealed by their relatively low homogenization temperatures ($\leq 40-50^{\circ}\text{C}$). of fluid
765 inclusions trapped within these cements. Deformation twining is either absent or weakly
766 developed, reflecting the lack of significant tectonic deformation after calcite precipitation.

767 These cements postdate the dolomitization events, high amplitude ~~bed-bed~~-perpendicular and
768 parallel stylolites, and are precipitated as cements bounding the breccia fragments within the
769 damage zone of the Montagna dei Fiori Fault. Salinities calculated from their fluid inclusions,
770 particularly in EV4C4, suggests precipitation from meteoric waters, which should have been
771 favored during the late evolutionary stages of antiformal stacking beneath the Montagna dei Fiori

772 Anticline, and eventual late extensional slip along the Montagna dei Fiori Fault (Storti et al.,
773 2018). The results obtained in this study are in relative agreement with the earlier work by
774 Ronchi et al. (2003) and Murgia et al. (2004) in the Central Apennines, assigning dolomitization
775 phases to the pre- and syn-orogenic deformations, although they did not specify the direct
776 relation between the local structures and the different types of dolomite.

777 The textures of the studied dolomites vary from planar-e to non-planar, the preponderance of
778 planar dolomite, as in D4, creates a rock with interesting poroperm characteristics (e.g. Woody et
779 al., 1996; Wilson et al., 2007; Wenzhi et al., 2012). This case-study is certainly relevant for
780 many potential reservoirs elsewhere in the world. Similar multistage burial dolomitization events
781 enhancing the reservoir quality have been reported from the carbonate successions of the Jurassic
782 in the Kopet-Dagh Basin, north eastern Iran (Adabi, 2009) and Devonian of the Rainbow sub-
783 Basin, western Canada (Qing and Mountjoy, 1989; Lonnee, 1999).

784 **6 Conclusions**

785 The Lower Jurassic limestones outcropping at the core of the Montagna dei Fiori
786 Anticline (Central Apennines, Italy) are massively affected by dolomitization, in damage zones
787 of the pre-orogenic faults inherited from the Tethyan rifting and the ones formed during the
788 Apenninic orogeny. Cross-cutting relationships between deformation structures, and results from
789 optical and cold cathodoluminescence petrography, fluid inclusion microthermometry, and
790 isotope geochemistry, support the occurrence of two major dolomitization events. The first event
791 is interpreted as having developed during the late stages of Tethyan rifting in Jurassic and
792 resulted in volumetrically significant dolostone geobodies. These dolostones are majorly-largely
793 matrix replacive, and their precipitation initiated prior to the significant burial as reflected in
794 their cross-cutting relationship with bed-bed-parallel stylolites, and by homogenization
795 temperatures in fluid inclusions that are dominantly below about 40-50°C. The second
796 dolomitization event corresponds to volumetrically less relevant replacive dolomite and dolomite
797 cements occluding fractures. These dolomites precipitated during hydrothermal fluid circulation
798 associated with contractional tectonics during the Apenninic orogeny, possibly at the onset of the
799 growth of the Montagna dei Fiori Anticline (Late Miocene).

800 Dolomitizing fluids in both events were most likely sourced from evaporitic brines
801 associated to the underlying Burano evaporites and their interaction with siliciclastics-siliciclastic
802 rocks and/or the crystalline basement.

803

804 *Author contributions.* M. Mozafari participated in fieldwork, performed petrographic and
805 microthermometric analyses, provided their interpretation, and wrote the manuscript; R.
806 Swennen participated in fieldwork, discussed the results of the diagenetic study, and critically
807 reviewed the manuscript; F. Balsamo contributed to collect and interpret structural data,
808 discussed structural diagenesis data interpretation, and critically reviewed the manuscript; H. El
809 Desouky collected $^{87}\text{Sr}/^{86}\text{Sr}$ data; F. Storti conceived the research, contributed to collect and
810 interpret structural data, discussed structural diagenesis data interpretation, and critically
811 reviewed the manuscript; C. Taberner participated in fieldwork, discussed the results of the
812 diagenetic study and their framing into the proposed structural evolution, and critically reviewed
813 the manuscript.

814

815 *Acknowledgments.* This research was performed by collaboration between Parma and KU
816 Leuven universities in the framework of a research project (PT12432 and GFSTE 1100942)
817 funded by Shell Global Solutions International (Carbonate Research Team, now Geology and
818 New Reservoir Types Team). We thank E.M. Selmo (Parma University) and M. Joachimski
819 (University of Erlangen, Germany) for the stable carbon and oxygen analysis. G. Davis (VU
820 Amsterdam, the Netherlands) is thanked for the strontium isotope analysis. A. Comelli and H.
821 Nijs are kindly thanked for the careful preparation of the wafers and thin sections. L. Barchi is
822 gratefully appreciated for his help in SEM analysis. We ~~gratefully~~ acknowledge A. Koopman for
823 the constructive discussions during field work. We appreciate D. Smith (Energie Beheer
824 Nederland, the Netherlands) for the careful reviewing of the manuscript. We are very grateful to
825 reviewers J. Hendry and E. Ukar for their suggestions that allowed us to significantly improve
826 the manuscript.

827

828 **References**

- 829 Adabi, M. H.: Multistage dolomitization of upper jurassic mozduran formation, Kopet-Dagh
830 Basin, NE Iran. Carbonates and Evaporites, 24, 16-32,
831 <https://doi.org/10.1007/BF03228054>, 2009.
- 832 Alvarez, W.: Evolution of the Monte Nerone Seamount in the Umbria-Marches Apennines; I,
833 Jurassic-Tertiary stratigraphy, B. Soc. Geol. Ital., 108, 3-21, 1989.
- 834 Amieux, P.: La cathodoluminescence: méthode d'étude sédimentologique des carbonates, B.
835 Cent. Rech. Explor.-Prod. Elf-Aquitaine, 6, 437-483, 1982.
- 836 Artoni, A.: Messinian events within the tectono-stratigraphic evolution of the Southern Laga
837 Basin (Central Apennines, Italy), B. Soc Geol. Ital., 122, 447-466, 2003.
- 838 Artoni, A.: The Pliocene-Pleistocene stratigraphic and tectonic evolution of the central sector of
839 the Western Periadriatic Basin of Italy, Mar. Pet. Geol., 42, 82-106,
840 <https://doi.org/10.1016/j.marpetgeo.2012.10.005>, 2013.
- 841 Banner, J. L.: Radiogenic isotopes: systematics and applications to earth surface processes and
842 chemical stratigraphy, Earth. Sci. Rev., 65, 141-194, [https://doi.org/10.1016/S0012-](https://doi.org/10.1016/S0012-8252(03)00086-2)
843 [8252\(03\)00086-2](https://doi.org/10.1016/S0012-8252(03)00086-2), 2004.
- 844 Barchi, M., Minelli, G., and Pialli G.: The CROP 03 profile: a synthesis of results of deep
845 structures of the Northern Apennines, Mem. Soc. Geol. It., 52, 383-400, 1998.
- 846 Barker, S. L., and Cox, S. F.: Evolution of fluid chemistry and fluid-flow pathways during
847 folding and faulting: an example from Taemas, NSW, Australia, Geol. Soc. London
848 Spec. Publ., 359, 203-227, <https://doi.org/10.1144/SP359.12>, 2011.
- 849 Bassetti, M. A., Ricci Lucchi, F., Roveri, M., Taviani, M.: Messinian facies in a critical section
850 of northern Apennines (Montepetra-Peticara, Pesaro), Giorn. Geol., 60, 261-263,
851 1998.
- 852 Bathurst, R. G. C. (Eds.): Carbonate sediments and their diagenesis, Dev. Sedimentol., Ser.,
853 Elsevier, 12, 658 pp., 1975.
- 854 Bathurst, R. G. C.: Deep crustal diagenesis in limestones: Revista del Instituto de Investigaciones
855 Geológicas, Deputacion Provincial, Universidad Barcelona, 34, 89-100, 1980.
- 856 Bernoulli, D., Kälin, O., and Patacca, E.: A sunken continental margin of the Mesozoic Tethys:
857 The Northern and Central Apennines, Symposium" Sédimentation jurassique W
858 Européen", Spec. Publ. Ass. Sedim. Francis, 1, 179-210, 1979.

- 859 Bodnar, R. J.: Revised equation and table for determining the freezing point depression of H₂O-
860 NaCl solutions, *Geochim. Cosmochim. Acta*, 57, 683-684, 10.1016/0016-
861 7037(93)90378-A, 1993.
- 862 Boles, J. R. and Franks, S. G.: Clay diagenesis in Wilcox Sandstone of southwest Texas:
863 Implications of smectite diagenesis and sandstone cementation, *J. Sediment. Petrol.*,
864 49, 55-70, <https://doi.org/10.1306/212F76BC-2B24-11D7-8648000102C1865D>,
865 1979.
- 866 Bollati, A., Corrado, S., and Marino, M.: Inheritance of Jurassic rifted margin architecture into
867 the Apennines Neogene mountain building: a case history from the Lucretili Mts.
868 (Latium, Central Italy), *Int. J. Earth Sci.*, 101, 1011-1031,
869 <https://doi.org/10.1007/s00531-011-0694-7>, 2012.
- 870 Bosence, D., Procter, E., Aurell, M., Kahla, A. B., Boudagher-Fadel, M., Casaglia, F., Cirilli, S.,
871 Mehdie, M., Nieto, L., Rey, J., Scherreiks, R., Soussi, M., and Waltham, D.: A
872 dominant tectonic signal in high-frequency, peritidal carbonate cycles? A regional
873 analysis of Liassic platforms from western Tethys, *J. Sediment. Res.*, 79, 389-415,
874 <https://doi.org/10.2110/jsr.2009.038>, 2009.
- 875 Boschetti, T., Venturelli, G., Toscani, L., Barbieri, M., and Mucchino, C.: The Bagni di Lucca
876 thermal waters (Tuscany, Italy): an example of CaSO₄ waters with high Na/Cl and
877 low Ca/SO₄ ratios, *J. Hydrol.*, 307, 270-293,
878 <https://doi.org/10.1016/j.jhydrol.2004.10.015>, 2005.
- 879 Brandano, M., Cornacchia, I., Raffi, I., and Tomassetti, L.: The Oligocene-Miocene stratigraphic
880 evolution of the Majella carbonate platform (Central Apennines, Italy), *Sediment.*
881 *Geol.*, 333, 1-14, <https://doi.org/10.1016/j.sedgeo.2015.12.002>, 2016.
- 882 Burke, W. H., Denison, R. E., Hetherington, E. A., Koepnick, R. B., Nelson, H. F., and Otto, J.
883 B.: Variation of seawater ⁸⁷Sr/⁸⁶Sr throughout Phanerozoic time, *Geology*, 10, 516-
884 519, [https://doi.org/10.1130/0091-7613\(1982\)10<516:VOSSTP>2.0.CO;2](https://doi.org/10.1130/0091-7613(1982)10<516:VOSSTP>2.0.CO;2), 1982.
- 885 Burkhard, M.: Calcite twins, their geometry, appearance and significance as stress-strain markers
886 and indicators of tectonic regime: a review, *J. Struct. Geol.*, 15, 351-368,
887 [https://doi.org/10.1016/0191-8141\(93\)90132-T](https://doi.org/10.1016/0191-8141(93)90132-T), 1993.
- 888 Calamita, F., Cello, G., Deiana, G., and Paltrinieri, W.: Structural styles, chronology rates of
889 deformation, and time-space relationships in the Umbria-Marche thrust system

890 (central Apennines, Italy), *Tectonics*, 13, 873-881,
891 <https://doi.org/10.1029/94TC00276>, 1994.

892 Cardello, G. L., and Doglioni, C.: From mesozoic rifting to Apennine orogeny: the gran Sasso
893 range (Italy), *Gondwana Res.*, 27, 1307-1334,
894 <https://doi.org/10.1016/j.gr.2014.09.009>, 2015.

895 Carpenter, B.: Origin and chemical evolution of brines in sedimentary basins, *Oklahoma Geol.*
896 *Surv.*, 79, 60-77, <https://doi.org/10.2118/7504-MS>, 1978.

897 Centamore, E., Chiocchini, U., and Moretti, A.. Geologia della zona tra Acerenza e Avigliano
898 (Prov. di Potenza), *Studi Geol. Camerti*, 1, 97-122,
899 <http://dx.doi.org/10.15165/studgeocam-1462>, 1971.

900 Chilovi, C., De Feyter, A. J., Minelli, G., and Barchi, M. R.. Neogene strike-slip reactivation of
901 Jurassic normal faults in the M. Nerone-M. Catria Anticline (Umbro-Marchean Apennines,
902 Italy), *Boll. Soc. Geol. It.*, 121, 199-207, 2002.

903 Choukroune, P., Gapais, D., and Merle, O.: Shear criteria and structural symmetry, *J. Struct.*
904 *Geol.*, 9, 525-530, [https://doi.org/10.1016/0191-8141\(87\)90137-4](https://doi.org/10.1016/0191-8141(87)90137-4), 1987.

905 Clemenzi, L., Storti, F., Balsamo, F., Molli, G., Ellam, R., Mucchez, P., and Swennen, R.: Fluid
906 pressure cycles, variations in permeability, and weakening mechanisms along low-
907 angle normal faults: The Tellaro detachment, Italy, *Am. Assoc. Pet. Geol. Bull.*, 127,
908 1689-1710, <https://doi.org/10.1130/B31203.1>, 2015.

909 Colacicchi, R., Passeri, L., and Piali, G.: Evidences of tidal environment deposition in the
910 Calcare Massiccio formation (Central Apennines-Lower Lias), in: *Tidal Deposits*,
911 edited by: Ginsburg, R. N., Springer, Berlin, Heidelberg, Germany, 345-353,
912 <https://doi.org/10.1007/978-3-642-88494-8>, 1975.

913 Cooper, J. C., and Burbi, L.: The geology of the central Sibillini Mountains, *Mem. Soc. Geol. It.*,
914 35, 323-347, 1986.

915 Crescenti, U.: Serie stratigrafiche della serie calcarea dal Lias al Miocene nella regione
916 Marchigiano Abruzzese: parte I and II, *Mem. Soc. Geol. It.*, 8, 155-420, 1969.

917 Davies, G. R., and Smith, L. B. J.: Structurally controlled hydrothermal dolomite reservoir
918 facies: an overview, *Am. Assoc. Pet. Geol. Bull.*, 90, 1641-1690, 2006.

919 Del Moro, A., Puxeddu, M., Radicati di Brozolo, F., and Villa, I. M.: Rb-Sr and K-Ar ages of
920 minerals at temperatures of 300-400°C from deep wells in the Larderello geothermal

- 921 field (Italy), *Contrib. Mineral. Petr.*, 81, 349-349,
922 <https://doi.org/10.1007/BF00371688>, 1982.
- 923 Dewever, B., Swennen, R., and Breesch, L.: Fluid flow compartmentalization in the Sicilian fold
924 and thrust belt: implications for the regional aqueous fluid flow and oil migration
925 history, *Tectonophysics*, 591, 194-209, <https://doi.org/10.1016/j.tecto.2011.08.009>,
926 2013.
- 927 Dewey, J. F., Helman, M. L., Turco, E., Hutton, D. H. W., and Knott, S. D.: Kinematics of the
928 western Mediterranean, in: *Alpine Tectonics*, edited by: Coward, M. P., Dietrich, D.,
929 Park, R. G., *Geol. Soc. London Spec. Publ.*, 45, 265-283,
930 <https://doi.org/10.1144/GSL.SP.1989.045.01.15>, 1989.
- 931 Dewit, J., Foubert, A., El Desouky, H. A., Muchez, P., Hunt, D., Vanhaecke, F., and Swennen,
932 R.: Characteristics, genesis and parameters controlling the development of a large
933 stratabound HTD body at Matienzo (Ramales Platform, Basque-Cantabrian Basin,
934 northern Spain), *Mar. Pet. Geol.*, 55, 6-25, [10.1016/j.marpetgeo.2013.12.021](https://doi.org/10.1016/j.marpetgeo.2013.12.021), 2014.
- 935 Dickson, J. A. D.: Carbonate identification and genesis as revealed by staining, *J. Sediment.*
936 *Petrol.*, 36, 491-505, [https://doi.org/10.1306/74D714F6-2B21-11D7-](https://doi.org/10.1306/74D714F6-2B21-11D7-8648000102C1865D)
937 [8648000102C1865D](https://doi.org/10.1306/74D714F6-2B21-11D7-8648000102C1865D), 1966.
- 938 Di Francesco, L., Fabbi, S., Santantonio, M., Bigi, S., and Poblet, J.: Contribution of different
939 kinematic models and a complex Jurassic stratigraphy in the construction of a
940 forward model for the Montagna dei Fiori fault-related fold (Central Apennines,
941 Italy), *Geol. J.*, 45, 489-505, <https://doi.org/10.1002/gj.1191>, 2010.
- 942 [Eichhubl, P., and Boles, J. R.: Rates of fluid flow in fault systems: evidence for episodic rapid](#)
943 [fluid flow in the Miocene Monterey Formation, coastal California, *Am. J. Sci.*, 300,](#)
944 [571-600, doi: 10.2475/ajs.300.7.571, 2000.](#)
- 945 Elter, P., Giglia, G., Tongiorgi, M., and Trevisan, L.: Tensional and contractional areas in the
946 recent (Tortonian to Present) evolution of the Northern Apennines, *B. Geofis. Teor.*
947 *Appl.*, 17, 3-18, 1975.
- 948 Emery, D., and Robinson, A. (Eds.): *Inorganic Geochemistry: Applications to Petroleum*
949 *Geology*, Blackwell Science, Oxford, United Kingdom, 101-128, 1993.
- 950 Fantoni, R., and Franciosi, R.: Tectono-sedimentary setting of the Po Plain and Adriatic foreland,
951 *Rend. Lincei*, 21, 197-209, <https://doi.org/10.1007/s12210-010-0102-4>, 2010.

- 952 [Ferraro, F., Agosta, F., Ukar, E., Grieco, D. S., Cavalcante, F., Belviso, C., and Prosser, G.:](#)
953 [Structural diagenesis of carbonate fault rocks exhumed from shallow crustal depths:](#)
954 [An example from the central-southern Apennines, Italy, *J. Struct. Geol.*, 122, 58-80,](#)
955 <https://doi.org/10.1016/j.jsg.2019.02.008>, 2019.
- 956 Flecker, R., De Villiers, S., and Ellam, R. M.: Modelling the effect of evaporation on the
957 salinity-⁸⁷Sr/⁸⁶Sr relationship in modern and ancient marginal-marine systems: the
958 Mediterranean Messinian Salinity Crisis, *Earth Planet. Sci. Lett.*, 203, 221-233,
959 10.1016/S0012-821X(02)00848-8, 2002.
- 960 Friedman, I.: Some investigations of the deposition of travertine from Hot Springs-I. The
961 isotopic chemistry of a travertine-depositing spring, *Geochim. Cosmochim. Acta*, 34,
962 1303-1315, [https://doi.org/10.1016/0016-7037\(70\)90043-8](https://doi.org/10.1016/0016-7037(70)90043-8), 1970.
- 963 Gale, J. F., Laubach, S. E., Marrett, R. A., Olson, J. E., Holder, J., and Reed, R. M.: Predicting
964 and characterizing fractures in dolostone reservoirs: Using the link between
965 diagenesis and fracturing, *Geol. Soc. London Spec. Publ.*, 235, 177-192,
966 <https://doi.org/10.1144/GSL.SP.2004.235.01.08>, 2004.
- 967 Giacometti, A., and Ronchi, P.: Early Lias Carbonate Platform: Facies and Diagenesis Analogies
968 between the Calcare Massiccio (Umbro-Marchean Apennines) and the Inici Fm.
969 (Sicily Channel), *Mem. Soc. Geol. It.*, 55, 271-278, 2000.
- 970 Ghisetti, F., and Vezzani, L.: Detachments and normal faulting in the Marche fold-and-thrust belt
971 (Central Apennines, Italy): inferences on fluid migration paths, *J. Geodyn.*, 29, 345-
972 369, [https://doi.org/10.1016/S0264-3707\(99\)00057-5](https://doi.org/10.1016/S0264-3707(99)00057-5), 2000.
- 973 Ghisetti, F., and Vezzani, L.: Interfering paths of deformation and development of arcs in the
974 fold-and-thrust belt of the central Apennines (Italy), *Tectonics*, 16, 523-536,
975 <https://doi.org/10.1029/97TC00117>, 1997.
- 976 Goldstein, R. H., and Reynolds, T. J.: Systematics of Fluid Inclusions in Diagenetic Minerals,
977 *Soc. Sediment. Geol., Short Course*, 31, 199 pp., 1994.
- 978 Gregg, J. M.: On the formation and occurrence of saddle dolomite-discussion, *J. Sediment.*
979 *Petrol.*, 53, 1025-1033, 1983.
- 980 Gregg, J. M., Shelton, K. L., Johnson, A. W., Somerville, I. D., and Wright, W. R.:
981 Dolomitization of the Waulsortian limestone (lower Carboniferous) in the Irish

982 Midlands, *Sedimentology*, 48, 745-766, <https://doi.org/10.1046/j.1365->
983 3091.2001.00397.x, 2001.

984 Habermann, D., Neuser, R. D., and Richter, D. K.: REE-activated cathodoluminescence of
985 calcite and dolomite: high-resolution spectrometric analysis of CL emission (HRS-
986 CL), *Sediment. Geol.*, 101, 1-7, [https://doi.org/10.1016/0037-0738\(95\)00086-0](https://doi.org/10.1016/0037-0738(95)00086-0),
987 1996.

988 Hendry, J. P., Gregg, J. M., Shelton, K. L., Somerville, I. D., and Crowley, S. F.: Origin,
989 characteristics and distribution of fault-related and fracture-related dolomitization:
990 Insights from Mississippian carbonates, Isle of Man, *Sedimentology*, 62, 717-752,
991 <https://doi.org/10.1111/sed.12160>, 2015.

992 Hiemstra, E. J., and Goldstein, R. H.: Repeated injection of hydrothermal fluids into downdip
993 carbonates: a diagenetic and stratigraphic mechanism for localization of reservoir
994 porosity, Indian Basin Field, New Mexico, USA, *Geol. Soc. London Spec. Publ.*,
995 406, 141-177, <https://doi.org/10.1144/SP406.1>, 2015.

996 [Hollis, C., Bastesen, E., Boyce, A., Corlett, H., Gawthorpe, R., Hirani, J. Rotevatn, A., and](#)
997 [Whitaker, F.: Fault-controlled dolomitization in a rift basin. *Geology*, 45, 219-222.](#)
998 <https://doi.org/10.1130/G38s394.1>, 2017.

999 Horita, J.: Oxygen and carbon isotope fractionation in the system dolomite-water-CO₂ to
1000 elevated temperatures, *Geochim. Cosmochim. Acta*, 129, 111-124,
1001 <https://doi.org/10.1016/j.gca.2013.12.027>, 2014.

1002 Horvath, F.: Towards a mechanical model for the formation of the Pannonian basin,
1003 *Tectonophysics*, 226, 333-357, [https://doi.org/10.1016/0040-1951\(93\)90126-5](https://doi.org/10.1016/0040-1951(93)90126-5), 1993.

1004 Hudson, J. D.: Stable isotopes and limestone lithification, *Geol. Soc. London*, 133, 637-660,
1005 <https://doi.org/10.1144/gsjgs.133.6.0637>, 1977.

1006 Koopman, A.: Detachment tectonics in the central Apennines, Italy, Ph.D. thesis, Utrecht
1007 University, The Netherlands, 155 pp., 1983.

1008 Land L. S.: The isotopic and trace element geochemistry of dolomite: the state of the art, in:
1009 Concepts and Models of dolomitization, edited by: Zenger D. H., Dunham J. B. and
1010 Ethington R. L., *Soc. Econ. Paleontol. and Mineral., Spec. Pub.*, 28, 87-110, 1980.

1011 Land L. S.: The application of stable isotopes to studies of the origin of dolomite and to
1012 problems of diagenesis of clastic sediments, in: *Stable Isotopes in Sedimentary*

- 1013 Geology, edited by: Arthur M. A., Soc. Econ. Paleontol. and Mineral, Short Course,
1014 10, 4-1 , 1983.
- 1015 Land L. S.: The origin of massive dolomite. Jour. Geol. Educ., 33, 112-125, 1985.
- 1016 Laubach, S. E., Eichhubl, P., Hilgers, C., and Lander, R. H.: Structural diagenesis, J. Struct.
1017 Geol., 32, 1866-1872, <https://doi.org/10.1016/j.jsg.2010.10.001>, 2010.
- 1018 Li, Z., Goldstein, R. H. and Franseen, E. K.: Meteoric calcite cementation: diagenetic response to
1019 relative fall in sea-level and effect on porosity and permeability, Las Negras area,
1020 southeastern Spain, Sediment. Geol., 348, 1-18,
1021 <https://doi.org/10.1016/j.sedgeo.2016.12.002>, 2017.
- 1022 Lind, I. L., Berger, W. H., and Kroenke, L. W.: Stylolites in chalk from leg 130, Ontong Java
1023 Plateau, in: Proceedings of the Ocean Drilling Program, scientific results, 445-451,
1024 1993.
- 1025 Lobato, L. M., Forman, J. M. A., Fazikawa, K., Fyfe, W. S., and Kerrich, R.: Uranium in
1026 overthrust Archean basement, Bahia, Brazil. Canadian Mineral., 21, 647-654, 1983.
- 1027 [Lonnee, J. S.: Sedimentology, dolomitization and diagenetic fluid evolution of the Middle](#)
1028 [Devonian Sulphur Point Formation, northwestern Alberta, Ph.D. thesis, University of](#)
1029 [Windsor, Canada, 133 pp., 1999.](#)
- 1030 Luczaj, J. A., and Goldstein, R. H.: Diagenesis of the Lower Permian Krider Member, southwest
1031 Kansas, USA: fluid-inclusion, U-Pb, and fission-track evidence for reflux
1032 dolomitization during latest Permian time, J. Sediment. Res., 70, 762-773,
1033 <https://doi.org/10.1306/2DC40936-0E47-11D7-8643000102C1865D>, 2000.
- 1034 Machel, H. G.: Effects of groundwater flow on mineral diagenesis, with emphasis on carbonate
1035 aquifers, Hydrol. J., 7, 94-107, <https://doi.org/10.1007/s100400050>, 1999.
- 1036 Machel, H. G., Mason, R. A., Mariano, A. N., and Mucci, A.: Causes and emission of
1037 luminescence in calcite and dolomite, in: Luminescence microscopy and
1038 spectroscopy : Qualitative and quantitative applications, edited by: Barker, C. E., and
1039 Kopp, O. C, Soc. Sediment. Geol., Short Course, 9-25, 1991.
- 1040 Machel, H. G., and Cavell, P. A.: Low-flux, tectonically-induced squeegee fluid flow, Bull. Can.
1041 Petrol. Geol., 47, 510-533, 1999.

- 1042 Major, R. P., Lloyd, R. M. and Lucia, F. J.: Oxygen isotope composition of Holocene dolomite
1043 formed in a humid hypersaline setting, *Geology*, 20, 586-588,
1044 [https://doi.org/10.1130/0091-7613\(1992\)020<0586:OICOHD>2.3.CO;2](https://doi.org/10.1130/0091-7613(1992)020<0586:OICOHD>2.3.CO;2), 1992.
- 1045 Marchegiani, L., Deiana, G., and Tondi, E.: Tettonica pre-orogenica in Appennino centrale, *Stud.*
1046 *Geol. Camerti*, 14, 211-228, <http://dx.doi.org/10.15165/studgeocam-807>, 1999.
- 1047 Marino, M., and Santantonio, M.: Understanding the geological record of carbonate platform
1048 drowning across rifted Tethyan margins: Examples from the Lower Jurassic of the
1049 Apennines and Sicily (Italy), *Sediment. Geol.*, 225, 116-137,
1050 <https://doi.org/10.1016/j.sedgeo.2010.02.002>, 2010.
- 1051 Marshall, J. D.: Climatic and oceanographic isotopic signals from the carbonate rock record and
1052 their preservation, *Geol. Mag.*, 129, 143-160,
1053 <https://doi.org/10.1017/S0016756800008244>, 1992.
- 1054 Mattei, M.: Analisi geologico-strutturale della Montagna dei Fiori (Ascoli Piceno, Italia
1055 Centrale), *Geol. Romana*, 26, 327-347, 1987.
- 1056 Mazzoli, S., Deiana, G., Galdenzi, S., and Cello, G.: Miocene fault-controlled sedimentation and
1057 thrust propagation in the previously faulted external zones of the Umbria-Marche
1058 Apennines, Italy, *EGU Stephan Mueller Spec. Publ. Ser.*, 1, 195-209, 2002.
- 1059 Mazzullo, S. J.: Geochemical and neomorphic alteration of dolomite: a review, *Carbonates*
1060 *Evaporites*, 7, 21-37, <https://doi.org/10.1007/BF03175390>, 1992.
- 1061 McArthur, J. M., Howarth, R. J., and Shields, G. A.: Strontium isotope stratigraphy, in: *The*
1062 *Geologic Time Scale 2012*, edited by: Gradstein, F. M., Ogg, J. G., Schmitz, M., and
1063 Ogg, G., Elsevier, 127-144, <https://doi.org/10.1016/C2011-1-08249-8>, 2012.
- 1064 McCaffrey, M. A., Lazar, B., Holland, H. D.: The evaporation path of seawater and the
1065 coprecipitation of Br- and K⁺ with halite, *J. Sediment. Res.*, 57, 928-937,
1066 <https://doi.org/10.1306/212F8CAB-2B24-11D7-8648000102C1865D>, 1987.
- 1067 McCaig, A. M.: Deep fluid circulation in fault zones, *Geology*, 16, 867-870,
1068 [https://doi.org/10.1130/0091-7613\(1988\)016<0867:DFCIFZ>2.3.CO;2](https://doi.org/10.1130/0091-7613(1988)016<0867:DFCIFZ>2.3.CO;2), 1988.
- 1069 McCaig, A. M., Wickham, S. M., and Taylor, H. P.: Deep fluid circulation in alpine shear zones,
1070 Pyrenees, France: field and oxygen isotope studies, *Contrib. Mineral. Petr.*, 106, 41-
1071 60, <https://doi.org/10.1007/BF00306407>, 1990.

- 1072 Montanez, I. P.: Late diagenetic dolomitization of Lower Ordovician, upper Knox carbonates: A
1073 record of the hydrodynamic evolution of the southern Appalachian Basin, *Am.*
1074 *Assoc. Pet. Geol. Bull.*, 78, 1210-1239, 1994.
- 1075 Moore, C. H. (Eds.): Carbonate diagenesis and porosity, *Dev. Sedimentol.*, 46, Elsevier Sci.
1076 Publ., Amsterdam, The Netherlands, 338 pp., 1989.
- 1077 Morettini, E., Santantonio, M., Bartolini, A., Cecca, F., Baumgartner, P. O., and Hunziker, J. C.:
1078 Carbon isotope stratigraphy and carbonate production during the Early-Middle
1079 Jurassic: examples from the Umbria-Marche-Sabina Apennines (central Italy),
1080 *Paleog., Paleocl., Paleoec.*, 184, 251-273, [https://doi.org/10.1016/S0031-](https://doi.org/10.1016/S0031-0182(02)00258-4)
1081 [0182\(02\)00258-4](https://doi.org/10.1016/S0031-0182(02)00258-4), 2002.
- 1082 Mountjoy, E. W., Machel, H. G., Green, D., Duggan, J., and Williams-Jones, A. E.: Devonian
1083 matrix dolomites and deep burial carbonate cements: a comparison between the
1084 Rimbe-Meadowbrook reef trend and the deep basin of west-central Alberta, *B. Can.*
1085 *Petrol. Geol.*, 47, 487-509, 1999.
- 1086 Murgia, M. V., Ronchi, P., and Ceriani, A.: Dolomitization processes and their relationships with
1087 the evolution of an orogenic belt (Central Apennines and peri-adriatic foreland,
1088 Italy), *AAPG Hedberg series*, 1, 277-294, <https://doi.org/10.1306/1025695H13121>,
1089 2004.
- 1090 Nelson, R. A: Significance of fracture sets associated with stylolite zones, *Am. Assoc. Pet. Geol.*
1091 *Bull.*, 65, 2417-2425, 1981.
- 1092 Parotto, M., and Praturlon, A.: Geological summary of the Central Apennines, *Quad. Ric. Sci.*,
1093 90, 257-311, 1975.
- 1094 Patacca, E., Sartori, R., and Scandone, P.: Tyrrhenian basin and Apenninic arcs: Kinematic
1095 relations since late Tortonian times, *Mem. Soc. Geol. It.*, 45, 425-451,
1096 <http://hdl.handle.net/11568/11610>, 1992.
- 1097 Piali, G.: Facies di piana cotidale nel Calcarea Massiccio dell'Appennino umbro marchigiano,
1098 *Boll. Soc. Geol. It.*, 90, 481-507, 1971.
- 1099 Pierantoni, P., Deiana, G., and Galdenzi, S.: Stratigraphic and structural features of the Sibillini
1100 Mountains (Umbria-Marche Apennines, Italy), *Ital. J. Geosci.*, 132, 497-520,
1101 <https://doi.org/10.3301/IJG.2013.08>, 2013.

- 1102 Purser, B., Tucker, M. and Zenger, D.: Problems, progress and future research concerning
1103 dolomites and dolomitization, in: Dolomites: a Volume in Honour of Dolomieu,
1104 edited by: Purser, B., Tucker, M. and Zenger, D., IAS Spec. Publ., 21, 3-20, 1994.
- 1105 [Qing, H., and Mountjoy, E. W.: Multistage dolomitization in Rainbow buildups, Middle](#)
1106 [Devonian Keg River Formation, Alberta, Canada. J. of Sediment. Res., 59, 114-126,](#)
1107 <https://doi.org/10.1306/212F8F30-2B24-11D7-8648000102C1865D>, 1989.
- 1108 Radke, B. M., and Mathis, R. L.: On the formation and occurrence of saddle dolomite, J.
1109 Sediment. Res., 50, 1149-1168, [https://doi.org/10.1306/212F7B9E-2B24-11D7-](https://doi.org/10.1306/212F7B9E-2B24-11D7-8648000102C1865D)
1110 [8648000102C1865D](https://doi.org/10.1306/212F7B9E-2B24-11D7-8648000102C1865D), 1980.
- 1111 Ronchi, P., Casaglia, F., and Ceriani, A.: The multiphase dolomitization of the Liassic Calcare
1112 Massiccio and Corniola successions (Montagna dei Fiori, Northern Apennines, Italy),
1113 Boll. Soc. Geol. It., 122, 157-172, 2003.
- 1114 Rosenbaum, J., and Sheppard, S. M.: An isotopic study of siderites, dolomites, and ankerites at
1115 high temperatures, Geochim. Cosmochim. Acta, 50, 1147-1150,
1116 [https://doi.org/10.1016/0016-7037\(86\)90396-0](https://doi.org/10.1016/0016-7037(86)90396-0), 1986.
- 1117 Roveri, M., Bassetti, M. A., and Lucchi, F. R.: The Mediterranean Messinian salinity crisis: an
1118 Apennine foredeep perspective, Sediment. Geol., 140, 201-214,
1119 [https://doi.org/10.1016/S0037-0738\(00\)00183-4](https://doi.org/10.1016/S0037-0738(00)00183-4), 2001.
- 1120 Saelen, G., Doyle, P., and Talbot, M. R.: Stable-isotope analyses of belemnite rostra from the
1121 Whitby Mudstone Fm., England: Surface water conditions during deposition of a
1122 marine black shale, Palaios, 11, 97-117, <https://doi.org/10.2307/3515065>, 1996.
- 1123 Santantonio, M, and Carminati, E.: Jurassic rifting evolution of the Apennines and Southern Alps
1124 (Italy): Parallels and differences, Geol. Soc. Am. B., 123, 464-484,
1125 <https://doi.org/10.1130/B30104.1>, 2011.
- 1126 Santantonio, M. and Muraro, C.: The Sabina Plateau, Palaeoescrapment, and Basin-Central
1127 Apennines, 6th international symposium on the Jurassic system, General Field Trip
1128 Guidebook, Palermo, Italy, 271-315, 2002.
- 1129 Santantonio, M., Fabbi, S., and Bigi, S.: Discussion on «Geological map of the partially
1130 dolomitized Jurassic succession exposed in the central sector of the Montagna dei
1131 Fiori Anticline, Central Apennines, Italy», Ital. J. Geosci., 136, 312-316,
1132 <https://doi.org/10.3301/IJG.2017.04>, 2017.

- 1133 Schulz, H. M., Wirth, R., and Schreiber, A.: Organic-inorganic rock-fluid interactions in
1134 stylolitic micro-environments of carbonate rocks: a FIB-TEM study combined with a
1135 hydrogeochemical modelling approach, *Geofluids*, 16, 909-924,
1136 <https://doi.org/10.1111/gfl.12195>, 2016.
- 1137 Scisciani V., Tavarnelli, E., and Calamita, F.: The interaction of extensional and contractional
1138 deformations in the outer zones of the Central Apennines, Italy, *J. Struct. Geol.*, 24,
1139 1647-1658, [https://doi.org/10.1016/S0191-8141\(01\)00164-X](https://doi.org/10.1016/S0191-8141(01)00164-X), 2002.
- 1140 Shackleton, N. J., and Kennett, J. P.: Paleotemperature History of the Cenozoic and the Initiation
1141 of Antarctic Glaciation Oxygen and Carbon Isotope Analyses in DSDP Sites 277, 279,
1142 and 281, Initial reports of Deep Sea Drilling Project, 29, 743-755, 1975.
- 1143 Sharp, I., Gillespie, P., Morsalnezhad, D., Taberner, C., Karpuz, R., Vergés, J., Horbury, A.,
1144 Pickard, N., J. Garland, J., and Hunt, D.: Stratigraphic architecture and fracture-
1145 controlled dolomitization of the Cretaceous Khami and Bangestan groups: an outcrop
1146 case study, Zagros Mountains, Iran, *Geol. Soc. London Spec. Publ.*, 329, 343-396,
1147 <https://doi.org/10.1144/SP329.14>, 2010.
- 1148 Shepherd, T., Rankin, A. H., and Alderton, D. H. M. (Eds.): *A Practical Guide to Fluid Inclusion*
1149 *Studies*, Glasgow: Blackie, 239 pp., 1985.
- 1150 Sibley, D. F., and Gregg, J. M.: Classification of dolomite rock textures, *J. Sediment. Petrol.*, 57,
1151 967-975, <https://doi.org/10.1306/212F8CBA-2B24-11D7-8648000102C1865D>,
1152 1987.
- 1153 Sibson, R. H.: Fluid flow accompanying faulting: field evidence and models, *Earthquake*
1154 *prediction: an international review*, AGU, 4, 593-603,
1155 <https://doi.org/10.1029/ME004p0593>, 1981.
- 1156 Slobodník, M., Muchez, P., Kral, J., and Keppens, E.: Variscan veins: record of fluid circulation
1157 and Variscan tectonothermal events in Upper Palaeozoic limestones of the Moravian
1158 Karst, Czech Republic, *Geol. Mag.*, 143, 491-508,
1159 <https://doi.org/10.1017/S0016756806001981>, 2006.
- 1160 Smith, R. E., Wiltschko, D. V.: Generation and maintenance of abnormal fluid pressures beneath
1161 a ramping thrust sheet: isotropic permeability experiments, *J. Struct. Geol.*, 18, 951-
1162 970, [https://doi.org/10.1016/0191-8141\(96\)00023-5](https://doi.org/10.1016/0191-8141(96)00023-5), 1996.

- 1163 Steiger, R., and Jäger, E.: Subcommittee on geochronology: convention on the use of decay
1164 constants in geo and cosmochemistry, *Earth Planet. Sci. Lett.*, 36, 359-362,
1165 [https://doi.org/10.1016/0012-821X\(77\)90060-7](https://doi.org/10.1016/0012-821X(77)90060-7), 1977.
- 1166 Storti, F., Balsamo, F., and Koopman, A.: Geological map of the partially dolomitized Jurassic
1167 succession exposed in the core of the Montagna dei Fiori Anticline, Central
1168 Apennines, Italy, *Ital. J. Geosci.*, 136, 125-135, <https://doi.org/10.3301/IJG.2016.05>,
1169 2017a.
- 1170 Storti F., Balsamo, F., and Koopman, A.: Reply to: discussion on «Geological map of the
1171 partially dolomitized Jurassic succession exposed in the central sector of the
1172 Montagna dei Fiori Anticline, Central Apennines, Italy» by Santantonio, M., Fabbi,
1173 S. and Bigi, S., *Ital. J. Geosci.*, 136, 317-319, <https://doi.org/10.3301/IJG.2017.04>,
1174 2017b.
- 1175 Storti, F., Balsamo F., Mozafari M., Koopman A., Swennen R. and Taberner C.: Syn-
1176 contractional overprinting between extension and shortening along the Montagna dei
1177 Fiori Fault during Plio-Pleistocene antiformal stacking at the Central Apennines
1178 thrust wedge toe, *Tectonics*, <https://doi.org/10.1029/2018TC005072>, 2018.
- 1179 Stueber, A. M., Pushkar, P., and Baldwin, A. D., JR.: Survey of $^{87}\text{Sr}/^{86}\text{Sr}$ ratios and total
1180 strontium concentrations in Ohio stream and ground waters, *Ohio J. Sci.*, 72, 98-104,
1181 1972.
- 1182 Sommer, S. E.: Cathodoluminescence of carbonates, 1. Characterization of cathodoluminescence
1183 from carbonate solid solutions, *Chemical Geology*, 9, 257-273,
1184 [https://doi.org/10.1016/0009-2541\(72\)90064-2](https://doi.org/10.1016/0009-2541(72)90064-2), 1972.
- 1185 Swennen, R., Dewit, J., Fierens, E., Muchez, Ph., Shah, M., Nader, F. H., Hunt, D.: Multiple
1186 dolomitisation events along the Ranero fault (Pozalagua Quarry, Basque-Cantabrian
1187 Basin): episodic earthquake activity, *Sedimentology*, 59, 1345-1374,
1188 <https://doi.org/10.1111/j.1365-3091.2011.01309.x>, 2012.
- 1189 Tavani, S., Storti, F., Salvini, F., and Toscano, C.: Stratigraphic versus structural control on the
1190 deformation pattern associated with the evolution of the Mt. Catria anticline, Italy, *J.*
1191 *Struct. Geol.*, 30, 664-681, <https://doi.org/10.1016/j.jsg.2008.01.011>, 2008.

- 1192 Taylor, H. P.: Oxygen and hydrogen isotope relationships in hydrothermal mineral deposits, In:
1193 Geochemistry of hydrothermal ore deposits, edited by: Barnes, H. L., Wiley and
1194 Sons, New York, 229-302, 1997.
- 1195 Thirlwall, M. F.: Long-term reproducibility of multicollector Sr and Nd isotope ratio analysis,
1196 Chemical Geology, 94, 85-104, [https://doi.org/10.1016/S0009-2541\(10\)80021-X](https://doi.org/10.1016/S0009-2541(10)80021-X),
1197 1991.
- 1198 Tongiorgi, M., Rau, A., and Martini, I. P.: Sedimentology of early-alpine, fluvio-marine, clastic
1199 deposits (Verrucano, Triassic) in the Monti Pisani (Italy), Sediment. Geol., 17, 311-
1200 332, [https://doi.org/10.1016/0037-0738\(77\)90051-3](https://doi.org/10.1016/0037-0738(77)90051-3), 1977.
- 1201 [Ukar, E., and Laubach, S. E.: Syn-and postkinematic cement textures in fractured carbonate](#)
1202 [rocks: Insights from advanced cathodoluminescence imaging, Tectonophysics, 690,](#)
1203 [190-205, <https://doi.org/10.1016/j.tecto.2016.05.001>, 2016.](#)
- 1204 Vai, G. B., and Ricci Lucchi, F.: Algal crusts, autochthonous and clastic gypsum in a
1205 cannibalistic evaporite basin: a case history from the Messinian of northern
1206 Apennines. Sedimentology, 24, 221-244, [https://doi.org/10.1111/j.1365-
1207 3091.1977.tb00255.x](https://doi.org/10.1111/j.1365-3091.1977.tb00255.x), 1977.
- 1208 Vandeginste, V., Swennen, R., Gleeson, S. A., Ellam, R. M., Osadetz, K., and Roure, F.: Zebra
1209 dolomitization as a result of focused fluid flow in the Rocky Mountains Fold and
1210 Thrust Belt, Canada. Sedimentology, 52, 1067-1095, [https://doi.org/10.1111/j.1365-
1211 3091.2005.00724.x](https://doi.org/10.1111/j.1365-3091.2005.00724.x), 2005.
- 1212 Vandeginste, V., Swennen, R., Gleeson, S. A., Ellam, R. M., Osadetz, K., and Roure, F.:
1213 Geochemical constraints on the origin of the Kicking Horse and Monarch Mississippi
1214 Valley-type lead-zinc ore deposits, southeast British Columbia, Canada, Mineralium
1215 Deposita, 42, 913-935, <https://doi.org/10.1007/s00126-007-0142-6>, 2007.
- 1216 Veizer, J., Ala, D., Azmy, K., Bruckshen, P., Buhl, D., Bruhn, F., Carden, G. A. F., Diener, A.,
1217 Ebner, S., Godderis, Y., Jasper, T., Korte, C., Pawellek, F., Podlaha, O. G., and
1218 Strauss, H.: $^{87}\text{Sr}/^{86}\text{Sr}$, $\delta^{13}\text{C}$ and evolution of Phanerozoic seawater, Chemical
1219 Geology, 161, 59-88, [https://doi.org/10.1016/S0009-2541\(99\)00081-9](https://doi.org/10.1016/S0009-2541(99)00081-9), 1999.
- 1220 Walker, G., Abumere, O. E., and Kamaluddin, B.: Luminescence spectroscopy of Mn²⁺ rock-
1221 forming carbonates, Mineral. Mag., 53, 201-11, [10.1180/minmag.1989.053.370.07](https://doi.org/10.1180/minmag.1989.053.370.07),
1222 1989.

1223 Wenzhi, Z., Anjiang, S., Suyun, H., Baomin, Z., Wenqing, P., Jingao, Z. and Zecheng, W.:
1224 Geological conditions and distributional features of large-scale carbonate reservoirs
1225 onshore China. *Petrol. Explor. Develop.*, 39, 1-14, [https://doi.org/10.1016/S1876-](https://doi.org/10.1016/S1876-3804(12)60010-X)
1226 [3804\(12\)60010-X](https://doi.org/10.1016/S1876-3804(12)60010-X), 2012.

1227 Wilson, A., and Ruppel, C.: Salt tectonics and shallow subsea floor fluid convection: models of
1228 coupled fluid-heat-salt transport, *Geofluids*, 7, 377-386,
1229 <https://doi.org/10.1111/j.1468-8123.2007.00191.x>, 2007.

1230 Wilson, M. E. J., Evans, M. J., Oxtoby, N. H., Nas, D. S., Donnelly, T. and Thirlwall, M.:
1231 Reservoir quality, textural evolution, and origin of fault-associated
1232 dolomites. *AAPB Bull.*, 91, 1247-1272, 2007.

1233 Woodcock, N. H., and Mort, K.: Classification of fault breccias and related fault rocks, *Geol.*
1234 *Mag.*, 145, 435-440, <https://doi.org/10.1017/S0016756808004883>, 2008.

1235 Woody, R. E., Gregg, J. M. and Koederitz, L. F.: Effect of texture on petrophysical properties of
1236 dolomite: Evidence from the Cambrian-Ordovician of Southeastern Missouri. *AAPG*
1237 *Bull.*, 80, 119-131, 1996.

1238 Zempolich, W. G., and Hardie, L. A.: Geometry of dolomite bodies within deep-water
1239 resedimented oolite of the Middle Jurassic Vajont Limestone, Venetian Alps, Italy:
1240 Analogs for hydrocarbon reservoirs created through fault-related burial
1241 dolomitization, in: *Reservoir quality prediction in sandstones and carbonates*, edited
1242 by: Kupecz, A., Gluyas, J., and Bloch, S., *AAPG Mem.*, 69, 127-162, 1997.

1243

1244

1245

1246

1247

1248

1249

1250

1251 **Table captions**

1252 **Table. 1.** Stable carbon and oxygen isotopes, $^{87}\text{Sr}/^{86}\text{Sr}$ ratios, and fluid inclusion
1253 microthermometry data (not pressure corrected) of host rocks and diagenetic phases in the
1254 Montagna dei Fiori Anticline. Stable carbon and oxygen isotopes values are expressed in
1255 ‰ V-PDB and salinity values in eq. wt. % NaCl.

1256 **Figure captions**

1257 Fig. 1. **Aa)** Simplified regional map (modified after Ghisetti and Vezzani, 1997) showing the
1258 tectonic outlines of the Central Apennines and the study area (rectangle). **Bb)** Schematic
1259 geological map of the Montagna dei Fiori Anticline showing the distribution of dolostones
1260 (modified after Storti et al., 2017a). **Cc)** Lithostratigraphical column of the successions exposed
1261 in Montagna dei Fiori (modified after Mattei, 1987; Di Francesco et al, 2010; Storti et al., 2018).
1262 Letter B stands for the Bugarone Formation. Lithologies are mentioned in the text. Note that the
1263 thickness of the not-outcropping formations (Triassic evaporites and the crystalline basement) is
1264 not to scale. **Dd)** Regional Geological-geological transect across present day Central Apennines
1265 and the Adriatic Sea (modified after Fantoni and Franciosi, 2010) with vertical exaggeration of
1266 2:1. The dashed rectangle indicates the Montagna dei Fiori Anticline region.

1267

1268 Fig. 2. **Aa, Bb)** Geological map of the central sector of the Montagna dei Fiori Anticline, and
1269 cross-section oriented parallel (a-b) to the hinge line representing the tectono-stratigraphic
1270 architecture of the faulted anticline (modified after Storti et al., 2017a). The stereonets (Schmidt
1271 equal area projection lower hemisphere) provide the attitude of the extensional faults. The
1272 locations of the corresponding field sites are indicated by ~~numbers~~letters. **c)** At this location, well
1273 exposed N-S striking extensional fault zones offset the dolomitized Corniola Formation. The
1274 fault zone is characterized by near-horizontal stylolites localized in the footwall damage zone (4
1275 fault data). **d, e and f)** These locations consist of mostly ~ E-W striking extensional fault zones.
1276 Particularly the boundary fault zones delimiting Calcare Massiccio Formation in the main horst
1277 block is evident (site d: 20 fault data; site e: 24 fault data; site f: 9 fault data). **g and h)** At these
1278 locations, dip-slip slickenlines support major extensional movements related to the Montagna dei
1279 Fiori Fault. Contractional deformation structures are preserved in the bed-perpendicular

1280 | stylolites, shear surfaces and tension gashes arranged as S-C arrays (site g: 21 fault data; site h:
1281 | 14 fault data). Equal area projection, lower hemisphere.

1282 |
1283 | Fig. 3. Aa) Field photograph showing the deformed Scaglia Formation in the hanging wall (HW)
1284 | and brecciated, dolomitized Calcare Massiccio Formation in the footwall (FW) of the Montagna
1285 | dei Fiori Fault. The red arrow indicates the sense of fault movement. Bb) A hand specimen from
1286 | the deformed Scaglia formation showing ~~the intensity of the abundant~~ pressure ~~solutions-solution~~
1287 | ~~seems~~ (TS), indicated by arrows, and their abutting relationship with cross-cutting calcite veins
1288 | (CV2C2). Cc) A transmitted light photomicrograph of the dolomitized, brecciated Calcare
1289 | Massiccio Formation. Note all the breccia fragments are composed of dolomite (D4 here).

1290 |
1291 | Fig. 4. Field photographs (Corano Quarry) showing the field relations between dolostones (only
1292 | D3 here), host limestones and the Montagna dei Fiori Fault: Aa) Panoramic view showing the
1293 | spatial relationship between limestones and dolostones (orange) in the damage zone of the
1294 | Montagna dei Fiori Fault (F). Note that the limestones and including dolostones of the Calcare
1295 | Massiccio and Bugarone Formations on the footwall (FW) and marly limestones of the Scaglia
1296 | Formation on the hangingwall (HW) are intensely deformed. Bb) Plan view of the dolomitized
1297 | Calcare Massiccio limestone in the footwall damage zone: intersected by calcite veins (CV4C1),
1298 | which are partially dolomitized, and affected by ~~bed-bed~~-perpendicular stylolites (arrows). Cc)
1299 | Distinct transition (dashed line) between dolomitized and undolomitized Calcare Massiccio
1300 | limestone in the footwall damage zone.

1301 |
1302 | Fig. 5. Field photograph (Aa) and a simplified sketch (Bb) in field site d showing of a dolomitic
1303 | pocket (grey color) ~~within the folded Calcare Massiccio (grey color)~~ and ~~their-its~~ relation with
1304 | ~~bed-bed~~-parallel stylolites within the Calcare Massiccio Formation (hammer is 40 cm long). Note
1305 | C1 is the only calcite cement here.

1306 |
1307 | Fig. 6. Undolomitized and dolomitized Calcare Massiccio Formation in field site d: Aa)
1308 | Transmitted light image showing a micritic peloid rimmed by ~~the~~-fibrous cements (FC) which
1309 | are ~~followed-overgrown~~ by ~~the~~-mosaic cements (MC). Bb) Transmitted light image showing
1310 | mosaic cements (MC) in a peloidal limestone over-printed by high amplitude ~~bed-bed~~-parallel

1311 stylolites (dotted white line). Note the core of some of the peloids is partially cemented as well.
1312 **Cc, Dd**) Respectively, transmitted light and corresponding cathodoluminescence image of FC
1313 and MC cements. **Ee**) Transmitted light photomicrograph showing D1 crystals (arrows) rimming
1314 lining a fracture which is cemented by EV1C1. The fracture is in turn affected by a bed-bed-
1315 parallel stylolite. **Ff**) Cathodoluminescence image showing D1 scattered in the host rock and
1316 riming the fracture. **Gg, Hh**) Respectively, transmitted light and corresponding
1317 cathodoluminescence image showing part of a bed-bed-parallel stylolite (dotted white line)
1318 overprinting D1 and D2 crystals.

1319

1320 Fig. 7. **Aa, Bb**) Photomicrographs of respectively, transmitted light and corresponding
1321 cathodoluminescence image showing the zoned rhombs of D2 with the remnants of D1 preserved
1322 in their cloudy core sampled from dolomitized Calcare Massiccio Formation in field site d. The
1323 pore space is occluded by D4. **Cc, Dd**) D3 cementing angular breccia fragments of the Bugarone
1324 Formation in the damage zone of the Montagna dei Fiori Fault in the Corano Quarry site. Note
1325 the breccia is overprinted by a fault-fault-parallel bed-bed-perpendicular stylolite. **Ee, Ff**)
1326 Photomicrographs of respectively, transmitted light and corresponding cathodoluminescence
1327 image showing the euhedral to subhedral crystals of D3 entirely replacing the matrix and also
1328 present as cement developing a bright subzone and rim sampled from dolomitized Corniola
1329 Formation in Osso-caprino road. **Gg, Hh**) D3 with a saddle crystal outline (SD) postdating calcite
1330 cements (MC) and a zoned D2 crystal. The saddle morphology is outlined by a dotted white line.

1331

1332 Fig. 8. Photomicrographs of respectively, transmitted light and corresponding
1333 cathodoluminescence image of dolomite types: **Aa, Bb**) The cross-cutting relationship between
1334 D3 and D4 sampled from dolomitized Corniola Formation in Osso-caprino road. Note the
1335 presence of D3 within the core of dolomite crystals overgrown by D4. **Cc, Dd**) Successions of
1336 dolomite types sampled from dolomitized Calcare Massiccio Formation in field site f. Note the
1337 green CL color of D4 crystals. Typically, luminescent dolomites are known to show yellow,
1338 orange to red colors (Machel et al., 1991). Green luminescence in carbonates including dolomite
1339 have been attributed by a number of researchers to the incorporation of three valent rare earth
1340 elements (REE) such as Dy^{3+} and U^{3+} as luminescence activators within their crystal lattice
1341 (Luczaj and Goldstein, 2000). Another possibility is the emplacement of Mn^{2+} , with yellow

1342 luminescence, in Ca²⁺ sites with blue luminescence in the dolomite crystal lattice instead of
1343 preferential incorporation in the Mg²⁺ site (Sommer, 1972b; Amieux, 1982; Walker et al., 1989;
1344 Habermann et al., 1999). Accordingly, non-stoichiometric, Ca-rich and poorly ordered dolomites
1345 may favor Mn²⁺ incorporation into their Ca²⁺ site. ~~Ee, Ff~~) Vuggy porosity rimmed by D4 (green
1346 CL). Note the porosity is filled with fine dolomite rhombs including traces of D2 in their core
1347 and D4 overgrowths.

1348

1349 Fig. 9. Photomicrographs showing respectively, transmitted light and corresponding
1350 cathodoluminescence image of D4 and D5 in relation to stylolites and fracturing: ~~Aa, Bb~~) D4,
1351 exploiting a ~~bed-bed~~-parallel stylolite that crossed-cuts D1 and D2 sampled from dolomitized
1352 Calcare Massiccio Formation in field site d. ~~Ec, Dd~~) A sub-horizontal fracture cemented by D4
1353 sampled from dolomitized Corniola Formation in field site f. ~~Ee, Ff~~) D5 microveins (arrows)
1354 intersecting all the predating dolomite types in the footwall brecciated zone of the Montagna dei
1355 Fiori Fault-, sampled from dolomitized Calcare Massiccio Formation in Castel Manfrino site.

1356

1357 Fig. 10. Field photographs showing the major calcite vein settings observed in Montagna dei
1358 Fiori: ~~Aa~~) Cross-sectional view of bed normal Calcite vein 1 (~~CV1C1~~) abutting ~~bed-bed~~-parallel
1359 stylolites in folded beds of the Calcare Massiccio Formation. ~~Bb~~) Plan view of the Calcite vein 2
1360 (~~CV2C2~~) intensely affecting the deformed Scaglia (Rossa) Formation. ~~Ec, Dd~~) Cross-sectional
1361 view of the Scaglia Formation, intensely affected by pressure solution seams of tectonic origin
1362 crossed-over by populations of bed-perpendicular Calcite veins (~~CV3C3~~) in en echelon
1363 extensional arrays.

1364

1365 Fig. 11. ~~Aa~~) Cathodoluminescence and transmitted light (in set) image showing blocky to
1366 elongated crystals of ~~CV1C1~~ with zoned CL pattern in the Corano Quarry site. ~~Bb~~) Transmitted
1367 light image showing intensely twinned ~~CV1C1~~ crystals overprinted by euhedral to subhedral
1368 crystals of D3 in the Corano Quarry site. Photomicrographs of respectively, transmitted light and
1369 corresponding cathodoluminescence image: ~~Ec, Dd~~) ~~CV2C2~~ in the Scaglia Formation abutted by
1370 a ~~bed-bed~~-perpendicular stylolite (indicated by white arrows and dashed line) in the Corano
1371 Quarry site. The crystals display blocky to fibrous morphologies, deformation twinning, and a
1372 similar orange luminescence pattern ~~comparable with~~ similar to the adjacent host rock. ~~Ee, Ff~~)

1373 | [EV3C3](#) cementing the breccia fragments in the damage zone of the Montagna dei Fiori Fault.
1374 | The crystals are blocky and show faint deformation twinning. They are brown-orange with
1375 | distinct darker luminescence sector zones. [Gg](#), [Hh](#)) [EV4C4](#) present as a cement within a
1376 | polygonal pore space rimmed by dolomite-, [sampled from dolomitized Calcare Massiccio](#)
1377 | [Formation in field site f](#). Note the blocky crystals, absence of deformation twinning and distinct
1378 | concentric luminescence zonation pattern. [EV4C4](#) is corroded and followed by a late telogenetic
1379 | calcite.

1380

1381 | Fig. 12. ~~A, B~~ Overview of the $\delta^{13}\text{C}$ and $\delta^{18}\text{O}$ values of dolomites ([Aa](#)) host rocks from
1382 | Montagna dei Fiori as well as calcite veins ([Bb](#)). The stable isotope value of Lower Jurassic
1383 | marine limestones based on Veizer et al. (1999) is indicated by a dashed rectangle in subset B.
1384 | The $\delta^{18}\text{O}$ values of the marine dolomites are considered to be 3-4‰ V-PDB higher than those of
1385 | marine limestones (Land, 1980; Major et al., 1992; Horita, 2014). [Cc](#)) Cross-plot of $^{87}\text{Sr}/^{86}\text{Sr}$
1386 | ratios and corresponding $\delta^{18}\text{O}$ values of host rocks, dolomites and calcite veins compared with
1387 | Lower Jurassic marine carbonates $^{87}\text{Sr}/^{86}\text{Sr}$ (dashed rectangle) framework reported by McArthur
1388 | et al. (2012).

1389

1390 | Fig. 13. Overview of microthermometry analysis of primary inclusions in Montagna dei Fiori:
1391 | [Aa](#)) Frequency distribution of the $T_{m_{ice}}$ ($^{\circ}\text{C}$) in dolomite [phases](#). [Bb](#)) Frequency distribution
1392 | of the T_h ($^{\circ}\text{C}$) in dolomite [phases](#). [Cc](#)) Salinity (eq. wt. % NaCl) versus T_h ($^{\circ}\text{C}$) of dolomite
1393 | and calcite phases. [Dd](#)) Isotopic fractionation diagram from Land (1983) used to determine the
1394 | isotopic composition (‰ V-SMOW) of parental fluids in equilibrium with dolomites in
1395 | Montagna dei Fiori.

1396

1397 | Fig. 14. ~~A~~) Generalized paragenesis of diagenetic phases in relation to deformational stages and
1398 | burial history of the Calcare Massiccio Formation in the Montagna dei Fiori Anticline. The
1399 | deformational stages are from Storti et al. (2018), and the burial curve is based on Ronchi et al.
1400 | (2003). [The burial curve was made based on paleo-depth, paleo-temperatures, sedimentation rate](#)
1401 | [and paleo-heat flow.](#)

1402

1403 Fig. 15. Sketch showing the successive fault-related diagenetic phases, of most importantly
1404 dolomitization, recorded in the carbonate succession exposed at the core of the Montagna dei
1405 Fiori Anticline (not scaled). Different diagenetic phases are indicated with different colors. **Aa)**
1406 The first dolomitization event is pre-orogenic (syn-rift), triggered from the fluids channelized
1407 along Jurassic ~ E-W and ~ N-S striking extensional faults. This event occurred during burial
1408 compaction and development of bed-bed-parallel stylolites (BS). It is represented by scattered
1409 dolomite rhombs (D1) followed by calcite cementation (**CV1C1**). The dolomitization continued
1410 with precipitation of larger crystals of D2. **Bb)** Second dolomitization event: syn-orogenic (early
1411 folding/ faulting) dolomitization from fluids that migrated from more internal regions of the
1412 thrust belt and were channelized along the basal detachment level into the fold core. This
1413 dolomitization event presents matrix replacive and cements displaying infrequent saddle outlines
1414 (SD) in pore spaces, within bed-bed-parallel veins and shear fractures. These dolostones postdate
1415 compaction but are affected by bed-bed-perpendicular stylolites (TS) generated by horizontal to
1416 sub-horizontal layer-layer-parallel shortening related to the growth of the Montagna dei Fiori
1417 Anticline. **Cc)** Extensional collapse of the anticline and development of the Montagna dei Fiori
1418 Fault, followed by buttressing of the Scaglia against Calcare Massiccio and Corniola Formations
1419 during positive inversion induced by continuing underthrusting at depth. Precipitation of D5 in
1420 micro-veins and cements in breccia zones, followed by late stage calcite cementation in the
1421 Montagna dei Fiori Fault damage zone (**CV2C2**, **CV3C3** and **CV4C4**).

	Stable isotopes		Sr isotopes	Fluid inclusion microthermometry		
	$\delta^{13}\text{C}$	$\delta^{18}\text{O}$	$^{87}\text{Sr}/^{86}\text{Sr}$	Th (°C)	Salinity	n
Calcare Massiccio Fm.	+2.4 to +3.1	-1.6 to 0.0	0.70766	-	-	
Corniola Fm.	+2.0 to +2.5	-3.1 to -1.4	0.70725	-	-	
Scaglia Fm.	+1.0 to +3.1	-2.2 to -1.0	0.70784-0.70791	-	-	
D1	+2.5	-1.9	0.70789	≤ 40-50	3.5 to 11.3	<u>27</u>
CV1	+1.6 to +2.1	-4.7 to -2.7	0.70773	-	-	<u>1</u>
D2	-	-	-	≤ 40-50 to 71	7.9 to 20.5	<u>37</u>
D3	+2.0 to +2.6	-2.8 to -1.9	0.70859-0.70964	70 to 73	9.2 to 16.9	<u>9</u>
D4	+2.4 to +2.5	-3.0 to -2.5	0.70790	79 to 105	12.8 to 18.6	<u>7</u>
CV2	+1.2 to +3.1	-1.7 to -1.6	0.70779 - 0.70787	-	-	
CV3	+0.5 to +2.4	-2.2 to 0.0	-	≤ 40-50	4.5 to 9.7	<u>9</u>
CV4	+3.8 to +4.9	-9.4 to -9.1	-	≤ 40-50	0.17 to 3.0	<u>19</u>

Table. 1

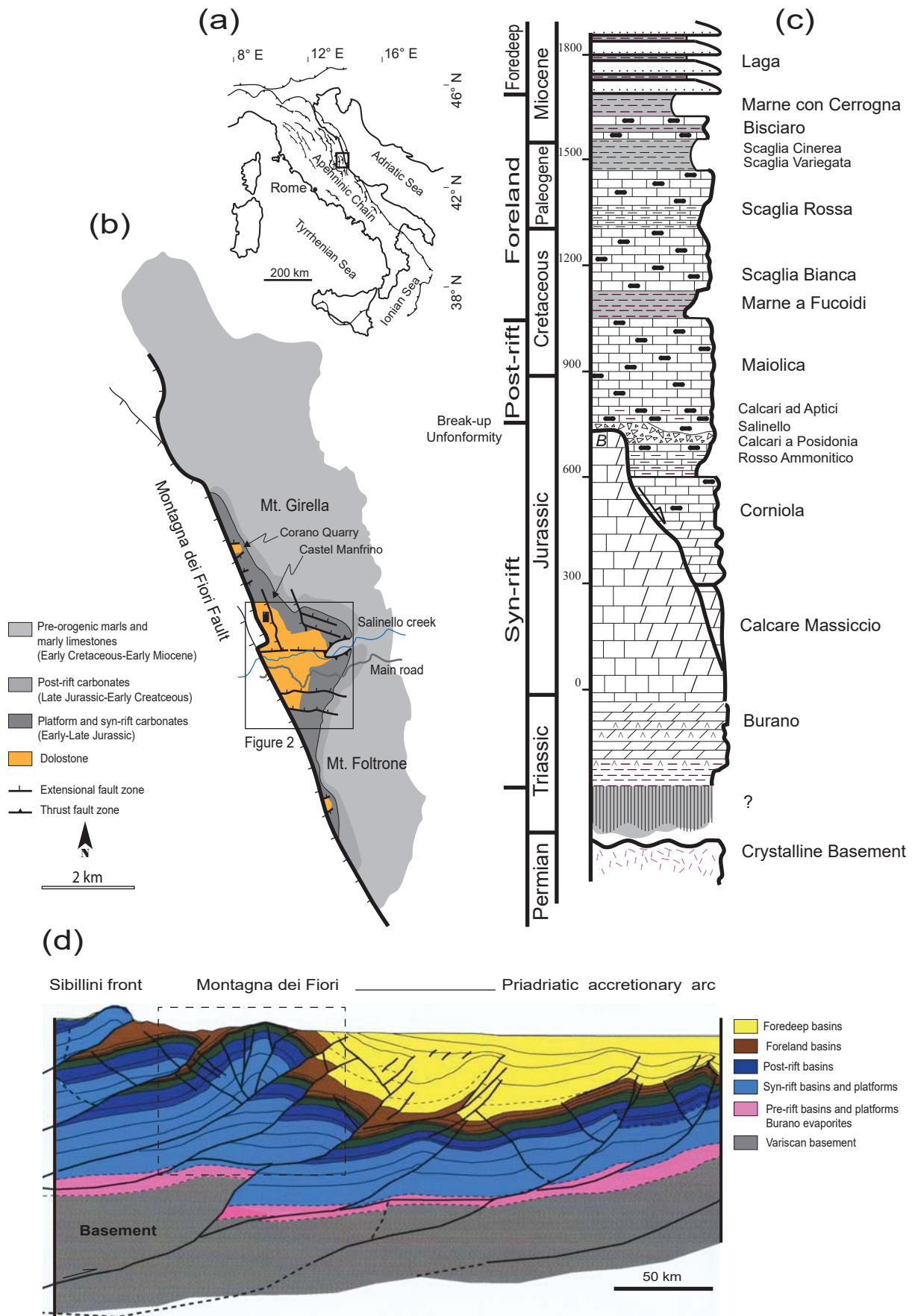


Fig. 1

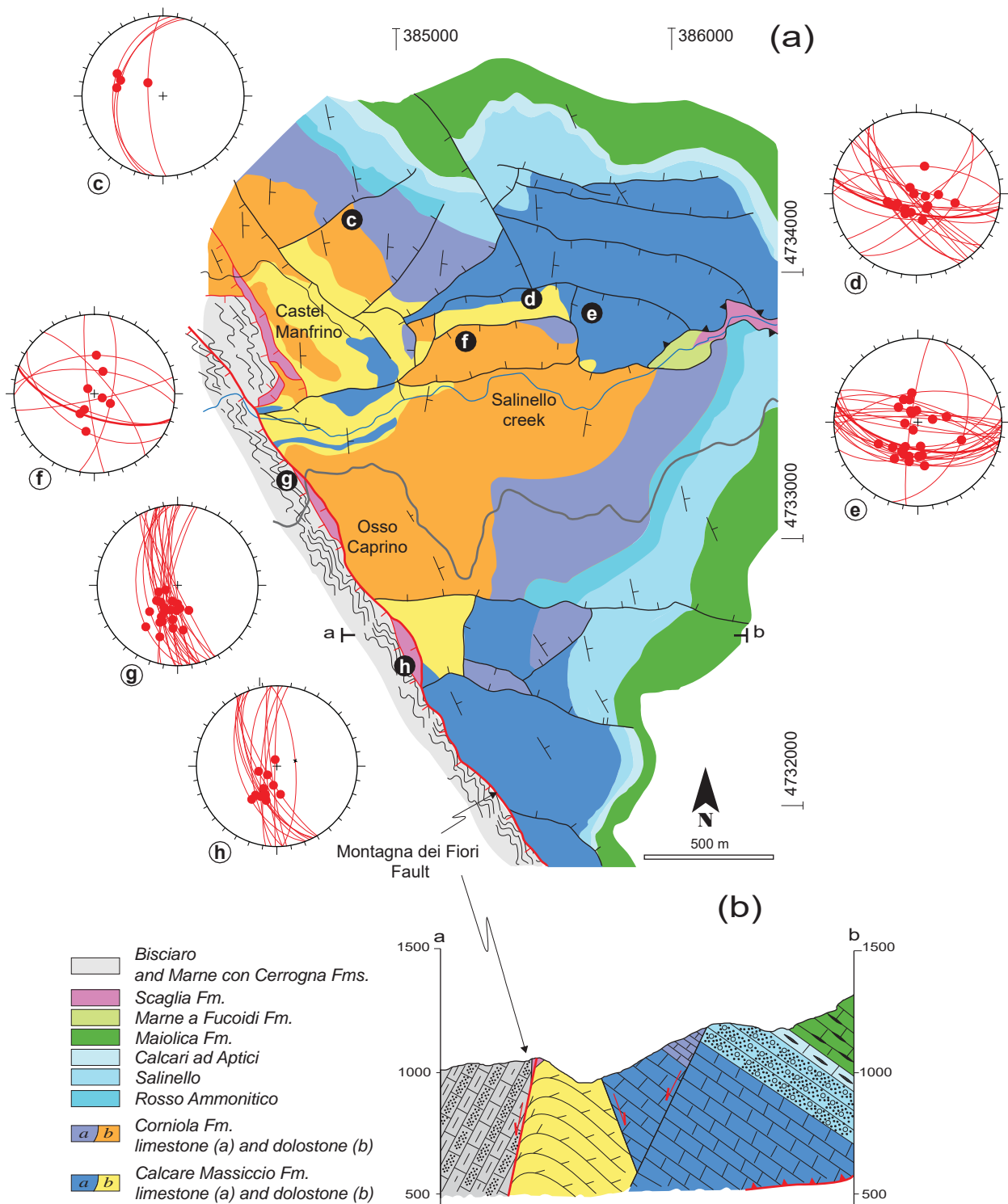


Fig. 2

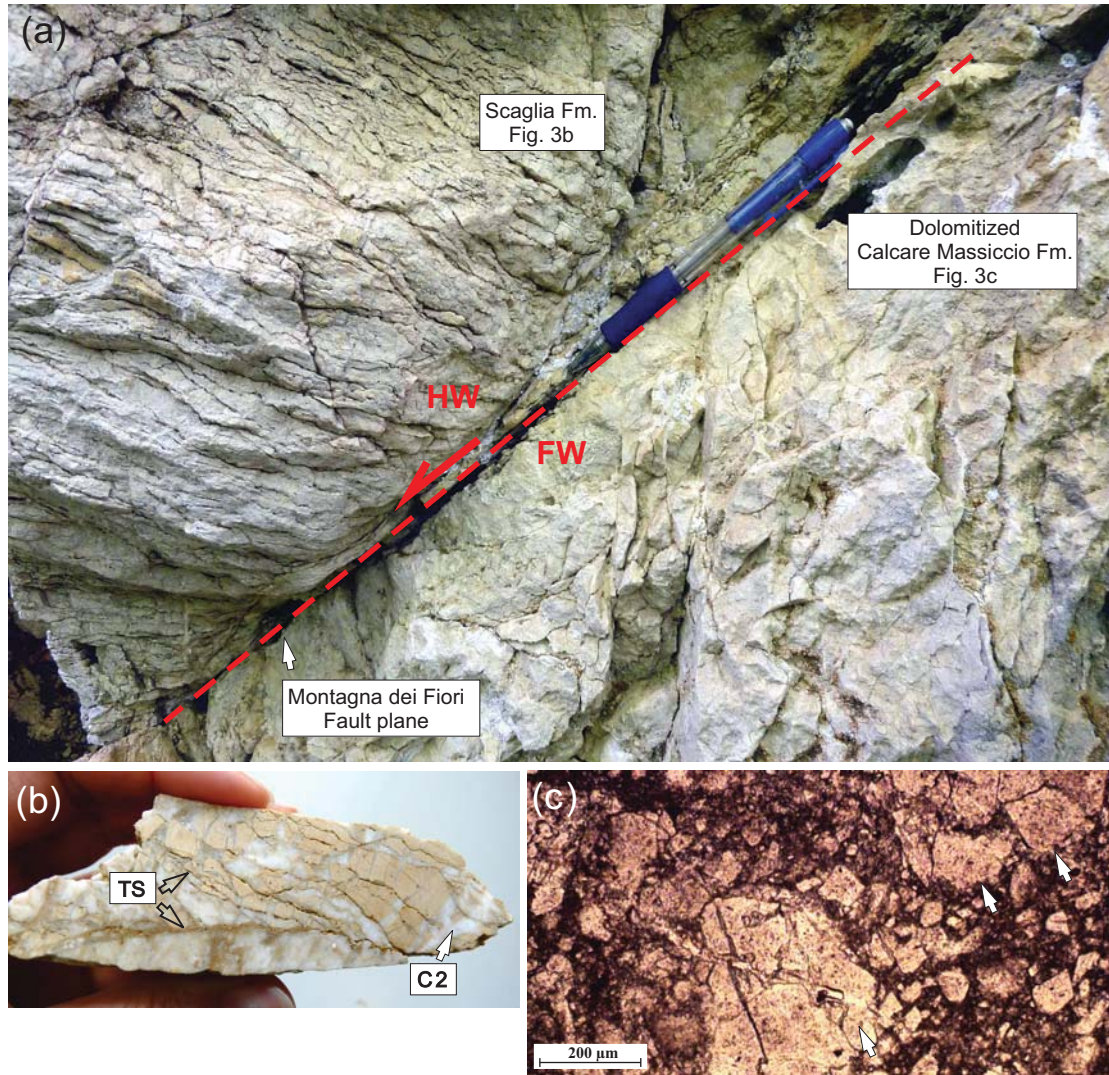


Fig. 3

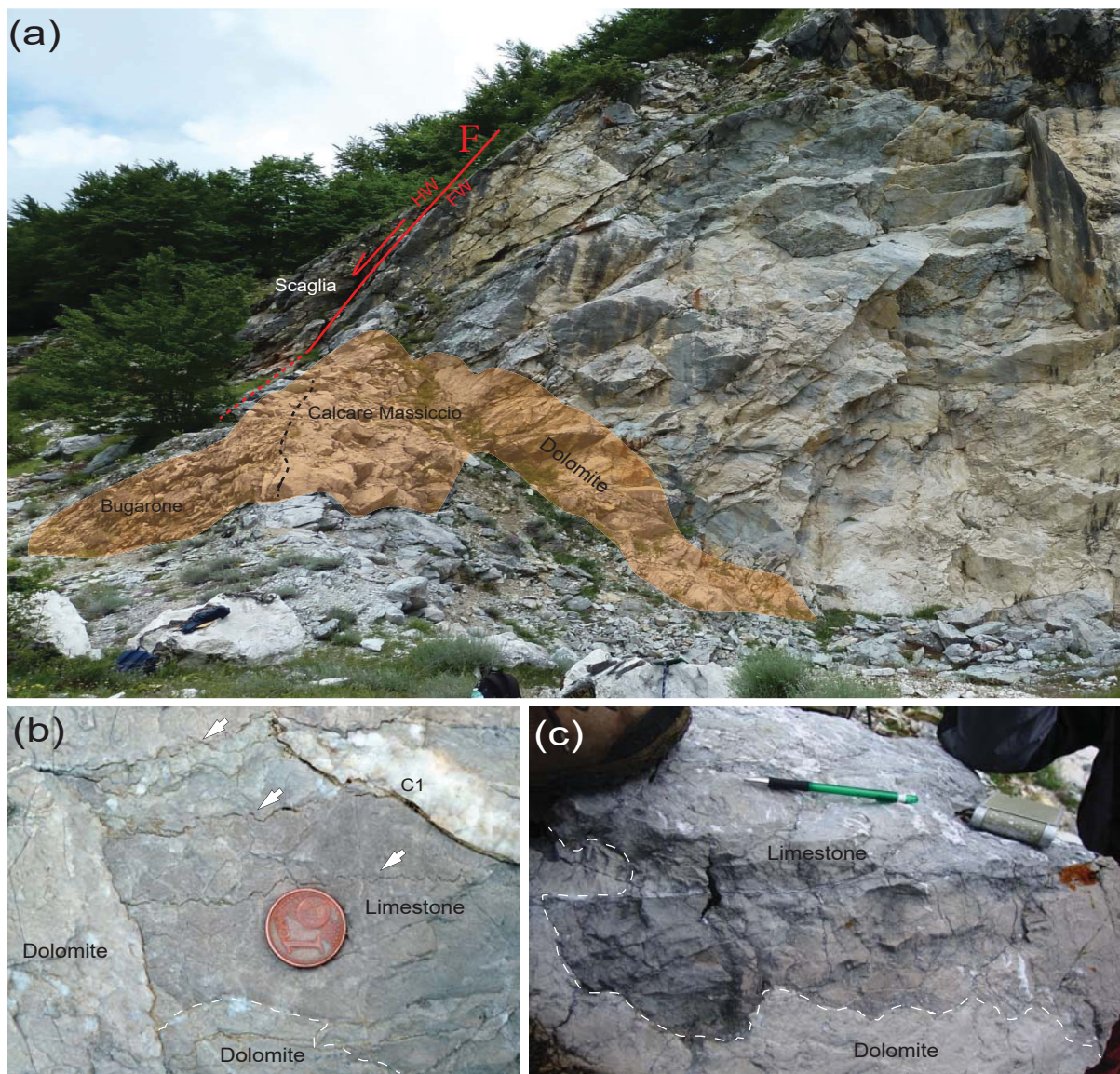


Fig. 4

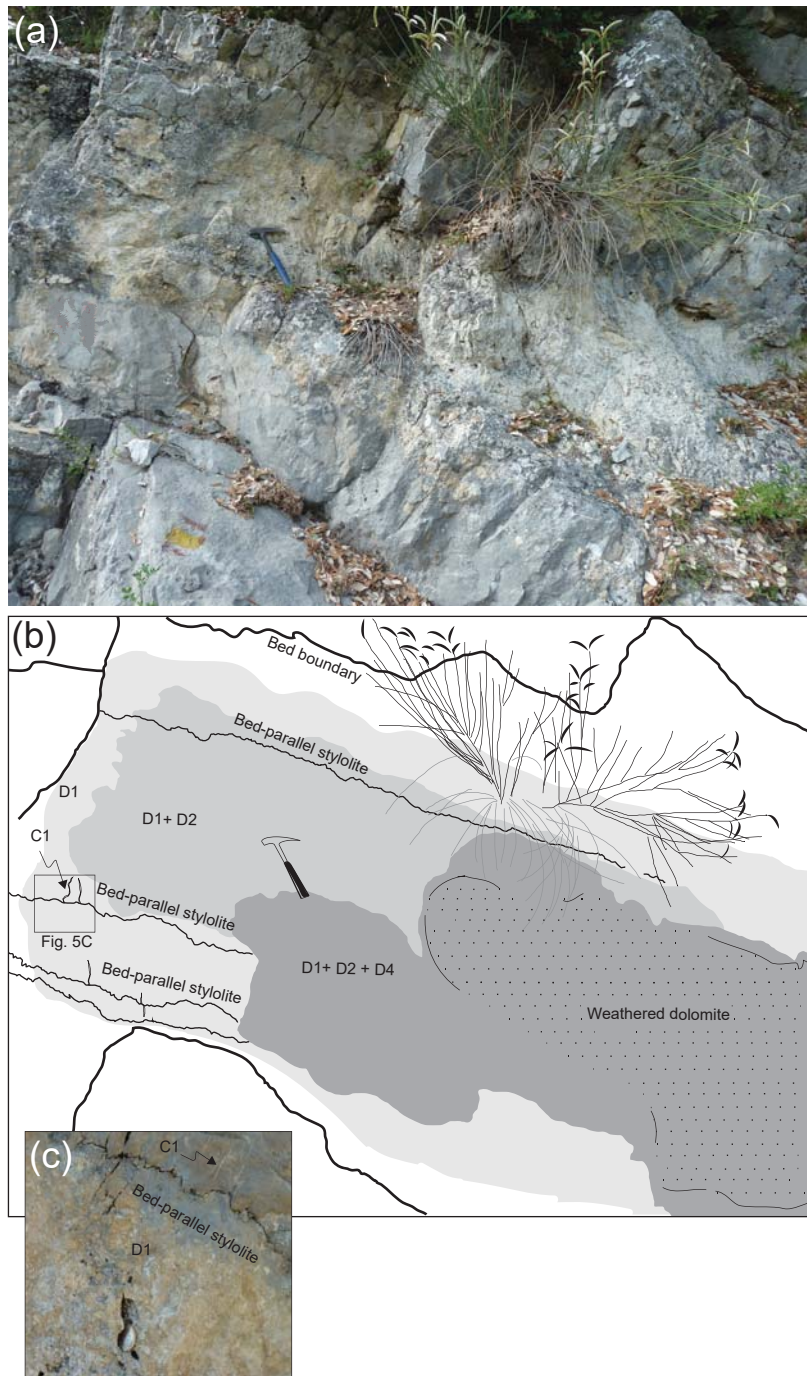


Fig. 5

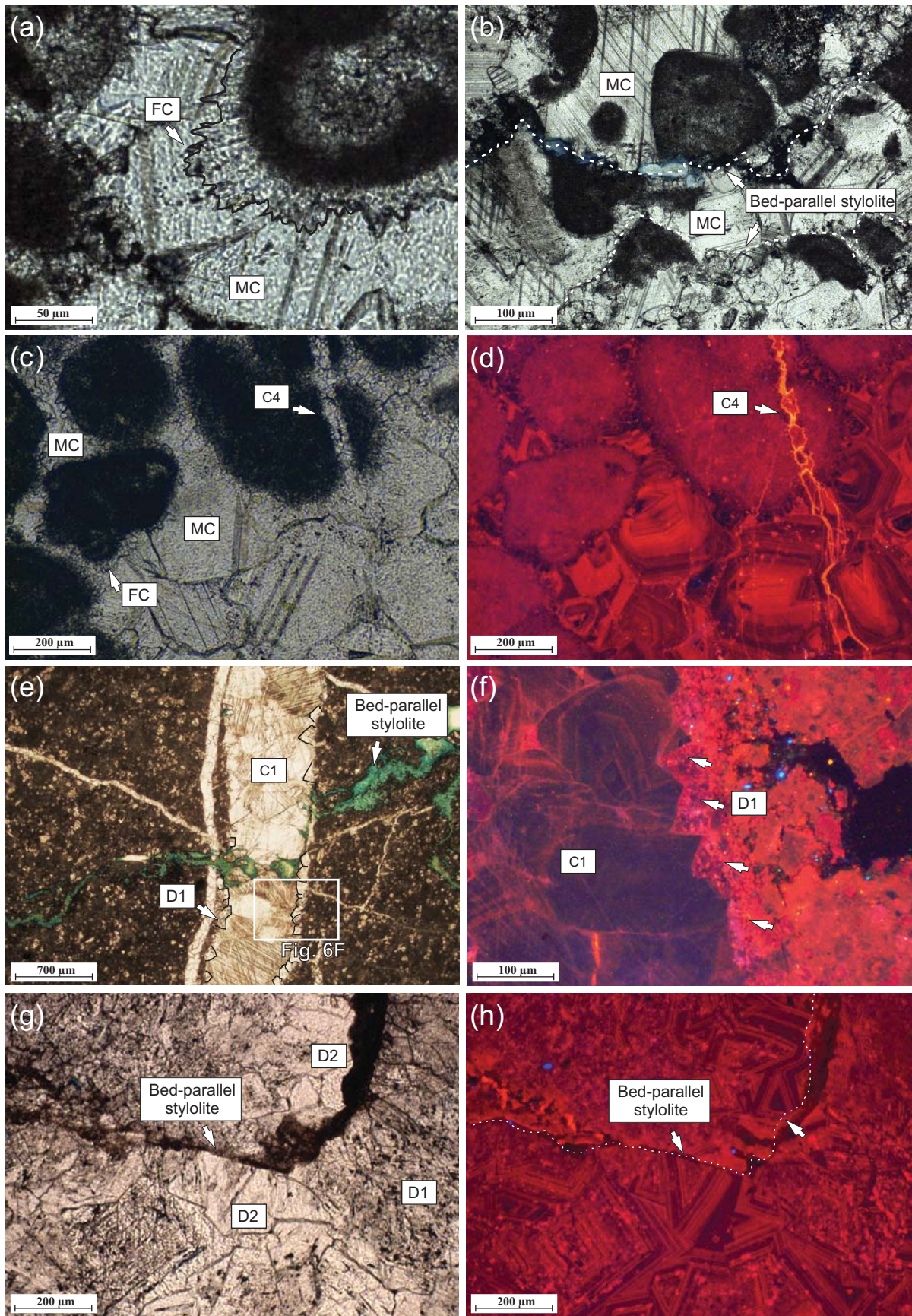


Fig. 6

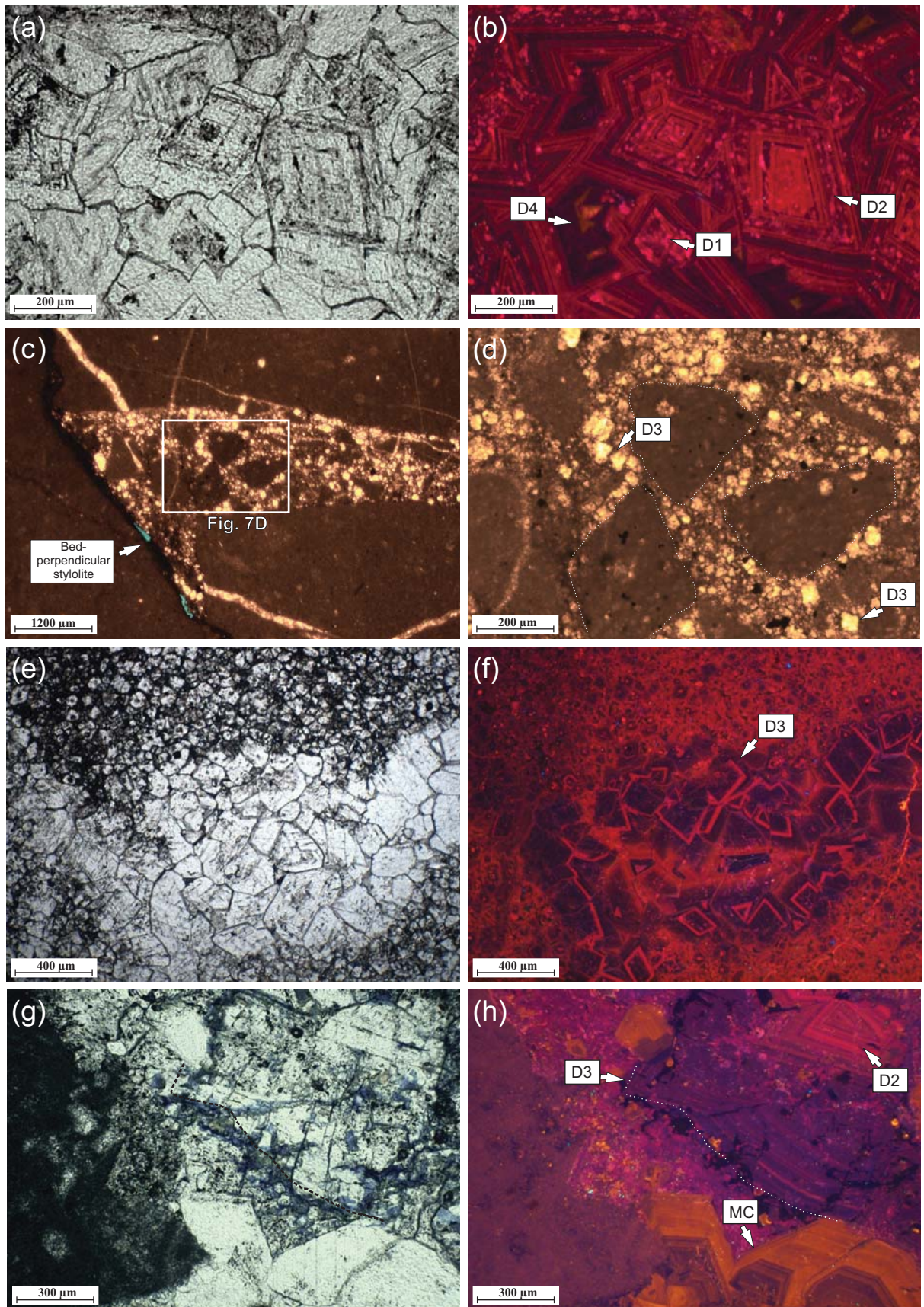


Fig. 7

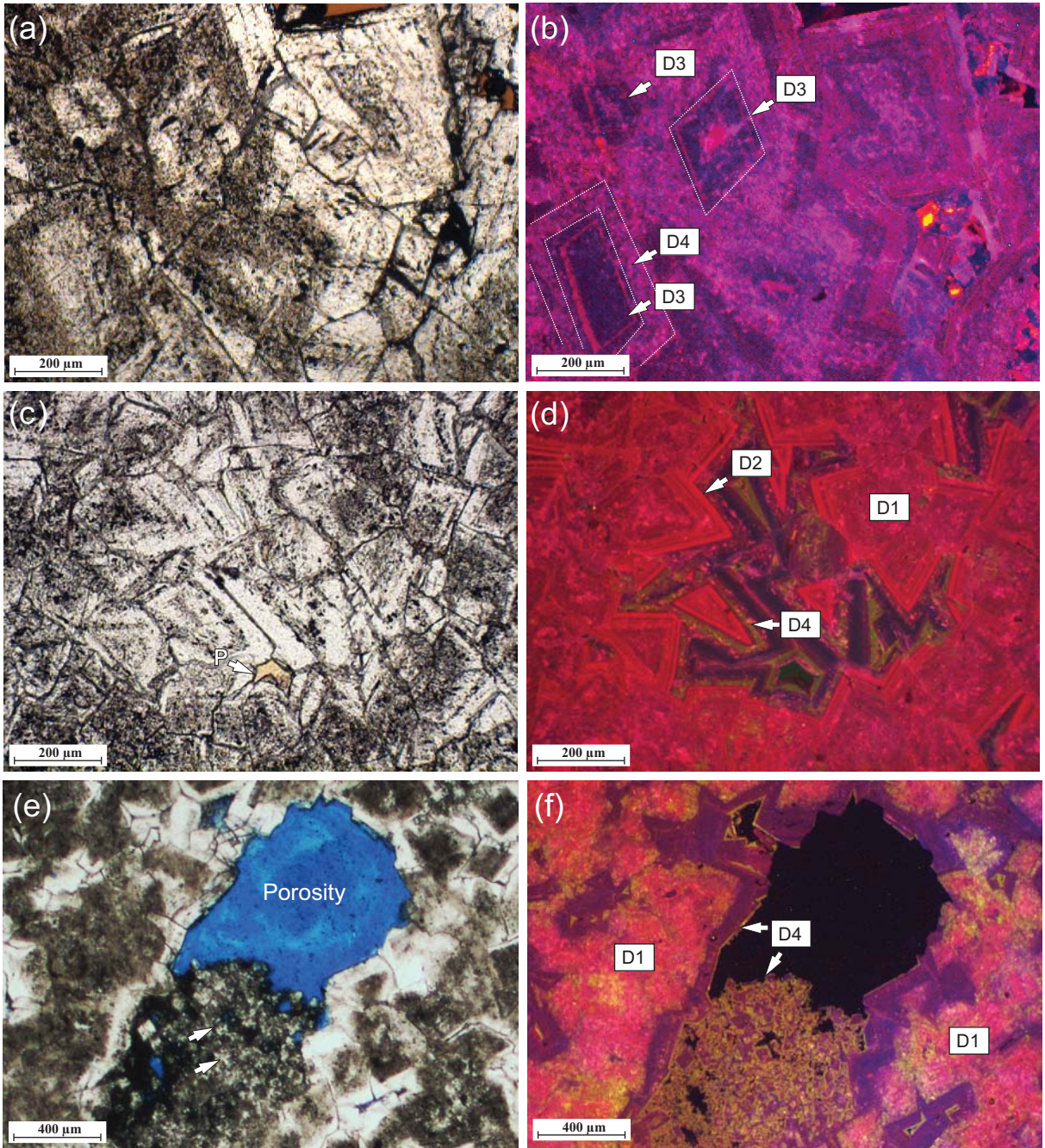


Fig. 8

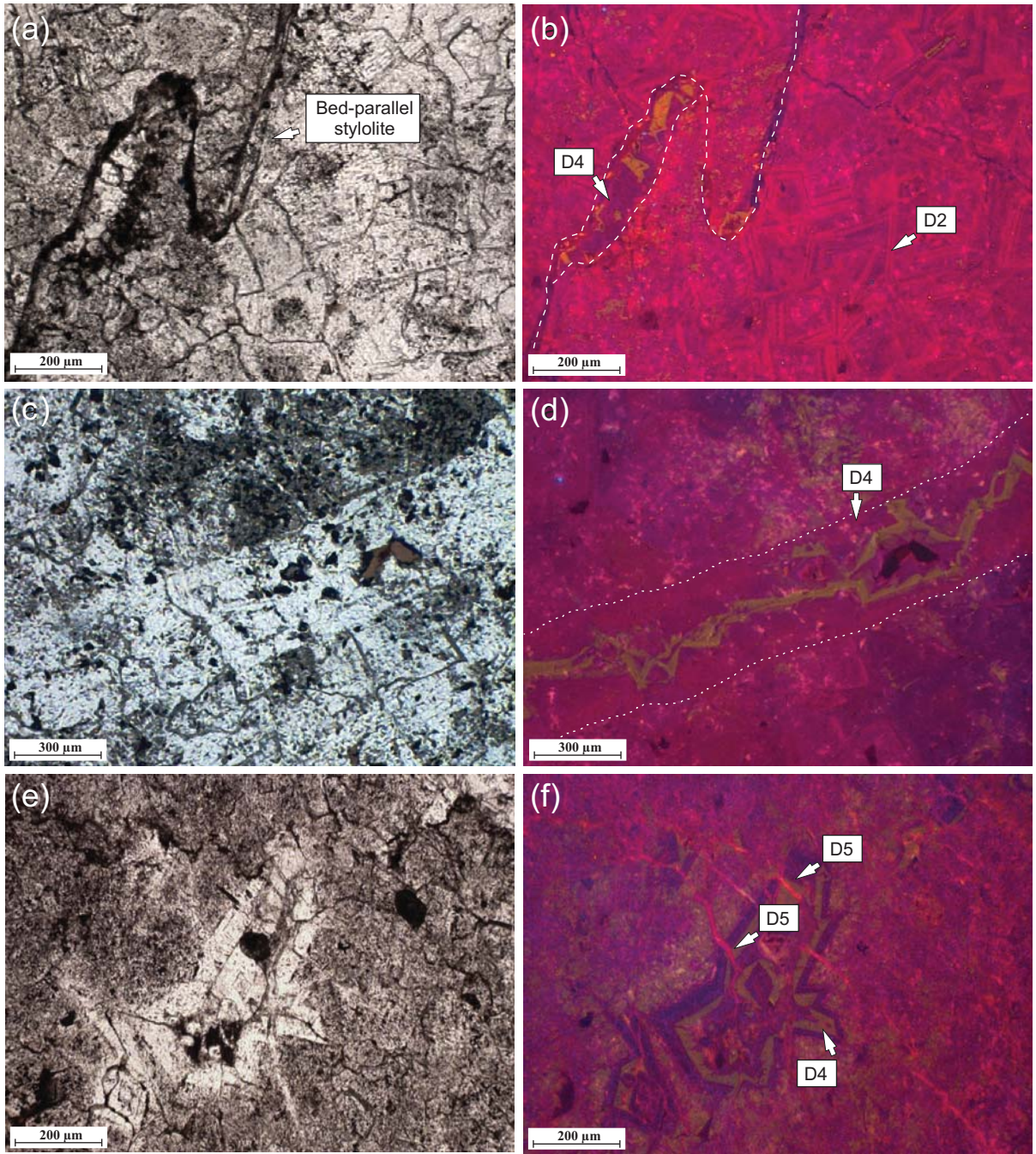


Fig. 9

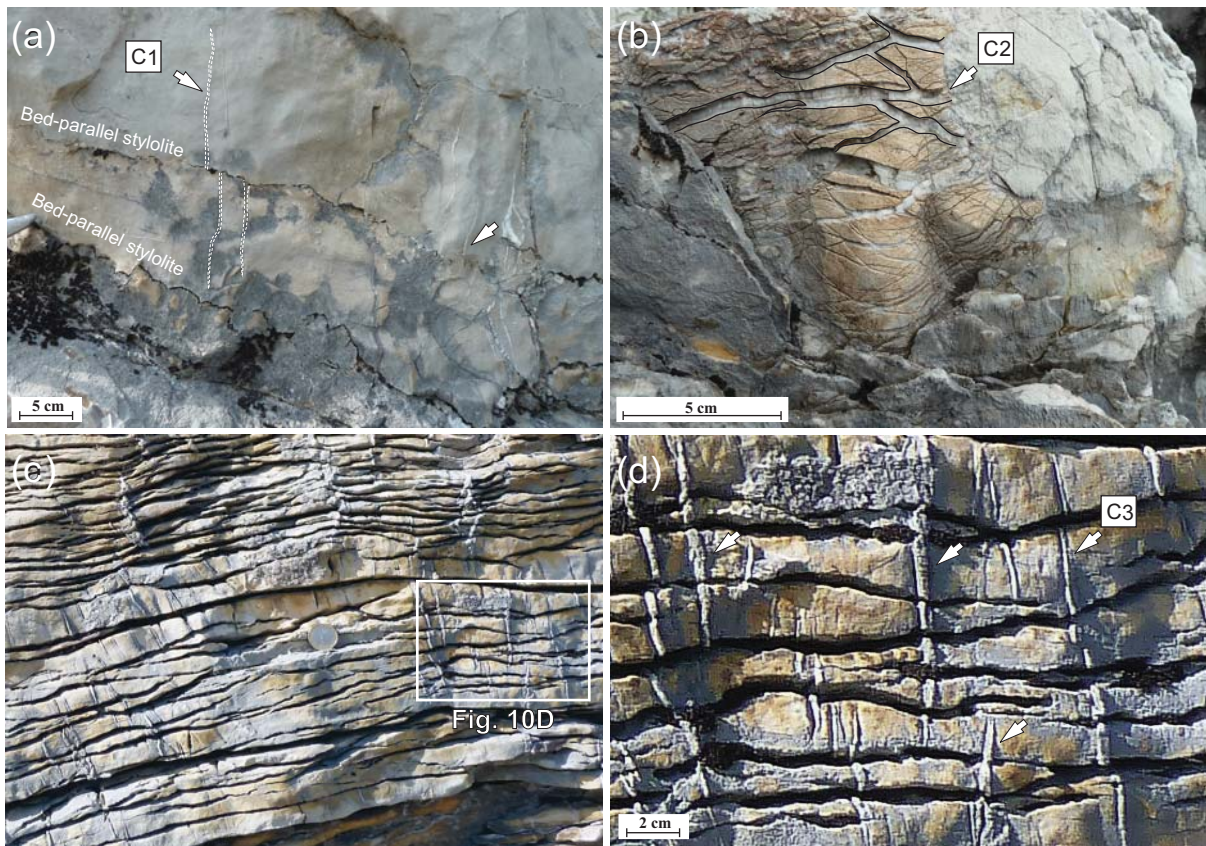


Fig. 10

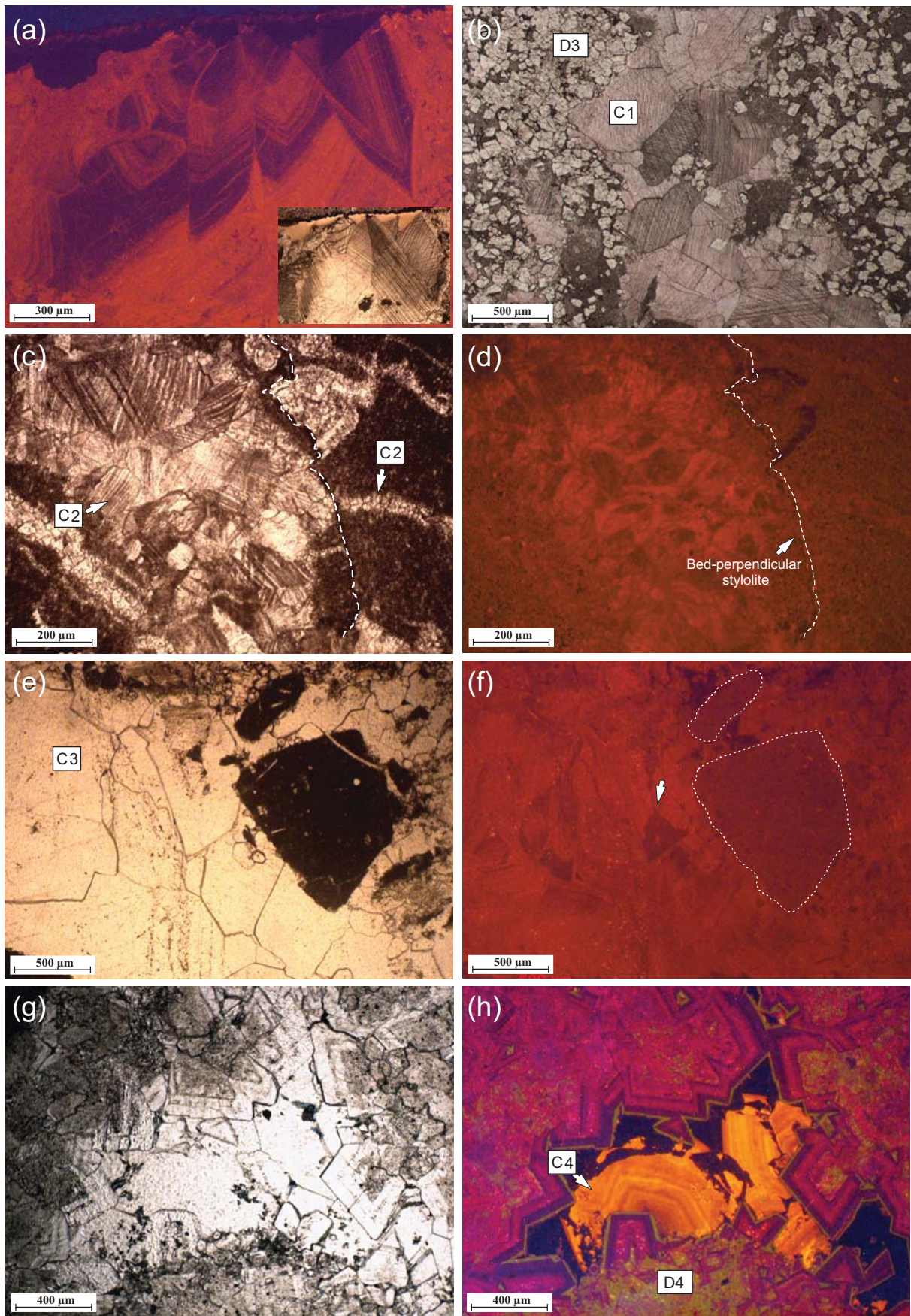


Fig. 11

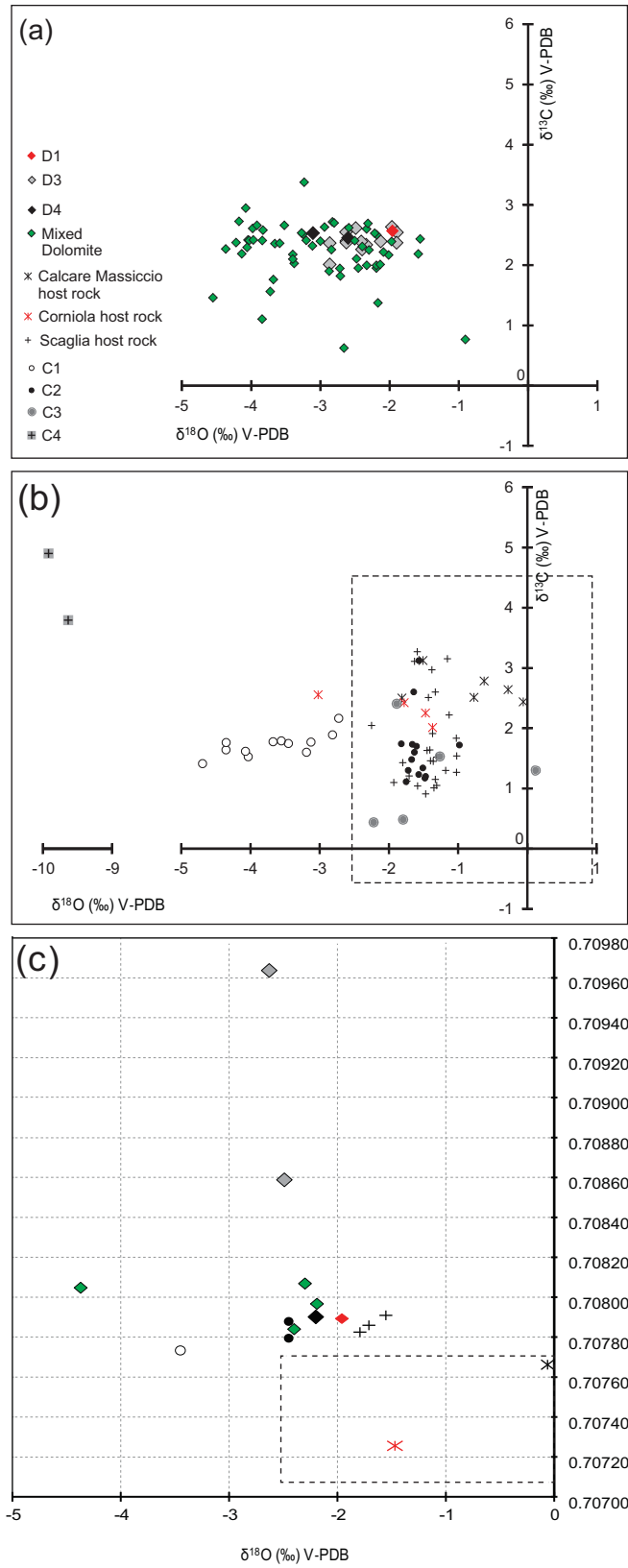


Fig. 12

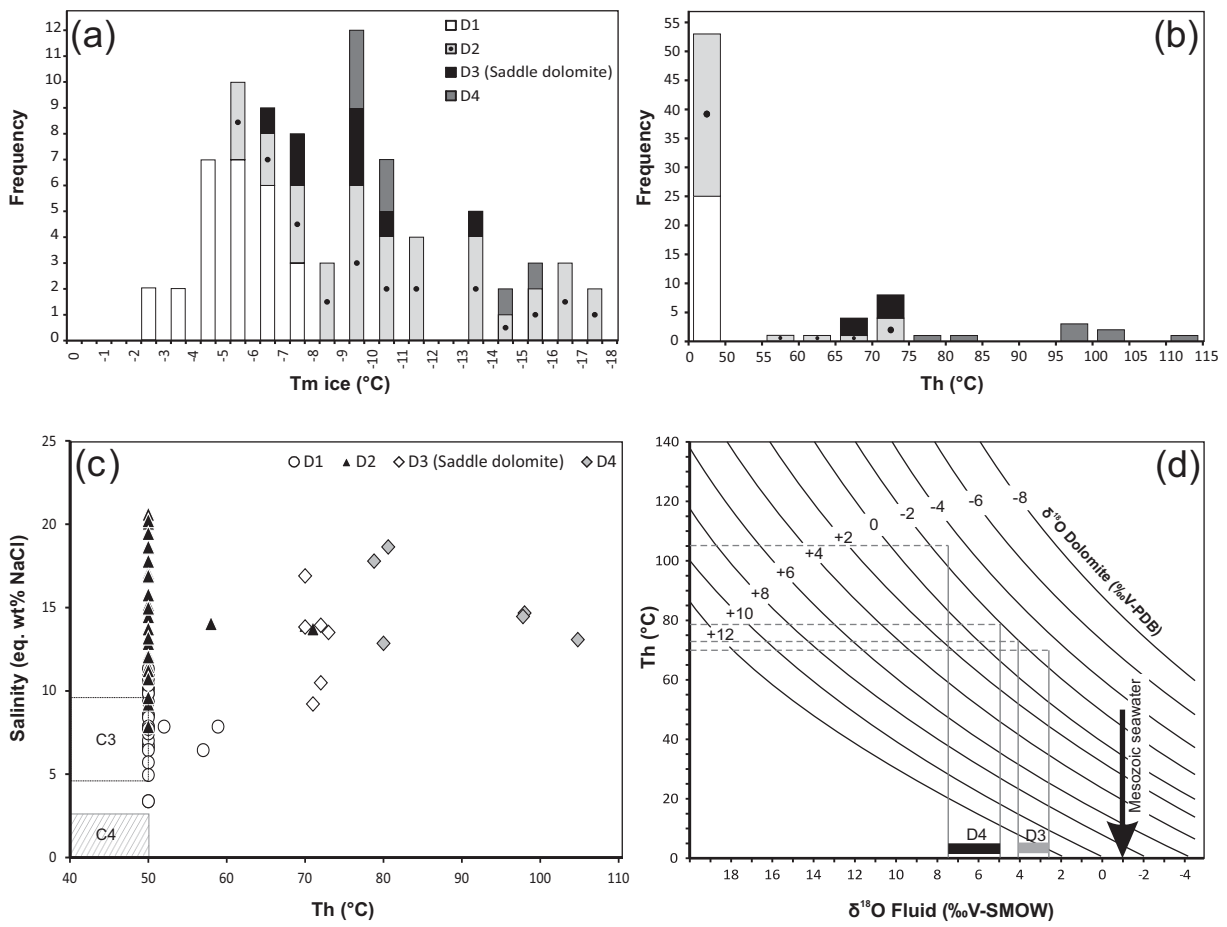


Fig. 13

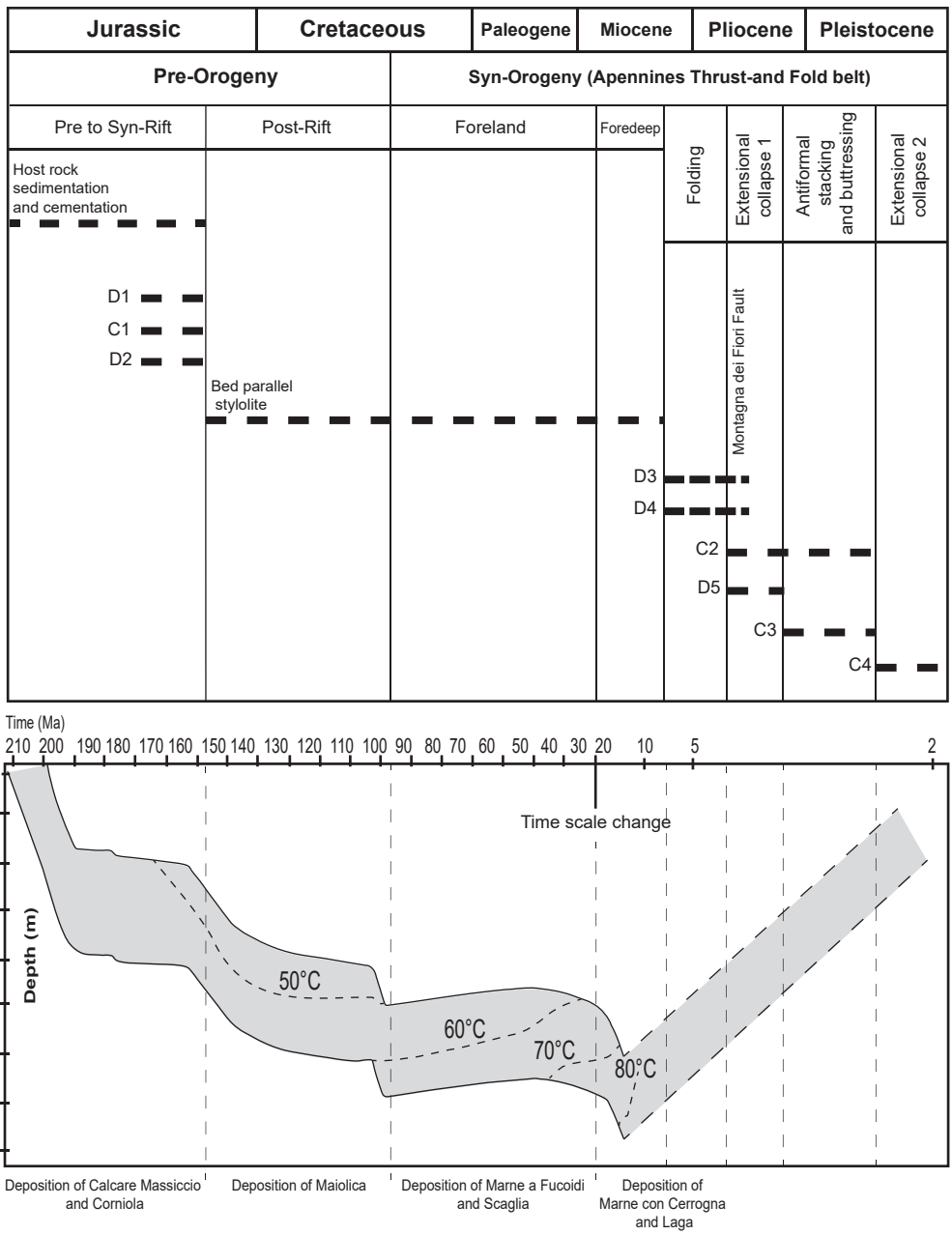


Fig. 14

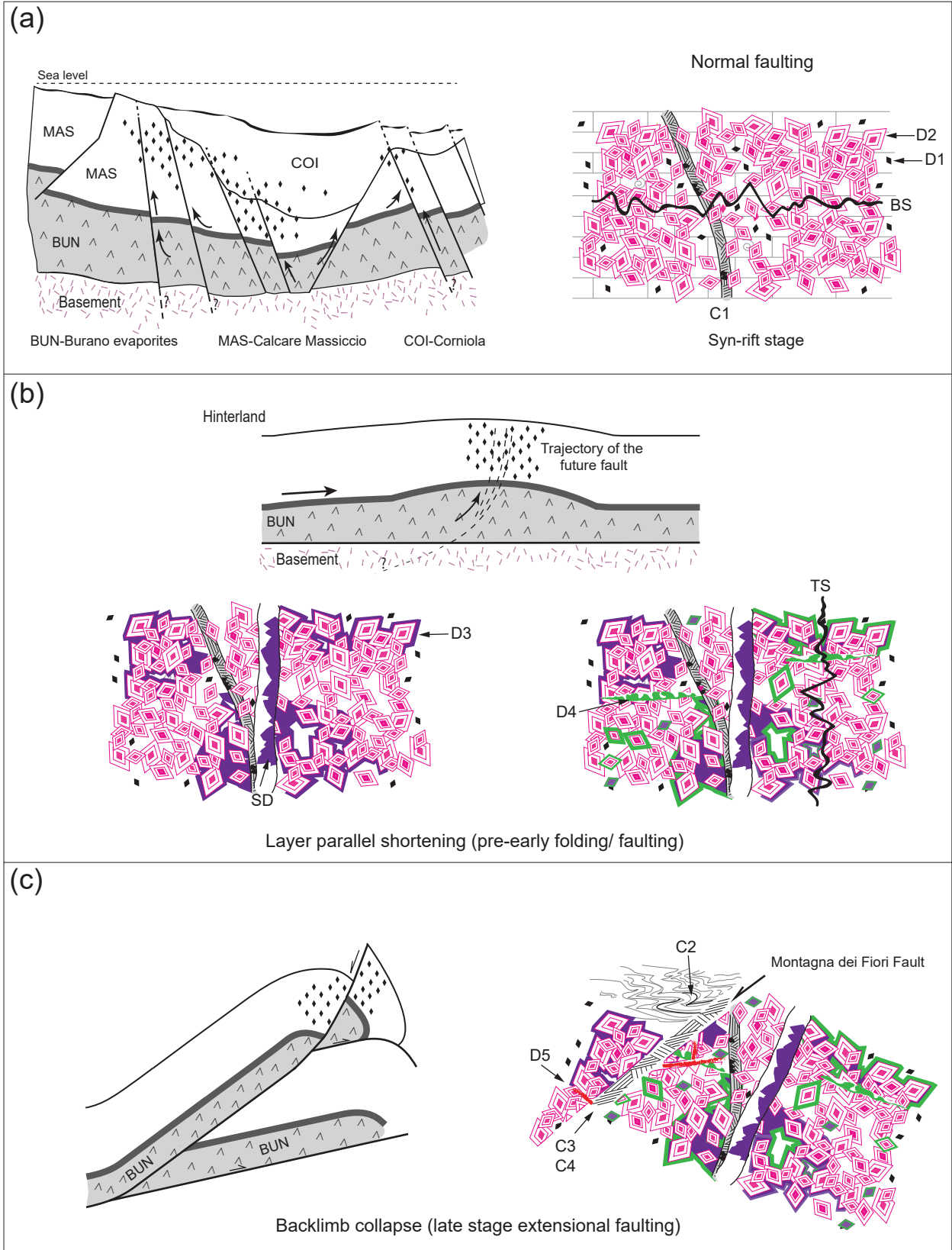


Fig. 15